DEVELOPMENT OF A NOVEL OXIDE-OXIDE CERAMIC MATRIX COMPOSITE FOR HIGH TEMPERATURE STRUCTURAL APPLICATIONS

by

SOPHIE CLARE DEARN

A thesis submitted to The University of Birmingham

For the degree of DOCTOR OF PHILOSOPHY

School of Metallurgy and Materials

College of Engineering and Physical Sciences

University of Birmingham

February 2015

To my husband, Karl

and my children Joshua Patrick Thackeray and Isabella Rose Endelienta

Abstract

The introduction of ceramic matrix composites (CMCs) for structural applications in the hot section of a gas turbine provides many potential benefits over conventional alloy materials, including facilitating elevated operating temperatures. The development of an oxide-oxide CMC composed of commercially available Nextel 720 (3M) fibres within a porous alumina matrix was presented.

A simple, low cost processing method involving slurry impregnation and subsequent consolidation and densification was developed, facilitating the production of dried pre-impregnated fabric ('pre-preg') that can be stored in ambient conditions. Detailed investigation into the effect of three types of PVA binder, the effect of 0-20wt% additions of an alumina precursor (ACH), the influence of a bimodal particle distribution and the effect of sintering at temperatures between 1100 and 1300°C on processing and mechanical properties was completed in order to optimise the material.

The optimised composite material, composed of Nextel 720 fibres within a submicron alumina particle matrix with 10wt% ACH sintered at 1200°C, exhibited mean flexural strength >205MPa, short beam shear strength >12MPa and tensile strength >146MPa. These results were comparable to similar oxide CMCs previously reported, validating this material.

Acknowledgements

I would like to express my deepest gratitude to my supervisor, Professor Paul Bowen, for his guidance, encouragement and support throughout this project.

This project would not have been possible without Dr Ted Butler (University of Birmingham), I am very grateful for his knowledge and expertise.

I would like to thank Dr Samantha Jones for her empirical wisdom and practical assistance, as well as Mr David Price and Dr Timothy Doel for their help in the mechanical testing laboratory.

I acknowledge those at Rolls-Royce plc.; my industrial supervisors, Dr Ian Edmonds and Dr Paul Andrews for their insightful comments and direction, as well as Steven Hillier and Danilo Di Salvo for their support throughout the project.

In addition, I offer thanks to Daniel Thompson, Grace Atkinson and Dr Quentin Fontana at Advanced Composites Group, now Cytec Industries Inc., whom it was a pleasure to work alongside.

I recognise that this research would not have been possible without the financial assistance of Rolls-Royce plc, the Engineering and Physical Sciences Research Council (EPSRC) and the Technology Strategy Board (TSB).

Sophie C Dearn

February 2015

Contents

List of Figures

List of Tables

Chapter 1 - Introduction

Many of our modern technologies require materials with unusual combinations of properties which cannot be met by conventional metallic alloys, ceramics or polymers. This is especially true for materials in the aerospace and transportation industry. Aircraft engineers are continually searching for high temperature structural materials with low densities that are not easily corroded. They seek materials that are both strong and stiff, and abrasion and impact resistant. This is a challenging combination of materials to find since it is generally accepted that increasing the strength or stiffness of a material results in a decrease in impact strength. Similarly, strong materials are usually more dense.

Material property combinations are being extended by the development of composite materials. A composite is considered to be any multiphase material that exhibits two or more chemically and/or physically distinct phases. Typically, composite materials are composed of a reinforcement phase and a continuous matrix phase. According to the principle of combined action, composite materials have characteristics better than or different from those of either constituent.

This thesis explored the development of a novel oxide-oxide ceramic matrix composite (CMC) composed of commercially available Nextel 720 fibres within an alumina matrix for high temperature structural applications. A summary of the thesis is outlined in Figure 1.1.

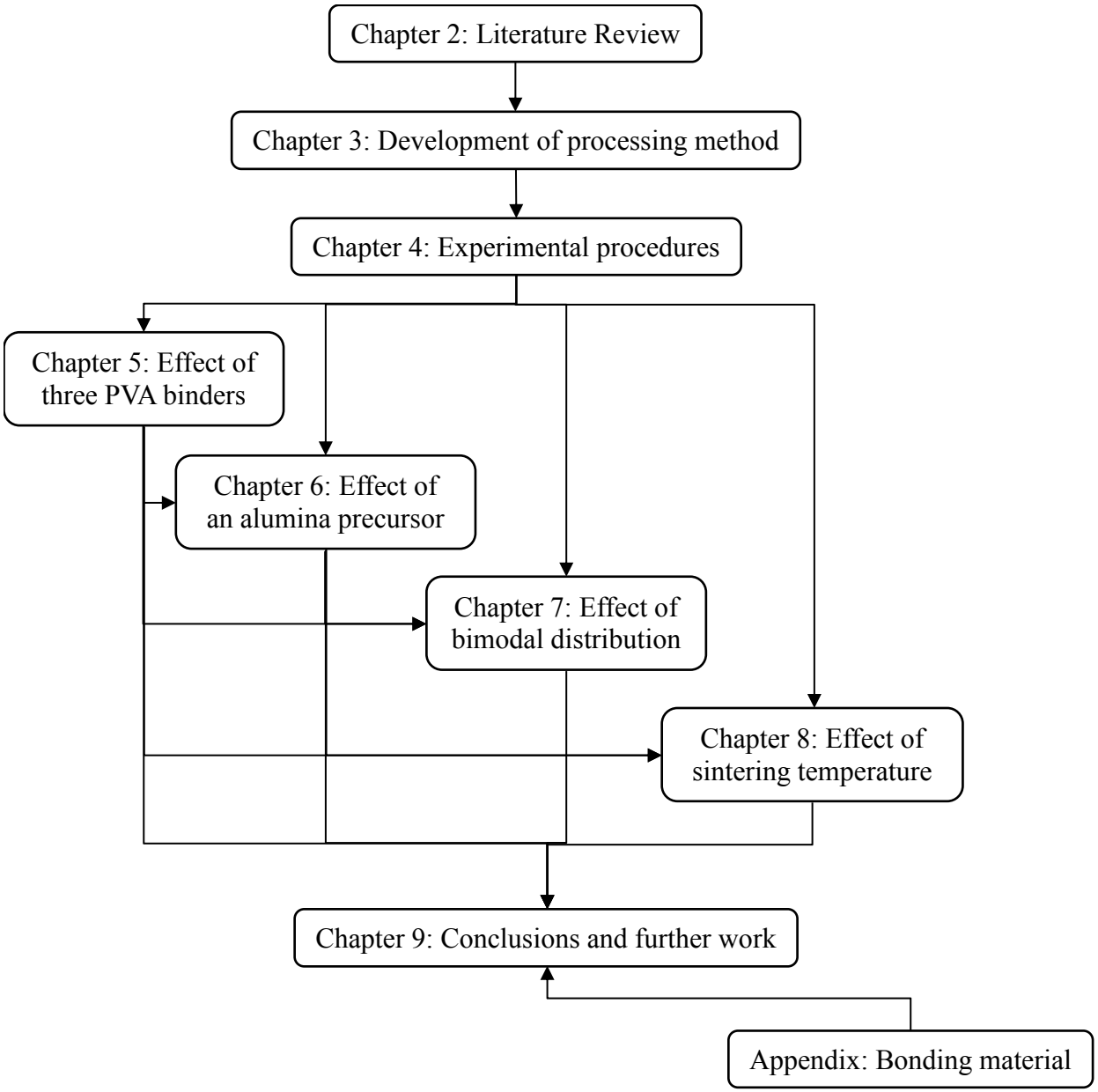

Figure 1.1. Outline of the thesis

Chapter 2 - Literature review

The introduction of ceramic matrix composites (CMCs) for structural applications in the hot section of a gas turbine (such as combustor tiles, nozzles and seal segments) provides many potential benefits over conventional alloy materials. Not only do CMCs have a reduced density compared to metallic alloys, but the use of such materials could enable components to operate at higher material temperatures (Figure 2.1) for longer hot times, with reduced levels of material degradation. This property combination could offer improvements in both operating efficiency and performance, in addition to a reduction in emissions. Whilst ceramic composites are unlikely to offer a benefit over traditional materials in terms of initial component cost, cycle cost may be reduced by extending the life of a component and eliminating the need for cooling air by operating at temperatures below the temperature capability of the material. The ability to cool a material depends on its thermal conductivity. Poor thermal conductivity can result in local hot spots and thermal strains (in addition to complicating thermal models) and thus eliminating the need for cooling air is highly desirable in turbine applications.

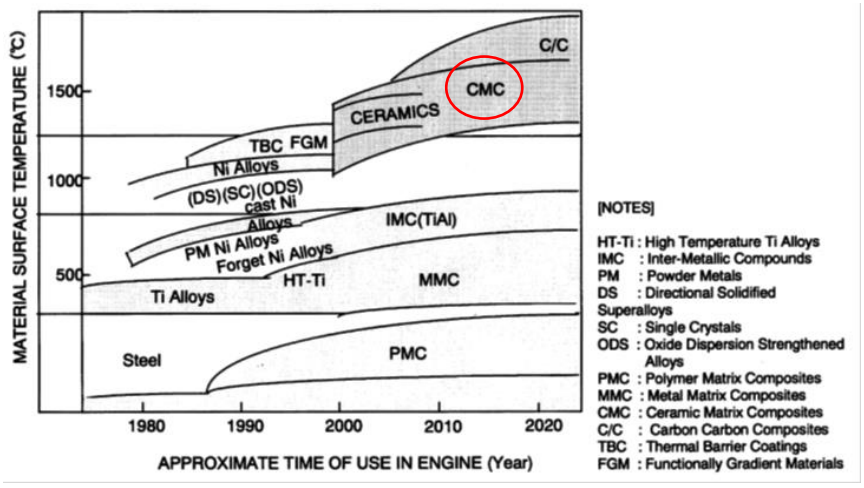

Figure 2.1. Trends in development of high temperature materials for turbine components [1].

Monolithic ceramics are in many ways suitable for applications in the gas turbine, but their brittleness renders them susceptible to failure under conditions of thermal or mechanical shock. By incorporating ceramic fibres into a ceramic matrix to produce a ceramic matrix composite (CMC), the toughness of the material can be improved to a sufficient degree for structural gas turbine applications [2]. The most common microstructural design path to promote toughness uses a fibre coating that forms a weak interface between the fibres and the matrix (Figure 2.2b). This weak interface provides a path for crack deflection parallel to the loading direction, allowing the crack to propagate along the fibre/matrix interface resulting in a non-brittle fracture behaviour. A low thermal mismatch stress between the fibres, fibre coating and matrix is essential in order to reduce internal frictional stress. Fibre coatings introduce high cost and processing complexity and thus alternative methods of creating damage tolerant behaviour have been sought.

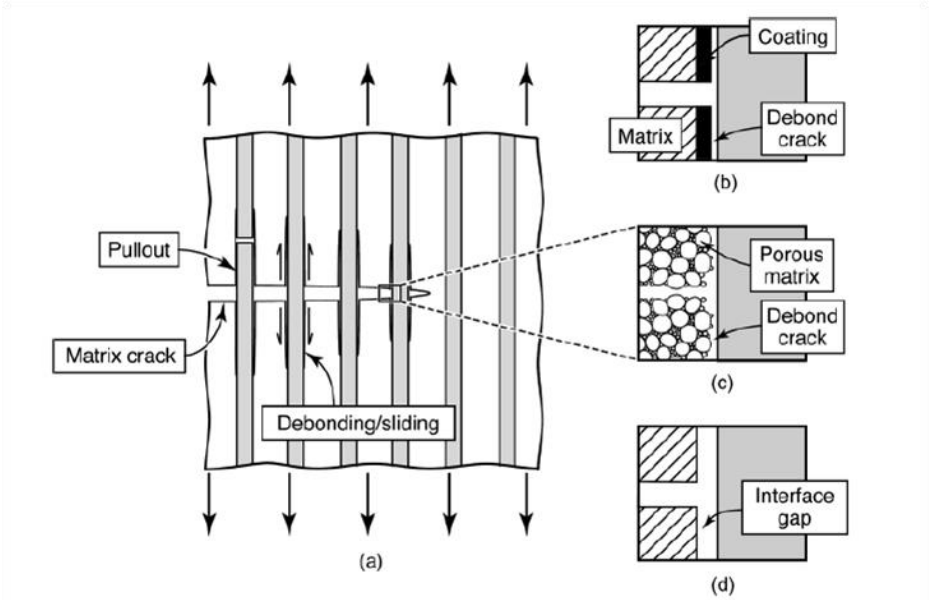

Figure 2.2. Microstructural concepts for enabling crack deflection in ceramic composites; a) fibre coating to form a weak interface b) porosity within the matrix to form a weak interface and c) fugitive coating to form an interface gap [3].

Similar crack deflecting behaviour can be achieved by means of a finely distributed porosity within the matrix (Figure 2.2c). The porous matrix allows the fibres to be isolated from cracks within the matrix, and thus fracture has to be reinitiated in the solid phase within the high stress field of the propagating crack, meaning that a continuous crack front cannot propagate through the material. In contrast to the fibre coating method, the fibres must have a larger thermal expansion coefficient than the matrix. In consequence, fibre bundles are in residual tension and matrix regions in residual compression [4]. Furthermore, the matrix must be chemically compatible with the fibres owing to their intimate contact in the absence of a coating [3], [5].

The fugitive coating concept, a less commonly used approach, relies on the retention of a coating (typically carbon) during composite processing and its subsequent removal through oxidation to form a narrow gap (Figure 2.2d). Ideally the gap formed is straight and thus fibre pull-out is unconstrained as the crack travels through the material, with no load transfer from the matrix, resulting in crack deflection. In reality, however, a straight gap does not form between the fibre and matrix, and thus mechanical interlocking and intermittent fibre/matrix bonding prevents damage tolerant behaviour. The thickness of the coating must be controlled as this defines the width of the interfacial gap. The optimal thickness is system-specific, since it relies on factors including thermal expansion mismatch and roughness effects from both fibre and matrix [3], [6].

CMCs can be classified into oxide and non-oxide materials. Over the past few decades, a vast amount of research has focussed on the development of non-oxide, silicon carbide (SiC) composites with a fibre/matrix interface (frequently carbon or boron nitride). Technology in this area has reached a high level of maturity and large components are routinely

manufactured for gas turbine applications [7]. SiC/SiC composites have attractive high temperature properties. They have a high temperature capability, high thermal conductivity and low thermal expansion, therefore reducing thermally induced strains. However, the oxidation sensitivity of the interface can cause oxidation embrittlement of the composite after service at elevated temperature for long times ($>10^4$ hours). Oxidation embrittlement is most severe with cyclic mechanical and thermal loading. Oxygen penetrates into the composite via matrix cracks that form during loading and reacts locally with the fibres and fibre coatings to form oxide products. Oxide products create strong bonds between the fibre and the matrix, preventing crack deflection and inhibiting the internal friction mechanisms that otherwise promote toughness [3], [8].

Oxide systems are immune to oxidation embrittlement and thus have emerged as leading contenders for applications requiring long term service lives in oxidising environments, such as those present in the hot section of the gas turbine. Since the constituents are fully oxidised, further damage by oxidation can be avoided even at high temperatures and after matrix cracking. Oxide composites are potentially low cost, however the primary difficulty with this approach is the lack of a suitable oxide-based debond layer equivalent to carbon or boron nitride. Whilst there have been a number of successful attempts to create an oxide debond layer, the majority of literature focuses on creating damage tolerant behaviour via a porous matrix [8], [9].

2.1. Material design

When designing a ceramic matrix composite, there are a number of factors that affect the performance of the material (Figure 2.3). The mechanical behaviour and chemical composition of the individual components (reinforcement and matrix), and the interaction between these components (the interface) is of vital importance. A number of characteristics must be considered when selecting the reinforcement and matrix materials including temperature capability, density, strength, coefficient of thermal expansion, creep behaviour and fracture toughness. The reinforcement and matrix materials must be environmentally stable, in addition to being chemically and thermally compatible [10], [11]. Many of these characteristics have an important bearing on the processing route chosen. The processing required to manufacture the composite is an integral part of the design process and will be discussed in section 2.2.

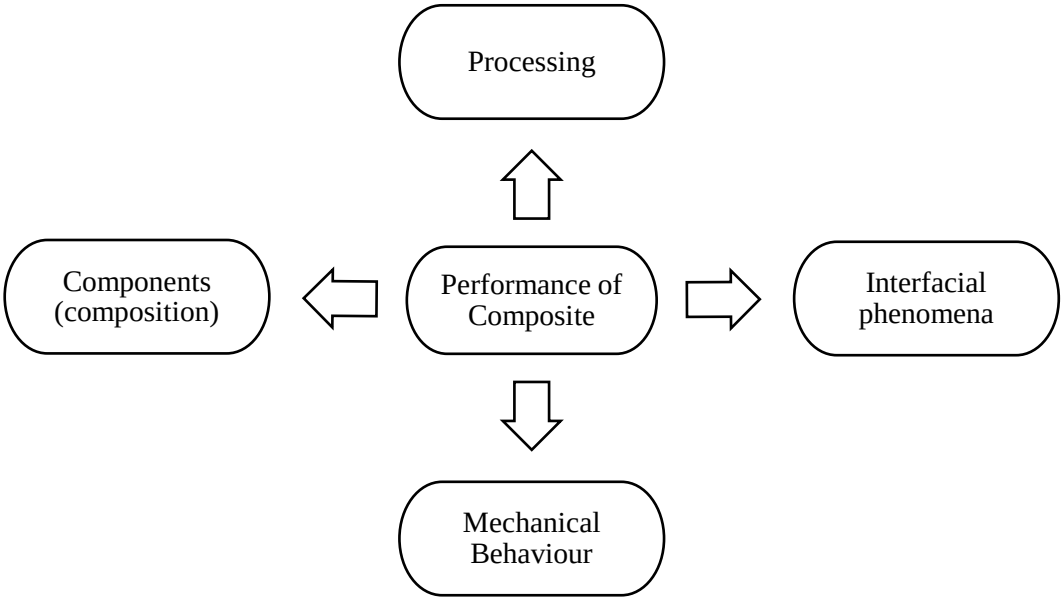

Figure 2.3. Performance of a composite is linked to the composition of components, their mechanical behaviour, processing and the characteristics of the interface between matrix and reinforcement (after [10]).

2.1.1. Ceramic reinforcements

Ceramic reinforcements include particles, whiskers, short fibres and continuous fibres. Table 2.1 highlights some noteworthy ceramic reinforcement materials. Continuous ceramic fibres are of particular interest for high temperature structural materials since they combine relatively high strength and elastic modulus with high temperature capability. Continuous fibres can be produced with a wide range of compositions, geometries and properties and are widely commercially available. It is common to classify continuous reinforcements into non-oxide and oxide fibres. Non-oxide fibres such as those containing carbon and silicon carbide are regularly utilised in CMCs however they are susceptible to oxidation at moderate temperatures and thus require an oxygen barrier protection. Oxide fibres are fully oxidised and therefore cannot suffer from oxidation embrittlement. There are a number of commercially available alumina-based oxide fibres; most significantly the Nextel family of fibres developed by Minnesota Mining and Manufacturing Co. (3M).

Table 2.1. Noteworthy ceramic reinforcement materials (after [12]**).**

Particles		SiC
		TiC
		Al_2O_3
Discontinuous Fibres	**Whiskers**	SiC
		TiB_2
		Al_2O_3
	Short Fibres	Glass
		Al_2O_3
		SiC
		$Al_2O_3 + SiO_2$
		Vapour-grown carbon fibres
Continuous Fibres	**Oxide**	Al_2O_3
		$Al_2O_3 + SiO_2$
		ZrO_2
		Silica-based glasses
	Non-oxide	B
		C
		SiC
		Si_3N_4
		BN

2.1.1.1. Non-oxide fibres

Carbon fibres were first developed in the 1960s for space and defence applications and are now used extensively in commercial, industrial and consumer applications, in a variety of different composite matrix systems (polymer, metal and ceramic matrices). Carbon fibres offer high strength, high stiffness, low density and low thermal expansion, in addition to high thermal and electrical conductivity. Furthermore, carbon fibres have the potential to operate at high temperatures (2200°C), providing the fibres have either an oxygen barrier protection or the environment is non-oxidising. Carbon fibres are generally produced by the pyrolysis of an organic hydrocarbon precursor in a non-reactive atmosphere. Commercial production usually includes a two-step process; spinning of the precursor followed by thermal conversion to carbon. Three commonly used precursors include rayon, polyacrylonitrile (PAN) and pitch. Rayon-based fibres dominated the market in the 1960s and 1970s however due to the low carbon yield and high processing costs, PAN- and pitch-based fibres are far more popular today. PAN-based fibres have a far greater tensile and compressive strength than pitch-based fibres, however pitch-based fibres exhibit the highest specific modulus. Carbon fibres are typically 5-15μm in diameter and can be woven in a range of different weaves (plain, satin, twill, basket) to produce fabrics [12], [13], [14].

Silicon carbide (SiC) fibres have excellent mechanical strength at high temperature and are commonly used to produce high performance composite materials [15]. SiC monofilaments, such as the 'SCS' fibres developed by Speciality Materials Inc., are produced by chemical vapour deposition (CVD), which typically uses methyltrichlorosilane to deposit SiC onto a carbon monofilament. Whilst SiC monofilaments display very high strength, their large diameters (70-140μm) are not conducive to fibre shaping into complex architectural preforms [16]. Small-diameter SiC fibres, which are sufficiently flexible to allow weaving and braiding,

are very desirable for use in CMCs [17]. Small-diameter (<15μm) SiC fibres are commonly fabricated by spinning and heat treating preceramic polymer precursors such as polycarbosilane. Preparation of first generation SiC fibres often resulted in significant amounts of oxygen which, when heated above 1200°C, led to weight loss, porosity and deteriorating mechanical properties [15]. Consequently, manufacturers sought alternative compositions and processing conditions in order to reduce the oxygen content within the fibres and to control grain size.

Ube Industries produce a range of high temperature grade SiC fibres named 'Tyranno' which incorporate titanium (S- and LoxM-grade), zirconium (ZMI-grade) and aluminium (SA-grade) to inhibit grain growth, resulting in high strength and high temperature stability. In addition, the ZMI-grade fibre has improved oxidation-resistance at high temperature. ATK COI Ceramics, formerly Dow Corning, manufacture a titanium- and boron-containing SiC fibre ('Sylramic') that has excellent strength and stiffness at both room temperature and elevated temperatures (1400°C). The fibre has a high density, high degree of crystallinity, fine grain size and very low oxygen content [17], [18]. Whilst fine grains are advantageous for tensile strength, they are detrimental to creep resistance. An alternative method that limits the oxide phase involves curing of the green fibre under electron irradiation. The Hi-Nicalon and Hi-Nicalon Type S fibres (Nippon Carbon Co.) are produced using this method and show significantly reduced oxygen content and consequently increased density, elastic modulus, thermal expansion and thermal conductivity compared with the original Nicalon fibre. The temperature capability of these fibres can be improved from 1200°C for Nicalon to 1600°C for the Hi-Nicalon and Hi-Nicalon Type S fibres [19]. As can be expected, an improvement in performance by the removal of oxygen using electron irradiation increases production costs

significantly. The Hi-Nicalon and Hi-Nicalon Type S production costs are 4-6 times greater than those of the Nicalon fibre [16].

2.1.1.2. Oxide fibres

Commercially available oxide reinforcements are typically alumina-based continuous, polycrystalline fibres produced by the sol-gel process. Whilst this method is more expensive than traditional melt-blow techniques, fibres with higher alumina content can be produced and greater microstructural control is possible. High alumina content provides improved chemical stability, an elevated melting point and superior strength up to 1200°C. The sol-gel process involves spinning chemically-derived precursors followed by pyrolysis and ceramisation. Precursors of commercially available fibres include aluminium chlorohydrate (Almax™ fibres), aluminium acetate (Nextel™ series of fibres) and aluminoxane polymers (Sumitomo Altex). The sol is pumped through a multiple orifice spinneret to form 400-1000 filaments simultaneously under controlled temperature, humidity and air flow. Varying the pump rate relative to the speed of the draw wheels enables control of fibre diameter. After spinning, the green fibres are heat treated, or pyrolysed, forming ceramic fibres. Gentle decomposition of the green fibre limits defects and flaws, which reduce fibre strength. To achieve high fibre strength at room temperature, a small grain size (<0.5μm) is desired. A low firing temperature will give a smaller grain size but generally leads to an unacceptable level of residual porosity caused by grain boundary migration. Porosity can be eliminated with higher processing temperatures but leads to excessive grain growth. To overcome this dilemma, it is common to introduce a second phase that prevents grain growth at high sintering temperatures whilst simultaneously eliminating porosity [12], [14], [20].

The first pure (99.9%) α-alumina continuous fibre was developed by Du Pont in the late 1970s. α-alumina is the most thermally stable and crystalline form of alumina. The FP fibre had a polycrystalline microstructure with a grain size of 0.5μm and good room temperature strength. However, the fibre exhibited a rapid degradation of mechanical properties above 1000°C owing to its fine microstructure, which led to grain sliding and high creep strain rates. In addition, its large diameter (18μm) and lack of ductility rendered it unsuitable for weaving and thus the fibre was not produced commercially [21], [22]. Du Pont developed a second polycrystalline continuous fibre, PRD-166, which consisted of 80wt% α-alumina with 20wt% yttria-stabilised zirconia particles. The presence of zirconia improved room temperature strength by phase transformation toughening and inhibited grain growth at high temperature. Nevertheless, these improvements were not sufficient to allow commercial development [23].

Nextel™ 610 (3M) and Almax™ (Mitsui Mining) fibres, developed in the early 1990s, are both 99% α-alumina with a diameter of 10μm. This reduction in diameter compared with FP and PRD-166 fibres has the immediate advantage of increasing the flexibility of the fibres, allowing weaving and thus the production of more complex shapes [22]. The Almax fibre has a grain size of 0.5μm; however, the fibre exhibits a large amount of intergranular porosity (8%) caused by a lack of control over grain growth during manufacturing. Consequently, mechanical properties are severely degraded above 1000°C. The Nextel 610 fibre has high strength and thermochemical stability, and maintains excellent high temperature strength and creep resistance below 1000°C [24]. A fine grained (0.1μm) α-Al_2O_3 fibre is obtained by seeding α-Al_2O_3 with a very fine hydrous colloidal iron oxide (Fe_2O_3), which acts to improve the nucleation rate of α-Al_2O_3. In addition, Nextel 610 contains 0.35% SiO_2 which acts to retard grain growth above 1000°C during manufacture. It is believed that silica does not form

a second phase at grain boundaries [22]. Nextel 610 fibres suffer from poor creep performance above 1000°C as a result of their small grain size [12].

Pure α-alumina fibres have superior chemical and thermal stability compared with silica-containing fibres and are therefore less reactive with potential oxide matrices during manufacture and are more stable in corrosive service environments. Nevertheless, difficulties remain in controlling porosity and grain growth during processing of pure α-alumina fibres, and fibres generally have a higher density and higher elastic modulus which lowers strain-to-failure and increases brittleness [14]. The introduction of silica allows the transformation to α-alumina to be limited since it reacts with alumina to form mullite ($3Al_2O_3$:$2SiO_2$). The presence of mullite at grain boundaries controls the grain growth of residual α-alumina. Silica-containing fibres are generally produced at lower cost than pure α-alumina fibres, and are stable up to 1200°C. The Altex fibre, produced by Sumitomo Chemicals Co., comprises 85% alumina and 15% silica to produce nano-scale γ-alumina grains intimately dispersed in amorphous silica. Silica inhibits the transformation to α-alumina below 1127°C in both oxidising and inert atmospheres [25]. The presence of silica in the Altex fibre does not reduce fibre strength at lower temperatures compared with pure alumina fibres; however lower activation energy is required for the creep of the fibre [22]. Nextel 720 fibres (3M) are also composed of 85% α-Al_2O_3 and 15% SiO_2 by weight. In contrast to the Altex fibre, heat treatment forms a two-phase mixture of α-Al_2O_3 and mullite with approximately 4% porosity. The fibres contain 0.3% Fe_2O_3 as a nucleating agent for the formation of α-alumina, as described for Nextel 610 fibres. Nextel 720 fibres exhibit superior creep performance compared with other oxide fibres owing to the high content of mullite, a highly creep-resistant compound, and due to the unique crystalline structure which reduces deformation by grain boundary sliding at high temperature. In addition, the larger grain size of Nextel 720 fibres

reduces creep, since creep is inversely proportional to grain size in fine-grained oxides. The high content of mullite lowers density by 13% and thermal expansion by 30% compared to pure α-alumina fibres (Nextel 610). Nextel 720 fibres have a circular cross section and a diameter of 12µm, woven in an 8-harness satin weave with approximately 400 filaments in each tow. The fibres have a single filament tensile strength and modulus of 2100MPa and 260GPa, respectively. The Nextel 720 fibre displays an in-service temperature capability of 1200°C, currently the highest of any commercially available oxide fibre. In addition, the fibres retain 90% room temperature multi-filament tensile strength at 1300°C (Figure 2.4) [24], [26], [27].

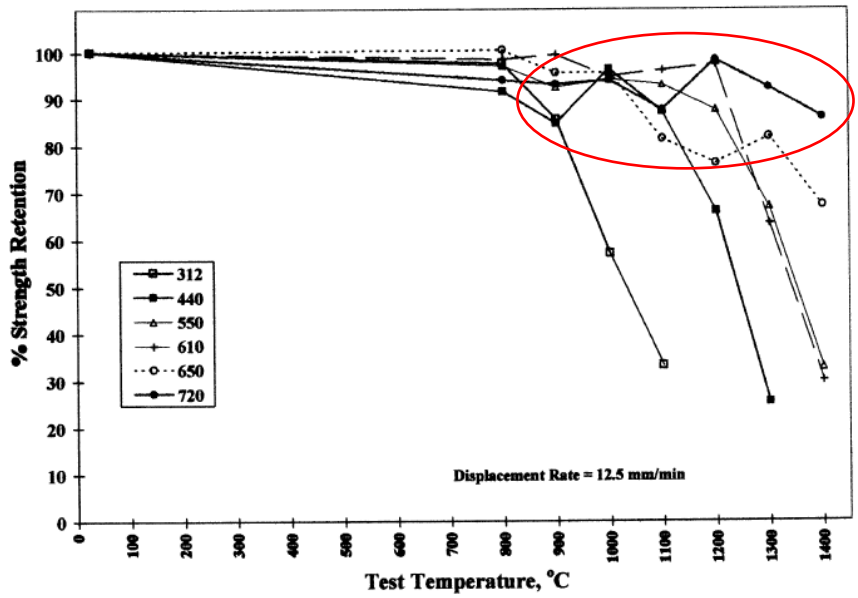

Figure 2.4. Tensile strength retention of multi-filament strands of Nextel fibres at elevated temperature [24].

The Nextel 650 fibre was developed for high temperature applications where the presence of mullite and other silicon-containing phases is not desirable. The fibre comprises 89% α-alumina, 10% cubic zirconia and 1% yttria (Y_2O_3) and is produced in continuous form with a diameter of 11.2µm. Zirconia with a grain size of 5-30nm is present on both grain boundaries and within alumina grains and limits α-alumina grain growth at high temperature. Nextel 650

fibres have an alumina grain size of 0.1μm, yet display 100 times lower creep than Nextel 610 fibres due to the presence of yttria. The single-filament tensile strength of Nextel 650 fibres is reported to be 2.75GPa, with only 73% strength retained at 800°C and just 30% strength retained at 1200°C (Figure 2.4). As such, the fibre has a maximum use temperature of 1080°C [24], [28].

The Saphikon fibre (Saint-Gobain Saphikon), a single crystal α-alumina fibre, was developed to allow higher temperature capability and better creep resistance than polycrystalline alumina fibres such as Nextel 610 or 720. Saphikon fibres are produced by the 'edge-defined film-fed growth' method whereby a single crystal is grown from a molten film of alumina. During growth, the melt wicks into a molybdenum die and the fibre growth, initiated by a seed crystal, occurs at the top of the die. The shape of the crystal is defined by the external shape of the die. Continuous growth lengths of more than 300m have been demonstrated. Whilst the Saphikon fibre displays thermochemical stability at 1400°C, its large diameter (125μm) prevents weaving and the production method is very expensive [8], [29], [30].

2.1.2. Ceramic matrices

The role of a matrix in fibre-reinforced CMCs is to bind the fibres together to form a structural unit, protect the fibres from environmental attack and mechanical abrasion, and to transfer and distribute applied stress to the fibres. Whilst the matrix contributes little to the tensile, load-bearing capacity of the CMC, it has a significant influence on the interlaminar shear and in-plane shear properties. In addition, the matrix influences to some extent the compressive strength of the composite, providing lateral support to resist fibre buckling. It is essential that the matrix forms a mechanical, chemical or frictional bond with the reinforcing fibres, without causing physical damage. The matrix must also be chemically stable and

chemically compatible with the reinforcing fibres, preventing undesirable reactions from taking place at the interface during fabrication or service. The temperature capability of the matrix material must also be considered, although high temperature applications are often limited by the reinforcing fibres. CMCs capable of withstanding temperatures in excess of 1000°C require the use of oxide, carbide or nitride matrices [31], [32], [33], [34]. Furthermore, it is desirable to reduce the coefficient of thermal expansion (CTE) mismatch, reducing thermal stresses. If the matrix CTE is greater than that of the fibre, a radial compression will result on cooling from elevated temperatures, causing the matrix to grip the fibre. Radial gripping increases the strength of the interface, preventing fibre debonding and pull-out, promoting brittle behaviour [35]. Matrices containing silicon carbide are regularly utilised in composites reinforced with non-oxide (silicon carbide or carbon) fibres, whilst alumina, alumina-silicate and mullite matrices are more commonly employed in oxide-fibre reinforced composites [36], [37].

The use of silicon carbide (SiC) as a matrix material is based on its low density, excellent high temperature strength and creep resistance, good oxidation and corrosion resistance at temperatures ≤1500°C and low CTE. Furthermore SiC can be easily deposited in a fibre preform by a number of processing techniques and is chemically compatible with commercially available SiC fibres [34], [38], [39]. Oxidation embrittlement of carbon or SiC fibres reinforced with SiC at intermediate temperatures (700-800°C) has been well documented. Matrix microcracking occurs at relatively low stress (100-200MPa), facilitating the in-depth diffusion of oxygen towards the oxidation-prone interfaces and/or fibres. A number of approaches have been investigated to impede oxygen diffusion and increase the durability of these composites in corrosive environments. The addition of boron to the matrix

results in the formation of B_2O_3 in the crack opening, acting to seal the crack and inhibit oxidation of the interface [40].

Alumina, silica and mullite matrices are predominantly used in oxide CMCs for their low density, high temperature capability and chemical stability with commercially available oxide fibres [36]. In addition, oxide matrices such as these can be fabricated at lower temperatures compared with SiC matrices, reducing manufacturing costs. Alumina (Al_2O_3) has good mechanical strength and stiffness, high hardness and wear resistance, good thermal conductivity and a low CTE [34]. Alumina has a melting point in excess of 2000°C and is stable in both oxidising and reducing environments. Whilst alumina can be used at temperatures up to ~1900°C, creep can occur at temperatures above 1200°C [41]. Silica-based matrices have excellent oxidation resistance and can be easily fabricated. Nevertheless, these matrices suffer from a significant loss in properties above 950°C and form a volatile oxide, SiO_2, in reducing conditions [41]. Mullite is a solid solution of alumina and silica, approximately $3Al_2O_3{\cdot}2SiO_2$. It has excellent strength and creep resistance in addition to a low CTE and relatively low elastic modulus [34], [41]. Owing to the sluggish sintering kinetics of mullite, temperatures in excess of 1300°C are required for the formation of bonds between particles. This presents a processing challenge since most commercially available oxide fibres degrade above 1200°C. It is common to combine large mullite particles, which are resistant to sintering, with smaller alumina particles which sinter more readily and form a continuous bonded network [42].

2.1.3. CMC interface design

The fibre/matrix interface plays a significant role in determining the ultimate performance of a CMC. The direct introduction of a ceramic fibre into a ceramic matrix results in a strong

chemical bond between the two components, allowing matrix cracks to penetrate directly into the fibres resulting in catastrophic failure. Thus the primary role of an interface is to provide a weak bond between fibre and matrix, allowing crack deflection through fibre debonding and pull-out. The predominant approach in developing a weak bond at the fibre/matrix interface is to form a thin coating (0.1-0.5μm) on the fibres which acts as a debond layer and as a low-friction sliding interface. Fibre coatings protect the fibres from environmental attack during both fabrication and use; however they introduce high production complexity and cost. Interface coatings on non-oxide reinforcements have reached a high level of maturity and are typically carbon or boron nitride [14], [35], [43], [40], [44].

The fugitive coating concept, a less commonly employed approach, relies on the retention of a coating (typically carbon) during processing which is subsequently removed through oxidation to form a narrow gap. Difficulties remain in controlling the width of the interface gap, and as such, mechanical interlocking and intermittent fibre/matrix bonding often prevents damage tolerant behaviour.

Similar damage tolerant behaviour can be achieved by means of a finely distributed porosity within the matrix. Research in this area has focused on oxide materials such as alumina and mullite. These composite systems offer low cost and straightforward processing methods; however it is essential that the fibres and matrix are chemically compatible owing to their intimate contact in the absence of a fibre coating.

2.1.3.1. Fibre coatings

Material selection for interfacial fibre coatings in CMCs is limited by a number of factors. Firstly, the coating material must be mechanically weak to allow fibre debonding and sliding

upon loading, whilst also providing high temperature chemical compatibility and stability in oxidising environments [45]. It is essential that fibre coatings have a uniform thickness, composition and morphology in order to prevent mechanical interlocking during fibre pull-out. Furthermore, the CTE of the coating material should be equivalent to that of the reinforcement to reduce internal residual stresses. In addition to promoting damage tolerant behaviour, interface coatings serve to protect the reinforcing fibres from chemical attack and high temperature degradation during both composite fabrication and service, and must therefore be crack and pore free [14]. The formation of a thin fibre coating poses a particular challenge for multifilament tows and 2D/3D weaves, where the fibres are in direct contact with one another.

Fibre coatings can be formed at the fibre/matrix interface as the result of *in situ* reactions during composite fabrication, whereby chemical species react at the fibre surface to form a weak layer (often carbon). This approach was used extensively during early development of glass-ceramic matrix composites; however these composites were limited by their oxidative stability at high temperature [46]. An alternative approach involves the deposition of a fibre coating prior to composite fabrication by either chemical vapour deposition (CVD) or liquid precursor coatings [14], [47]. This method allows superior control of coating thickness, composition and morphology and is independent of composite processing conditions. During CVD, a gaseous precursor reacts locally at the fibre surface, decomposing to form a ceramic coating. The microstructure and properties of the resultant coating depend significantly on the deposition conditions [40]. Coating thicknesses can range from nanometers to several micrometres, depending on deposition rates and times. Whilst a wide range of compositions can be formed by CVD including carbides, nitrides and oxides, non-oxide coatings of pyrolytic carbon (PyC) and hexagonal boron nitride (hex-BN) are most commonly employed

since the high temperatures involved in CVD generally limit the process to non-oxide reinforcements. The well-known oxidation embrittlement problem with non-oxide composites in the intermediate temperature range has led to the development of alternative deposition methods which allow oxide reinforcements to be coated.

Liquid precursor coating techniques, such as the sol-gel approach, require much lower temperatures for ceramic conversion than CVD and as such can be used to coat oxide fibres such as Nextel 720. Liquid precursor techniques involve coating the fibres with an aqueous liquid which is subsequently heat-treated to form the desired ceramic coating. Multiple coating/conversion steps are often required with this process since high shrinkage occurs during drying and conversion. Liquid precursor techniques can be used to form single and mixed oxides of silicon, aluminium, zirconium and titanium, in addition to rare-earth phosphates such as monazite.

$LaPO_4$ (monazite) has been identified as an effective interface material for its stability at high temperature in both reducing and oxidising environments. Monazite has been shown to form a low toughness interface with oxide fibres such as Nextel 610 and 720, and exhibits an unusually low hardness (5GPa), deforming relatively easily at room temperature [48], [49]. Monazite has a melting temperature of 2072°C, is stable in air and water-containing environments, and has good chemical compatibility with commonly used oxide composite materials such as alumina and mullite [29], [43], [50]. Monazite coatings can be formed by liquid precursor routes or *in situ,* although there are a number of fabrication challenges to overcome with both methods. Coating uniformity can be difficult to control, often resulting in fibre bridging and incomplete fibre coverage, subsequently affecting the performance of the material. The use of different monazite precursors have been shown to produce large

differences in the strength of the composite, with many resulting in degradation of fibre strength due to the formation of by-products. Fibre degradation can also occur with long term exposure to high temperatures during coating fabrication [51]. Nevertheless, successful coating of Nextel 610 and 720 fibres by the use of an aqueous colloidal rhabdophane precursor has been shown, producing thick coatings without strength degradation after heat treatment at 1200°C for 100 hours [52]. During *in situ* formation of a monazite coating, capillary forces draw the monazite precursor solution to the fibre surface, forming a uniform monazite coating. Eliminating the need for a separate fibre coating step greatly simplified composite processing. The composite exhibited good mechanical properties and damage tolerant behaviour was evident [53]. The mechanical behaviour of a Nextel 610/alumina composite with a monazite coating formed via a liquid precursor route prior to composite fabrication was investigated by Ruggles-Wrenn et al. [54]. During monotonic tensile loading, at all temperatures investigated (900-1200°C), the addition of a monazite coating produced a significant improvement in ultimate tensile strength, however the presence of a monazite coating was detrimental to both elastic modulus and failure strain. The application of a monazite coating considerably improved the creep resistance at 900°C, with specimens exhibiting extensive fibre pull-out.

Porous zirconia has also been shown to be a suitable interface material for oxide CMCs [8], [43]. Zirconia, a thermochemically stable material, is mechanically strong and thus it is necessary to reduce the strength of the zirconia coating by introducing porosity (~30%). Holmquist et al. suggested that individual zirconia grains form at the interface, acting as ball-bearings between the fibre and matrix to allow fibre debonding and pull-out [8]. Four-point bend testing of a Nextel 610/alumina composite with a zirconia coating produced via a

precursor method prior to composite fabrication indicated a significant improvement in flexural strength and better retained strength at high temperatures (800-1000°C) [43].

2.1.3.2. Fugitive interfaces

The fugitive interface concept requires the retention of a coating during composite fabrication followed by its removal through oxidation, creating a void at the fibre/matrix interface. In contrast to the fibre coating approach, the interface is debonded prior to loading rather than relying on the stress intensity at the crack front to initiate fibre debonding. Carbon coatings have received the most attention in this area since carbon can be deposited with ease onto fibre tows or woven fabrics by either CVD or liquid precursor techniques (sol-gel) and is readily oxidised at moderate temperatures. Composite densification must be performed in an inert (non-oxidising) environment. The fugitive coating prevents possible fibre/matrix interaction during processing and defines the width of the interfacial gap after oxidation.

The optimal width of the interfacial gap is system-specific and is determined by factors including thermal expansion mismatch and fibre/matrix roughness. If the interfacial gap is too wide, little interaction can occur between fibre and matrix. Conversely, if the gap is too narrow, matrix damage will penetrate directly into the fibres causing catastrophic failure. In principle, oxidation of the coating forms a smooth, straight void, allowing fibre pull-out without constraint (Figure 2.5a). In reality, however, mechanical interlocking caused by intermittent fibre/matrix bonding and fibre/matrix surface roughness limits fibre sliding (Figure 2.5b). Once the coating has been oxidised, fibres are exposed and thus it is vital that the reinforcement and matrix materials are chemically compatible. In addition, non-oxide reinforcements are generally limited by their susceptibility to oxidation at elevated temperatures in the absence of a protective coating [6], [14], [40].

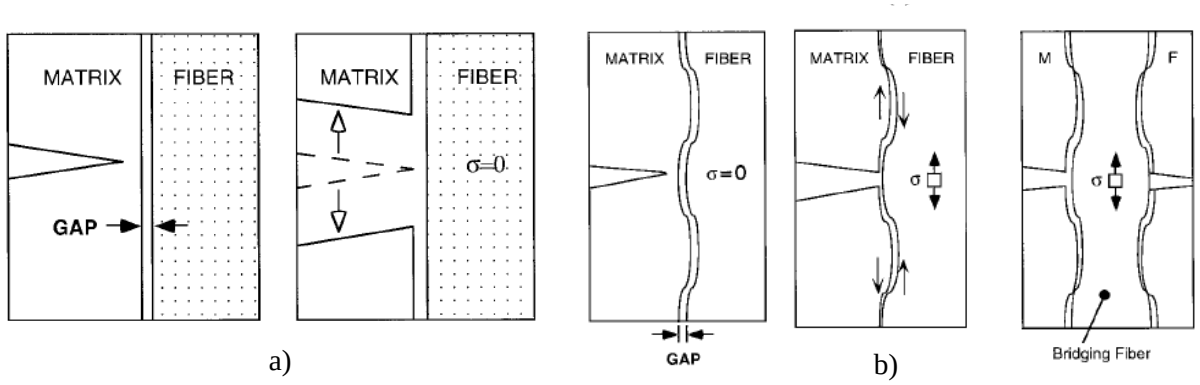

Figure 2.5. a) A straight interfacial gap allows fibres to pull-out without constraint b) Fibre/matrix roughness results in mechanical interlocking, limiting fibre pull-out [6].

The fugitive interface concept in oxide CMCs has received surprisingly little attention, despite encouraging results from early work in this area. When carbon-coated Nextel 720 fibres were embedded in a dense calcium aluminosilicate (CAS) matrix and the carbon subsequently oxidised, significant enhancements in fibre pull-out were obtained compared with non-coated fibres. Composites retained ~80% of their as-processed strength after long-term heat treatment in air at 1000°C for 500 hours. Carbon coatings of both 20 and 40nm were deposited using CVD, with the thicker coating producing better results in unidirectional samples while the thinner coating was more advantageous in ±45° samples. Coating thickness was limited by fibre bridging. Attempts to produce a coating thickness of 100nm resulted in extensive cementing of the fibres within tows [6].

The presence of a fugitive interface has also been demonstrated in porous matrix CMCs. Keller et al. demonstrated that carbon-coated Nextel 720 fibres within an 80% mullite/20% alumina porous matrix exhibited improved fibre pull-out as well as higher notched strength. These improvements were attributed to the combined effects of matrix porosity and the interfacial gap [6]. Conversely, Saruhan et al. demonstrated that the interfacial gap of a carbon-coated Nextel 720/aluminosilicate composite reduced from 200nm to 80nm after 2

hours at 1200°C, and heat treatment at 1300°C for 1000 hours led to almost total closure of the interface gap, resulting in a decrease in damage tolerant behaviour [55].

2.1.3.3. Porous matrices

Porous matrix CMCs have been developed since the mid-1990s and are generally limited to oxide systems containing alumina, aluminosilicate and mullite matrices. The porosity level required to enable damage tolerant behaviour is typically 30-40% and is achieved by means of a fine, uniformly distributed porosity within a contiguous particle network. It is vital to the damage tolerance of the material that the matrix maintains a stable pore structure during long-term service at elevated temperatures. The fibre and matrix materials must be chemically compatible at elevated temperatures owing to their intimate contact. Furthermore, in the absence of a fibre coating the fibres are susceptible to environmental attack, thus limiting this concept to oxidation immune reinforcements such as alumina-based fibres. Porous matrix CMCs offer significant benefits in their ease and low cost of manufacture as a result of not requiring fibre coatings or elaborate matrix densification techniques [14], [36], [56]. Processing techniques for porous matrix CMCs include polymer impregnation and pyrolysis (PIP), slurry infiltration and hot pressing, and the sol-gel process. These processing routes will be discussed in further detail in section 2.2.

The optimum matrix strength often involves a compromise in properties: the matrix must be weak enough to allow crack deflection and prevent damage from extending into the fibres whilst maintaining sufficient off-axis, interlaminar and compressive strength [44]. Furthermore, the particle size of the matrix has a significant influence on the properties of the CMC. Fine, submicron particles enhance the strength of the matrix by improving packing density and uniformity within the fibre preform. Nevertheless, fine particles reduce the

stability of the matrix during densification, often forming undesirable flaws such as shrinkage cracks [42].

In contrast to conventional CMCs with a dense matrix and weak fibre coating, fracture in a porous matrix CMC must be reinitiated in the solid phase for the crack to extend, meaning that a continuous crack front does not exist (Figure 2.6b). Fibre fracture, therefore, does not occur by the propagation of a crack within the matrix but must initiate within the fibre itself (from surface flaws or flaws within the fibre) [5]. The mechanical properties of porous matrix CMCs will be discussed in further detail in section 2.3.

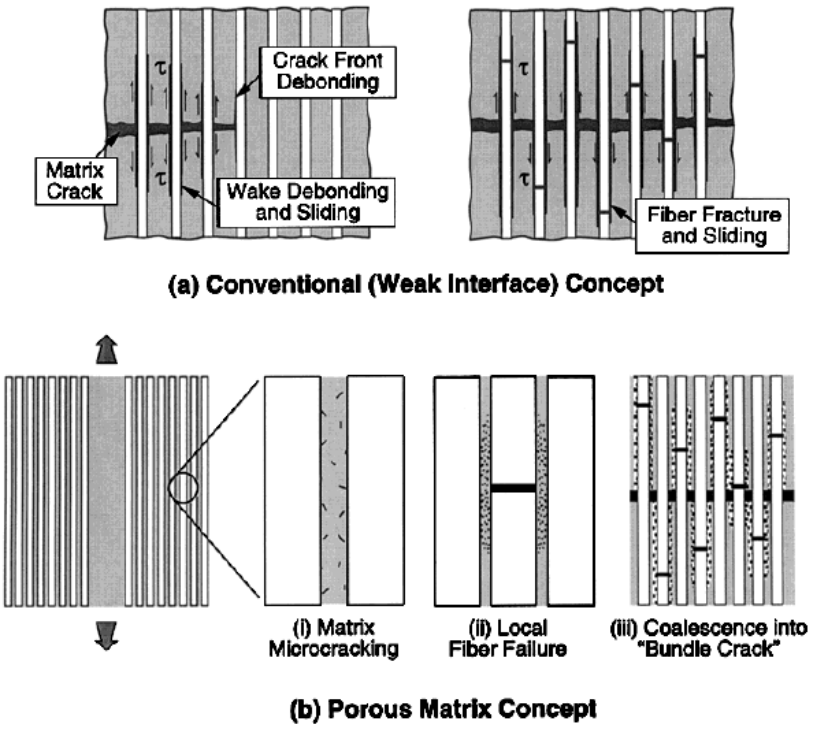

Figure 2.6. Schematics of the damage processes that allow damage tolerance in a) conventional dense-matrix weak-interface CMCs and b) porous matrix CMCs without fibre coatings [36].

2.2. Conventional processing of CMCs

The processing of a CMC should be considered as an integral part of the whole process of designing a CMC component. For example, any damage to the reinforcement because of processing will result in less than desirable performance in the final product. Characteristics such as melting point and chemical compatibility of both the reinforcing and matrix material also have an important bearing on the processing route chosen as well as the final properties and performance of the resultant composite. There are a number of processing methods commonly used for the manufacture of CMCs including chemical vapour infiltration, polymer impregnation and pyrolysis, reactive melt infiltration, slurry infiltration and hot pressing and the sol-gel process. It is not uncommon to combine two or more processing methods to optimise the densification and/or microstructure of the composite system [38]. Chemical vapour infiltration is generally used to deposit interphases, regardless of the technique employed for the infiltration of the matrix, since it yields deposits of uniform composition, structure and thickness.

2.2.1. Chemical vapour infiltration

Chemical vapour infiltration (CVI) is a processing technique whereby a solid (e.g. a ceramic material) is deposited within the pore network of a heated substrate from a chemical reaction taking place between gaseous species which flow (either by diffusion or convection) into the pores. In theory, CVI can be applied to any porous substrate as long as the pores are interconnected and large enough in diameter (microns), and the substrate is both thermally and chemically stable under the CVI conditions [57]. Whilst it has been suggested that CVI originated in efforts to densify porous graphite bodies by infiltration with carbon [58], Professor Roger Naslain of the University of Bordeaux designed and experimentally validated the CVI process for carbon fibre reinforced SiC composites for aerospace applications [59],

[47], [60]. The CVI process has subsequently been used to produce both oxide and non-oxide CMCs of various compositions. Examples of gas precursors and infiltration conditions are outlined in Table 2.2.

Table 2.2. Examples of gas precursors and infiltration conditions used for the preparation of various CMCs according to the isothermal/isobaric CVI process [61].

Matrix	Precursor	Temperature (°C)	Pressure (kPa)
SiC	CH_3SiCl_3(MTS)–H_2	900–1100	10–100
B_4C	BCl_3–CH_4–H_2	900–1000	1–5
TiC	$TiCl_4$–CH_4–H_2	950	1–5
BN	BF_3–NH_3	900–1100	1–5
Al_2O_3	$AlCl_3$–CO_2–H_2	950–1000	2–3
ZrO_2	$ZrCl_4$–CO_2–H_2	900–940	1–5
Si_3N_4	$SiCl_4$–NH_3	900–1000	

The CVI process typically consists of fabrication of the porous fibre preform followed by the application of a thin (0.1-1μm) debonding interphase deposited on the fibre surface. The preform is then infiltrated with a gaseous precursor, which decomposes and forms a ceramic deposit on the fibre surface. The process continues until the open porosity on the preform surface is closed and typically requires multiple cycles of infiltration. An additional layer protecting the composite surface from oxidation may be applied.

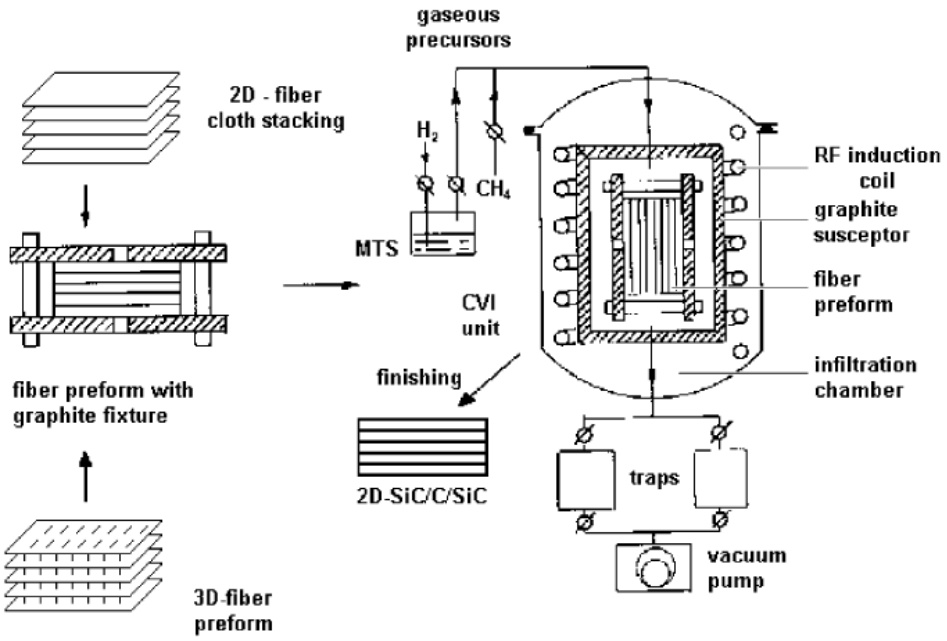

Figure 2.7. Schematic of isothermal/isobaric CVI process for the fabrication of C/SiC or SiC/SiC composites from a fibre preform and gaseous precursors [38].

It is generally accepted that there are five conditions under which the preform is infiltrated; isothermal/isobaric, thermal gradient, isothermal/forced flow, thermal gradient/forced flow and pulsed flow [62]. Isothermal/isobaric CVI maintains the fibre preform at a uniform temperature and pressure, and is a very slow process due to its low diffusion rate. In addition, the surface pores tend to close first, restricting the gas flow to the interior of the preform and therefore necessitating multiple cycles of infiltration, surface machining and re-infiltration to obtain an adequate density [61], [63]. A schematic of isothermal/isobaric CVI is illustrated in Figure 2.7. In thermal gradient CVI, a temperature gradient is achieved by heating the top region and cooling the bottom region of the precursor chamber, therefore enhancing gas diffusion [64], [65]. The precursor decomposes mostly in the hot inner regions since the rate of the chemical reaction is greater at higher temperatures. Thermal gradient CVI allows better densification of the ceramic matrix compared with isothermal/isobaric CVI due to prevention of early closing of the surface pores. Isothermal/forced flow CVI utilizes a pressure gradient

to enhance infiltration into a uniformly heated preform [66]. A pressure gradient is determined by the difference in pressure between the entering and exhausting gases. Forced flow/thermal gradient CVI combines the effects of both temperature gradients and forced flow enhancing the infiltration of the vapour precursor, reducing densification time to as little as 3 hours [57], [67]. In pressure-pulse CVI the precursor gas pressure changes rapidly by cyclic filling and evacuation of the reactant gas in order to enhance diffusion [68]. Pressure-pulsed CVI also has the ability to yield highly engineered interphases or matrices through the sequential use of several precursors [38].

CVI can occur at temperatures usually well below the melting point of the deposit, therefore subjecting the fibres to very little thermal stress. Additionally, the process imparts little mechanical stress to the preform compared with more traditional techniques such as hot pressing. CMCs produced by CVI possess good mechanical properties, good thermal shock resistance, and increased creep and oxidation resistance. Matrices of high purity can be fabricated and large, complex shapes can be produced in a near net shape [57], [11].

One of the major limitations of the CVI process is the high capital and production costs incurred. CVI is a very slow process due to its low diffusion rate and it can take several weeks to produce a CMC, resulting in high production costs. Thus, it is desirable to maximise the rate of matrix deposition to reduce time and cost, yet increasing the rate of deposition usually results in an inhomogeneous structure with almost complete densification near the external surfaces and much lower densities in the interior regions. Deposition rates increase exponentially with temperature and whilst relatively low temperatures produce a more uniform structure, the deposition rate is simply uneconomical. Similarly, low pressure decreases the diffusive flux to the deposition surface, slowing deposition rate. Nevertheless,

high pressure may impart residual internal stresses [57], [58]. The residual porosity of a CMC fabricated by CVI is typically 10-15%, resulting in relatively low thermal conductivity and a poor hermeticity with respect to gas and liquid fluids [38].

2.2.2. Polymer impregnation and pyrolysis

Polymer impregnation and pyrolysis (PIP) is widely used to consolidate CMCs since it produces a relatively dense composite at lower temperatures than alternative methods. The PIP process involves impregnating a fibre reinforcement with a polymeric precursor followed by curing at ~150-250°C. The polymer precursor is then pyrolysed at 800-1200°C, converting the polymer to a ceramic. This is typically performed in either a low temperature press or an autoclave for densification. Weight loss during pyrolysis, coupled with shrinkage in converting the precursor to ceramic material results in 20-30% porosity and thus re-impregnation and pyrolysis is usually necessary. Typically 6-10 cycles are performed until the desired density is achieved [14], [69]. A schematic of the PIP process is illustrated in Figure 2.8.

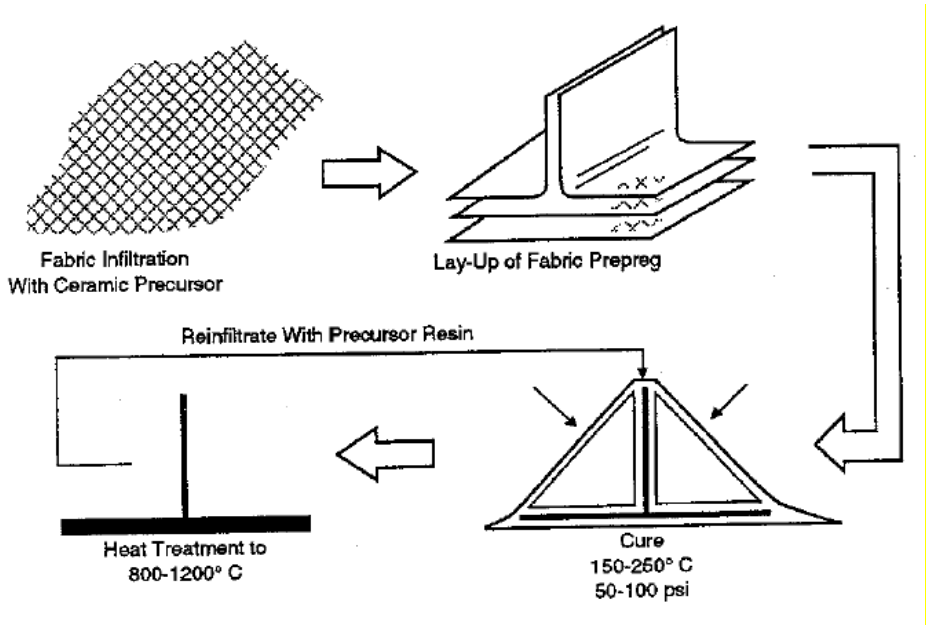

Figure 2.8. Processing of polymer derived ceramics [14].

The PIP process utilises simple processing equipment at low temperatures, resulting in low production costs compared with alternative methods [70],[71]. Low-temperature processing also prevents degradation of the fibres and inhibits sintering at the interfaces between the fibres and the matrix, a characteristic desirable for promoting damage tolerance. PIP allows control of the microstructure, nanostructure and chemical composition, and the process yields a high purity ceramic structure [72]. The PIP method is able to produce large and complex shapes by use of consolidation in an autoclave [69]. The PIP process is very similar to the process employed for polymer composites and thus any process that has been used for polymer shape making can be utilised. Nevertheless, sufficient densification in bulk component production via the PIP method is very difficult due to significant volume shrinkage and gas evolution of the precursor during pyrolysis. A reduction in porosity and an improvement in mechanical properties can be improved by filler loading of the polymer with ceramic particles [72]. However, loading the precursor with a powder considerably increases its viscosity, hindering flow into the fibre preform [38].

2.2.3. Reactive melt infiltration

Reactive melt infiltration (RMI) is a fast and relatively cost effective method of producing ceramic composites. RMI is used predominantly for the fabrication of silicon carbide (SiC) matrix composites. This process, known as Liquid Silicon Infiltration (LSI), involves infiltration of a carbon containing preform with molten silicon. When oxides are formed, such as when liquid aluminium is infiltrated into a preform in an oxidising atmosphere, the process is termed Directed Metal Oxidation (DIMOX). RMI has shorter processing than alternative methods, and has the ability to produce near-net, complex shapes. In addition, infiltration takes place by capillary action and no external pressure is applied to the system, causing little damage to the fibre reinforcement [73], [74].

2.2.3.1. Liquid silicon infiltration

Liquid Silicon infiltration (LSI), or silicon melt infiltration, was first developed by General Electric Company and DLR (German Aerospace Research Establishment) [75]. In LSI, a ceramic matrix forms as a result of a chemical interaction between liquid metal infiltrated into a porous reinforcing preform and the substance surrounding the melt. The reinforcing fibres are first consolidated with a carbon deposit either by CVI or PIP and cut and stacked to produce a preform. Following this, the preform is infiltrated with molten silicon or a silicon-refractory metal alloy (Figure 2.9). The liquid silicon wets the surface of the preform and the melt soaks into the porous structure, reacting with the carbon deposit to form silicon carbide. Silicon carbide fills the preform pores and forms the ceramic matrix. Commonly, at least 5% of residual free silicon remains in the carbide matrix. The final products in silicon-refractory metal alloy infiltration are silicon carbide, refractory disilicide and residual silicon. The physical properties of the preform such as pore size, pore volume and deposited carbon particle size determine the composition and microstructure of the reaction-formed silicon carbide ceramic. The rate of infiltration is dependent on wetting behaviour, reaction kinetics and mechanism, and infiltration temperature [73], [74], [76].

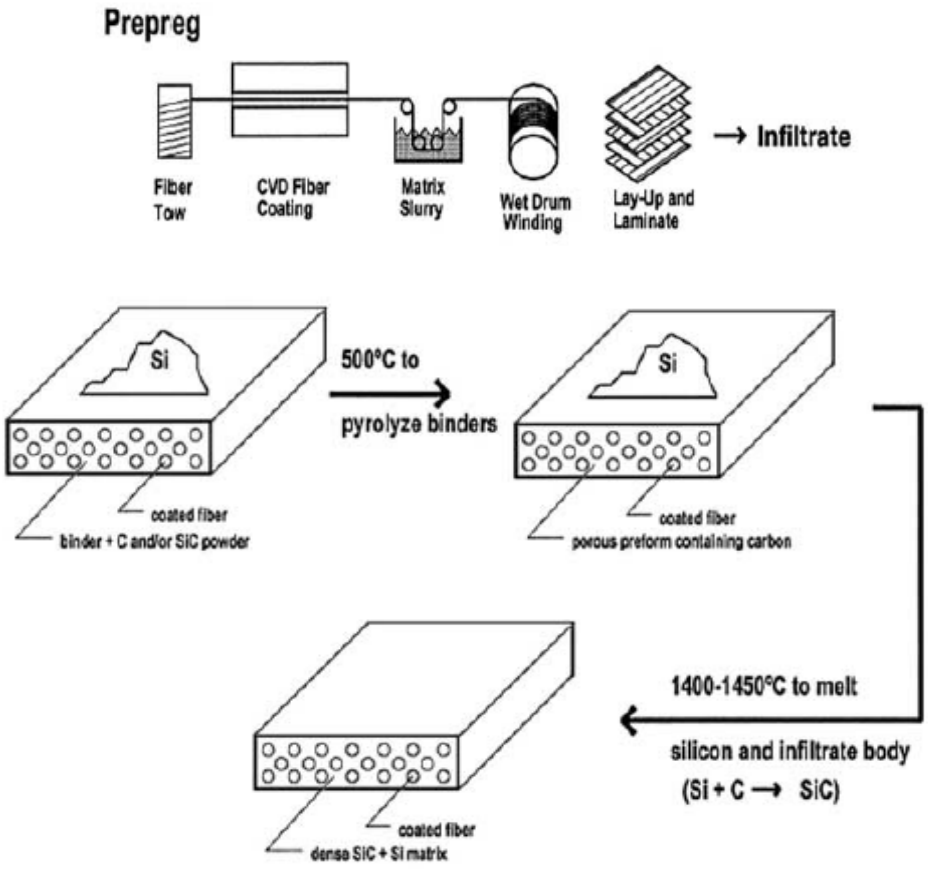

Figure 2.9. Fabrication of a SiC-matrix composite by the liquid silicon infiltration process [38].

LSI has many advantages over alternative methods including its simplicity and short processing time. It does not require multiple cycles of infiltration, and yields composites with almost no residual open porosity. Composites produced by LSI have a high thermal and electrical conductivity and complex, near-net shapes may be fabricated [38]. However, infiltration occurs at relatively high temperatures (1400-1600°C) and therefore only fibres with high thermal stability such as carbon or quasi-stochiometric SiC can be employed. Additionally, liquid silicon is a corrosive medium and can cause damage to both interphases and fibres. As with the CVI process, it is essential that pore entrances remain open until the composite is fully densified to avoid inhomogeneity. This is difficult due to the fast

densification process. Finally, at least 5% of residual free silicon remains in the carbide matrix which limits its refractoriness and creep resistance [38].

2.2.3.2. Directed metal oxidation

The Directed Metal Oxidation process (DIMOX), often referred to as the Lanxide process, was developed by Lanxide Corporation in the 1980s (now Honeywell Advanced Composites, Inc.) [77]. The DIMOX process forms a ceramic composite by the directed reaction of a molten metal with an oxidant. DIMOX is commonly used to fabricate aluminium oxide matrix composites but can also be used to fabricate a large number of composite matrices, as listed in Table 2.3. Reinforcing fibres are first coated with an interface material (typically carbon or boron nitride) to protect the fibres from the molten metal and to provide a weak interface, which is desirable to enhance toughness. The reinforcement and the parent metal alloy are heated to 900-1200°C (for aluminium oxide systems) allowing rapid oxidation of the parent metal alloy outward and into the fibre preform. The reaction is sustained by the wicking action of liquid metal along interconnected microscopic channels in the oxidation product to the reaction front promoting growth away from the original metal surface. The resulting composite is free of pores and impurities, however some unreacted metal (5-30% of the material volume) remains in the intergranular spaces of the ceramic matrix. The percentage of metal remaining in the composite depends upon the processing conditions and the starting materials [11], [14], [78], [79].

Table 2.3. Examples of DIMOX/Lanxide ceramic matrix systems (after [80]).

Parent Metal	**Reaction Product**
Aluminium	Oxide
	Nitride
	Boride
	Titanate
Silicon	Nitride
	Boride
	Carbide
Titanium	Nitride
	Boride
	Carbide
Zirconium	Nitride
	Boride
	Carbide
Hafnium	Boride
	Carbide
Tin	Oxide
Lanthanum	Boride

The DIMOX process offers several potential advantages over alternative fabrication methods. The process allows the production of large, complex, fully dense composite materials using inexpensive and simple equipment and reasonably short production times (one to three days). Growth of the matrix into the preform typically involves little or no change in dimension and thus problems associated with densification shrinkage in traditional ceramic processing can be avoided. Composites produced by the DIMOX method possess good mechanical properties at high temperature due to the absence of impurities. It is possible to design duplex interphases providing a weak bond between the matrix (reaction product) and the reinforcement, allowing fibre debonding and pull-out to promote toughness. Nevertheless, it is difficult to control the chemistry and produce an all-ceramic matrix by this process. A fully densified composite produced by this method will always contain some residual metal (typically 5-30% of the material volume) [78], [80].

2.2.4. Slurry infiltration and hot pressing

The slurry infiltration and hot pressing method of fabrication, adapted from monolithic ceramic forming, can be used to form ceramic, ceramic-glass and glass matrices such as alumina, silica, mullite, silicon carbide and silicon nitride. Firstly, the reinforcing fibres are passed through a bath containing ceramic powder particles dispersed within a liquid carrier (usually water or alcohol), known as a slurry. The slurry may also contain an organic binder and a wetting agent to improve infiltration. The infiltrated fibres are cut and stacked, dried to remove the organic binder (burnout), and hot pressed. Figure 2.10 shows a schematic of this process. Hot pressing involves high temperatures and pressures, which enhances the consolidation of ceramic particles, resulting in a low porosity composite. An alumina/silica system typically requires hot pressing at 1250-1300°C with 15MPa applied pressure [81]. Composites produced by this method generally possess good mechanical properties due to their low porosity and high density. However, the reinforcing fibres may be damaged by the high pressures applied, and they may also suffer damage caused by a reaction with the matrix at high temperatures. The equipment required for hot pressing is relatively expensive. In addition, components are limited to simple plate shapes and thus high cost machining is often required [82], [83], [84].

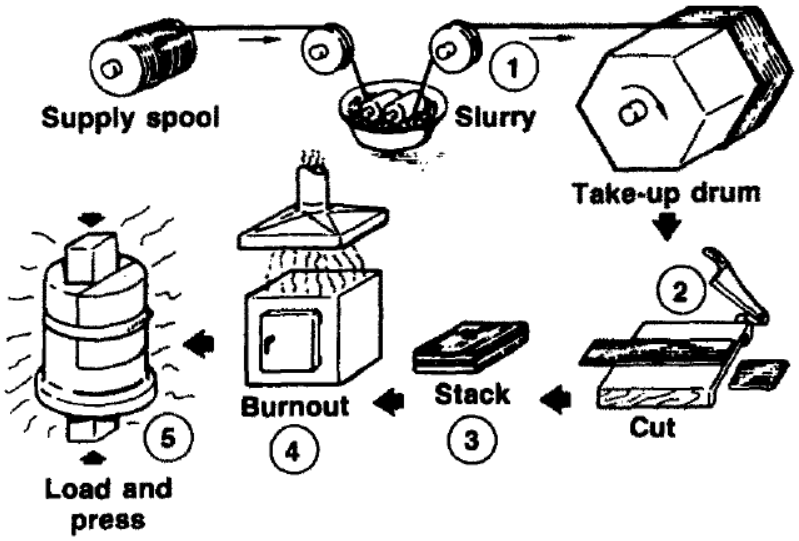

Figure 2.10. Schematic of the slurry infiltration and hot pressing process [84].

2.2.5. Sol-gel

The sol-gel process, discussed previously in section 2.1.1.2 as a processing method for oxide fibres, can also be used to produce glass, glass-ceramic or ceramic matrices. A colloidal suspension of fine ceramic particles (~1-1000nm) within a liquid, termed a sol, is converted to a gel at elevated temperatures by either hydrolysis or condensation [85]. The gel is then subjected to controlled heating to produce a ceramic or glass. The reinforcement material can be in the form of a porous preform, fibre tow, or woven fabric. Liquids sols such as those derived from alkoxides have a low viscosity, aiding infiltration into fibre preforms or fibre weaves. In contrast to the slurry infiltration method, the binder burnout stage is not required since the binder, or sol in this case, becomes part of the matrix during heating. Consequently, the sol-gel process offers excellent compositional homogeneity in single phase matrices, and also has the potential for producing unique multiphase matrices. The gel-to-ceramic conversion temperature is typically much lower than that required in traditional sintering processes and thus fibre damage by high processing temperatures can be eliminated. The equipment required to produce CMCs by this method are relatively inexpensive, and large, complex, near-net shapes can be fabricated, reducing machining costs. Traditional sols such

as those derived from alkoxides are very expensive however the use of polymeric precursors and commercially available colloidal salts can help to reduce raw material costs. Sol-gel composites traditionally demonstrate poor mechanical properties, necessitating research into control of matrix cracking during drying, matrix densification and fibre/matrix interface control. The ceramic yield achieved by the sol-gel process is low compared with slurry techniques, resulting in high shrinkage and large cracks within the matrix. Repeated impregnations are generally required to produce a suitably dense matrix. Furthermore, acidic gases evolved during pyrolysis can cause fibre damage [11], [14], [83], [86].

2.3. Processing and properties of Nextel 720/porous-matrix CMCs

Nextel 720 fibres have been identified by many as potential reinforcements for oxide CMCs owing to their high temperature capability in addition to good creep performance, as discussed in section 2.1.1.2. Porous oxide matrices are immune from oxidation embrittlement and offer low cost manufacturing routes. More specifically, alumina-based matrices offer chemical compatibility with Nextel 720 fibres, have high temperature capability, low density and good mechanical properties. The following section will describe the processing and properties of oxide CMCs composed of Nextel 720 fibres within a porous, alumina-based matrix previously highlighted in the literature.

2.3.1. University of California at Santa Barbara (UCSB)

The development of porous-matrix oxide composites has received significant attention at the University of California at Santa Barbara (UCSB). Two processing routes have been described. The first processing method uses pressure filtration to pack particles around fibres within a preform. The matrix is then strengthened by the cyclic infiltration and pyrolysis of a precursor. This relatively simple, low cost method is limited to the production of flat plates [9], [42], [87], [88], [89]. The second method, named VibroIntrusion, is capable of producing complex geometries such as T-joints and tubes. The powder is first consolidated to a very high volume fraction and then infiltrated into the fibre preform via vibration-assisted flow. Similarly to pressure infiltration, subsequent precursor impregnation/pyrolysis cycles are required to strengthen the matrix [5], [90], [91].

2.3.1.1. Pressure infiltration

The pressure infiltration approach to the fabrication of an all-oxide CMC is summarised in Figure 2.11. This process has been demonstrated using both Nextel 610 and 720 fibres. In this

process, the matrix is produced in two steps. Firstly, an aqueous slurry containing 30vol% solids comprising 80% ~1μm diameter MU-107 mullite (Showa Denko K.K.) and 20% ~0.2μm diameter AKP-50 alumina (Sumitomo Chemical) is infiltrated into a stack of fibre cloths. Studies of the effect of submicron particle size alumina additions on the sintering of mullite were used to select the matrix composition [42]. HNO_3 is used to adjust the pH to ~3, allowing repulsive interactions to develop between the oxide particles, providing the appropriate rheology to facilitate their flow into the fibre preform and promote packing. The fibres are cut, stacked and placed between two perforated stainless-steel plates within a chamber with evacuation capabilities. An amount of slurry calculated to fill the preform is then poured on top, and the chamber is evacuated from both top and bottom to drive the filtration process. After consolidation, the panels are dried over a period of ~48hours producing green panels with a packing density of ~60%. The green panels are given an initial sintering treatment at 900°C for 2 hours to promote the development of alumina bridges between the mullite particle network. The composites are then impregnated with an alumina precursor solution (aluminium hydroxychloride) under vacuum, dried in air, and pyrolysed at 900°C for 2 hours. Precursor impregnation and pyrolysis is repeated twice, as determined by Mattoni et al. [9], who investigated the effect of repeated impregnations on matrix porosity and composite properties. Porosity decreased slightly from 35% for 2 impregnations to 29% for 10 impregnations, yet flexural strength decreased significantly from ~210MPa for 2 impregnations to ~80MPa for 10 impregnations. The panels are given a final sintering treatment at 1200°C for 2 hours which serves to stabilize the precursor-derived alumina to the corundrum (α) structure and to enhance the integrity of the alumina bridges [88].

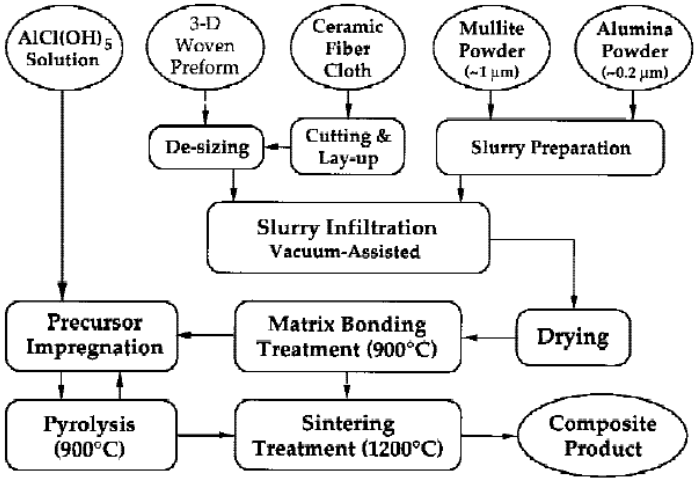

Figure 2.11. Pressure infiltration approach to the fabrication of an all-oxide CMC [42].

Levi et al. and Carelli et al. reported the tensile strength of composites composed of Nextel 720 fibres within an alumina-mullite matrix produced by the pressure infiltration method to be ~145MPa in the 0°/90° orientation with a modulus of ~60GPa. Tensile strength decreased to ~50MPa in the ±45° orientation [42], [88]. Mattoni et al. reported the flexural strength of such composites to be ~210MPa, whilst the interlaminar shear strength (established by short beam shear) was ~10MPa with two repeat precursor impregnations. Interlaminar shear stress increased to ~12MPa with four repeat impregnations, however this was detrimental to flexural strength [9].

The effect of thermal ageing following long-term exposure (1000h) at temperatures of 1000-1200°C in air were investigated by Carelli et al. [88]. The study revealed that tensile strength and failure strain in the 0°/90° orientation after ageing remained unchanged, whilst the modulus and tensile strength exhibited a two-fold increase after ageing at 1200°C in the ±45° orientation as a result of matrix strengthening. In addition, the failure mechanism changed from predominantly matrix damage accompanied by interply delamination to failure dominated by fibre fracture with minimal delamination.

Mattoni and Zok investigated the strength and notch sensitivity of composites with zero, two and four precursor impregnation and pyrolysis cycles. It was concluded that the unnotched tensile and shear strength (established using the Iosipescu shear test) can be increased by increasing the number of impregnations and subsequently strengthening the matrix, however these improvements were offset by an increase in notch sensitivity. Furthermore, it was observed that an improvement in tensile strength with increasing impregnations was accompanied by a reduction in fibre pull-out [89].

2.3.1.2. VibroIntrusion

The VibroIntrusion method was first introduced by Haslam et al. [5] and is summarised in Figure 2.12. Firstly, an aqueous slurry is prepared with 20vol% solids, containing 70% ~1μm diameter MU-107 mullite (Showa Denko K.K.) and 30% ~0.2μm diameter AKP-50 alumina (Sumitomo Chemical). The mullite to alumina ratio was selected to achieve a high packing density and low shrinkage during sintering. Tetramethylammonium hydroxide (TMA-OH) is used to maintain pH ~11, allowing electrostatic repulsive interactions to develop between oxide particles. 2wt% (relative to solids) PEG-silane is added to induce a steric dispersing effect by the adsorption of molecules due to a reaction with –OH surface sites on both powders. The slurry is placed on mechanical rollers for 12 hours, after which tetramethylammonium nitrate (TMA-N) salt is added to form weakly attractive pair potentials between the particles. The slurry is then returned to the mechanical rollers for a further 12 hours. After mixing, the slurry is consolidated by pressure filtration and stored in sealed plastic bags to prevent drying. Fibre cloths are cut and placed in separate plastic bags, and an excess of the preconsolidated slurry distributed to both sides of each fibre cloth. Assisted by vibration, the slurry is manually rolled across the surface of the fibre cloth until the cloth is fully infiltrated to form prepreg that can be frozen and stored. The preconsolidated slurry

exhibits shear-rate thinning and thus vibration reduces the viscosity and allows rapid intrusion of the particles into the fibre cloth. Prepregs are then removed from their plastic bags and stacked in the desired orientation. The stack is then vibrated whilst being lightly pressed under vacuum to cause the preconsolidated slurry to flow and complete the infiltration. The infiltrated stack is very flexible and can be shaped. The green body is dried before an initial sintering treatment at 900°C for 2 hours to promote the development of alumina bridges between the mullite network. The composite is subsequently impregnated with an alumina precursor solution under vacuum in a dry nitrogen atmosphere to prevent premature gelation of the precursor. The composites are left in the precursor solution for 2 hours at atmospheric pressure, after which they are transferred to ammoniated water (pH 10) for 4 hours to gel the precursor. The composite is then heated to 900°C in order to pyrolyse the precursor. Precursor impregnation and pyrolysis is repeated multiple times, and subsequently sintered at 1200°C for 2 hours [90]. The ability to manufacture tubular shapes with a homogenous microstructure has been demonstrated by Holmquist et al. [91].

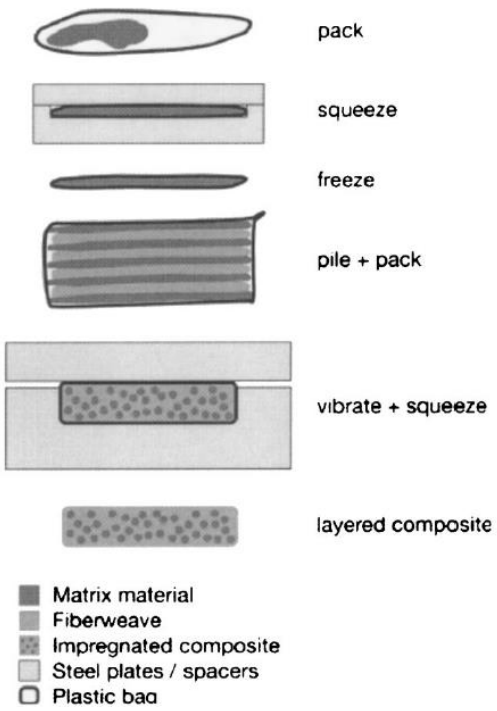

Figure 2.12. VibroIntrusion approach to the fabrication of an all-oxide CMC [5].

Holmquist and Lange investigated the flexural and shear properties of composites composed of Nextel 720 fibres within an alumina-mullite matrix produced by the VibroIntrusion method [90]. The flexural strength of as-processed composites was ~172MPa with an elastic modulus of ~61GPa. Interlaminar shear strength (determined by short beam shear) was shown to be a function of matrix porosity, with shear strength decreasing from ~9MPa to ~7MPa with only a slight increase in matrix porosity from 42.0 to 43.2%. Thermal stability was studied by ageing the specimens in air for 100 hours at 1200°C and 1300°C. Flexural strength tests at room temperature revealed that there was no significant effect on either strength or stiffness after ageing at 1200°C, however a slight improvement in interlaminar shear strength was evident. Whilst there was no evidence of matrix densification, the authors concluded that an improvement in shear strength after ageing was caused by strengthening of the mullite/alumina matrix network. Flexural strength decreased by ~20% after ageing at 1300°C and this was accompanied by a slight increase in stiffness. It was concluded that this reduction in strength was caused partially by degradation of the fibre and partially due to a stronger and denser matrix after ageing. It was proposed that a denser matrix induces higher stress concentrations around fibre breaks and therefore the probability of failure in adjacent fibres increases. This was confirmed by a significant reduction in fibre pull-out length. The in-plane notch sensitivity of the material was also investigated. The net-section flexural strength of both as-processed notched specimens and notched specimens aged at 1200°C for 100 hours was ~75-90% of unnotched specimens, indicating moderate notch sensitivity.

2.3.2. COI Ceramics

COI Ceramics, Inc., founded in 1976 and based in San Diego (CA, USA), manufactures and markets composite products for the aerospace and space industry. A significant body of research has been conducted at the Air Force Institute of Technology (OH, USA) into the

properties of COI manufactured Nextel 720/oxide matrix CMCs. The COI processing method is outlined in Figure 2.13. Firstly, Nextel 720 fibres are infiltrated with matrix via a sol-gel process (described in section 2.2.5). Following lay-up, the laminate is dried with a vacuum bag process under low pressure (<0.7MPa) and low temperature (<150°C), followed by a pressureless sintering technique [92], [93]. Early work focussed on the development of composites composed of Nextel 720 fibres within an alumina-silicate matrix for military exhaust systems. It was soon recognised that this system did not meet design requirements, exhibiting ~40% strength degradation after 100 hours exposure to 1100°C [92]. Further development saw the use of a pure alumina matrix and, more recently, an alumina-mullite matrix for high temperature structural aerospace applications. Substantial investigation into the properties of the COI manufactured Nextel 720/alumina matrix (N720/A) composite has been carried out. The composite plates studied typically comprise 12 plies in a 0°/90° orientation (2.8mm thick) with density ~2.7g/cc, fibre volume fraction ~44% and matrix porosity ~24%.

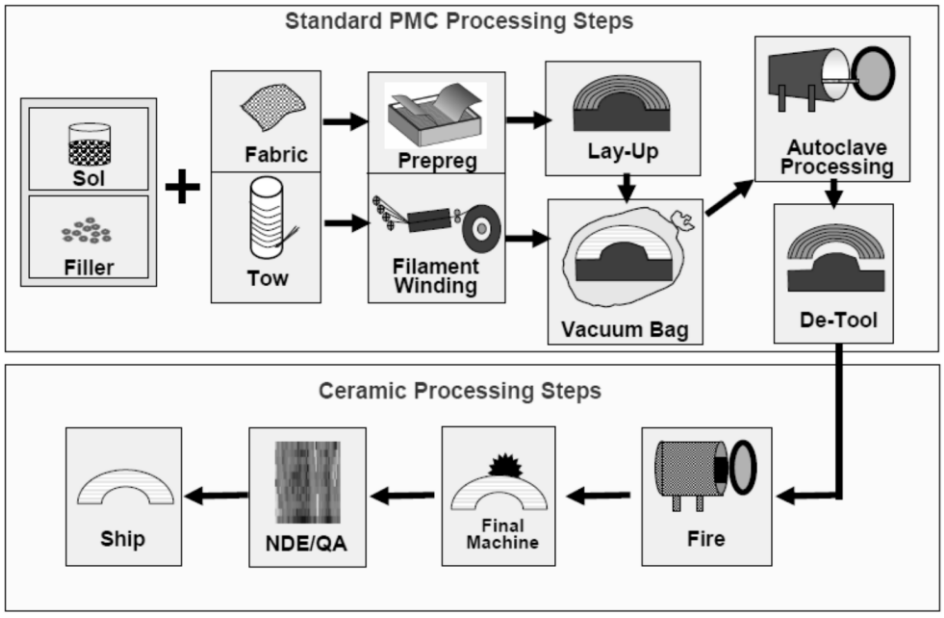

Figure 2.13. COI Ceramics oxide CMC fabrication process [93].

The tensile behaviour of the COI manufactured N720/A CMC has been investigated extensively. At room temperature (23°C), the ultimate tensile strength (UTS) has been reported to be 144-169MPa with an elastic modulus of 60-70GPa and failure strain of 0.25-0.35% [94], [95], [96]. With the exception of Steel et al. [94], an increase in UTS has been observed during monotonic tensile loading at elevated temperatures. Ruggles-Wrenn and Braun investigated the tensile behaviour at 800, 900, 1000 and 1100°C and it was concluded that the tensile properties change little as temperature increases from 800 to 1100°C. Average UTS was 189MPa, elastic modulus, 72GPa and failure strain, 0.33% [97]. Similar values have been obtained during tensile loading at 1200°C with UTS equal to 190-192MPa, elastic modulus, 75-76GPa and failure strain, 0.38%. The stress-strain behaviour at all temperatures investigated was nearly linear to failure indicating that there was little matrix cracking or fibre-matrix debonding. Fibre fracture appeared to be the dominate damage mode [95], [98], [99], [100]. Tensile behaviour has been shown to change dramatically during loading at 1330°C; UTS and elastic modulus decreased to 120MPa and 42GPa, respectively, whilst failure strain increased almost tenfold to 1.7%. The stress-strain curve reached a proportional limit at ~74MPa, after which non-linear behaviour was evident [95].

Ruggles-Wrenn et al. [101] established that both tensile strength and failure strain are strongly dependent on loading rate. Monotonic tensile tests were performed at 1200°C under load control with constant rates of 0.0025 and 25MPa/s. UTS decreased from 181MPa with loading at 25MPa/s to 154MPa with loading at 0.0025MPa/s. The stress-strain behaviour was nearly linear to failure at the higher loading rate, but departed early from linearity (~15MPa) at the lower rate causing failure strain to increase from 0.36% to 0.73-1.06%. Ruggles-Wrenn et al. suggested that the observed behaviour can be attributed to diffusion creep controlling the deformation of the fibres at 1200°C. Similar behaviour was observed by Ruggles-Wrenn and

Szymczak who investigated the effect of loading rate on the compressive properties of the N720/A composite at 1200°C. Compressive strength decreased 16% with decreased loading rate from 25MPa/s to 0.0025MPa and compressive modulus decreased 45%. Compressive stress-strain curves obtained for the higher loading rate displayed two nearly linear portions with a decrease in slope occurring at ~100MPa. The curve departed early from linearity (~40MPa) for the lower loading rate [102].

The N720/A composite exhibits excellent tension-tension fatigue resistance in laboratory air at 1200°C, with a fatigue limit (based on run-out of 10^5 cycles) of 170MPa (88% UTS). The material retained 100% of its tensile strength, however considerable stiffness loss was observed (30-50%) [101]. Mehrman et al. investigated the effect of hold times at maximum stress during fatigue tests**.** At the lower stress investigated (125MPa), the introduction of a hold period up to 100 seconds had no effect on fatigue life and run-out was achieved in all specimens. On the contrary, for the higher stress level investigated (154MPa), the introduction of a 10 second hold period caused a significant reduction in fatigue life and increasing the hold period to 100 seconds further reduced fatigue life by an order of magnitude [98].

The influence of cycling frequency on fatigue behaviour has been investigated at room temperature [96] and at 1200°C [103]. Mall and Ahn concluded that at room temperature, increasing cycling frequency from 1 to 100Hz had an insignificant effect, whilst fatigue life increased significantly with a further increase to 900Hz. It was proposed that local bonding at the fibre/matrix interface due to frictional heating at the higher frequency inhibited damage progression leading to an increase in fatigue life [96]. On the contrary, Ruggles-Wrenn at al.

concluded that at 1200°C, fatigue life appears to be independent of loading frequency. The fatigue limit (based on run-out of 10^5 cycles) of 170MPa was achieved at both 0.1 and 1.0Hz.

The tensile creep properties of the N720/A composite have been studied comprehensively. Ruggles-Wrenn et al. demonstrated that at applied stresses ≤26MPa at 1200°C, specimens exhibited only negative creep deformation (decrease in strain under constant stress). It was concluded that specimens exposed to 1200°C at stresses ≤26MPa for prolonged periods of time undergo additional matrix densification, explaining the negative creep deformation [101]. Creep curves obtained at temperatures 1000-1200°C with applied stresses 80-154MPa exhibit very short primary creep, which rapidly transitions into secondary creep. Secondary creep remains nearly linear to failure. The accumulated creep strain significantly exceeds failure strain obtained in tension tests [95]**,** [97]. Creep run-out of 100 hours was achieved at 150MPa at both 1000°C and 1100°C. At 1200°C, creep run-out stress was 80MPa. Fracture surfaces of specimens exposed to 1000°C and 1100°C are dominated by regions of fibrous fracture, whilst nearly planar fracture prevails for specimens exposed to 1200°C. It has been suggested that at 1200°C, the composite exhibits decreased damage tolerance, brittle fracture behaviour and a short creep lifetime [97].

The presence of steam has been shown to cause a significant reduction in both fatigue [101] and creep performance, with the detrimental effect of steam becoming more pronounced with increasing temperature [97]. It has been suggested that the use of this composite may be limited to temperatures below 1000°C in a moisture containing environment, especially for components subjected to considerable sustained loads [97]. Wannaparhun and Seal [104] and Ruggles-Wrenn et al. [103] have shown evidence of silicon leaching from the mullite phase of the fibre to the matrix after ageing in steam. No silicon was found in the matrix of the as-

processed material. Nevertheless, Ruggles-Wrenn et al. concluded that the degree of silicon migration could not be readily correlated with fatigue life and therefore may not be the cause of reduced performance in a steam environment [103].

Monotonic tensile loading of specimens with a ±45° fibre orientation at 1200°C revealed UTS and elastic modulus values considerably lower than the corresponding values in the 0°/90° orientation (55MPa and 46GPa, respectively, compared with 190-192MPa and 75-76GPa). Non-linear stress-strain behaviour was evident at low stress (~15MPa) and appreciable inelastic strains developed at near constant stress after UTS was reached [101]. The creep-rupture behaviour with ±45° fibre orientation was investigated for stresses between 15 and 45MPa at 1200°C. Creep strain rates ranged from $4.2x10^{-6}$ to $9.4x10^{-3}$ s^{-1} with increased applied stress. For stress levels <35MPa, specimens exhibited primary and secondary creep regimes and creep run out of 100 hours was achieved for all specimens. Run-out specimens exhibited an increase in stiffness and strength. Primary, secondary and tertiary creep regimes were observed at 45MPa and creep strain rates increased by three orders of magnitude [99].

Ruggles-Wrenn and Laffey investigated the interlaminar shear properties of the N720/A composite [105]. Interlaminar shear strength (ILSS) in air at 1200°C, determined by double notch shear, was 8.25MPa. Failure occurred primarily through delamination of just one fibre layer, with minimal fibre fracture. The creep performance in interlaminar shear was investigated. Creep run-out was achieved for all specimens tested at 6.5MPa and run-out specimens exhibited a substantial increase in ILSS (11.2MPa). The composite exhibited primary and secondary creep regimes. Fracture surfaces exhibited considerable fibre fracture and it was suggested that the matrix undergoes additional sintering during creep testing. Prior ageing of specimens in steam for 24 hours at 1200°C had an insignificant effect on ILSS (τ =

8.44MPa). On the contrary, exposure to steam considerably degraded the creep resistance in interlaminar shear. Creep run-out was only achieved at 4MPa and run-out specimens retained just 75% ILSS (6.13MPa). Primary, secondary and tertiary creep regimes were observed and creep strains accumulated were at least an order of magnitude larger than those produced in air. It was suggested that poor creep performance in steam was caused by hydrothermal weakening of the alumina matrix.

Mall and Sullivan demonstrated that under monotonic tensile loading conditions at 1200°C, there was only a 5% decrease in UTS from 200±18 MPa to 190±15 MPa with the presence of a central hole (diameter to width ratio of 0.33). The central hole had no effect on the fatigue life of the composite in tension-tension fatigue tests. Additionally, creep rupture behaviour showed rupture lives better than the unnotched geometry. Mall and Sullivan suggested that whilst the net section stress near the hole was the same as that in the unnotched geometry, the stress away from the hole was less and thus cracks grew slower [106]. On the contrary, the composite was found to be mildly notch sensitive with the presence of a double edge sharp notch, exhibiting a 15% decrease in UTS from 200±18MPa to 175±15MPa and ~20% reduction in fatigue strength for a given number of cycles to failure. In addition, there was ~15% reduction in the stress rupture strength in the presence of a sharp notch [107].

2.3.3. The “colloidal route”

Simon [108] developed a novel process for the manufacture of porous matrix oxide CMCs; named the “colloidal route”. The colloidal route is summarised in Figure 2.14 and can be described in five steps; dispersion, lamination, setting, drying and sintering.

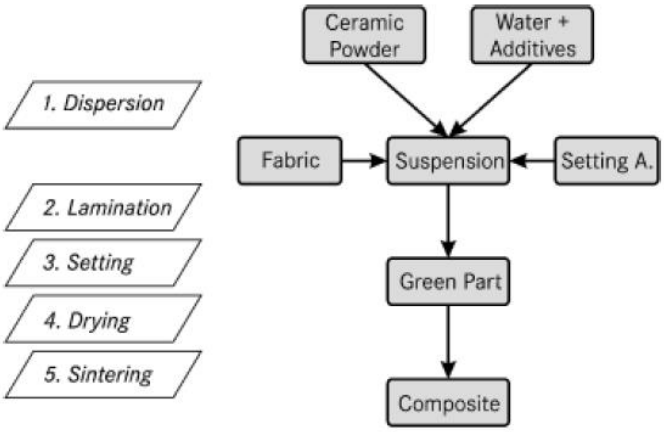

Figure 2.14. The "colloidal route" used for the manufacture of oxide/oxide composite panels [108].

A colloidal suspension is first prepared by dispersing equal quantities of 1 micron mullite particles and <100nm nano-particles in deionised water. The addition of an acid to adjust the pH to ~4 allows the development of electric double-layer repulsive forces between the oxide particles, producing a well dispersed solution with low viscosity and high solid loading (~47vol%). An aluminium nitride setting agent is added to the suspension (~1wt%) before lamination to shift the pH to ~9.5 during consolidation. Nextel 720 fibres are cut into the desired geometry and impregnated with the matrix suspension, after which components can be formed using a conventional hand lay-up technique. Setting (or consolidation) is achieved by an *in situ* reaction which takes place over 24 hours, resulting in a stiff, coagulated particle network. After consolidation, the green composite is dried in ambient air followed by sintering at temperatures >1200°C.

Simon [108] explored the basic tensile and interlaminar shear properties of the as-processed composite plates. During monotonic tensile loading at room temperature, the Nextel 720/mullite system exhibited an average tensile strength of 195-205MPa, Young's modulus of 68-74GPa and failure strain of 0.35-0.6%. Specimens exhibited an almost linear regime

followed by quasi-ductile fracture behaviour. The interlaminar shear strength (ILSS), determined by short beam shear, was 10-11.5MPa. Ageing experiments were carried out at temperatures between 1100°C and 1300°C for 1000 hours. Specimens exhibited a slight increase in both tensile strength and ILSS after ageing at temperatures ≤1200°C. After ageing at temperatures above 1200°C a gentle decrease in tensile strength was detected whilst ILSS increased considerably to ~17MPa. These findings were attributed to further densification of the porous matrix as well as by a loss in fibre strength due to extensive grain growth within the Nextel 720 fibres [108]. Simon and Danzer [109] investigated the off-axis properties of the Nextel 720/mullite composite. Tensile strength decreased significantly in the ±45° fibre orientation and specimens exhibited in-elastic behaviour with high failure strains. The interlaminar properties of the composite were unaffected by fibre orientation with specimens exhibiting ILSS of 10-12MPa in the ±45° orientation [109].

2.4. Summary of literature review

There are a number of factors that affect the performance of a ceramic matrix composite (CMC) including the mechanical properties and chemical composition of the reinforcing and matrix materials, the interaction between those constituents and the processing route employed to manufacture the CMC.

Ceramic reinforcements are available in the form of particles, whiskers, discontinuous and continuous fibres. Continuous ceramic fibres are of particular interest for high temperature structural materials since they combine relatively high strength and stiffness with high temperature capability. Continuous ceramic fibres can be produced with a wide range of compositions, geometries and properties and are widely commercially available. Non-oxide fibres such as those containing carbon and silicon carbide are regularly utilised in CMCs

owing to their excellent mechanical strength and potential to operate at high temperatures provided they have either an oxygen barrier protection or the environment is non-oxidising. Silicon carbide fibres, whilst being regularly employed in high performance composite materials, have high production costs owing to difficulties in removing oxygen impurities which cause deteriorating mechanical properties at elevated temperatures. Oxide fibres are fully oxidised and therefore cannot suffer from oxidation embrittlement. The Nextel 720 fibre (3M), composed of 85wt% α-alumina and 15wt% silica, exhibits superior creep performance in comparison with pure α-alumina fibres owing to the presence of mullite at grain boundaries. Nextel 720 fibres display an in-service temperature capability of 1200°C which is currently the highest of any commercially available oxide fibre. As such, they have been identified by many as a potential ceramic reinforcement for high temperature structural components.

Ceramic matrices bind the reinforcing fibres to form a structural unit, and protect fibres from environmental attack or mechanical abrasion. Whilst the matrix contributes little to the tensile strength of the composite, it has a significant influence on the interlaminar and compressive properties. Matrices containing silicon carbide are regularly utilised in composites reinforced with non-oxide fibres, whilst alumina-based matrices are more commonly employed in oxide-fibre reinforced composites. Alumina has good mechanical strength and stiffness, high hardness and wear resistance, good thermal conductivity and a low CTE. Most importantly, alumina-based matrices are chemically compatible with Nextel 720 fibres.

The direct introduction of a ceramic fibre into a ceramic matrix results in a strong chemical bond between the two components, allowing matrix cracks to penetrate directly into the fibres resulting in catastrophic failure. Thus, the primary role of a fibre/matrix interface is to create a

weak layer, promoting damage tolerant behaviour. Conventional interface design employs the use of a thin coating on the fibres which acts as a debond layer and a low friction sliding interface. Fibre coatings introduce high production complexity and cost, and difficulties remain in coating fibre weaves. Similar damage tolerant behaviour can be achieved by means of a finely distributed porosity within the matrix. Porous matrices offer the potential for low cost, straightforward processing methods to be utilised and are generally preferred for oxide systems.

The processing of a ceramic composite should be considered as an integral part of the design process. There are a number of processing methods commonly used for the manufacture of CMCs including chemical vapour infiltration (CVI), polymer impregnation and pyrolysis (PIP), reactive melt infiltration (RMI), slurry infiltration and hot pressing, and the sol-gel process.

CVI involves the deposition of a ceramic material within a fibre preform by a chemical reaction taking place between gaseous species. The CVI process can be used to produce both oxide and non-oxide CMCs of various compositions. Composites produced by CVI possess good mechanical properties and matrices of high purity can be fabricated. In addition, large, complex shapes can be produced in a near net shape. Nevertheless, the CVI process involves high capital and production costs.

The PIP process involves impregnating a fibre preform with a polymeric precursor followed by curing and pyrolysis, converting the polymer to a ceramic. The PIP process utilises simple processing equipment at low temperatures, resulting in low production costs compared with

alternative methods. However, 6-10 repeat impregnations are typically required to achieve sufficient matrix densification.

RMI has many advantages over alternative methods including its simplicity and short processing times, in addition to yielding dense matrices without requiring multiple infiltration cycles. RMI is used predominantly for the fabrication of silicon carbide (SiC) matrix composites; a process termed Liquid Silicon Infiltration (LSI). LSI requires relatively high temperatures and therefore only SiC or C fibres can be employed. Furthermore, liquid silicon is a corrosive medium and can cause damage to both interphases and fibres. RMI can be used to form oxide matrices; a process termed Direct Metal Oxidation (DIMOX). Due to the nature of the RMI process, porous matrix interface design is not possible.

The slurry infiltration and hot pressing method can be used to form matrices of alumina, silica, mullite, silicon carbide and silicon nitride. Hot pressing enhances the consolidation of ceramic particles, resulting in a low porosity composite. However, the reinforcing fibres may be damaged by the high pressures applied, and they may also suffer damage caused by a reaction with the matrix at high temperatures. Furthermore, the equipment required for hot pressing is relatively expensive and components are limited to simple plate shapes.

The sol-gel process involves the conversion of a sol (a colloidal suspension of fine ceramic particles within a liquid) to a gel by either hydrolysis or condensation, followed by controlled heating to produce a ceramic. The sol-gel process offers excellent compositional homogeneity in single phase matrices, and also has the potential for producing unique multiphase matrices. In addition, the gel-to-ceramic conversion temperature is typically much lower than that required in traditional sintering processes and thus fibre damage by high processing

temperatures can be eliminated. Furthermore, the equipment required is relatively inexpensive, and large, complex, near-net shapes can be fabricated, reducing machining costs. However, the ceramic yield is low compared with slurry techniques, resulting in high shrinkage and large cracks within the matrix. Thus, repeated impregnations are generally required to produce a suitably dense matrix.

The development of porous-matrix oxide composites containing Nextel 720 fibres has received significant attention at the University of California at Santa Barbara (UCSB). Two processing routes have been described in the literature; pressure filtration and VibroIntrusion. The pressure filtration method is limited to the production of flat plates whilst the VibroIntrusion method is capable of producing complex geometries. Composites produced by the pressure filtration method exhibited tensile strength of 145MPa in the 0°/90° orientation with a modulus of ~60GPa. Tensile strength decreased to ~50MPa in the ±45° orientation. The flexural strength of such composites was reported to be ~210MPa, whilst the interlaminar shear strength (established by short beam shear) was ~10MPa. Composites produced by the VibroIntrusion method exhibited flexural strength of 172MPa and interlaminar shear strength of 7-9MPa. No significant effect on flexural strength was evident after thermal ageing at 1200°C for 100 hours, however shear strength improved slightly.

A significant body of research has been conducted at the Air Force Institute of Technology (OH, USA) into the properties of COI Ceramics, Inc. manufactured Nextel 720/alumina matrix CMCs. Composites are manufactured by the sol-gel method. At room temperature, the ultimate tensile strength (UTS) has been reported to be 144-169MPa with an elastic modulus of 60-70GPa and failure strain of 0.25-0.35%. At 1200°C, UTS increased to 190-192MPa, elastic modulus, 75-76GPa and failure strain, 0.38%. Tensile behaviour changed dramatically

during loading at 1330°C; UTS and elastic modulus decreased to 120MPa and 42GPa, respectively, whilst failure strain increased almost tenfold to 1.7%. It was established that both tensile and compressive strength are strongly dependent on loading rate, with higher loading rates producing greater strength. The N720/A composite exhibited excellent fatigue and creep resistance in laboratory air at 1200°C however the presence of steam caused a significant reduction in both fatigue and creep performance. It was suggested that the use of this composite may be limited to temperatures below 1000°C in a moisture containing environment, especially for components subjected to considerable sustained loads. Interlaminar shear strength (ILSS) in air at 1200°C, determined by double notch shear, was 8.25MPa.

2.5. Research gaps

The introduction of CMCs for structural applications in the hot section of a gas turbine provides many potential benefits over conventional metallic alloy materials including facilitating elevated operating temperatures. Whilst non-oxide SiC/SiC composites have received a great deal of attention and are routinely manufactured for gas turbine applications, their sensitivity to oxidation at elevated temperatures has prompted research into oxide-oxide CMCs. Commercially available oxide reinforcements are typically alumina-based, continuous, polycrystalline fibres. Nextel 720 fibres (3M) have been identified as a potential ceramic reinforcement for high temperature applications, displaying an in-service temperature capability of 1200°C. A number of Nextel 720/alumina-based CMCs have been reported in the literature, however currently employed processing methods involve either simultaneous infiltration and consolidation, or repeat impregnation and pyrolysis cycles. Whilst the VibroIntrusion method allows storage of frozen pre-impregnated fibres, there is yet to be a process described for oxide CMC systems whereby pre-impregnated fibres or fabric can be

mass produced and stored at room temperature until required, a commonly employed process in the polymer matrix composite industry. Conventional CMC processing methods often involve high raw material and equipment costs, or high applied temperatures and pressures that are unsuitable for oxide systems. This highlights a need to develop a simple, low cost processing method, whilst simultaneously allowing mass production of pre-impregnated fibres, facilitating the use of oxide-oxide CMCs as a commercially viable alternative to metallic components.

2.6. Research objectives

1. To develop an oxide-oxide ceramic matrix composite capable of withstanding temperatures up to and including 1200°C.
2. To develop a composite system that meets or exceeds the mechanical properties of commercially available oxide-oxide systems identified in the literature.
3. To develop a simple, low cost processing method suitable for oxide-oxide CMC systems that can be easily replicated to produce reliable results.
4. To develop a means of storing pre-impregnated fabric (‘pre-preg’) at ambient temperature that can later be reactivated, allowing pre-preg to be mass-manufactured followed by a hand lay-up approach similar to that utilised in the polymer composite industry.

Chapter 3 - Development of processing method

The overall objective of this project was to develop an oxide-oxide ceramic matrix composite via a simple, low cost processing method for high temperature structural applications, whilst simultaneously allowing mass production of pre-impregnated fibres. A number of CMC fabrication methods were identified in the literature and it was concluded that conventional ceramic forming methods must be adapted to meet the requirements of the desired system. The slurry infiltration method allows excellent infiltration of matrix into the fibre weave, however hot pressing can cause damage to the reinforcing fibres and increases manufacturing costs owing to the high temperatures and pressures required. As such, the slurry infiltration method was pursued but an alternative method involving low temperature consolidation followed by pressure-less sintering was investigated.

Five key processing steps were identified by the author and are outlined in Figure 3.1. They include 1) preparation of a polymer binder system, 2) preparation of slurry, 3) slurry impregnation to produce pre-preg, 4) reactivation and consolidation of plies under low temperature and load to produce a green composite and 5) pressure-less sintering to produce an environmentally stable oxide/oxide ceramic matrix composite. The following chapter discusses the preliminary research and development undertaken in collaboration with Dr E.G. Butler in light of the literature review in order to produce a viable processing method.

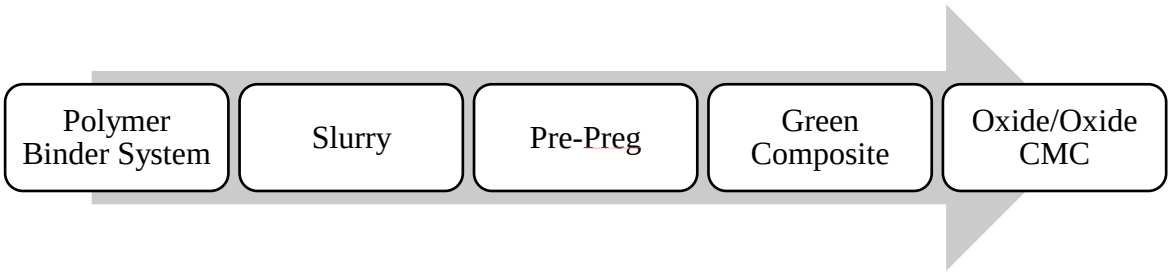

Figure 3.1. Important production steps in the manufacture of an oxide/oxide ceramic matrix composite highlighted from the literature.

3.1. Preparation of polymer binder system

It was determined from the literature that ceramic materials are commonly prepared by mixing powdered ceramic oxides with an aqueous solution containing one or more polymers (a polymer binder system) to produce slurry. The polymer binder serves to improve the flow characteristics of the ceramic powder and to hold the green body in the desired shape prior to sintering [110], [111]. Polyvinyl alcohol (PVA or PVOH) has been identified as a suitable temporary binder owing to its water solubility, chemically stability, and good bonding strength. PVA is obtained through saponification of polyvinyl acetate and is commercially available both partially and fully saponified, in both powder and liquid form. Furthermore, some commercially available PVAs are considered remoistening adhesives, allowing reactivation with the application of water upon the adhesive surface. This is a particularly attractive property for the reactivation of dried pre-preg. Three commercially available PVAs were investigated, exploring the effect on both manufacturing and mechanical properties, and will be discussed in chapter 5.

Polymer binder systems often include plasticisers that improve the flexibility and workability of the green composite. Plasticisers are low molecular weight additives that lower the glass transition temperature of the binder at room temperature, leading to better plasticity [112], [113]. This is a desirable characteristic for improving the handleability of dried pre-preg. Plasticisers must be both compatible and stable with other binder constituents, and must be emulsible in the same solvent used to carry the binder. Furthermore, the binder/plasticiser ratio must be optimised. Polyethylene glycol is commonly employed as a plasticiser in combination with a PVA binder to form an alumina slurry [114]. PEG 400, a low molecular weight polyethylene glycol, was therefore used in this project.

Interparticle forces are one of the major factors controlling the density to which powder consolidates to form a solid. Interparticle forces are controlled by surface chemistry which in turn is controlled by pH. Incorporating nitric acid (HNO_3) into the polymer binder system ensures the pH of slurry is acidic (~3). In the literature, this has been shown to create repulsive forces which acts as a lubricant to allow particles to rearrange and pack to their highest density [4], [42], [115].

3.2. Preparation of slurry

Slurry composition can greatly affect the microstructure and consequently the properties of a composite [112]. Excessive volumes of polymeric substances in slurry reduce composite density and degrade matrix strength [116]. Nevertheless, slurry must have a low enough viscosity to flow uniformly into the fibre weave. It was recognized in section 2.3 that the pressure filtration method requires the preparation of an aqueous solution containing 30vol% solids, whilst the VibroIntrusion process requires just 20vol% solids. The colloidal route, conversely, requires a solution with low viscosity and high solid loading (47vol%). During preliminary investigation, composites produced from slurry containing equal parts (by weight) polymer binder and alumina particles delaminated on sintering; displaying matrix dry regions on ply surfaces. On the contrary, composites produced from slurry containing one part polymer binder to five parts alumina proved very difficult to impregnate, displaying matrix rich regions on ply surfaces and matrix dry regions within the fibre weave, suggesting that slurry viscosity was too great to infiltrate into the fibre weave. These observations led to an optimised slurry ratio of 1 part polymer binder solution to 2.5 parts alumina powder (~30% solids).

Slurry is often produced by ball milling as this ensures an even distribution of oxide particles amongst the polymer binder. The effect of ball milling compared with manually shaking slurry was investigated and was shown to improve flexural strength from ~140MPa to ~155MPa for composites produced like-for-like. Ball milling caused the slurry to foam due to the reduced surface tension of water caused by dissolution of PVA within the polymer binder solution, particularly when using PVA with a low degree of saponification [117]. It was therefore necessary to include a small volume (0.1%) of antifoam agent prior to ball milling.

The production of ceramic components is highly dependent on particle size and size distribution. Large particles tend to pack inefficiently, leading to the formation of large pores which persist during sintering. Small particles have the ability to pack efficiently but often crack on sintering. Lange et al. [4] stated that when powder particles are packed against a fibre surface in a composite material, extra spaces exist that would have been partially filled with particles if the surface did not exist (the 'wall effect'). It was stated that if the ratio of particle-to-fibre diameter (R) is greater than 0.1, a limited number of particles can fill the interstices between the fibres (Figure 3.2). This geometrical restriction highlights the requirement for submicron diameter particles in a composite system [4].

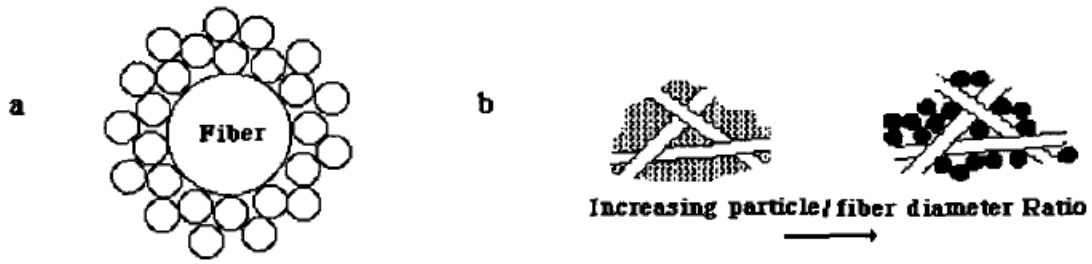

Figure 3.2 a) Fibre disrupts particle packing at surface because of the 'wall effect' b) Increasing the particle-to-fibre diameter results in fewer particles packed within the fibre interstices (after [4]).

Taimicron TM-DAR powder (Taimei Chemicals Co., ltd) is considered ultra-fine, high purity α-alumina particles and was identified as a suitable matrix material in this system [118]. The particles have a mean diameter of 0.1μm and therefore a high packing density can be theoretically achieved when combined with 12μm Nextel 720 fibres (R=0.008). In addition, the powder is considered to be low temperature sinterable alumina and has been shown to be fully densified at 1300°C [119].

3.3. Slurry impregnation to form 'pre-preg'

An objective of this project was to develop a processing method whereby pre-impregnated fibres ('pre-preg') can be dried and stored at ambient temperature until required, allowing the ability to semi-automate manufacturing by mass producing pre-preg, as seen in polymer matrix composite technology. CMC manufacturing techniques such as polymer impregnation and pyrolysis (PIP) necessitate infiltration and consolidation simultaneously and it is therefore not possible to dry and store pre-preg. The slurry infiltration technique involves passing fibres through a bath of slurry and, whilst it has not been shown previously, in theory allows the ability to interrupt manufacturing after infiltration. Nevertheless, slurry uptake by this method is dependent on viscosity and therefore matrix content is not easily controlled. Matrix content and consequently matrix porosity is critical to the mechanical behaviour of an oxide CMC with a weak, porous matrix. The matrix must provide adequate interlaminar and compressive strength, whilst simultaneously facilitating energy absorbing mechanisms such as crack deflection and fibre debonding. An alternative method of infiltration was explored in this project, using a long pile woven roller to 'drive' slurry into the fabric weave, allowing much better control of matrix infiltration.

During preliminary investigation, slurry impregnation was controlled by varying the volume of slurry loaded on the roller. Fabric strips were weighed before and after impregnation (wet), and after drying overnight to calculate pre-preg matrix content. When the roller was heavily loaded, slurry collected on the surface of the fabric strip in pools. When the fabric was overturned to expose the lower surface, slurry had evidently infiltrated through the weave and onto the plastic sheet below. Matrix content after impregnation with a heavily loaded roller was calculated to be >50wt%. Composites revealed regions of dense matrix between fibre layers after sintering and subsequently demonstrated poor flexural strength (<150MPa). When the roller was loaded with little slurry, slurry did not penetrate the fibre weave, necessitating additional impregnations and increasing the possibility of fibre damage. Matrix content after impregnation with little slurry was calculated to be <45wt% and consequently composites possessed low density (~2.2g/cc) and poor strength (σ_{flex} < 150MPa; τ ~7MPa). When the roller was moderately loaded with slurry, slurry penetrated the fibre weave without creating pools on the surface and with minimal roller strokes. Fabric weight increased by ~58-63% after impregnation with a moderately loaded roller, and subsequently lost ~13% after drying, resulting in a pre-preg matrix content of ~45-50%. Composites consequently demonstrated flexural strength >160MPa.

3.4. Reactivation and consolidation

The reactivation of dried pre-preg is a unique process in oxide CMC manufacture and therefore required considerable investigation. As previously mentioned, the use of a polymer binder containing a remoistening adhesive (PVA) allows reactivation upon application of water. Spraying the surface of plies with deionised water was briefly investigated however it was found that water did not penetrate into the fibre weave and plies did not become malleable. Plies did not consolidate under low temperature and load, and subsequently

delaminated on sintering. Immersing the plies into a bath of deionised water ensured penetration into the fibre weave, yet plies were subsequently 'too wet' for lay-up. As a result, a substantial volume of slurry was expelled during consolidation (12.5%) and the composite exhibited poor flexural strength (~140MPa). Consequently, plies were left to partially dry horizontally on wire racks until the correct 'wetness' was achieved. A number of variables were considered during reactivation and consolidation including duration of immersion, moisture content after immersion (by weight increase), duration of partial drying, moisture content on lay-up, method of stacking, load and temperature during consolidation and slurry loss after consolidation. During preliminary research, it was noted that prolonged immersion in water (>5 seconds) led to both slurry wash out and an impractical duration of partial drying (> 1 hour). When plies were immersed and removed immediately (1 second immersion), plies were dry to the touch within 10 minutes yet did not become adhesive within that time. This suggests that remoistening PVAs require a certain time to reactivate. Plies were weighed before immersion, immediately after immersion and on lay-up. Water content was calculated by weight increase. Plies with greater than 20wt% water content on lay-up were very difficult to handle due to their 'wetness' and did not remain in place during stacking. Additionally, a substantial volume of slurry was expelled during consolidation resulting in poor composite strength. On the contrary, plies containing little water on lay-up (<10wt%) lost malleability and did not appear to adhere to one another. It was deduced that immersion for 3 seconds followed by partial drying for 15 minutes allowed adequate time for PVA to reactivate. After 3 seconds immersion, plies of 80x150mm exhibited a water content of ~22wt% which reduced to ~17wt% after 15 minutes partial drying. Plies were 'tacky' to the touch and remained malleable, allowing manipulation during lay-up. This is particularly desirable for the manufacture of complex geometries.

Lay-up, or stacking, is a process used in both polymer and ceramic composite forming whereby plies are stacked one-by-one on a tooling block in the desired geometry. During preliminary investigation, it was recognised that light pressure must be applied to the laminate stack during lay-up in order to remove trapped air and improve adhesion between plies. This was performed with a solid roller, from the centre of the stack outwards and in all directions. It has been suggested that the orientation of reinforcing fibres has a significant effect on the mechanical behaviour of CMCs [11]. Nextel 720 fibres are woven in a non-symmetrical, 8-harness satin weave. Luo & Daniel [120] stated that the symmetry of an 8-harness satin weave can be improved by rotating alternate plies by 90° during lay-up, ensuring to mirror the laminate stack about the mid-plane. A schematic of this laminate orientation can be seen in Figure 3.3. The fill signifies fibre tows that run crosswise in a Nextel 720 fabric roll, whilst warp denotes fibre tows that run lengthwise [26].

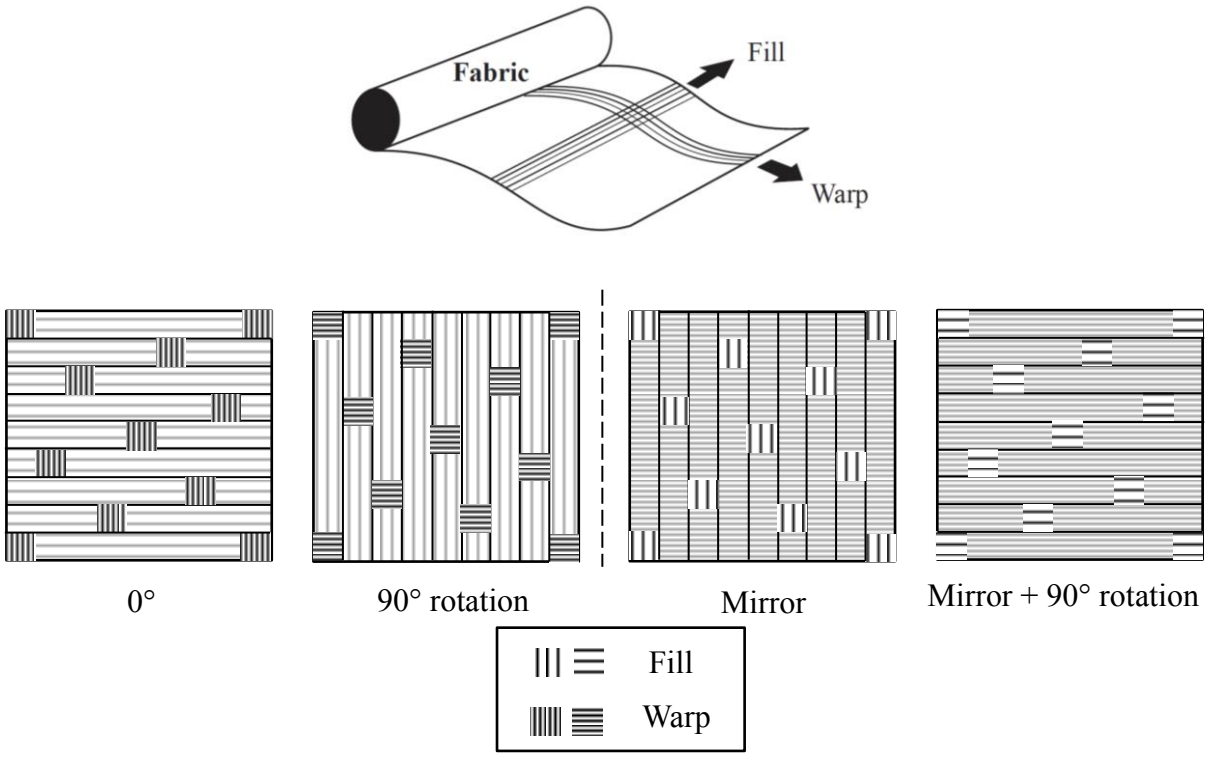

Figure 3.3. Laminate orientation during lay-up for an 8-harness satin weave (after [26] and [120].

Following lay-up, the laminate stack must be consolidated to form a green composite. In polymer composite manufacture this is commonly performed in either a heated press or an autoclave. Autoclaves allow the production of complex geometries; however they increase production costs significantly. It is generally accepted that for small flat plates, such as produced in this project to allow simple comparative studies, a heated press is sufficient. The laminate stack must be placed between two metal mould plates, with a sheet of plastic release film between the metal and laminate. Dimensional stops prevent the composite from crushing under the applied load. Preliminary research highlighted the need to apply load slowly, reducing the amount of trapped air and also to prevent slurry from being expelled under pressure. As such, load was applied over 5 minutes and allowed to stabilise at room temperature for 30 minutes. The laminate stack must be heated above 100°C to ensure all moisture is removed from the system, and temperature must be raised slowly to avoid rapid evaporation and consequently large voids in the composite. Accordingly, temperature was raised at 2°C/min to 90°C for 3 hours, followed by heating to 105°C at 0.5°C/min for 4 hours. The green composite must be cooled naturally to room temperature to avoid thermal shock. It was observed that composites of 11 ply thickness (80x150mm) produced under 3 tonnes load were noticeably thinner than those produced under 1 tonne load (thickness ~2.6mm compared with ~2.8mm), despite the same thickness dimensional stops, and consequently exhibited greater flexural strength. After further investigation it was found that during consolidation the laminate stack expanded during heating, causing the top plate to be lifted from the dimensional stop under 1 tonne load, but this was not observed with 3 tonnes load.

3.5. Sintering

Sintering has been identified as the final phase in the production of an oxide CMC and is often performed over a long period of time (24-48 hours). Ceramic powder compacts undergo

several significant changes during this phase including binder burnout, decomposition, phase transformations and densification. Binder burnout involves raising the temperature of the composite to the degradation temperatures of the polymer additives, thus volatilising and removing the polymer from the composite [110]. It is essential that this process is performed slowly since it has been shown elsewhere that heating PVA above the decomposition temperature (228°C) causes a rapid chain-stripping elimination of water, which when coupled with polymer melting causes foaming and can create large voids in the composite [121]. It was therefore decided to include a dwell period at 250°C for 1 hour to limit this behaviour. Sintering is a diffusional process that occurs at temperatures usually between 0.5 and 0.75 of the melting temperature (Tm) of the ceramic particles. During the diffusion process the pores between particles close up, resulting in densification of the composite and an improvement in mechanical properties. It is important to note that the sintering temperature of a ceramic matrix composite is generally limited by the temperature capabilities of the reinforcing fibres. Nextel 720 fibres exhibit a maximum temperature capability of 1200°C, currently the highest capability of any commercially available oxide reinforcement. As previously mentioned, Taimicron TM-DAR particles have been identified as a suitable matrix material for their low temperature sinterability, exhibiting full densification at 1250-1300°C [119]. Generally, sintering is performed without pressure to avoid damage to the composite however graphite tooling can be used where concerns over thermally induced distortions exist [14].

It is important to ensure that reinforcing fibres and matrix materials are chemically compatible at elevated temperatures during both sintering and in-service as chemical interaction such as leaching of silicon from fibres into the matrix could affect the performance of the composite. During preliminary investigation, energy-dispersive X-ray spectroscopy was carried out before and after sintering at 1200°C. Spot analysis indicated that both fibre and matrix

composition remained unchanged after the sintering process and there was no evidence of silicon leaching from the fibres into the matrix. It was therefore concluded that Nextel 720 fibres are chemically compatible with TM-DAR alumina powder at temperatures up to and including 1200°C.

Chapter 4 - Experimental procedures

4.1. Materials and processing

15g powder PVA (Gohsenol GL-05/NL-05, Nippon Gohsei Uk Ltd.) was combined with 360ml deionised water in a glass beaker and heated to 95°C. The solution was agitated until the powder was fully dissolved and allowed to cool. For PVA in solution (PAF 2, Optapix), 75g PVA was combined with 300ml deionised water and agitated well. 25ml PEG 400 (Sigma Aldrich) was then added to the solution, followed by 30ml HNO_3 (10% solution in deionised water). The polymer binder system was stored in an air tight container until required.

250g Taimicron TM-DAR alumina powder (Taimei Chemicals Co., ltd) was slowly added to 100ml polymer binder system, mixing at each addition of powder. 5 drops of Contraspum K1012 (Zschimmer & Schwarz) antifoam agent was added to the mixture which was subsequently ball milled with 500g alumina grinding media (7mm diameter, 90% alumina; Dynamic Ceramic) for 24 hours. The grinding media was removed using a metallic sieve and the slurry was continually turned on rollers in an air tight container until use.

Nextel 720 fabric was cut across the width of the fabric roll using a rotary cutter and placed on a plastic sheet. A high pile roller moderately loaded with slurry was used to impregnate the fabric along its length, imparting a modest amount of force with minimal strokes. The fabric was then overturned to expose the lower surface and slurry impregnated in the same manner. The fabric was then lifted carefully from one end and allowed to dry vertically overnight. The pre-impregnated fabric (‘pre-preg’) was stored flat until required.

Pre-impregnated fabric ('pre-preg') was cut into the required geometry using a rotary cutter. Each ply was individually immersed into a bath of deionised water for 3 seconds and placed on a drying rack for 15 minutes. Plies were handled with 'spade end' tweezers to limit damage to fibres. A sheet of nylon release film (Tygavac Advanced Materials Ltd) was placed on a metal mould plate. The plies were stacked individually, rotating the plies by 0/90°, mirrored at the mid-plane. A solid roller was used to apply pressure to the laminate stack after each ply was positioned. Dimensional stops with a thickness of 0.25mm per ply were placed 10mm from the edge of the laminates. A second sheet of release film was placed on the laminate stack and the top metal mould carefully positioned. The laminates were then placed into a press, and the press plates were brought slowly together until touching. Load was applied slowly over 5 minutes until the top metal mould plate came into contact with the dimensional stops. 3 tonnes was applied for an 11 ply, 80x150mm, composite. The laminates were left to stabilise at room temperature for 30 minutes. The press plates were then heated to 90°C at 2°C/min and held for 3 hours, followed by heating to 105°C at 0.5°C/min for 4 hours. The consolidated plies were cooled naturally to room temperature under load. The green composite was then removed from the mould.

The green composite was placed into a furnace and heated at 10°C/min to 250°C and held for 1 hour, followed by heating at 10°C/min to 525°C for 2 hours and finally heated at 10°C/min to 1200°C for 3 hours. The composite was then cooled at 20°C/min to room temperature.

Mechanical test specimens were wet diamond cut from composite flat plates in both the longitudinal and transverse direction (Figure 4.1).

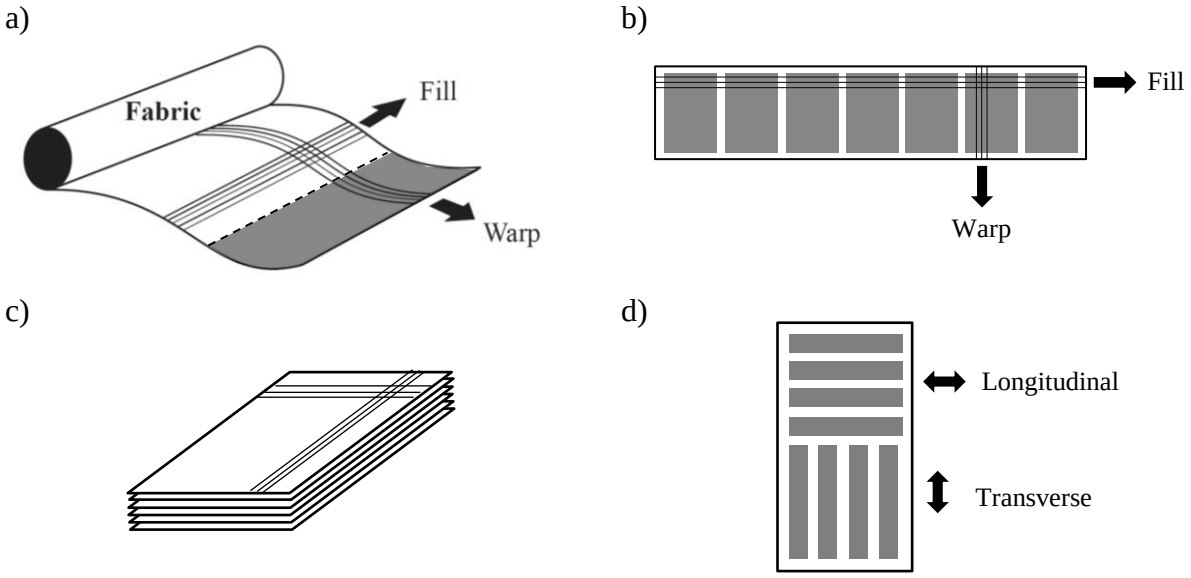

Figure 4.1. Illustration of specimen orientation a) Nextel 720 fabric cut along the 'fill', b) plies cut from pre-impregnated fibres, c) plies stacked and consolidated d) specimens cut in both longitudinal and transverse direction.

4.2. Mechanical testing

4.2.1. Flexural strength test parameters

Flexural strength parameters were adapted from ASTM C1341 for continuous fibre-reinforced advanced ceramic composites [122]. Specimens were in the form of rectangular bars 50mm by 10mm with their thickness dependent on the final sintered thickness of an 11 ply laminate (~2.6mm). A three point loading system was utilized whereby the bar rests on two supports 5mm in diameter and force is applied by means of a loading roller midway between the supports 12mm in diameter. Tests were performed in position control at a constant displacement rate of 0.05mm/min (Figure 4.2). Flexural strength was determined by Equation 4.1.

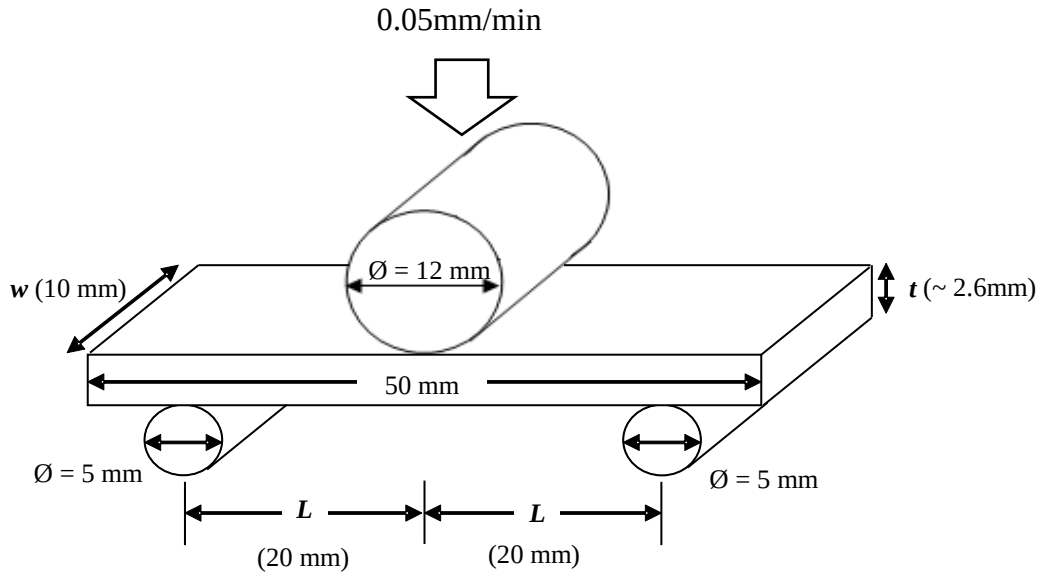

Figure 4.2. Flexural strength parameters adapted from ASTM C1341 for continuous fibre-reinforced advanced ceramics [122].

$$\sigma = \frac{P_{max}\ 3L}{w\ t^2} \qquad \textbf{Equation 4.1}$$

Where P_{max} is the maximum load observed during test, L is span size, w is specimen width and t is specimen thickness.

4.2.2. Short beam shear test parameters

A desirable property of a woven, layered composite is to have sufficient interlaminar shear strength to resist delamination. This type of failure might be encountered in a bending type of loading through the thickness as encountered with a through-thickness temperature gradient. For a given specimen thickness, the shorter the span, the greater the probability that failure will occur by delamination of the layers, rather than crack extension through the layers. Flexural testing with small values of span to thickness is called short beam shear testing and can be used to characterise the interlaminar shear strength of a composite material [5].

The short beam shear strength testing procedure was adapted from ASTM D2344 for polymer matric composite materials [123] and can be used to calculate the interlaminar shear properties of a composite. Specimens were in the form of rectangular bars 15mm by 5mm with their thickness dependent on the final sintered thickness of an 11 ply laminate (~2.6mm). A three point loading system was utilized whereby the bar rests on two supports 3mm in diameter and force is applied by means of a loading roller midway between the supports 6mm in diameter. Short beam shear tests were performed in position control at a constant displacement rate of 0.05mm/min (Figure 4.3). Short beam shear strength can be calculated using Equation 4.2.

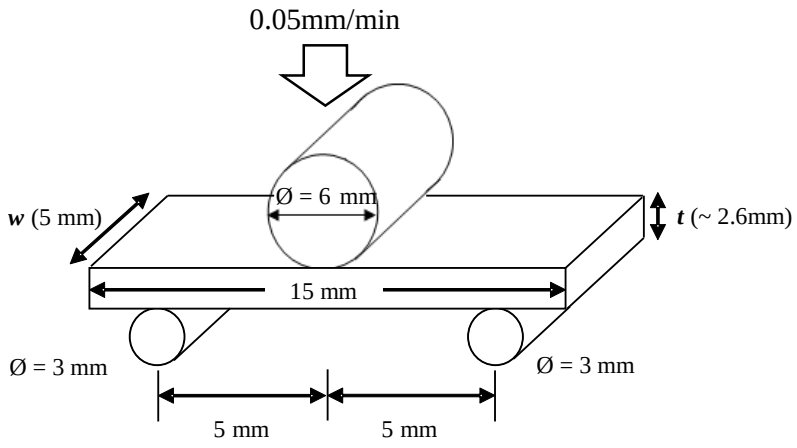

Figure 4.3. Short beam shear parameters adapted from ASTM D2344 for polymer matric composite materials [123].

$$\tau = \frac{3 P_{max}}{4 w t} \qquad \textbf{Equation 4.2}$$

Where P_{max} is the maximum load observed during test, w is specimen width and t is specimen thickness.

4.2.3. Tensile test parameters

Tensile test parameters were adapted from ASTM C1295 for monotonic tensile behaviour of continuous fibre-reinforced advanced ceramics [124]. Specimens were in the form of dog bone specimens with an inner width of 6mm and an outer width of 12mm, and a radius of curvature of 100mm. The gage section had a length of 20mm, with an overall length of 190mm. The specimen thickness was determined by the sintered thickness of a 12 ply laminate (approx. 2.8mm). Tensile tests were performed in position control at a constant displacement rate of 0.5mm/min (Figure 4.4). Self-tightening mechanical grips were used to apply force uniaxially. Tensile strength was calculated using Equation 4.3.

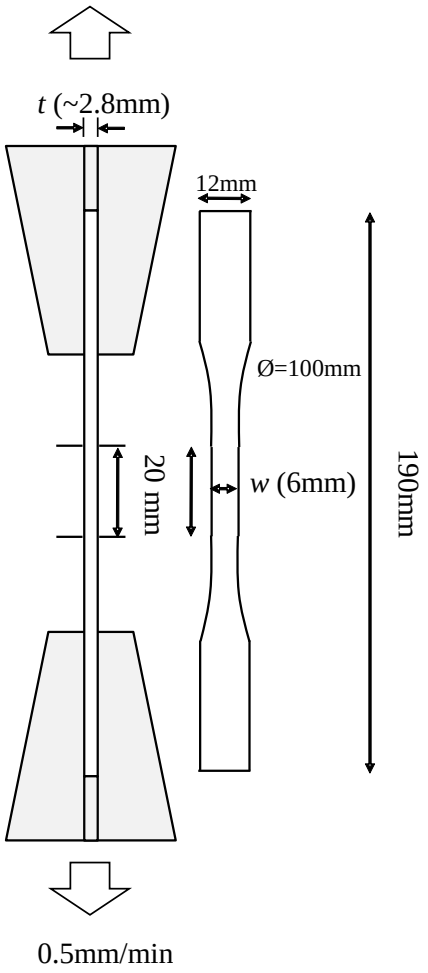

Figure 4.4. Tensile strength parameters adapted from ASTM C1295 for monotonic tensile behaviour of continuous fibre-reinforced advanced ceramics [124].

$$\sigma = \frac{P_{max}}{w\,t} \qquad \textbf{Equation 4.3}$$

Where P_{max} is the maximum load observed during test, w is specimen thickness and t is specimen thickness.

4.3. Microscopy

Non-coated three-point bend specimens were observed using a field emission scanning electron microscope (Hitachi S4000 FEG SEM) operating at 4kV acceleration voltage. Micrographs of the front surface directly beneath the central support roller were compared before and after loading in order to capture composite failure (Figure 4.5). The front surface was wet polished to 3µm.

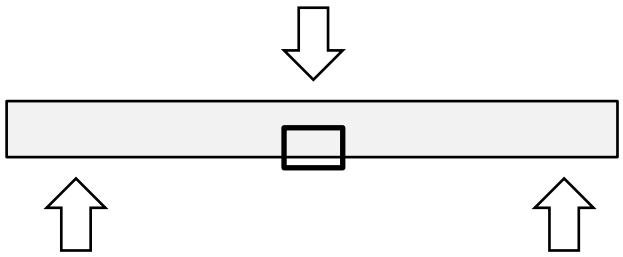

Figure 4.5. Position of SEM micrographs before and after loading in three point bend.

A JEOL 6060 SEM was also used to observe conductive, mounted samples operating at 20kV acceleration voltage. Samples were vacuum impregnated in EpoFix resin (Struers) and wet polished to 3µm. A sputter coater was used to create a conductive gold coating.

4.4. Statistical analysis

Welch's t-test was used to test whether the mean values of two groups are statistically different from each other. Welch's t-test assumes that both groups are sampled from a normal distribution but does not assume that both groups have equal variance. The test statistic, t, was calculated by the difference in the means divided by the standard error of this difference

(Equation 4.4). The degrees of freedom (df) for Welch's test was computed using Equation 4.5 and takes into account the discrepancy between the two standard deviations. Since this calculation usually leads to a value which is not an integer, it is common practice to round down to the next whole number. All tests conducted in this project tested the null hypothesis that both groups are the same (two-tailed). The p-value is the probability of attaining the observed values when the null hypothesis is true and was calculated using statistical software (GraphPad) comparing t and df. A small p value means that the observed difference would occur rarely due to random sampling. The null hypothesis was rejected when $p<0.05$.

$$t = \frac{\chi_1 - \chi_2}{\sqrt{\frac{s_1^2}{n_1} + \frac{s_2^2}{n_2}}}$$ **Equation 4.4**

$$df = \frac{\left[\frac{s_1^2}{n_1} + \frac{s_2^2}{n_2}\right]^2}{\frac{(s_1^2/n_1)^2}{n_1 - 1} + \frac{(s_2^2/n_2)^2}{n_2 - 1}}$$ **Equation 4.5**

Where $\boldsymbol{\chi_1}$ $\boldsymbol{and}$ $\boldsymbol{\chi_2}$ is the mean value of groups 1 and 2, respectively, $\boldsymbol{s_1^2}$ $\boldsymbol{and}$ $\boldsymbol{s_2^2}$ is the variance, and $\boldsymbol{n_1}$ and $\boldsymbol{n_2}$ is the sample size.

Chapter 5 - The effect of three PVA binders on processing and properties of Nextel 720 fibres within an alumina matrix

Polyvinyl alcohol (PVA) has been identified as a suitable temporary binder owing to its water solubility, chemically stability, and good bonding strength. PVA is obtained through saponification of polyvinyl acetate and is commercially available both partially and fully saponified, in both powder and liquid form.

Pre-preg laminates of 120x120mm composed of Nextel 720 fibres within a submicron particle diameter alumina matrix (TM-DAR powder) were produced using three different commercially available PVAs within the polymer binder solution: a partially saponified powder preparation (Gohsenol GL-05, Nippon Gohsei UK Ltd.), a fully saponified powder preparation (Gohsenol NL-05, Nippon Gohsei UK Ltd.) and a partially saponified liquid preparation (Optapix PAF 2, Zschimmer & Schwarz GmbH). Laminates were immersed in deionised water for 5 seconds and left to dry horizontally on wire racks, replicating the reactivation process of manufacturing. The weights of the laminates were noted before immersion, immediately after immersion and at 4 minute intervals until 10wt% water content was achieved. Water content was calculated as a percentage weight increase.

Composites of 11 ply thickness (80x120mm) were manufactured by both the author and Dr E.G. Butler from laminates containing GL-05, NL-05 and PAF 2. Three flat plates were manufactured for each PVA investigated and twelve flexural specimens (6 longitudinal, 6 transverse) were diamond cut from each plate. Specimens were tested in three-point bend using the parameters outlined in section 4.2.1.

5.1. Results

5.1.1. Drying rate

After 5 seconds immersion in deionised water, pre-preg processed using a partially saponified liquid PVA (PAF 2) increased in weight by 19.45% whilst pre-preg processed with a partially saponified powder PVA (GL-05) increased by 20.44% and a fully saponified powder PVA NL-05 increased by 21.54% (Figure 5.1). Laminates were left to partially dry until 10wt% water content was achieved, allowing drying rate to be calculated. Pre-preg processed with NL-05 exhibited a drying rate of 0.19wt% per minute, whilst pre-preg processed with GL-05 exhibited a drying rate of 0.21wt% per minute. Pre-preg processed using PAF 2 exhibited the quickest drying rate of 0.26wt% per minute (Table 5.1).

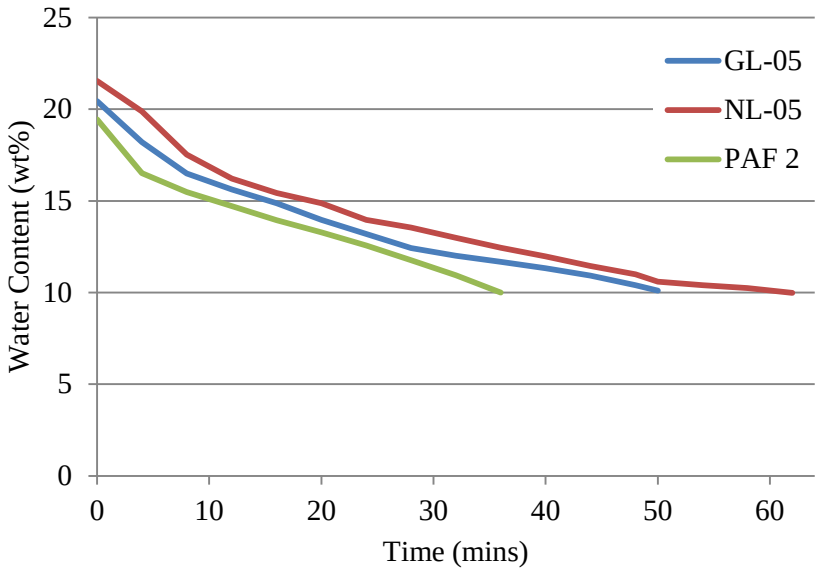

Figure 5.1. Water content by weight increase after 5 seconds immersion in deionised water and at 4 minute intervals during drying for laminates prepared using a partially saponified powder preparation (GL-05), a fully saponified powder preparation (NL-05) and a partially saponified liquid preparation (PAF 2).

Table 5.1. Drying rate calculated for laminates immersed in deionised water for 5 seconds and allowed to partially dry to 10wt% water content.

PVA	Drying Rate (wt% per min)
GL-05	0.21
NL-05	0.19
PAF 2	0.26

5.1.2. Flexural strength

Composite test pieces prepared from a partially saponified powder preparation (GL-05) exhibited a mean flexural strength of 158.6 MPa, whilst those prepared from a partially saponified liquid preparation (PAF 2) exhibited a mean flexural strength of 158.3 MPa. Composite test pieces prepared from a fully saponified powder preparation (NL-05) exhibited a mean flexural strength of 154.0 MPa (Table 5.2, Figure 5.2, Figure 5.3). Standard deviation and interquartile range calculated for NL-05 was substantially larger than both GL-05 and PAF 2 (Figure 5.2, Figure 5.3). Furthermore, frequency histograms illustrating the distribution of data for NL-05 exhibited a random distribution (Figure 5.4), GL-05 displayed a normal distribution with a slight positive (right) skew, and PAF 2 displayed a normal distribution.

Table 5.2. Flexural strength data for composites composed of Nextel 720 fibres within an alumina matrix processed using three commercially available PVAs within the polymer binder solution; GL-05, NL-05 and PAF 2.

PVA	Min.	Q1	Median	Q3 (MPa)	Max.	Mean	St.Dev.	No. Tests
GL-05	91.1	150.9	163.5	167.7	183.4	158.6	18.3	37
NL-05	112.1	122.0	151.4	179.9	223.4	154.0	32.5	35
PAF 2	134.9	149.2	155.3	167.3	201.2	158.3	13.1	84

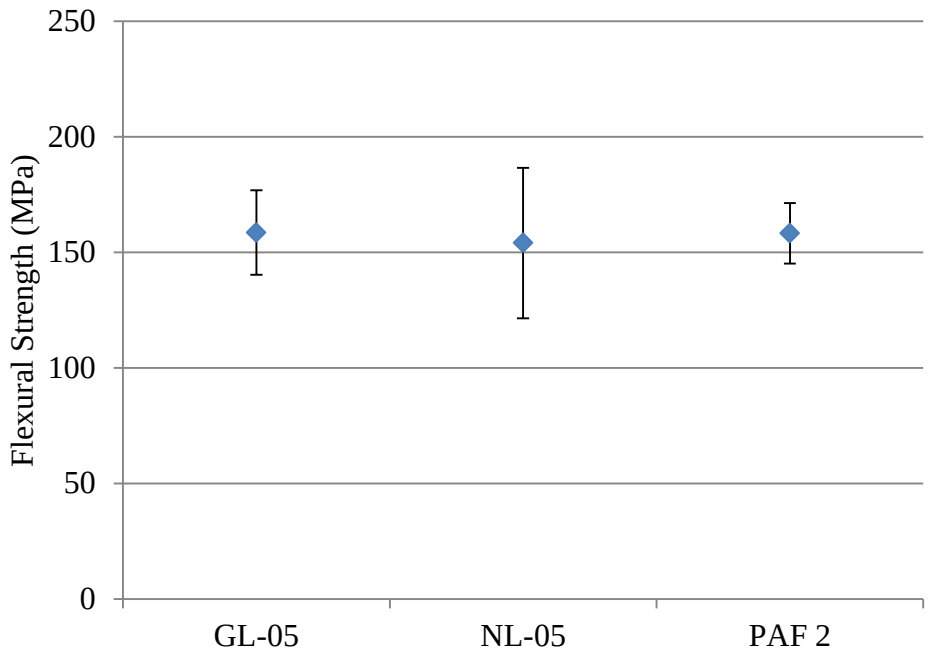

Figure 5.2. Flexural strength data represented by mean and standard deviation for composites processed using three commercially available PVAs within the polymer binder solution; GL-05, NL-05 and PAF 2.

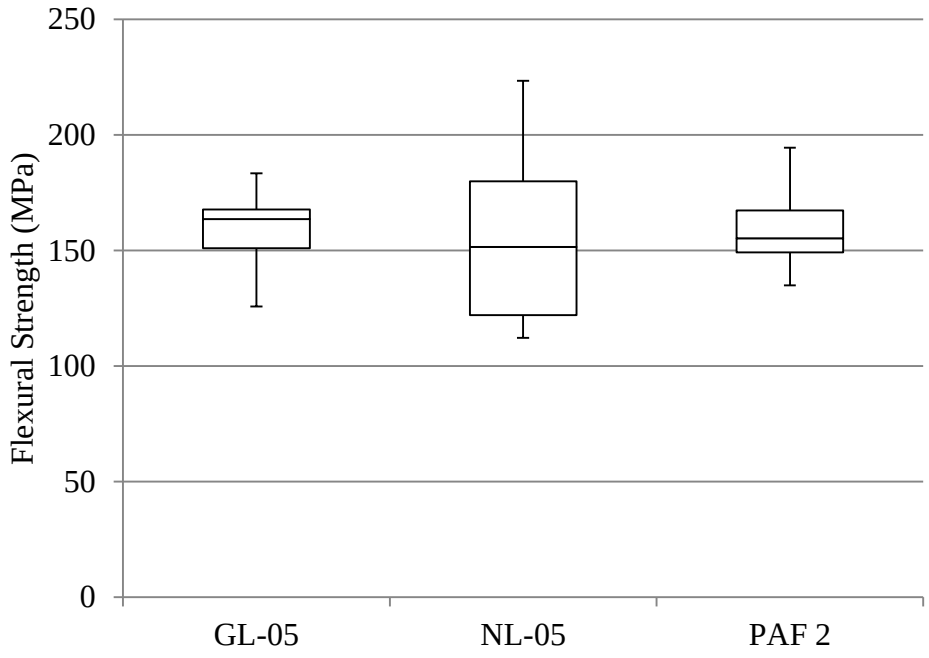

Figure 5.3. Box and whisker diagram comparing flexural strength values for composites prepared using three commercially available PVAs within the polymer binder solution; GL-05, NL-05 and PAF 2.

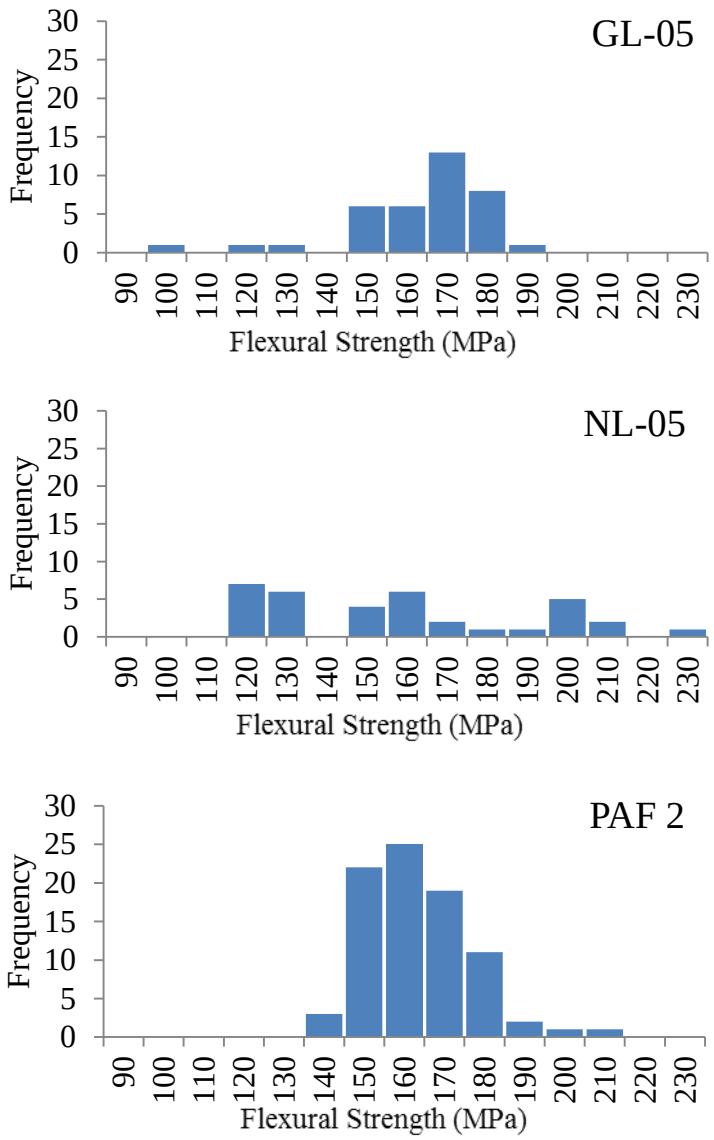

Figure 5.4. Frequency histograms comparing flexural strength values for composites processed using three commercially available PVAs within the polymer binder solution; GL-05, NL-05 and PAF 2.

Welch's t-test was conducted to compare mean flexural strength values obtained for composites processed using GL-05, NL-05 and PAF 2 (Table 5.3). In all circumstances, $p \nless 0.05$ and therefore the results were not statistically significant. These findings suggest that, at the 95% confidence level, the choice of PVA during processing does not affect composite flexural strength.

Table 5.3. Intermediate and p values obtained from Welch's t-test comparing flexural strength values for composites processed using three PVAs; GL-05, NL-05 and PAF 2.

Grp 1	Grp 2	$X_1 - X_2$	95% CI		$\sqrt{\frac{s_1^2}{n_1} + \frac{s_2^2}{n_2}}$	t	df	p
			Min	Max				
GL-05	NL-05	4.51	-8.07	17.10	6.27	0.72	52	0.48
GL-05	PAF 2	0.29	-6.40	6.98	3.33	0.09	52	0.93
NL-05	PAF 2	-4.21	-15.72	7.29	5.68	0.74	38	0.46

The stress-displacement response of specimens loaded in three-point bend was typically linear elastic until peak load was achieved, after which a non-catastrophic mode of failure was observed (Figure 5.5). After initial investigation, it was decided to cease testing after peak load had been achieved.

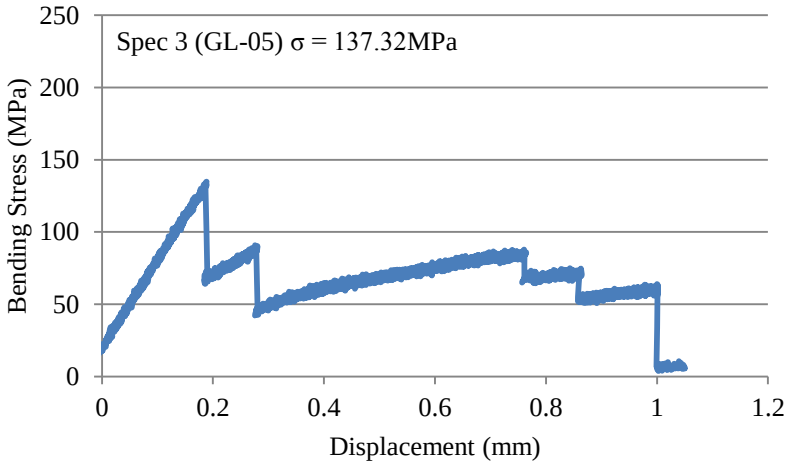

Figure 5.5. Representative stress-displacement curve for specimens composed of Nextel 720 fibres within an alumina matrix prepared with a partially saponified powder preparation, GL-05.

Representative stress-displacement curves for minimum, maximum and average strength values are presented in Figure 5.6 - Figure 5.8 for specimens processed using GL-05, NL-05 and PAF 2. In most cases the stress-displacement response followed the same form; a region of linear elasticity followed by a significant decrease in load bearing capacity. In some cases such as those presented in Figure 5.6 (Specimen 94) and Figure 5.8 (Specimen 150) a region of non-linear behaviour was observed prior to peak load.

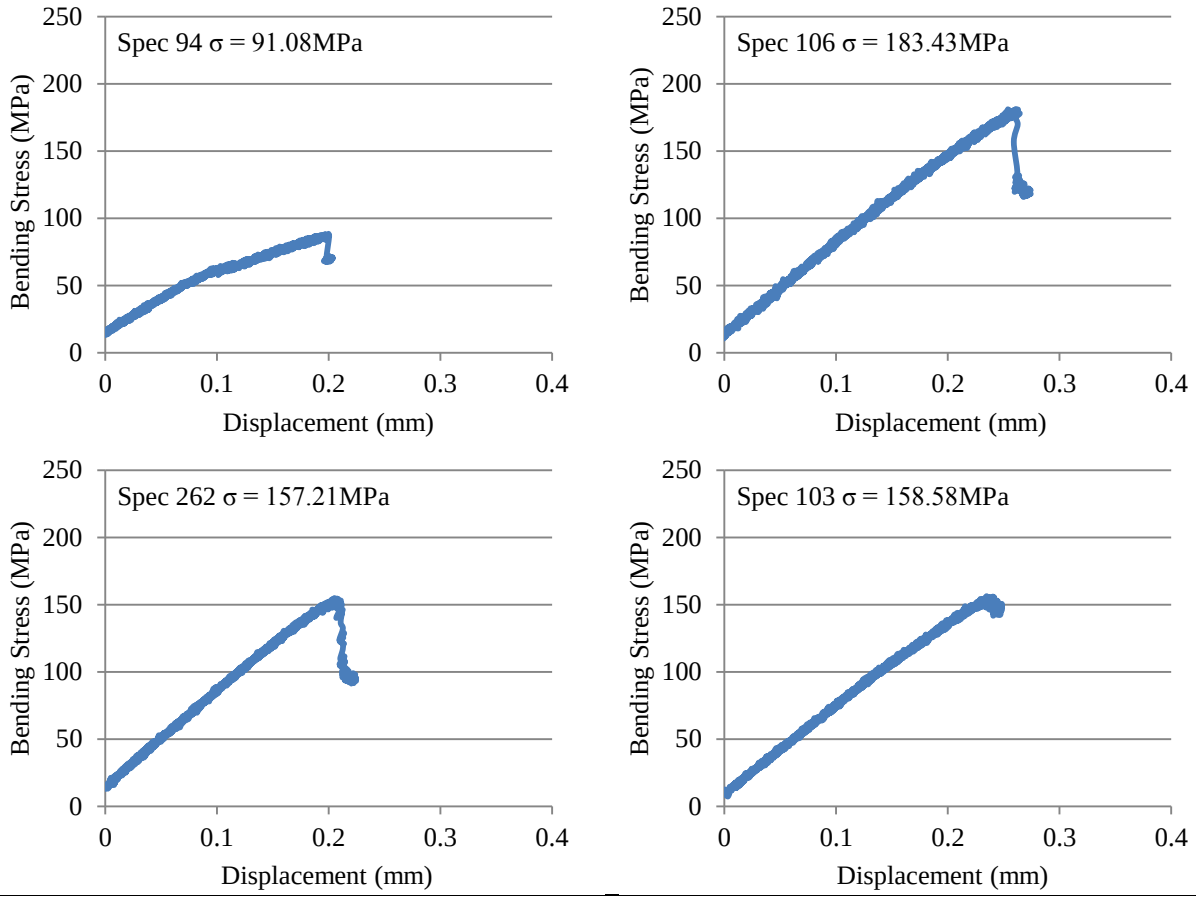

Figure 5.6. Representative stress-displacement curves for specimens composed of Nextel 720 fibres within an alumina matrix prepared with GL-05 showing minimum (Spec 94), maximum (Spec 106) and 2 average strength values (Spec 262 & 103).

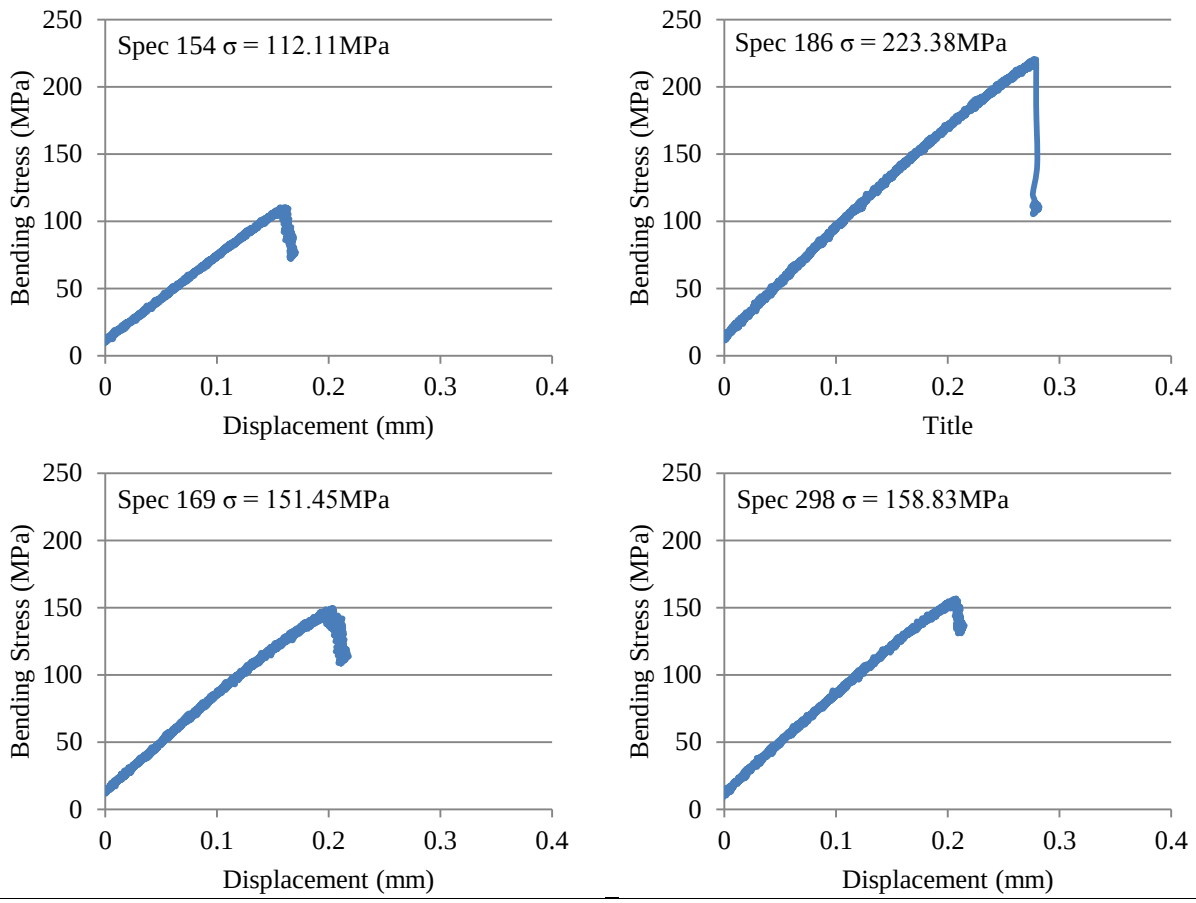

Figure 5.7. Representative stress-displacement curves for specimens composed of Nextel 720 fibres within an alumina matrix prepared with NL-05 showing minimum (Spec 154), maximum (Spec 186) and 2 average strength values (Spec 169 & 298).

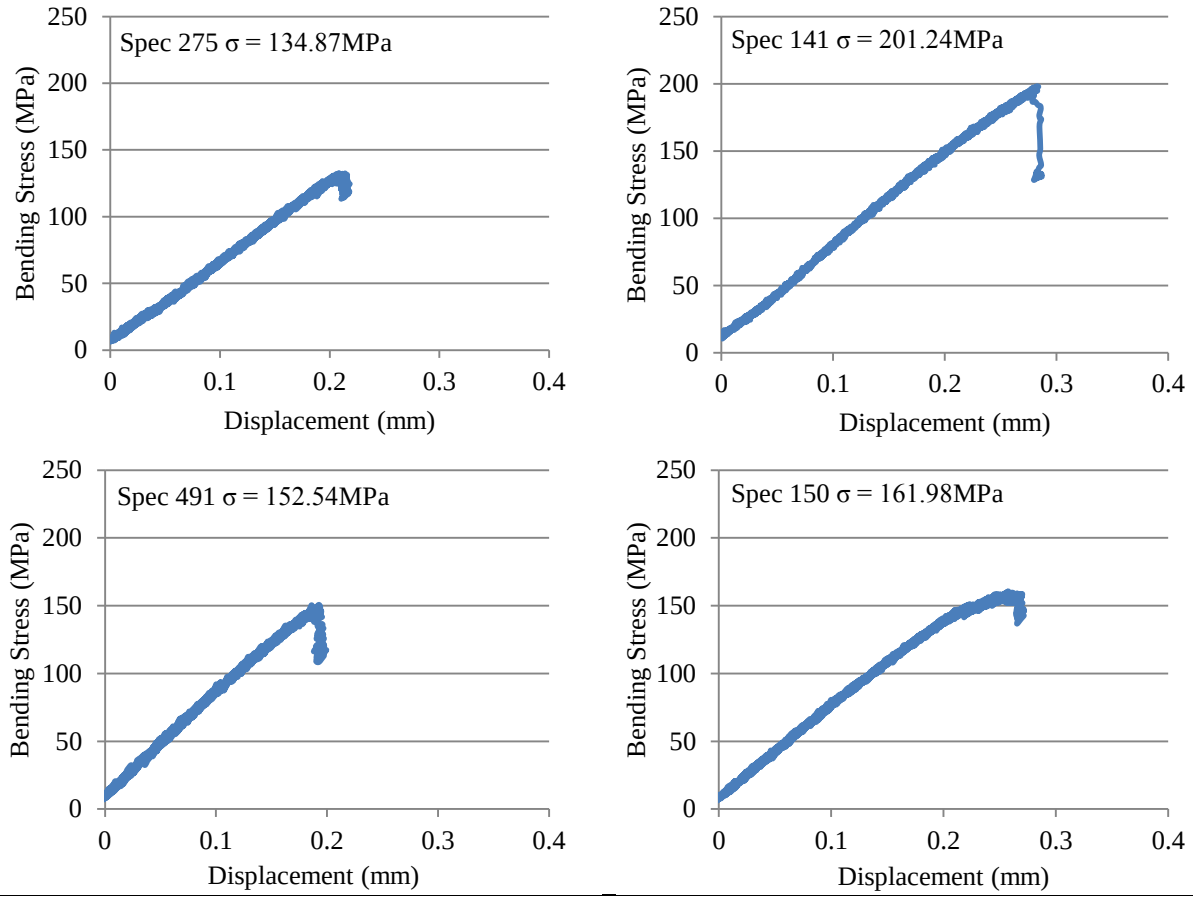

Figure 5.8. Representative stress-displacement curves for specimens composed of Nextel 720 fibres within an alumina matrix prepared with PAF 2 showing minimum (Spec 275), maximum (Spec 141) and 2 average strength values (Spec 491 & 150).

5.2. Discussion

Pre-preg laminates were immersed in deionised water and left to partially dry horizontally on wire racks, replicating the reactivation stage of manufacture. Laminates processed with PAF 2 absorbed the least amount of water during 5 seconds immersion, whilst pre-preg produced from NL-05 absorbed the most amount of water. The degree of saponification is the prime factor that influences the water solubility of PVA [117]. It signifies the number of acetate groups that have been replaced with hydroxyl groups during hydrolysis of polyvinyl acetate to form polyvinyl alcohol. During immersion in water, attractive forces develop between the hydrogen of one electronegative atom (PVA hydroxyl group) and the oxygen of a different electronegative atom (water molecule), allowing the polymer to absorb water. Thus, a fully saponified PVA (NL-05) will be able to form additional hydrogen bonds compared with a partially saponified PVA (GL-05 or PAF 2), owing to a greater number of hydroxyl groups present, and will therefore more readily absorb water. Equally, the more hydrogen bonds that are formed during immersion, the more hydrogen bonds there are to break during drying, resulting in a slower drying rate as suggested in this study. Pre-preg processed with PAF 2 exhibited the fastest drying rate to 10wt% water content suggesting that laminates produced using PAF 2 would have a shorter reactivation time during manufacturing compared with laminates produced using NL-05. It is favourable to decrease reactivation time in order to reduce ‘dead time’ in manufacturing. Nevertheless, it is important to allow the PVA to remoisten and become ‘tacky’, aiding adhesion between plies. Heating pre-preg during reactivation to decrease manufacturing time would therefore not be suitable since plies would dry too quickly and not become tacky, reducing bonding between plies and consequently resulting in delamination after sintering.

Mean flexural strength for composites processed using GL-05, NL-05 and PAF 2 were statistically not different at the 95% confidence level. PVA is a temporary binder, employed to improve strength of the green body prior to sintering and to aid reactivation of dried pre-preg. PVA decomposes during sintering of the composite and provided the furnace temperature is raised slowly, decomposition gases escape through a network of open porosity without causing damage to reinforcing fibres. In-plane properties such as flexural strength are fibre-dominated and therefore minor changes to the matrix properties are not likely to play a significant role in composite strength. The results of this study suggest that neither the level of saponification, nor the physical form of the PVA (powder or liquid) influence mean flexural strength. Nevertheless, flexural strength values obtained for composites processed with NL-05 displayed a substantially larger scatter than those obtained for composites processed with GL-05 and PAF 2, and the data was randomly distributed. Whilst manufacturing inherently results in variability due to the hand lay-up approach, the nature of three-point bend testing in composite materials can also lead to scatter between specimens. When a specimen is loaded in three-point bend, only a small volume of material is subjected to maximum load and therefore the test is sensitive to variation in the material. For example, if a shrinkage crack formed during sintering lies directly beneath the central load where load is most concentrated, the specimen will likely fail prematurely. Similarly, placement of porosity within the matrix could cause similar effect. NL-05 is a fully saponified PVA and therefore requires heating and agitation to aid dissolution. If the PVA was not fully dissolved, it is possible that ‘clumps’ of polymer formed, which subsequently decomposed to form large pores within the matrix during sintering. Further investigation into porosity distribution would be required to confirm this suggestion.

The stress-displacement response was typically linear elastic until peak load was achieved, after which a non-catastrophic mode of failure was observed. This behaviour was observed for all three PVAs investigated. Damage tolerant behaviour in oxide CMCs is facilitated by a weak, porous matrix. During loading, a series of cracks form in the matrix perpendicular to the load axis. Load is consequently transferred to the reinforcing fibres. Energy absorbing mechanisms such as fibre/matrix debonding and crack deflection allow the fibres to be isolated, impeding crack propagation. Fibre fracture occurs at the onset of peak load. Upon continued loading, cracks must be reinitiated in the matrix, resulting in a non-catastrophic failure as shown in Figure 5.5. In a small number of tests, a region of non-linear behaviour was evident prior to failure, indicating the onset of matrix cracking before composite failure. This is likely caused by the placement of cracks and porosity within the matrix.

Flexural test specimens were diamond cut from composite flat plates orientated in two directions, as illustrated in section 4.1. There was no observed strength difference between the longitudinal and transverse direction in any composite plate tested, and therefore results were combined. Similarly, placement within the composite flat plate (centre specimens compared with edge specimens) did not affect flexural strength.

A number of advantages were observed during manufacturing with the use of PAF 2. Firstly, PAF 2 is a liquid preparation and therefore the polymer binder solution did not require heating to aid dissolution of PVA, such as was necessary for GL-05 and NL-05. Additionally, it was observed that slurry prepared from PAF 2 was more viscous under static conditions but became less viscous under the stress of the roller during impregnation compared with slurry prepared from GL-05 and NL-05. This apparent shear thinning behaviour allowed slurry to infiltrate readily into the fibre weave and remain evenly distributed along the length of the

fabric during vertical drying. Furthermore, the use of PAF 2 reduced reactivation time of pre-preg as shown in section 5.1.1, and plies were seemingly more adhesive therefore aiding consolidation.

Mean flexural strengths of composites manufactured in this investigation of 154-159MPa are substantially lower than values reported in the literature for similar oxide CMCs, highlighting the need to optimise composite processing and/or constituents in order to achieve the objectives of this project. The flexural strength of composites composed of Nextel 720 fibres within an alumina-mullite matrix produced by the pressure infiltration method was reported to be ~210MPa [9], whilst those produced by the VibroIntrusion method exhibited flexural strength of ~172MPa [90].

5.3. Concluding remarks

The use of PAF 2 revealed statistically indifferent mean flexural strength values compared with GL-05 and NL-05. Nonetheless, the use of PAF 2 offers practical advantages over both GL-05 and NL-05 and will therefore be pursued throughout the remainder of the project. Comparison of flexural strength with similar oxide CMCs revealed a need to optimise composite processing and/or constituents in order to achieve the objectives of this project.

Chapter 6 - The effect of aluminium chlorohydrate (ACH) on processing and properties of Nextel 720 fibres within an alumina matrix

The effect of an alumina precursor, aluminium chlorohydrate (ACH), on manufacturing and material properties was explored. ACH is commonly employed as a polymer precursor to strengthen the matrix of composites in the polymer impregnation and pyrolysis method of fabrication [42]. ACH is an organic polymer with the molecular formula $Al_2Cl(OH)_5$. It is a highly concentrated solution of polyaluminium hydroxychloride (23wt% alumina in 50% aqueous solution) which decomposes to form pure alumina (Equation 6.1).

$$Al_2Cl(OH)_5 \rightarrow Al_2O_3 + HCl + 2H_2O \qquad \textbf{Equation 6.1}$$

Composites were manufactured using the process outlined in section 4.1 including two additional stages. Chlorohydrol 50 (Summit Reheis), a 50% solution of aluminium chlorohydrate, was added to slurry after 24 hours ball milling and slurry was ball milled for one further hour. An additional dwell period during sintering was necessary to ensure that residual chloride ions produced in the decomposition of ACH did not react with Nextel 720 reinforcing fibres at high temperatures. Thermogravimetric analysis provided by Dr Butler revealed that decomposition of ACH was complete by 800°C (Figure 6.1) and therefore a dwell period for 5 hours at this temperature was included to ensure the dissipation of chloride ions.

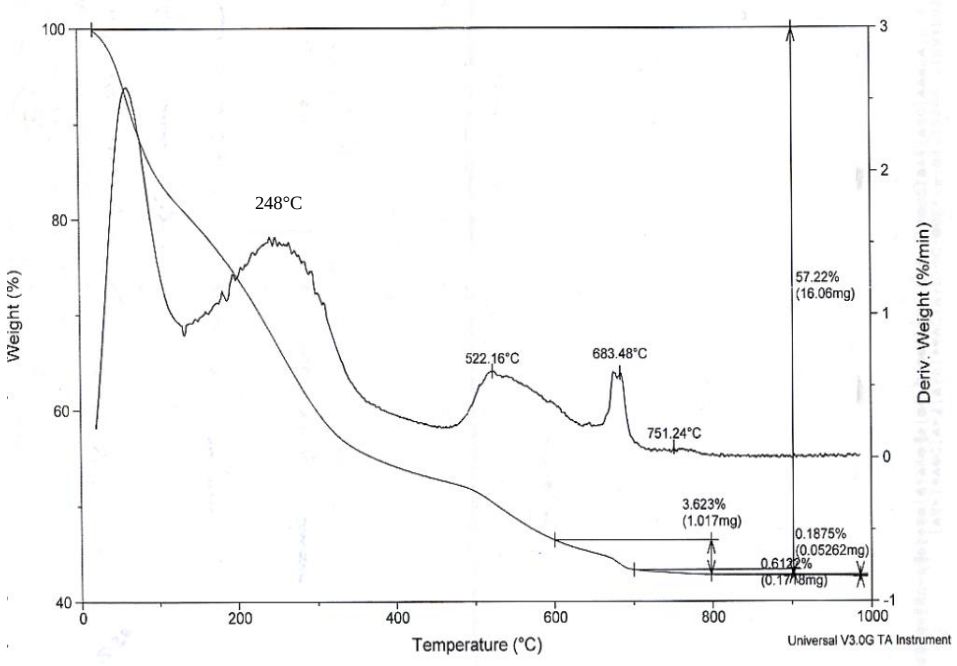

Figure 6.1. Thermogravimetric analysis of Chlorohydrol 50 (Summit Reheis), a 50% solution of aluminium chlorohydrate (courtesy of Dr E.G. Butler).

Composite flat plates of 11 ply thickness (80x150mm) were manufactured by both the author and Dr E.G. Butler with 0-20% additions of Chlorohydrol 50 (ACH) by weight of alumina powder. Twelve flexural (6 longitudinal, 6 transverse) and eight shear (4 longitudinal, 4 transverse) specimens were diamond cut from each plate. Specimens were tested in both three-point bend and short beam shear using the parameters outlined in sections 4.2.1. and 0. Dog-bone specimens containing 10wt% ACH were loaded in monotonic tension using the parameters outlined in section 4.2.3. Non-coated flexural and tensile specimens were observed using a field emission scanning electron microscope (FEG SEM) operating at 4kV acceleration voltage.

6.1. Results

6.1.1. Flexural strength

Composite test pieces processed without ACH (0%) exhibited a mean flexural strength of 158.3MPa (previously denoted PAF 2). Mean flexural strength increased to >200MPa for specimens containing 7-15wt% ACH. Composite test pieces containing 20wt% ACH exhibited a mean flexural strength of 158.6MPa. Standard deviation ranged from 8.4MPa for specimens containing 12wt% ACH to 25.8MPa for specimens containing 2wt% ACH (Table 6.1, Figure 6.2). 12wt% ACH exhibited the smallest interquartile range, whilst 2wt% ACH exhibited the largest (Figure 6.3). Frequency histograms illustrating the distribution of data revealed that composites manufactured with 0, 2 and 5wt% ACH demonstrated a slight positive skew, whilst composites manufactured with 12 and 15wt% ACH demonstrated a slight negative skew. Composites manufactured with 7 and 10wt% ACH exhibited a normal distribution (Figure 6.4).

Table 6.1. Flexural strength data for composites composed of Nextel 720 fibres within an alumina matrix containing 0-20wt% aluminium chlorohydrate (ACH).

% ACH	Min.	Q1	Median	Q3 (MPa)	Max.	Mean	St. Dev	No. Tests
0	134.9	149.2	155.3	167.3	201.2	158.3	13.1	84
2	138.3	156.9	177.9	201.4	227.2	179.6	25.8	66
5	146.9	171.0	185.3	210.3	241.9	190.0	23.7	146
7	176.7	204.0	211.8	218.9	242.0	211.7	11.8	68
10	162.4	191.6	205.8	219.8	251.3	205.3	20.4	138
12	178.5	199.7	206.2	208.9	217.4	204.9	8.4	24
15	143.5	188.9	210.8	223.5	240.1	206.9	22.2	83
20	116.4	148.5	163.9	174.6	184.8	158.6	22.6	13

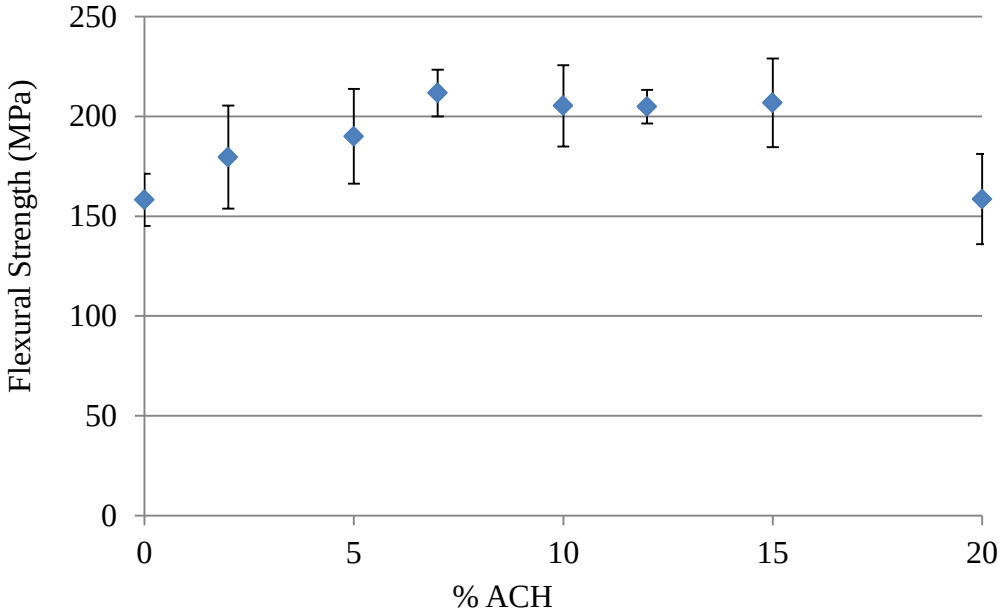

Figure 6.2. Flexural strength values illustrated by mean and standard deviation for composites composed of Nextel 720 fibres within an alumina matrix containing 0-20wt% aluminium chlorohydrate.

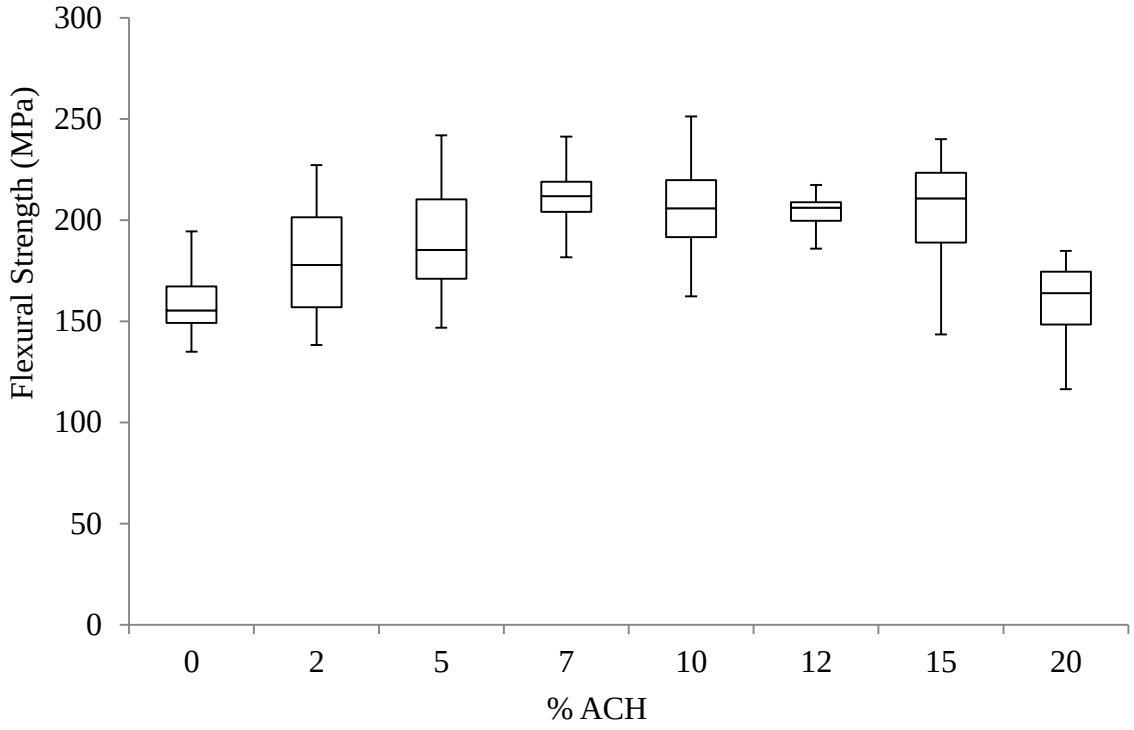

Figure 6.3. Box and whisker diagram comparing flexural strength values for specimens composed of Nextel 720 fibres within an alumina matrix containing 0-20wt% aluminium chlorohydrate (ACH) (whiskers represent ±1.5 x interquartile range).

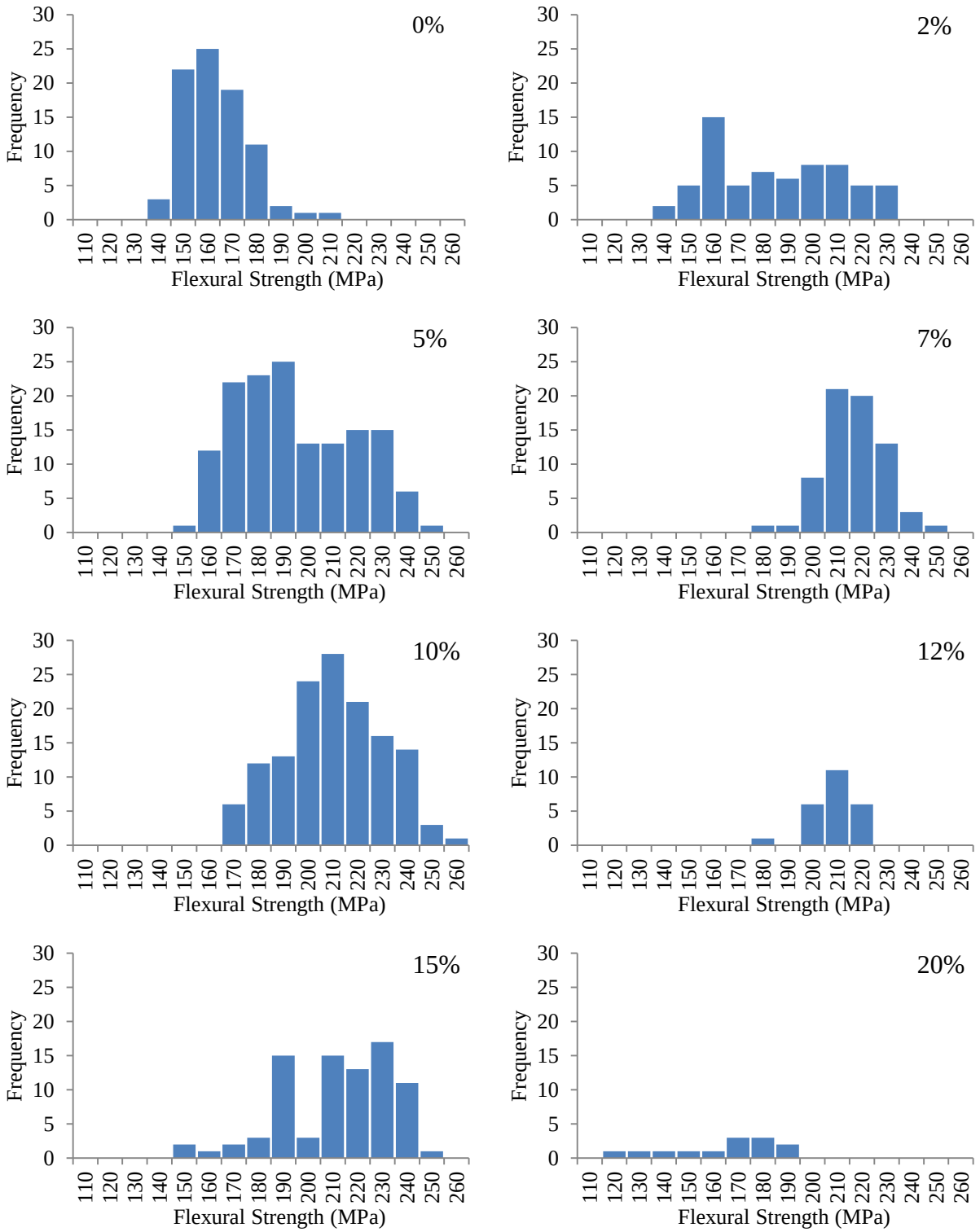

Figure 6.4. Frequency histograms comparing flexural strength values for composites composed of Nextel 720 fibres within an alumina matrix containing 0-20wt% aluminium chlorohydrate (ACH).

Welch's t-test was conducted to compare mean flexural strength values obtained for composites containing 0-20wt% additions of aluminium chlorohydrate (Table 6.2). The findings suggest that, at the 95% confidence level, mean flexural strength of specimens containing 2, 5, 7, 10, 12 and 15wt% ACH differs significantly ($p<0.05$) from flexural strength of specimens not containing ACH (0%). On the contrary, the results suggest that mean flexural strength of 20wt% ACH is not statistically different from 0% ACH ($p>0.05$). Mean flexural strengths of 7, 10 and 12wt% ACH were found to be not statistically different from 15wt% ACH, and 10wt% ACH was found to be not statistically different from 12wt% ACH.

Table 6.2. Intermediate and p values obtained from Welch's t-test comparing flexural strength values for composites containing 0-20wt% additions of ACH.

Grp 1 (wt% ACH)	Grp 2 (wt% ACH)	$X_1 - X_2$	95% CI		$\sqrt{\frac{s_1^2}{n_1} + \frac{s_2^2}{n_2}}$	t	df	p
			Min	Max				
0	2	-21.30	-28.22	-14.38	3.48	6.11	90	**2.40×10^{-08}**
0	5	-31.78	-36.56	-27.01	2.42	13.11	227	**1.22×10^{-29}**
0	7	-53.45	-57.44	-49.46	2.02	26.47	148	**4.78×10^{-58}**
0	10	-47.06	-51.48	-42.63	2.25	20.96	219	**2.81×10^{-54}**
0	12	-46.67	-51.13	-42.21	2.23	20.94	58	**8.74×10^{-29}**
0	15	-48.60	-54.19	-43.01	2.83	17.20	132	**1.47×10^{-35}**
0	20	-0.32	-14.20	13.55	-0.32	0.05	13	0.96
2	5	-10.48	-17.88	-3.09	3.74	2.81	116	**0.0059**
5	7	-21.66	-26.44	-16.88	2.43	8.93	211	**2.10×10^{-16}**
7	10	6.39	1.96	10.82	2.28	2.84	198	**0.0049**
10	12	0.38	-4.47	5.23	2.44	0.16	80	0.88
7	15	4.84	-0.75	10.44	2.83	1.71	129	0.089
10	15	-1.55	-7.46	4.36	2.99	0.52	161	0.61
12	15	-1.93	-7.84	3.98	2.98	0.65	97	0.52
15	20	48.28	33.96	62.61	6.72	7.18	15	**2.29×10^{-06}**

Representative stress-displacement curves for minimum, maximum and average strength values are presented in Figure 6.5 - Figure 6.12 for specimens containing 0-20wt% ACH. The stress-displacement response of specimens loaded in three-point bend was typically linear elastic until peak load was achieved, after which load bearing capacity decreased significantly. As stated in section 5.1.2, load was removed once maximum load had been achieved. If the test had continued, a non-catastrophic mode of failure would have been evident. A small number of specimens, such as Specimen 618 (Figure 6.6) and Specimen 880 (Figure 6.10) demonstrated a region of linear elasticity followed by non-linear behaviour prior to failure.

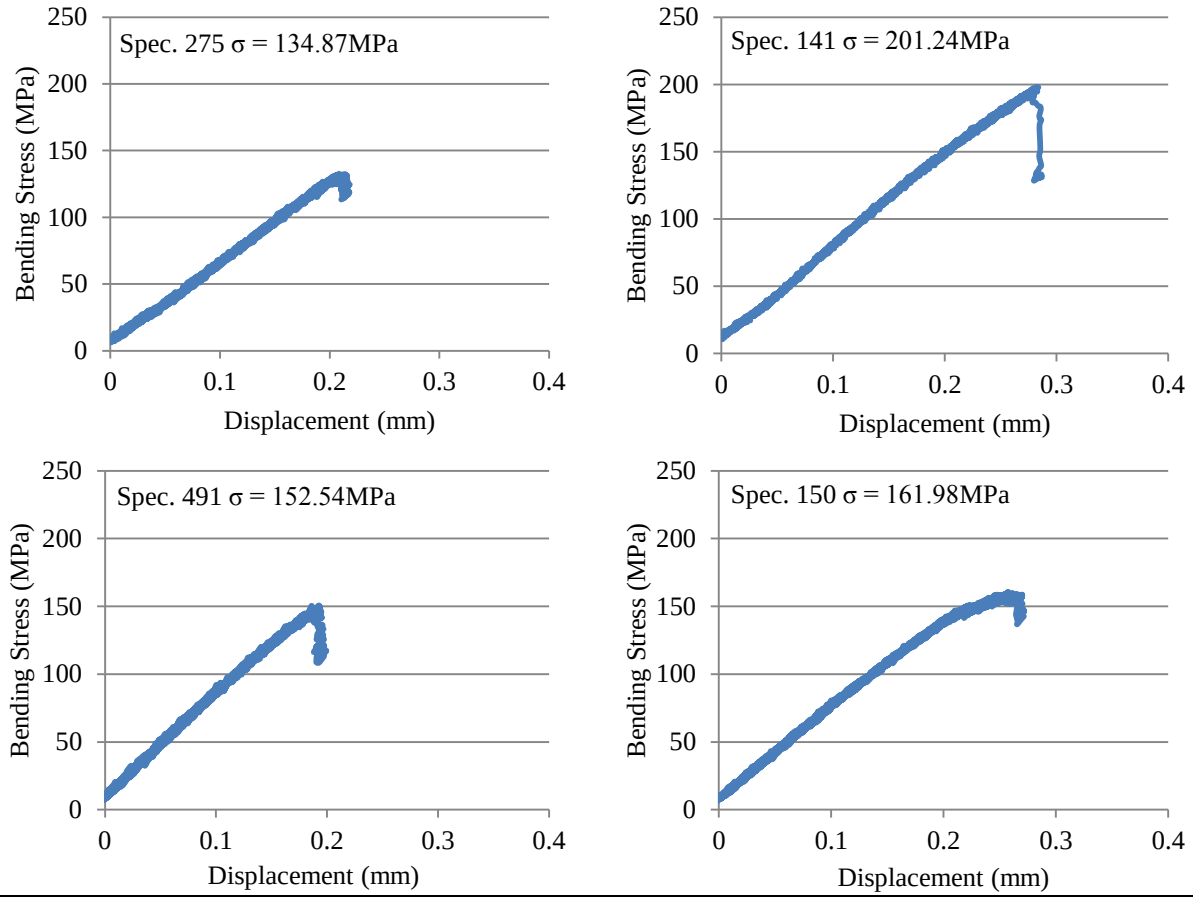

Figure 6.5. Representative stress-displacement curves for specimens composed of Nextel 720 fibres within an alumina matrix without ACH (0%) showing minimum (Spec 275), maximum (Spec 141) and 2 average strength values (Spec 491 & Spec 150).

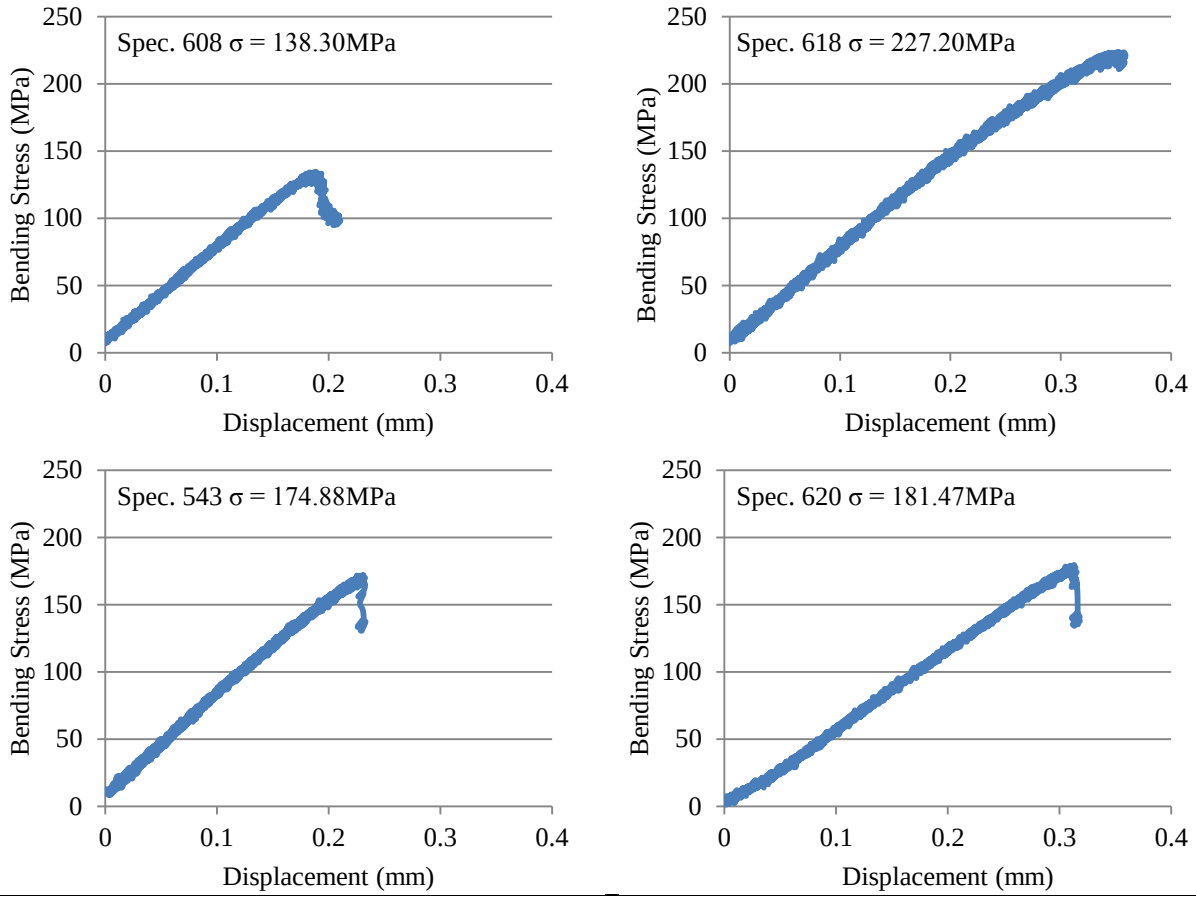

Figure 6.6. Representative stress-displacement curves for specimens composed of Nextel 720 fibres within an alumina matrix with 2% ACH showing minimum (Spec 608), maximum (Spec 618) and 2 average strength values (Spec 543 & Spec 620).

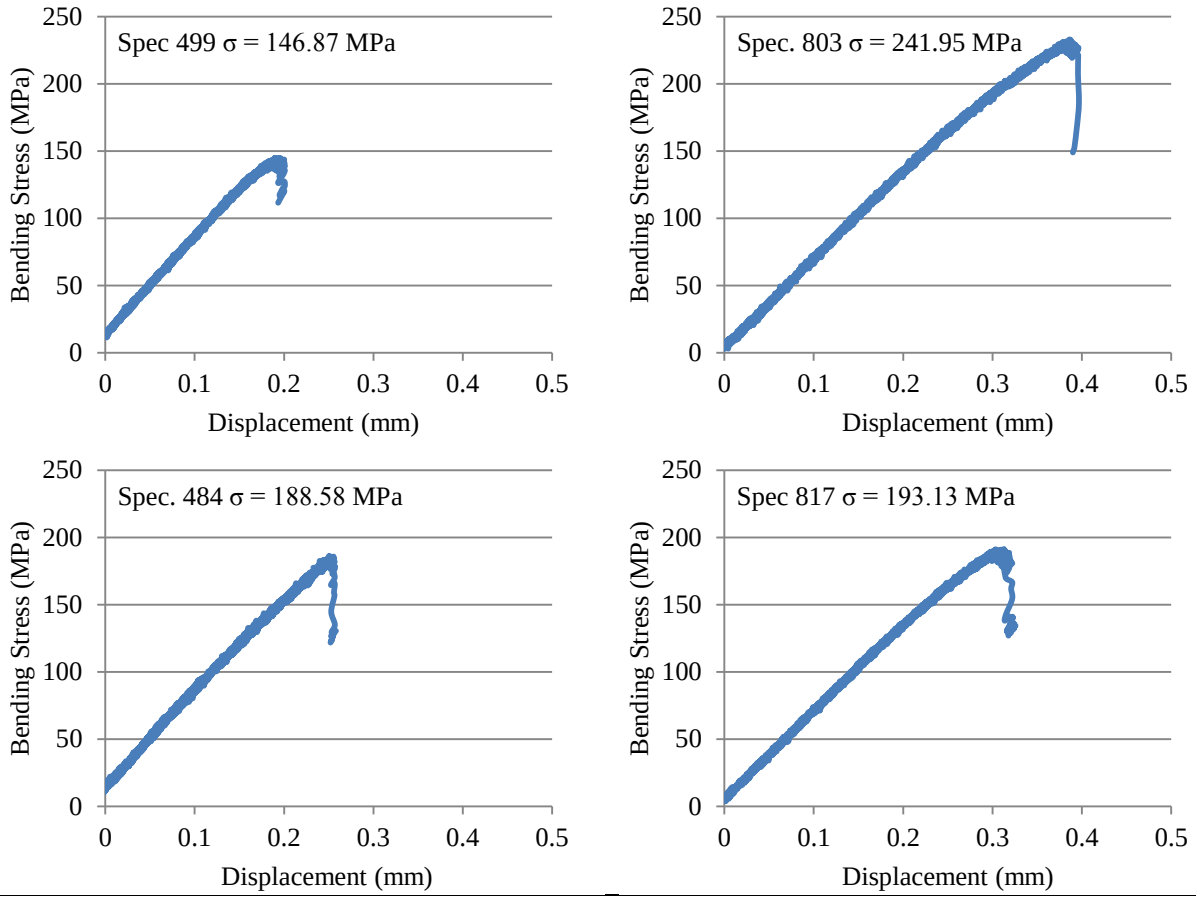

Figure 6.7. Representative stress-displacement curves for specimens composed of Nextel 720 fibres within an alumina matrix with 5% ACH showing minimum (Spec 499), maximum (Spec 803) and 2 average strength values (Spec 484 & Spec 817).

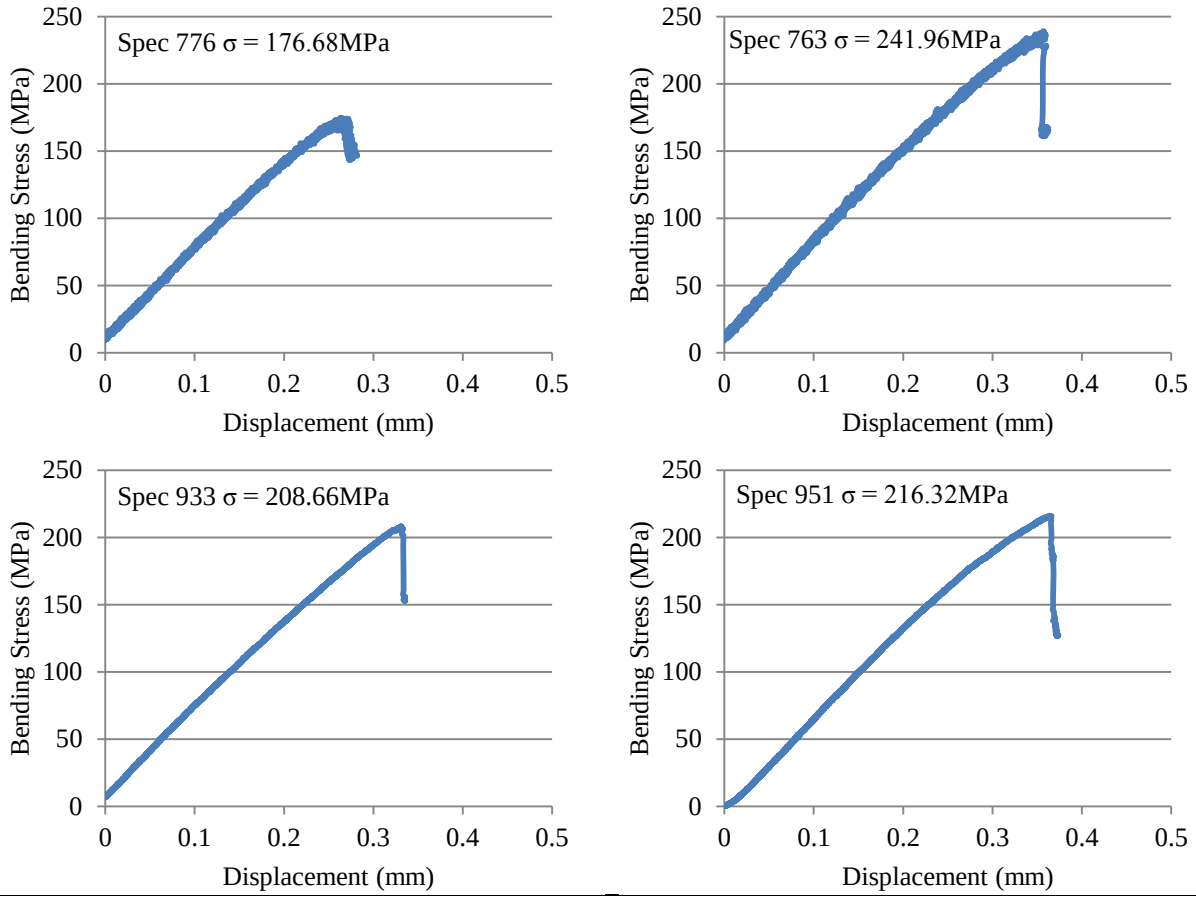

Figure 6.8. Representative stress-displacement curves for specimens composed of Nextel 720 fibres within an alumina matrix with 7% ACH showing minimum (Spec 776,), maximum (Spec 763) and 2 average strength values (Spec 933 & Spec 951).

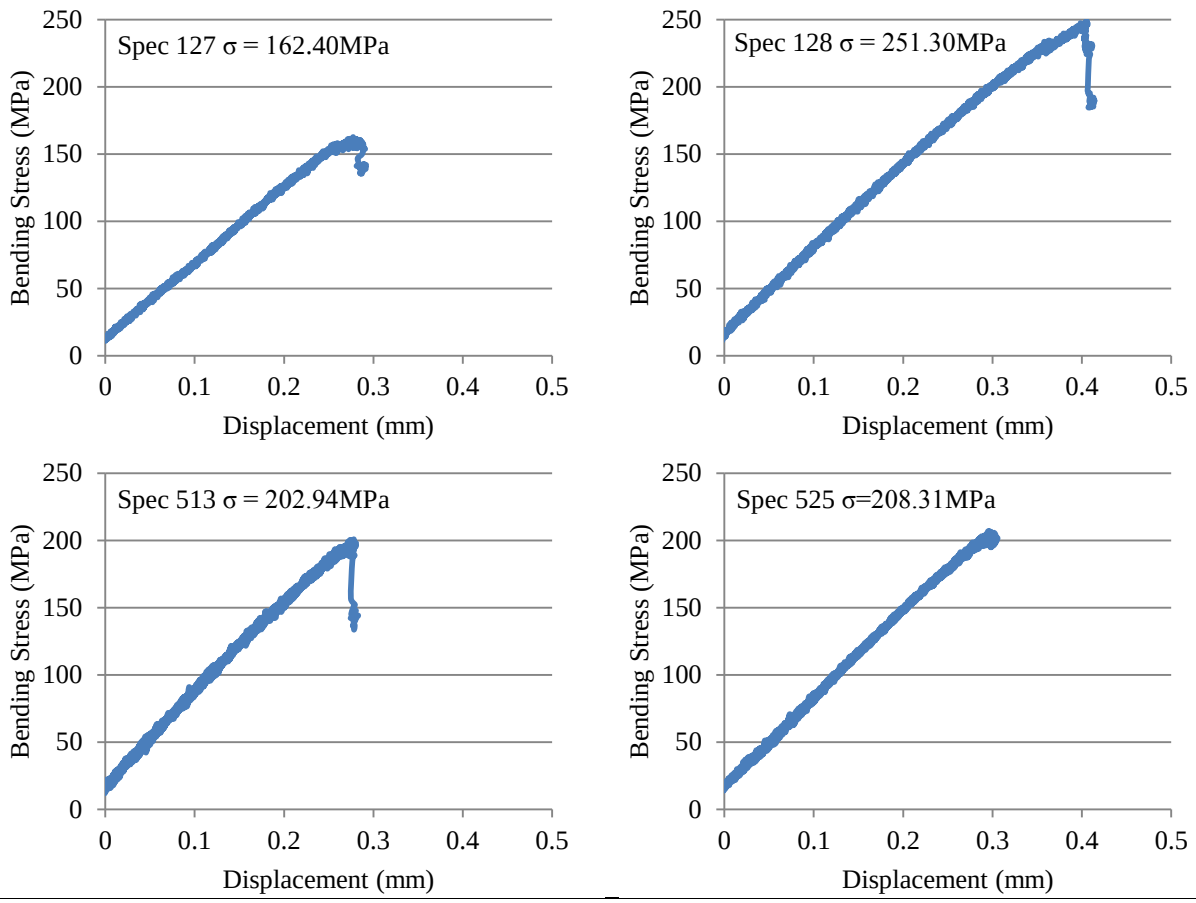

Figure 6.9. Representative stress-displacement curves for specimens composed of Nextel 720 fibres within an alumina matrix with 10% ACH showing minimum (Spec 127,), maximum (Spec 128) and 2 average strength values (Spec 513 & Spec 525).

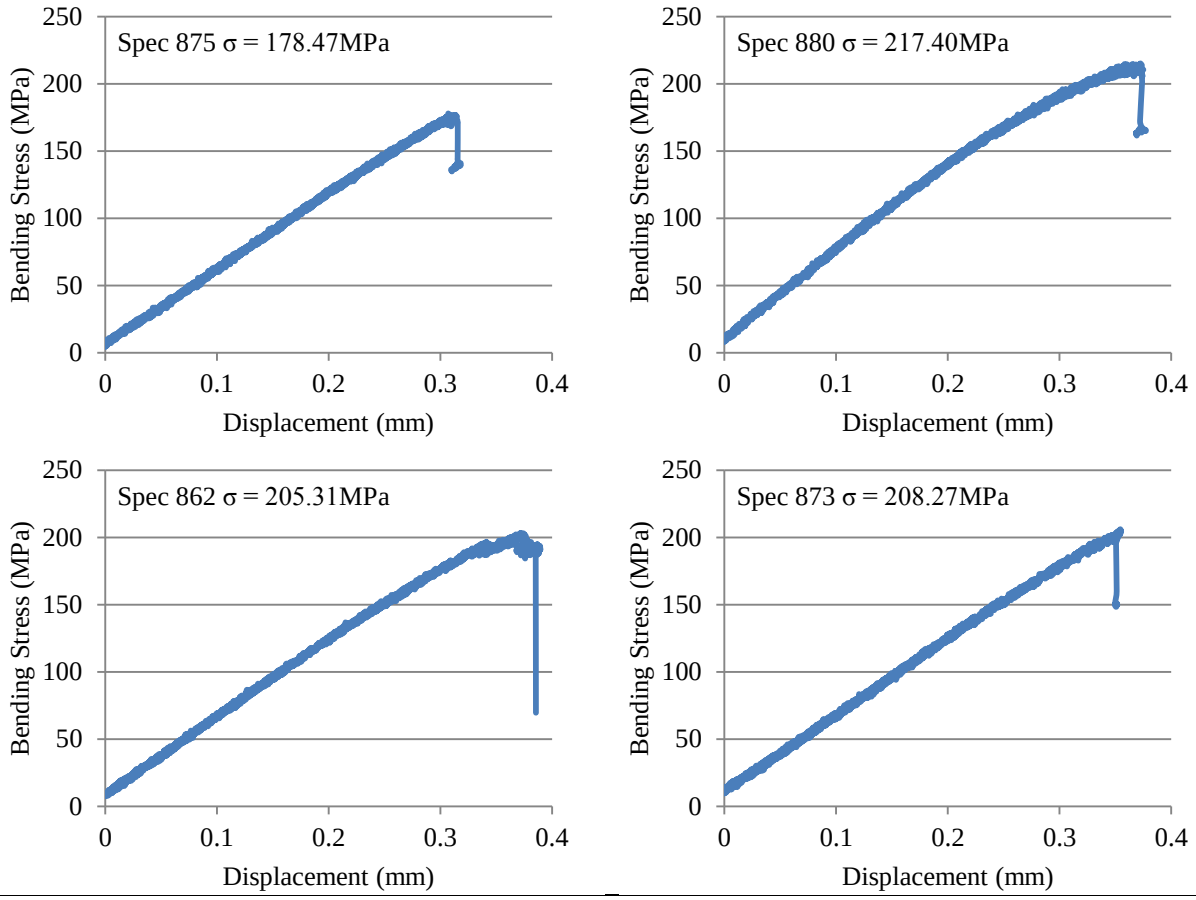

Figure 6.10. Representative stress-displacement curves for specimens composed of Nextel 720 fibres within an alumina matrix with 12% ACH showing minimum (Spec 875,), maximum (Spec 880) and 2 average strength values (Spec 862 & Spec 873).

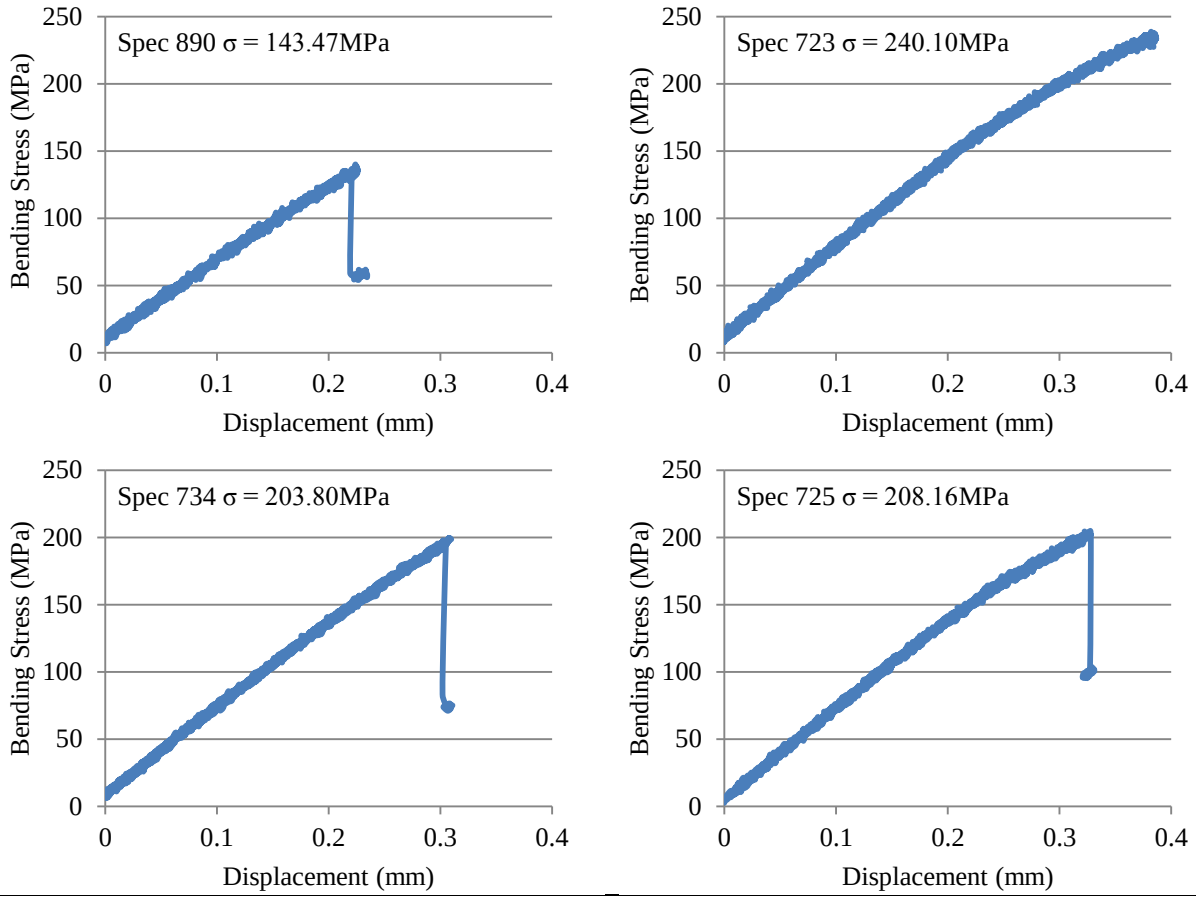

Figure 6.11. Representative stress-displacement curves for specimens composed of Nextel 720 fibres within an alumina matrix with 15% ACH showing minimum (Spec 890), maximum (Spec 723) and 2 average strength values (Spec 734 & Spec 725).

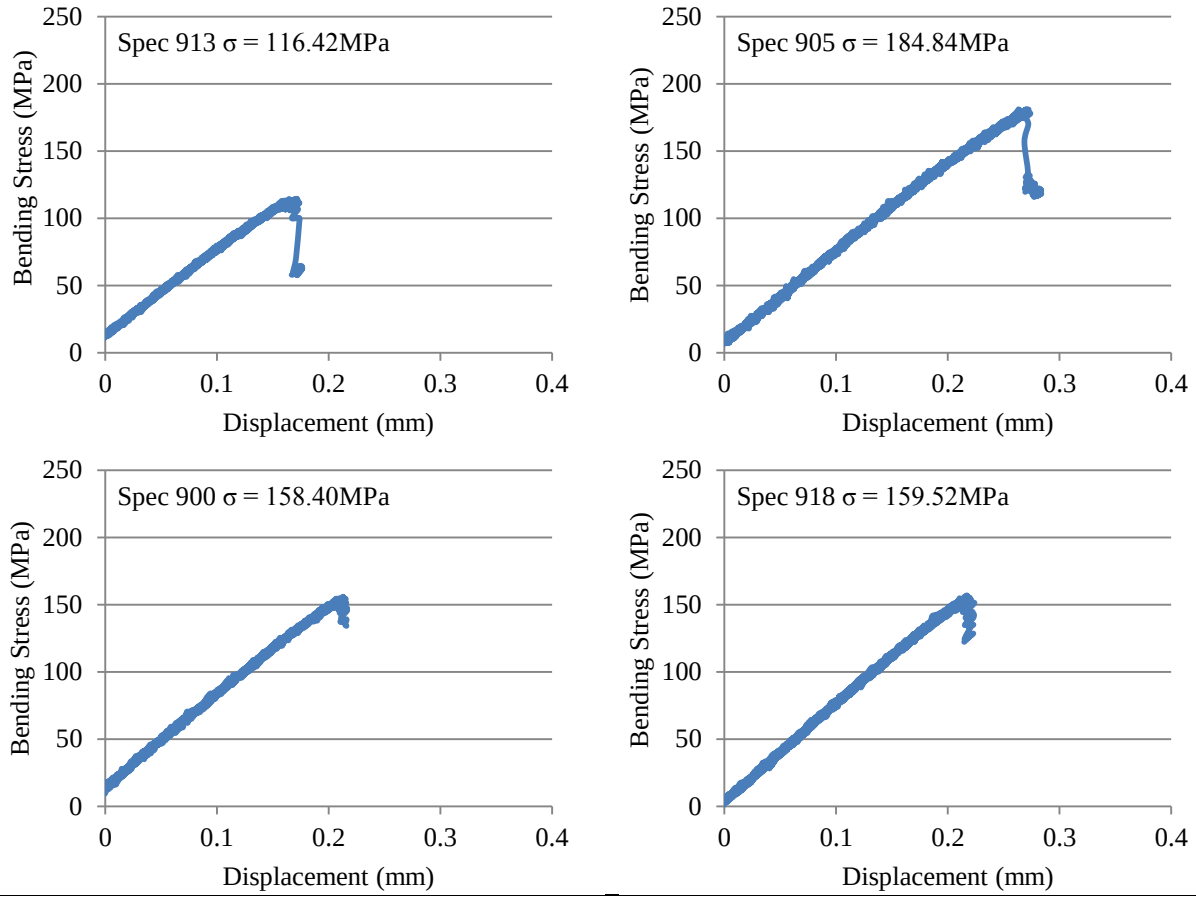

Figure 6.12. Representative stress-displacement curves for specimens composed of Nextel 720 fibres within an alumina matrix with 20% ACH showing minimum (Spec 913), maximum (Spec 905) and 2 average strength values (Spec 900 & Spec 918).

Low magnification SEM micrographs of the in-plane composite structure manufactured with 5wt% ACH prior to testing reveal a two-dimensional fibre weave, demonstrating layers of fibre tows both parallel and perpendicular to the length of the specimen, separated by matrix-rich regions (Figure 6.13 a and c). Fibre tows are seemingly well infiltrated with matrix material, however large-scale pores of irregular size and distribution, and crack-like flaws perpendicular to the fibre layers in matrix-rich regions were observed. SEM observations of Specimen 783 revealed no discernible changes in composite structure before and after testing (Figure 6.13 a compared with b), whilst Specimen 814 demonstrated a slight opening between layers after testing (Figure 6.13 c compared with d). It must be noted that specimens remained intact after testing, owing to termination of the test at the onset of peak load.

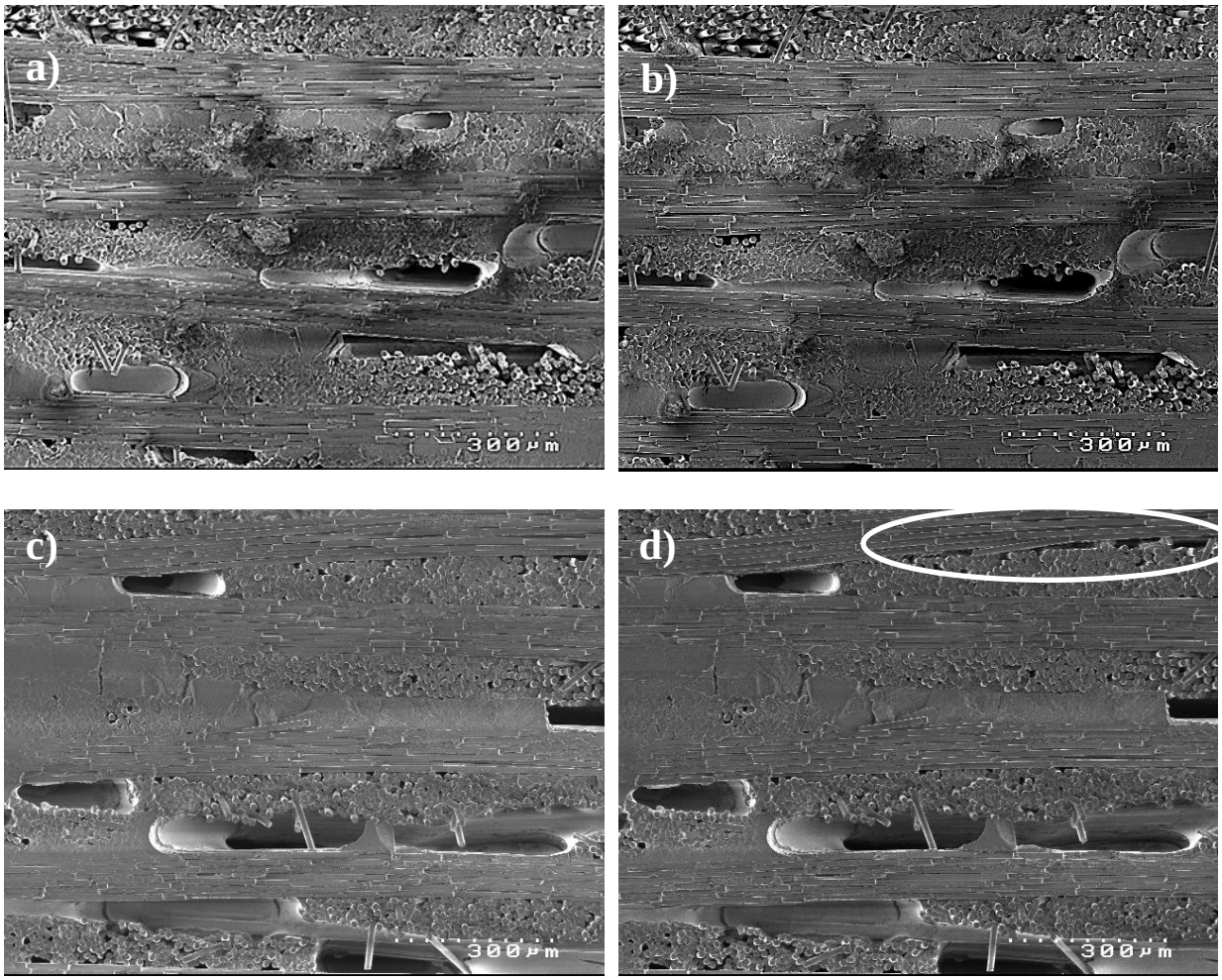

Figure 6.13. SEM micrographs of flexural specimens manufactured with 5wt% ACH. Figures a) & b) Specimen 783 before and after loading, respectively, illustrating no visible change after testing. Figures c) & d) Specimen 814 before and after loading, respectively, illustrating a slight opening between layers.

SEM observations of Specimen 811 (5wt% ACH) at higher magnification revealed fibres both parallel and perpendicular to the front surface of ~12 µm diameter, well infiltrated with matrix material. Figure 6.14 a illustrates a crack propagating through the material, debonding at the fibre/matrix interface, whilst Figure 6.14 b shows a fragment of matrix material bonded to the surface of a fractured fibre.

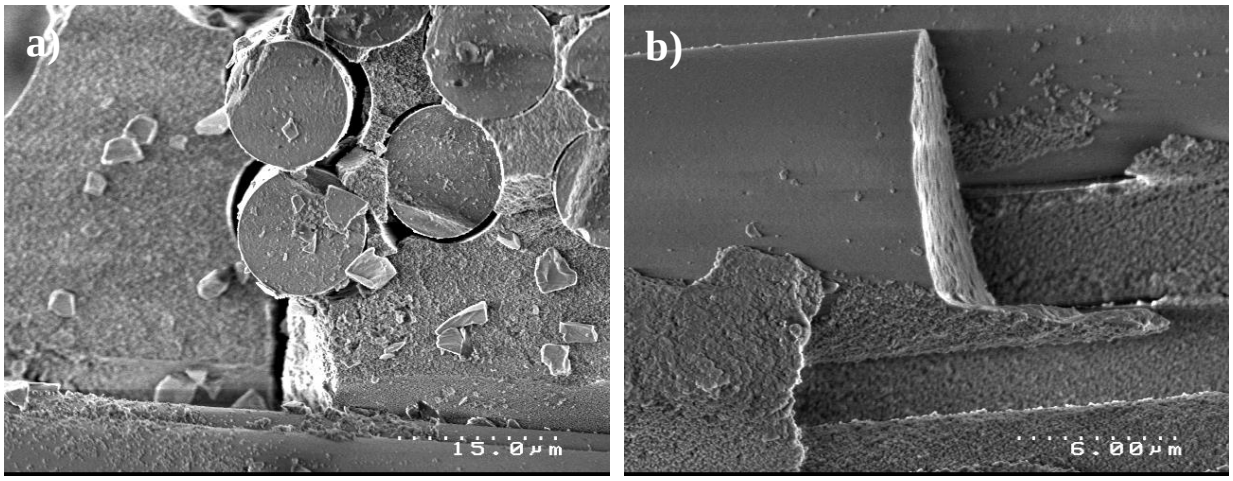

Figure 6.14. SEM observation of fracture surface (Specimen 811, manufactured with 5wt% ACH); a) fibre/matrix debonding as crack propagates through matrix material and b) fibre fracture with matrix bonded to fibre surface.

SEM observations of specimens manufactured with 12wt% ACH revealed an increased number of large-scale pores compared with 5wt% ACH prior to loading. Additionally, fibre tows perpendicular to the length of the specimen were seemingly less well infiltrated (Figure 6.15a). Nevertheless, there were no discernible changes in composite structure after loading in three-point bend (Figure 6.15 a compared with b).

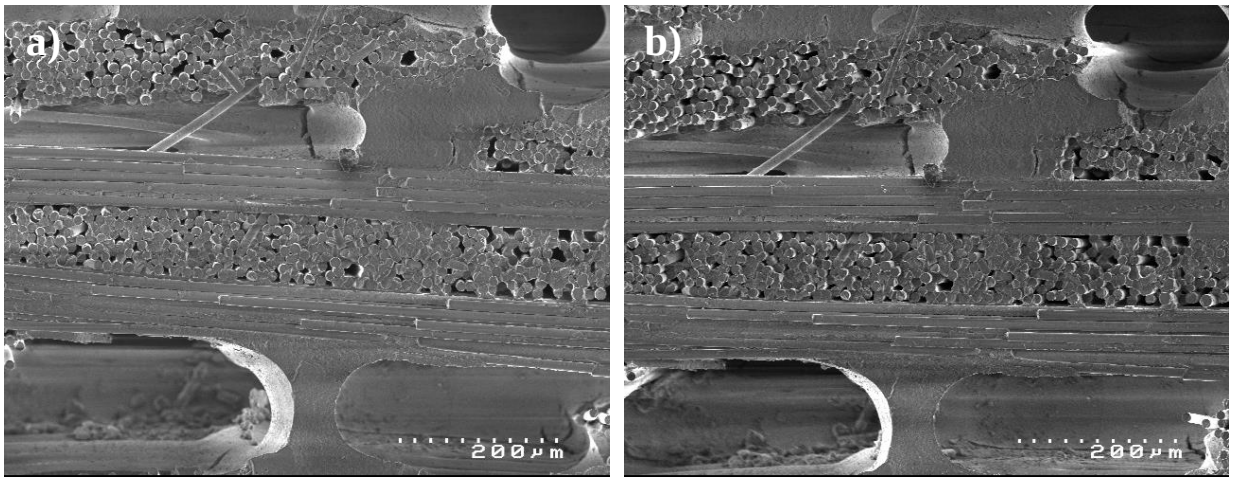

Figure 6.15. SEM micrographs of Specimen 876 manufactured with 12% ACH a) before and b) after loading in three-point bend illustrating no discernible changes in composite structure.

6.1.2. Short beam shear

Composite flat plates containing 5, 7 & 10wt% ACH exhibited mean short beam shear strengths of >12MPa. Specimens containing 12wt% ACH exhibited a mean shear strength of 8.86MPa, whilst 15wt% ACH exhibited a mean shear strength of 10.29MPa. Standard deviation varied from 0.90MPa for 10wt% ACH to 1.39MPa for 5wt% ACH (Table 6.3, Figure 6.16). 12wt% ACH exhibited the largest interquartile range, whilst 10wt% ACH exhibited the smallest interquartile range (Figure 6.17). Frequency histograms illustrating the distribution of data for 5, 7 & 10wt% ACH revealed normal distributions; whilst 12 & 15wt% ACH both demonstrated a slight negative skew (Figure 6.18).

Table 6.3. Short beam shear values for composites composed of Nextel 720 fibres within an alumina matrix containing 5-15wt% aluminium chlorohydrate (ACH).

% ACH	Min.	Q1	Median	Q3	Max.	Mean	St. Dev	No. Tests
				(MPa)				
5	8.57	11.53	12.05	12.83	15.63	12.13	1.39	35
7	10.93	11.92	12.53	13.28	14.60	12.58	0.94	54
10	10.52	11.63	12.06	12.79	13.53	12.10	0.90	14
12	6.56	7.72	8.97	10.12	10.85	8.86	1.37	16
15	6.37	9.81	10.63	11.12	11.95	10.29	1.34	29

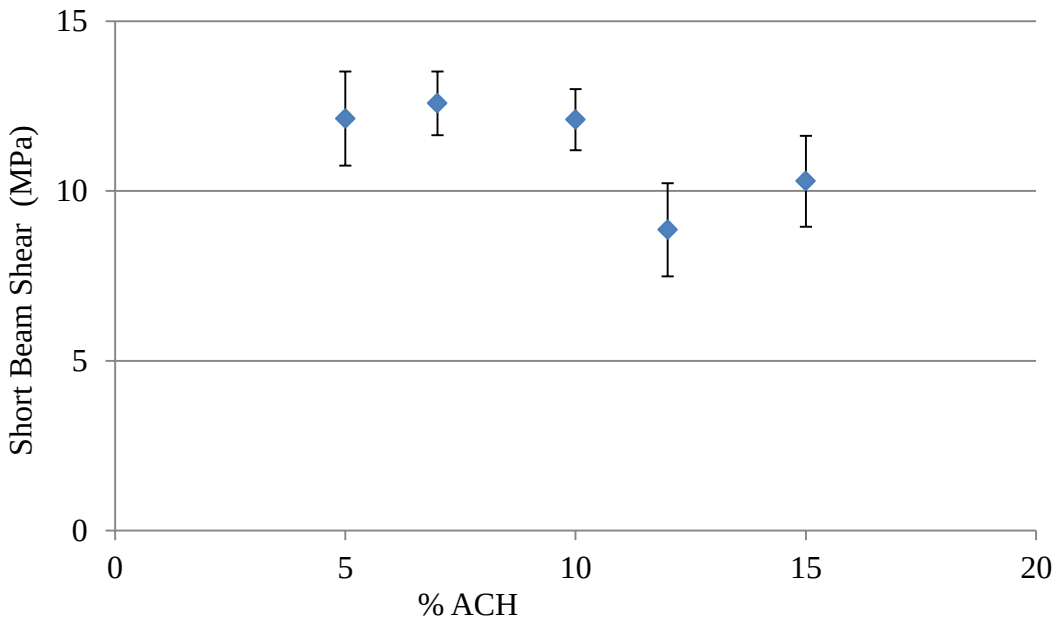

Figure 6.16. Short beam shear values illustrated by mean and standard deviation for composites composed of Nextel 720 fibres within an alumina matrix containing 5-15wt% aluminium chlorohydrate (ACH).

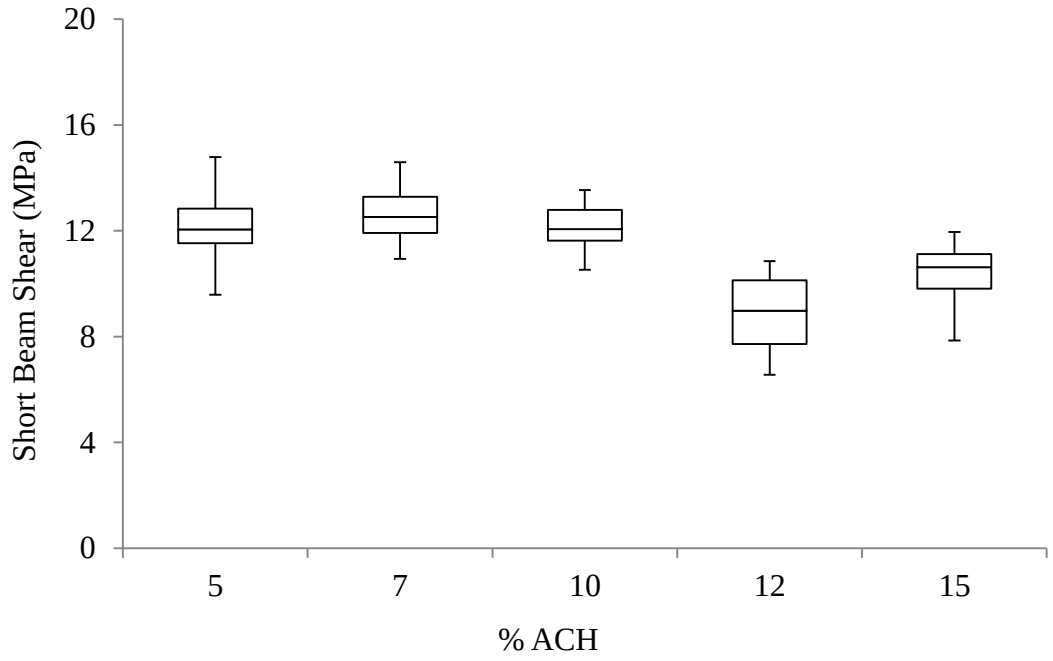

Figure 6.17. Box and whisker diagram comparing short beam shear values for composites composed of Nextel 720 fibres within an alumina matrix containing 5-15wt% aluminium chlorohydrate (ACH).

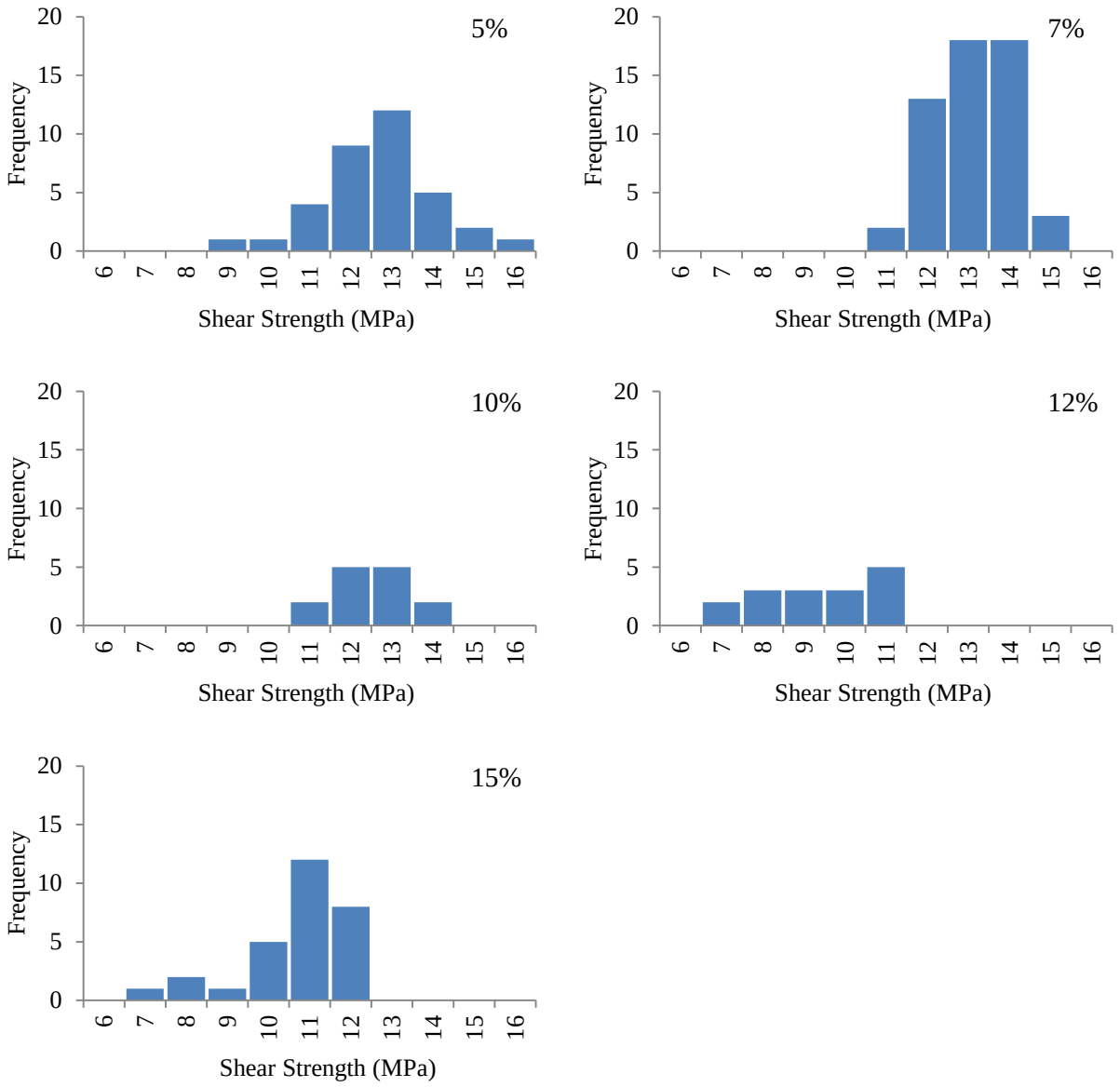

Figure 6.18. Frequency histograms comparing short beam shear values for composites composed of Nextel 720 fibres within an alumina matrix containing 5-15wt% aluminium chlorohydrate (ACH).

Welch's t-test was conducted to compare short beam shear strength values for specimens containing 5-15wt% ACH. Mean short beam shear strengths of specimens manufactured with 7 and 10wt% ACH were statistically not different compared with 5wt% ACH. On the contrary, mean shear strengths of 12 and 15wt% ACH were extremely statistically different from 5wt% ACH. Furthermore, mean shear strength for 10wt% ACH was statistically

different compared with 12wt% ACH, and 12wt% was statistically different from 15wt% ACH.

Table 6.4. Intermediate and p values obtained from Welch's t-test comparing short beam shear values for composites containing 5-15wt% additions of ACH.

Grp 1 (wt% ACH)	Grp 2 (wt% ACH)	$X_1 - X_2$	95% CI Min	95% CI Max	$\sqrt{\frac{s_1^2}{n_1} + \frac{s_2^2}{n_2}}$	t	df	p
5	7	-0.45	-0.99	0.09	0.27	1.69	53	0.098
5	10	0.03	-0.65	0.71	0.34	0.09	36	0.93
5	12	3.28	2.43	4.13	0.42	7.88	29	**9.73×10^{-09}**
5	15	1.84	1.16	2.53	0.34	5.39	60	**1.20×10^{-06}**
7	10	0.48	-0.08	1.05	0.27	1.77	20	0.091
10	12	3.24	2.38	4.10	0.42	7.75	26	**3.16×10^{-08}**
12	15	-1.43	-2.30	-0.57	0.42	3.38	30	**0.002**

6.1.3. Density

The densities of composites containing 0 to 20wt% ACH, as determined by mass/volume calculations, are presented in Figure 6.19. Mean density decreased from 2.65g/cc for composite flat plates manufactured without ACH (0%) to 2.28 g/cc for composites manufactured with 20wt% ACH (Table 6.5). Composites manufactured with 12wt% ACH exhibited the largest standard deviation, whilst 20wt% exhibited the smallest.

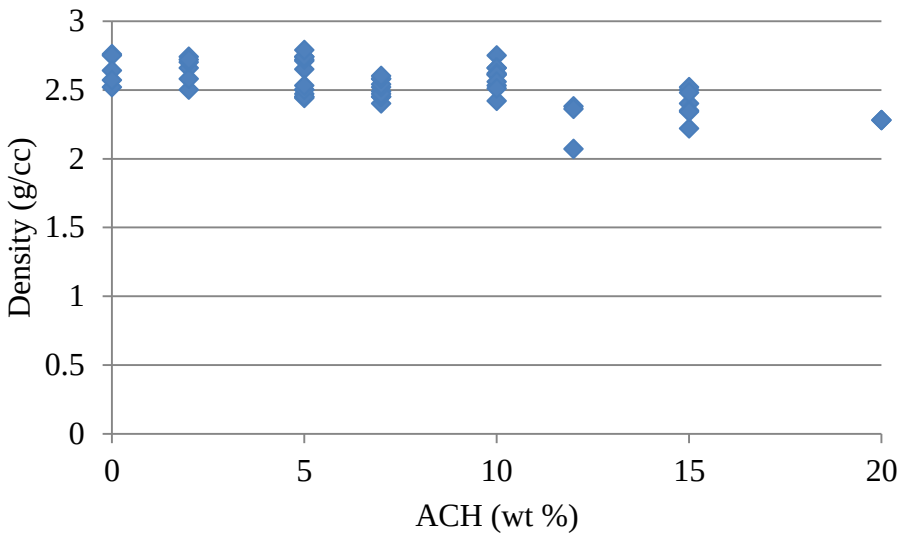

Figure 6.19. Density of composites composed of Nextel 720 fibres within an alumina matrix containing 0-20wt% aluminium chlorohydrate (ACH) (error bars represent ±1 standard deviation).

Table 6.5. Density values for composites composed of Nextel 720 fibres within an alumina matrix containing 0-20wt% aluminium chlorohydrate (ACH).

% ACH	Mean (g/cc)	St. Dev.	No. Plates
0	2.65	0.11	5
2	2.65	0.09	6
5	2.59	0.13	13
7	2.51	0.07	10
10	2.59	0.09	10
12	2.27	0.17	3
15	2.40	0.11	7
20	2.28	0.00	2

Welch's t-test was conducted to compare mean density values obtained for composites manufactured with 0-20wt% additions of ACH. The findings suggest that, at the 95% confidence level, mean densities of composites manufactured with 2, 5 and 10wt% ACH are not statistically significantly different from mean density of composites manufactured without

ACH (0%) ($p>0.05$). Similarly, mean density of composites manufactured with 7, 10 and 12wt% ACH are not statistically significantly different from 5wt% ACH. On the contrary, mean densities of 7, 12, 15 and 20% ACH were statistically different from composites manufactured without ACH (0%) ($p<0.05$), and mean density of 15wt% ACH was statistically significantly different from 5wt% ACH.

Table 6.6. Intermediate and p values obtained from Welch's t-test comparing density values for composites containing 0-20wt% additions of ACH.

Grp 1 (wt% ACH)	Grp 2 (wt% ACH)	$X_1 - X_2$	95% CI		$\sqrt{\frac{s_1^2}{n_1} + \frac{s_2^2}{n_2}}$	t	df	p
			Min	Max				
0	2	-0.002	-0.14	0.14	0.061	0.033	8	0.975
0	5	0.057	-0.08	0.19	0.060	0.934	9	0.374
0	7	0.140	0.01	0.27	0.052	2.684	5	**0.039**
0	10	0.550	-0.08	0.19	0.056	0.983	7	0.358
0	12	0.378	-0.10	0.86	0.111	3.407	2	**0.044**
0	15	0.247	0.10	0.39	0.063	3.936	8	**0.004**
0	20	0.368	0.24	0.50	0.048	7.717	4	**0.002**
5	7	0.084	-0.01	0.17	0.043	1.953	18	0.067
5	10	-0.001	-0.10	0.10	0.047	0.031	20	0.976
5	12	0.322	-0.14	0.78	0.107	3.009	2	0.095
5	15	0.190	0.07	0.31	0.055	3.452	15	**0.004**

6.1.4. Tensile strength

Six dog-bone specimens containing 10wt% ACH loaded in monotonic tension exhibited a mean tensile strength of 146.95 MPa, with a standard deviation of 4.94 MPa (Table 6.7). Stress-strain curves presented for specimens that failed within the gage section revealed evidence of slipping within the grips (Figure 6.20). After a brief period of linearity, the stress-strain response was typically non-linear to failure. SEM observations revealed a non-catastrophic, brushy fracture surface with evidence of a strong fibre/matrix bond.

Table 6.7. Tensile strength data for composites composed of Nextel 720 fibres within an alumina matrix containing 10wt% aluminium chlorohydrate (ACH).

Specimen No.	Tensile Strength (MPa)	Observations
1	150.41	Failure below gage section
2	146.07	Failure above gage section
3	153.02	Failure within gage section
4	138.59	Failure within gage section
5	145.75	Failure above gage section
6	147.88	Failure within gage section
Mean	**146.95**	
St. Dev.	**4.94**	

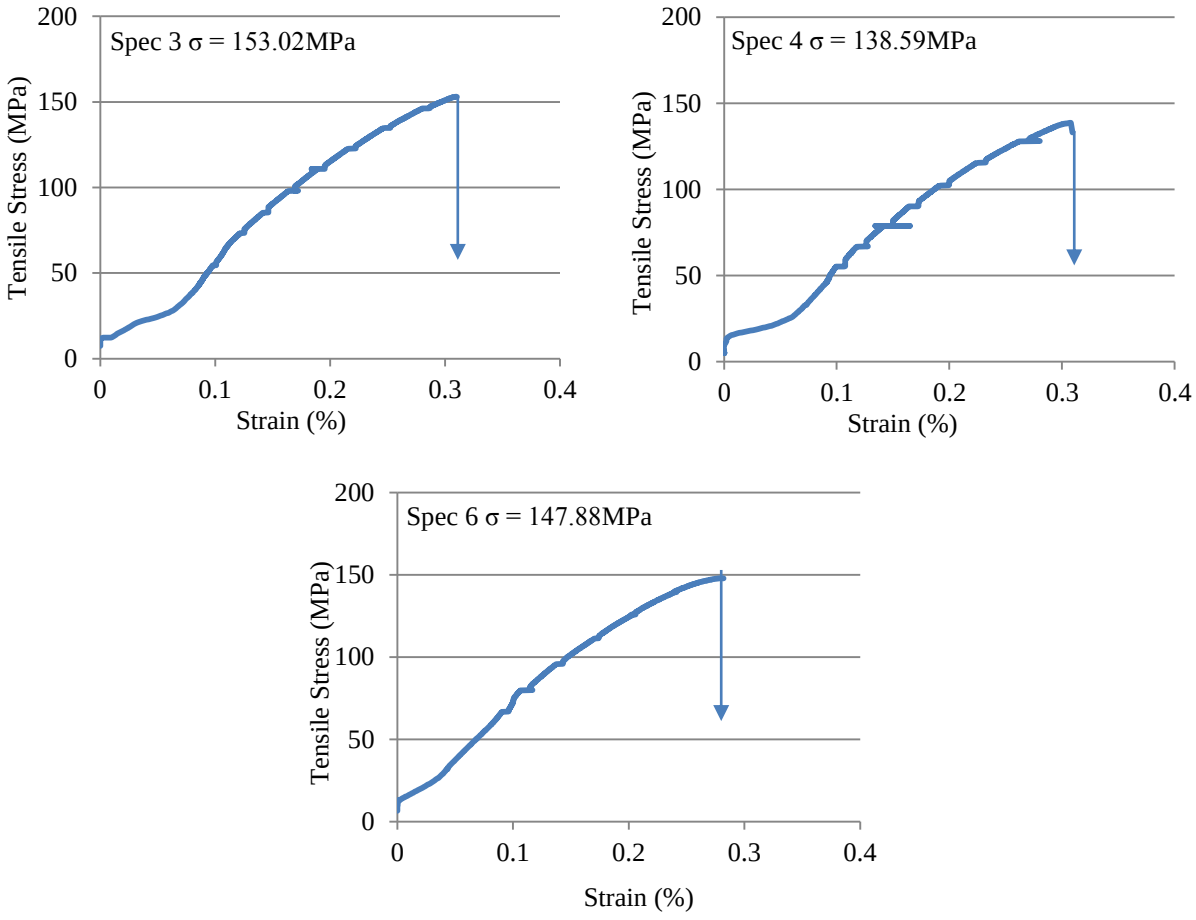

Figure 6.20. Stress-strain curves for specimens composed of Nextel 720 fibres within an alumina matrix containing 10wt% ACH loaded in monotonic tension.

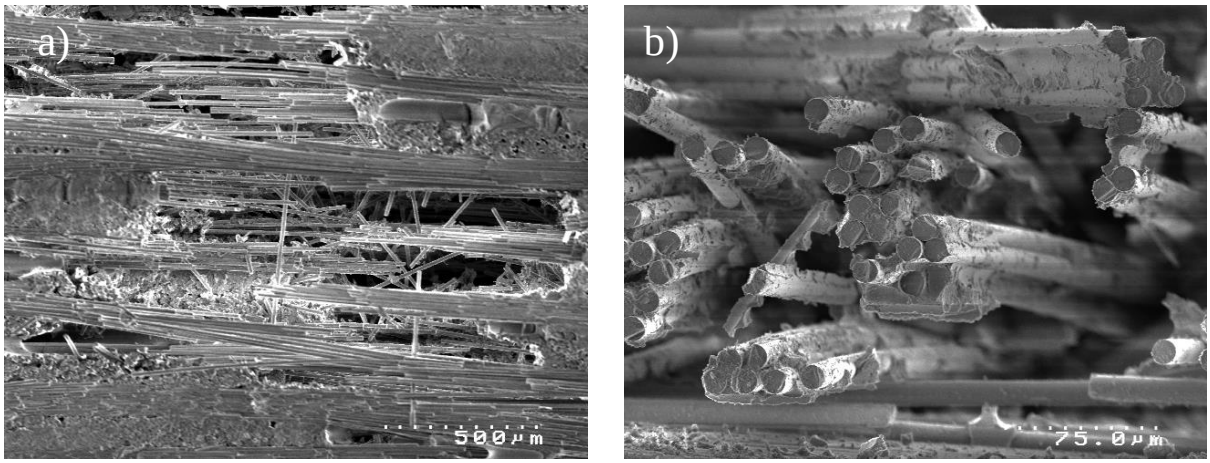

Figure 6.21. SEM micrographs of a porous oxide CMC composed of Nextel 720 fibres within an alumina matrix containing 10wt% ACH loaded in tension showing a) non-catastrophic mode of failure and b) strong fibre/matrix bond.

6.2. Discussion

Mean flexural strengths for composites processed with 2-15wt% ACH were statistically different, at the 95% confidence level, to mean flexural strength for composites processed without ACH (0%). Chlorohydrol 50 (ACH) is a highly concentrated solution of polyaluminium hydroxychloride which decomposes to form pure alumina. Alumina precursors are commonly employed during manufacturing to strengthen the matrix of porous matrix oxide CMCs. Polymer Impregnation and Pyrolysis (PIP) involves cyclic infiltration and pyrolysis of the precursor to decrease matrix porosity and increase composite density [42], [69]. Mattoni et al. [9] observed that the matrix porosity of a Nextel 720/alumina-mullite system decreased from 35% for two impregnation cycles to 29% for 10 impregnation cycles of alumina chlorohydrate (ACH). Flexural strength decreased from ~210MPa for 2 impregnations to ~80MPa for 10 impregnations. Mattoni et al. suggested that a reduction in matrix porosity leads to higher stress concentrations around fibre breaks, thereby increasing the failure probability in adjacent fibres. This system is relatively simple; ACH infiltrates into

the porous preform, decomposing to form pure alumina and therefore ‘filling the holes’ within the system. Perhaps a more interesting result for the purpose of this study would have been to compare flexural strength prior to any impregnation cycles with flexural strength after impregnation and pyrolysis of ACH. In contrast to Mattoni et al., this project saw the incorporation of ACH during slurry manufacture, prior to consolidation, and therefore ACH does not have the same ‘filling’ affect. The results of mass/volume density calculations revealed that density decreased with the addition of ACH, and mean densities of composites manufactured with 12, 15 and 20wt% ACH were significantly different from composites manufactured without ACH. Using density as a measure of porosity (a less dense composite will likely have greater porosity than a more dense composite of the same constituents); these results suggest that porosity increased significantly with the addition of 12-20wt% ACH. Furthermore, mean densities of 2, 5 and 10wt% ACH were not statistically different from composites manufactured without ACH, indicating that an increase in flexural strength for 2-15wt% ACH as demonstrated in this study was not due to a change in composite density or matrix porosity.

Notable improvements to the manufacturing process were observed following the addition of ACH. It was observed that slurry prepared with as little as 2wt% ACH was more viscous under static conditions but became less viscous under the stress of the roller during impregnation. This apparent shear thinning behaviour was noted previously with the use of PAF 2 in Chapter 5 -. During reactivation, plies were more adhesive or ‘tackier’ to the touch therefore aiding consolidation. Furthermore, the volume of slurry lost during consolidation decreased from 6.2% to 3.0% with the addition of 2% ACH (Figure 6.22), presumably due to slurry having a greater viscosity and therefore less slurry being expelled upon the application of load. It is beneficial to reduce the volume of slurry lost during consolidation in order to

achieve better control over matrix volume fraction and to improve the economic viability of the process. Solid loss increased from 3.0% to 6.6% with the addition of 5 to 15% ACH. During immersion in deionised water, hydrogen bonds created between the hydrogen of polymer groups within slurry and the oxygen of water molecules allow slurry to absorb water. Increasing the volume fraction of ACH, a polymer precursor of alumina, promotes additional hydrogen bonding and thus plies are more able to absorb water during immersion and consequently contain more water upon lay-up. As load is applied during consolidation, water (and therefore slurry) in the laminate stack is expelled, reducing matrix volume fraction. Furthermore, excess water in the system creates additional voids in the material as it evaporates on heating. SEM observations of specimens manufactured with 12wt% ACH revealed an increased number of large-scale pores compared with 5wt% ACH. Additionally, fibres perpendicular to the specimen length were seemingly less well infiltrated. Further investigation into porosity distribution would be required to confirm this suggestion.

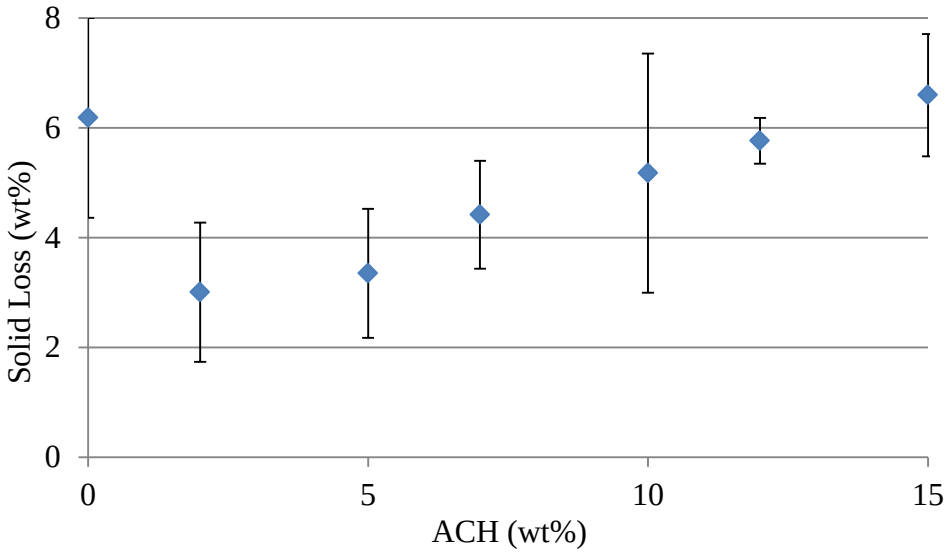

Figure 6.22. Percentage solid loss during consolidation for composite flat plates composed of Nextel 720 fibres within a pure alumina matrix containing 0-15wt% ACH (error bars represent ± 1 standard deviation).

Mean flexural strength of 20wt% ACH was found to be statistically not different from mean flexural strength of specimens manufactured without ACH (0%). ACH was incorporated into the matrix by weight of alumina powder such that for 20wt% slurry, 20g Chlorohydrol 50 ACH was added for every 100g TM-DAR alumina powder. Thus, the proportion of alumina powder and polymer binder solution in slurry effectively decreased for increasing additions of ACH. The polymer binder system developed within this project composes 90% water, whilst commercially available Chlorohydrol 50 is a 50% aqueous solution. Water content therefore increased from 25.7% for slurry not containing ACH to 28.8% for slurry containing 20% ACH (Figure 6.23). Assuming TM-DAR alumina powder yields 100% alumina, and Chlorohydrol 50 ACH yields 23% alumina after decomposition and sintering (manufacturers data), the total alumina yield decreases from 71.4% for composites not containing ACH to 65.4% for composites containing 20% ACH (Figure 6.24). Consequently, for composites of equal fibre content and thickness, reducing alumina yield and thus matrix volume fraction results in an increase in porosity. As previously discussed, mean density of composite plates containing 20wt% ACH was statistically different from mean density of composite plates manufactured without ACH, reflecting an increase in composite porosity. It was therefore assumed that improvements to impregnation and consolidation observed after the addition of ACH were outweighed by a decrease in density (and increase in porosity), resulting in flexural strength statistically not different from composites manufactured without ACH.

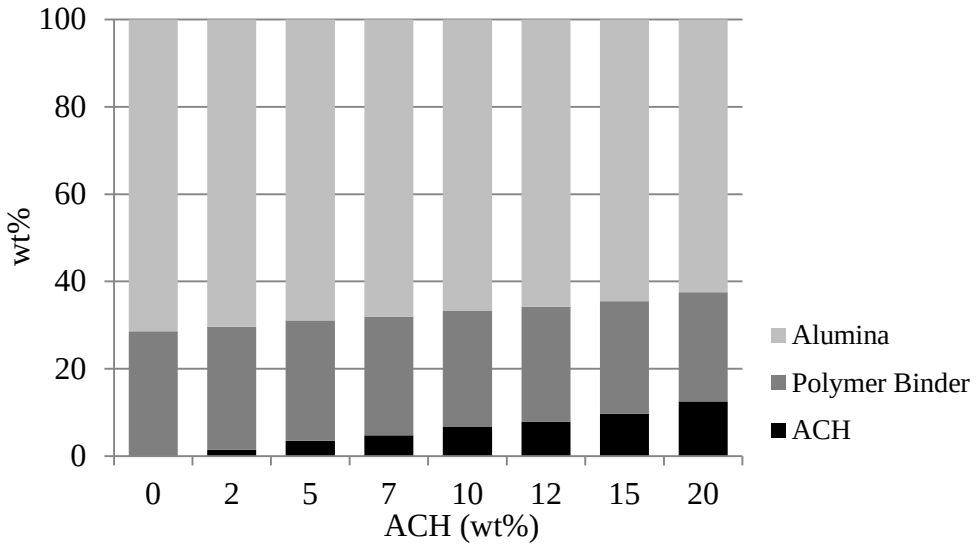

Figure 6.23. Effect of aluminium chlorohydrate (ACH) addition on relative proportions of alumina powder and polymer binder solution in slurry form.

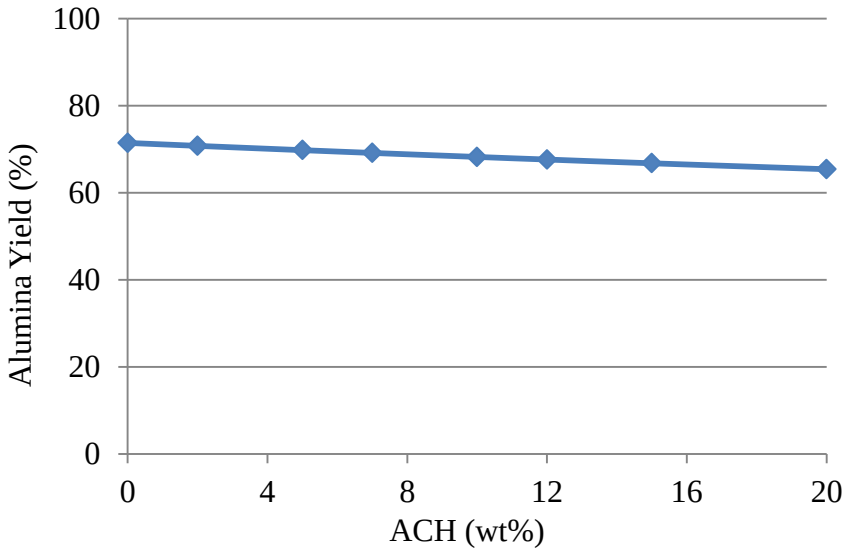

Figure 6.24. Alumina yield after sintering for composites composed of Nextel 720 fibres within a pure alumina matrix containing 0-20wt% ACH.

Mean shear strengths of specimens manufactured with 12 and 15wt% ACH were extremely significantly different compared with 5wt%. In contrast to flexural testing in three-point bend, the bending moment generated in a short beam shear specimen is limited by the short span relative to the thickness, reducing the tensile and compressive stresses at the outer surfaces

and maximising the induced shear stresses at the mid-plane. When transverse shear stresses exceed the interlaminar shear strength of the composite, a delamination failure will occur [125], [126], [127]. Out-of-plane properties such as short beam shear are matrix dominated and therefore composite materials with good matrix strength and good adhesion between fibre and matrix will perform better in short beam shear than composite materials with poor matrix strength and poor fibre/matrix adhesion. It can be assumed, therefore, from the results of short beam shear testing that composites manufactured with >10wt% ACH possess a weaker matrix than composites manufactured with <10wt% ACH, presumably owing to a decrease in alumina yield after sintering. Consequently, the composite is less able to withstand shear stresses at the mid-plane, resulting in premature delamination. Mean shear strength of specimens manufactured with 5wt% ACH was statistically not different compared with 7 and 10wt% ACH. Equally, mean density of composites manufactured with 5wt% ACH was statistically not different from 7 and 10wt% ACH, indicating that composites manufactured with 5-10wt% ACH contain comparable porosity and matrix strength, and subsequently equivalent short beam shear strength. Owing to limited data, it cannot be determined whether or not ACH improves short beam shear strength. Mean densities of composites manufactured with 2 and 5wt% ACH were statistically not different from composites manufactured without ACH, suggesting composites manufactured with 0-5wt% ACH contain statistically indifferent matrix properties. It was observed, however, that laminates manufactured with ACH were more ‘tacky’ upon lay-up, perhaps resulting in better adhesion and consolidation, and consequently an improvement in shear stress. Further evidence would be required to confirm these suggestions.

There were no observable differences in the stress-displacement response for specimens loaded in three-point bend manufactured with 0-20wt% ACH. The response was typically

linear elastic until peak load was achieved, after which load bearing capacity decreased significantly. These observations suggest that despite significantly different flexural strength, the method of failure remains the same. A small number of specimens demonstrated a region of linear elasticity followed by non-linear behaviour prior to failure. During loading, a series of cracks form in the matrix perpendicular to the load axis. Load is consequently transferred to the reinforcing fibres. Energy absorbing mechanisms such as fibre/matrix debonding and crack deflection allow the fibres to be isolated, impeding crack propagation and resulting in non-linear deformation as shown in a small number of specimens. When a specimen is loaded in three-point bend, only a small volume of material is subjected to maximum load and therefore the test is sensitive to variation in the material. Matrix porosity is critical to the damage tolerance of oxide CMCs without a fibre coating. Nevertheless, placement of both porosity and shrinkage cracks within the matrix can lead to variability between specimens. It has already been suggested that if a pore or shrinkage crack formed during sintering lies directly beneath the central roller where load is most concentrated, the specimen will likely fail prematurely. Equally, a specimen may exhibit superior strength if the area subjected to maximum load does not contain any large-scale porosity. Scatter between specimens is anticipated, particularly given the nature of both three-point bend testing and the hand lay-up manufacturing route. Composites manufactured with 12wt% ACH exhibited the smallest variability between specimens, whilst 2wt% exhibited the largest. There was no apparent relationship between variability and volume of ACH. Nevertheless, frequency histograms illustrating the distribution of data revealed that composites manufactured with ≤5wt% ACH demonstrated a slight positive skew, by which the mass of the distribution is concentrated at lower strength and the mean value is greater than the median value. Composites manufactured with 7-10wt% ACH displayed normal distribution whereby the mean, median and mode values are approximately equal, and the data is approximately symmetrical. Composites

manufactured with ≥12wt% ACH demonstrated a slight negative skew, indicating that the mass of the distribution is concentrated at higher strengths and the mean value is smaller than the median value. Frequency histograms illustrating the distribution of data for specimens loaded in short beam shear revealed similar findings. Composites manufactured with 5-10wt% ACH exhibited normal distribution, whilst those manufactured with 12-15wt% ACH demonstrated negative skew (mean < median). These observations suggest that mean flexural and shear values calculated for composites manufactured with >12wt% ACH were affected by a small number of specimens failing prematurely. It has already been suggested that increasing ACH leads to an increase in porosity, owing to a decrease in composite density. Thus if a specimen contains greater porosity, above what is necessary for damage tolerant behaviour, it is more likely to fail prematurely owing to an increased number of stress concentrations directly beneath the central load.

Low magnification SEM observations of flexural specimens manufactured with moderate additions of ACH (0-10wt%) prior to testing demonstrated comparable microstructures. A two-dimensional fibre weave was evident, showing fibre tows both parallel and perpendicular to the length of the specimen, illustrating the eight-harness satin weave of commercially available Nextel 720 fibres. Fibre tows were well infiltrated with matrix material, indicating that slurry was effectively impregnated during manufacturing. Matrix-rich regions separated fibre layers within which crack-like flaws, perpendicular to the fibre layers, were observed. These cracks were attributed to the constraint the fibres impose on matrix shrinkage during sintering/densification. Large-scale pores of irregular size and distribution were also evident. These were likely caused by trapped air during consolidation. Consolidation under vacuum, such as within an autoclave, may help to prevent these large-scale pores however this method was not pursued within this project due to the additional manufacturing costs and complexity.

Examination of composites manufactured with higher volumes of ACH (12-20wt%) showed fibre tows visually less well-infiltrated and an increase in the number of large-scale pores. As discussed previously, this was not attributed to incomplete impregnation but a decrease in alumina yield after decomposition and sintering with increasing ACH. Comparison of the in-plane microstructure at low magnification before and after loading in three-point bend revealed no discernible failure mechanism. Nevertheless, it was apparent that specimens failed in a non-catastrophic manner, on account of specimens being in-tact. Further analysis is required to capture the failure mechanism; however it is assumed that specimens fail by tension on the top surface.

Specimens manufactured with 7-10wt% ACH exhibited flexural strength of 205-212MPa and short beam shear strength of 12.1-12.6MPa. These findings are comparable with those reported for similar oxide CMCs highlighted in the literature. In fact, short beam shear strength far exceeds the values reported previously. The flexural strength of composites produced by the pressure infiltration method was reported to be ~210MPa [9], whilst those produced by the VibroIntrusion method exhibited flexural strength of ~172MPa. The short beam shear strength of composites produced by the VibroIntrusion method was reported to be 8MPa [90], whilst COI manufactured composites revealed double notch shear strength of 8.25MPa.

Preliminary investigation into the tensile properties of specimens manufactured with 10wt% ACH revealed a mean tensile strength of 146.95MPa. Stress-strain curves revealed a similar response as described for specimens loaded in three-point bend. After an initial linear region, stress developed in a non-linear manner with strain to maximum load, representative of permanent deformation. Stress-strain curves revealed evidence of the specimen slipping

within the grips, despite the use of self-tightening grips, meaning that elastic modulus was difficult to calculate. This suggests the need for a tabbing arrangement in future testing. Low magnification SEM observations exposed a brushy fracture surface, representative of a non-catastrophic mode of failure. Higher magnification SEM observations illustrated the presence of matrix strongly bonded to fractured reinforcing fibres, suggesting that failure occurred within the matrix, as opposed to at the fibre/matrix interface. Further investigation into the tensile properties of Nextel 720/alumina composites manufactured with ACH is required, with particular attention drawn to the gripping arrangement. Nevertheless, mean tensile strength obtained in this preliminary investigation is comparable with that achieved for similar oxide composites highlighted in the literature. The tensile strength of composites composed of Nextel 720 fibres within an alumina-mullite matrix produced by the pressure infiltration method was reported to be ~145MPa [42], [88], whilst tensile strength of the COI manufactured Nextel 720/alumina matrix CMC was reported to be 144-169MPa at room temperature [94], [95], [96].

6.3. Concluding remarks

It has been demonstrated that the addition of Chlorohydrol 50 ACH improved composite properties, with composites containing 7-15wt% ACH demonstrating flexural strength greater than 205MPa and composites containing 5-10wt% ACH demonstrating short beam shear strength greater than 12MPa. Furthermore, the addition of ACH was advantageous to the manufacturing process, aiding impregnation, reactivation and consolidation. The addition of 10wt% ACH was therefore pursued throughout the remainder of the project.

Chapter 7 - The effect of a bimodal particle distribution on processing and properties of Nextel 720 fibres within an alumina matrix containing ACH

The effect of combining large alumina particles with submicron alumina particles to create a bimodal particle size distribution was investigated. A multi-modal particle size distribution is commonly used in monolithic ceramics where fine particles within the powder fill the voids between larger particles in order to reduce cracking caused by contraction of small particles during sintering. A similar approach was described by Levi et al. [42], whereby relatively large (~1μm) mullite powder particles were combined with small alumina particles (~0.2μm) to form a Nextel 720-alumina/mullite composite processed by the polymer impregnation and pyrolysis method. Equally, Simon [108] combined relatively large 1μm mullite particles with mullite nanoparticles (<0.1μm) in equal volumes. A colloidal processing route was employed whereby inter-particle forces were controlled to ensure a core-shell structure.

1 micron diameter alumina particles (OCON-016, Logitech UK) were combined with 0.1 micron diameter alumina particles (TM-DAR powder) during slurry preparation in 10, 20, 30, 40, 50 and 80% increments. 10wt% Chlorohydrol 50 ACH was incorporated into slurry after 24 hours ball milling and ball milled for one further hour. Composite flat plates of 11 ply thickness, 80x150mm, manufactured by both the author and Dr E.G. Butler with a bimodal particle distribution were compared with those manufactured with purely submicron particles (0%), reported in the previous chapter as 10wt% ACH. Twelve flexural (6 longitudinal, 6 transverse) and eight shear (4 longitudinal, 4 transverse) specimens were diamond cut from each flat plate. Specimens were tested in three point bend and short beam shear using the parameters outlined in sections 4.2.1. and 0. Non-coated specimens were observed using a

field emission scanning electron microscope (FEG SEM) operating at 4kV acceleration voltage.

7.1. Results

7.1.1. Flexural strength

Specimens composed of purely submicron particles (0%) exhibited a mean flexural strength of 205.3MPa. Specimens containing 10-50% 1 micron particles demonstrated mean flexural strengths between 195 and 220MPa, whilst those containing 80% 1 micron particles exhibited a mean flexural strength of 144.1MPa (Table 7.1). Standard deviation ranged from 9.7MPa for specimens including 80% 1 micron particles, to 35.4MPa for those containing 30% 1 micron particles (Figure 7.1). Equally, specimens containing 30% 1 micron particles exhibited the largest interquartile range (Figure 7.2). Frequency histograms presented in Figure 7.3 illustrating the distribution of flexural strength values typically revealed a normal distribution with the exception of composites manufactured with 30% 1 micron particles which demonstrated a random distribution.

Table 7.1. Flexural strength values for composites composed of Nextel 720 fibres within an alumina matrix containing 0-80% 1µm alumina particles.

% 1µm	Min.	Q1	Median	Q3 (MPa)	Max.	Mean	St. Dev	No. Tests
0	162.4	191.6	205.8	219.8	251.3	205.3	20.4	138
10	157.8	194.6	203.5	210.8	242.3	204.6	18.0	24
20	185.2	213.1	222.8	230.4	247.5	220.1	14.4	42
30	115.0	167.7	202.8	220.9	262.0	195.3	35.4	37
40	169.8	204.7	219.4	229.8	254.8	217.1	19.8	32
50	181.1	210.3	217.3	222.2	234.5	214.7	12.9	20
80	121.8	138.1	143.7	150.3	162.6	144.1	9.7	20

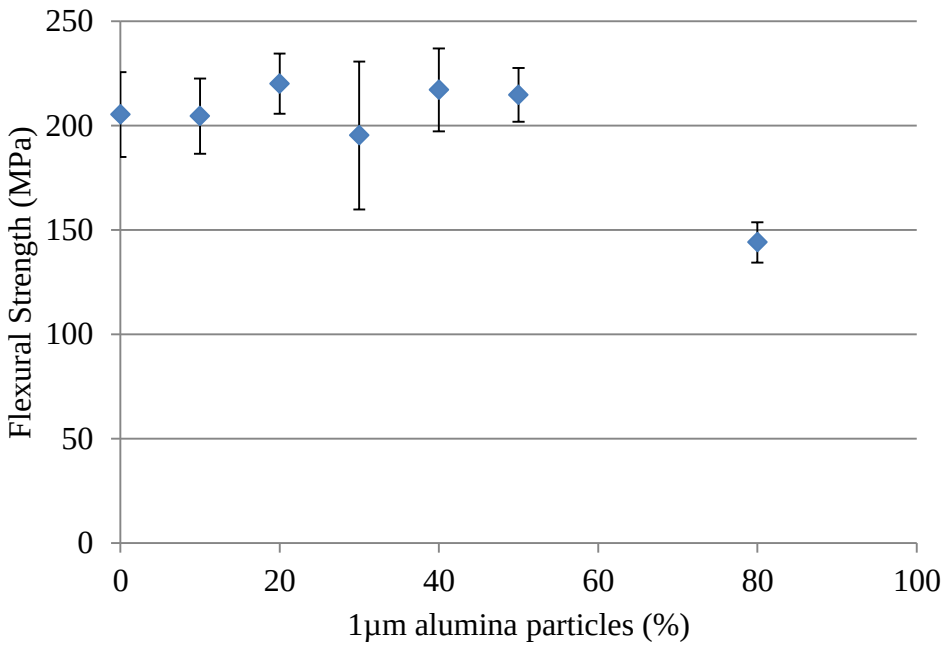

Figure 7.1. Flexural strength values illustrated by mean and standard deviation comparing composites composed of Nextel 720 fibres within an alumina matrix containing 0-80% 1 micron particles.

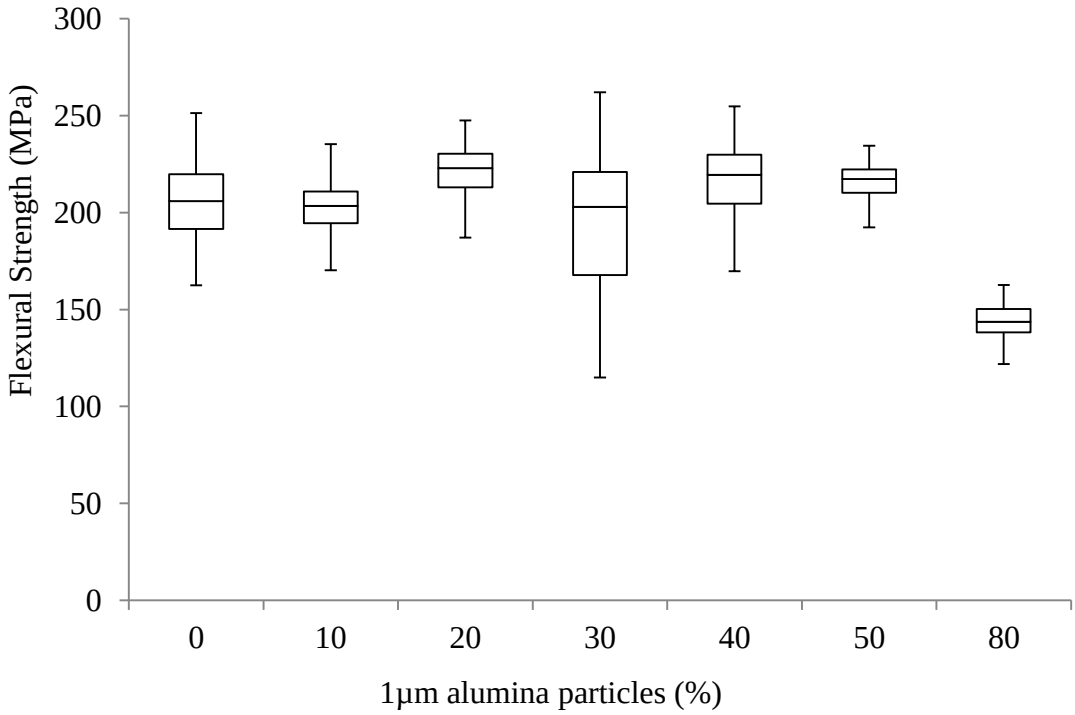

Figure 7.2. Box and whisker diagram comparing flexural strength values for composites composed of Nextel 720 fibres within an alumina matrix containing 0-80% 1 micron particles.

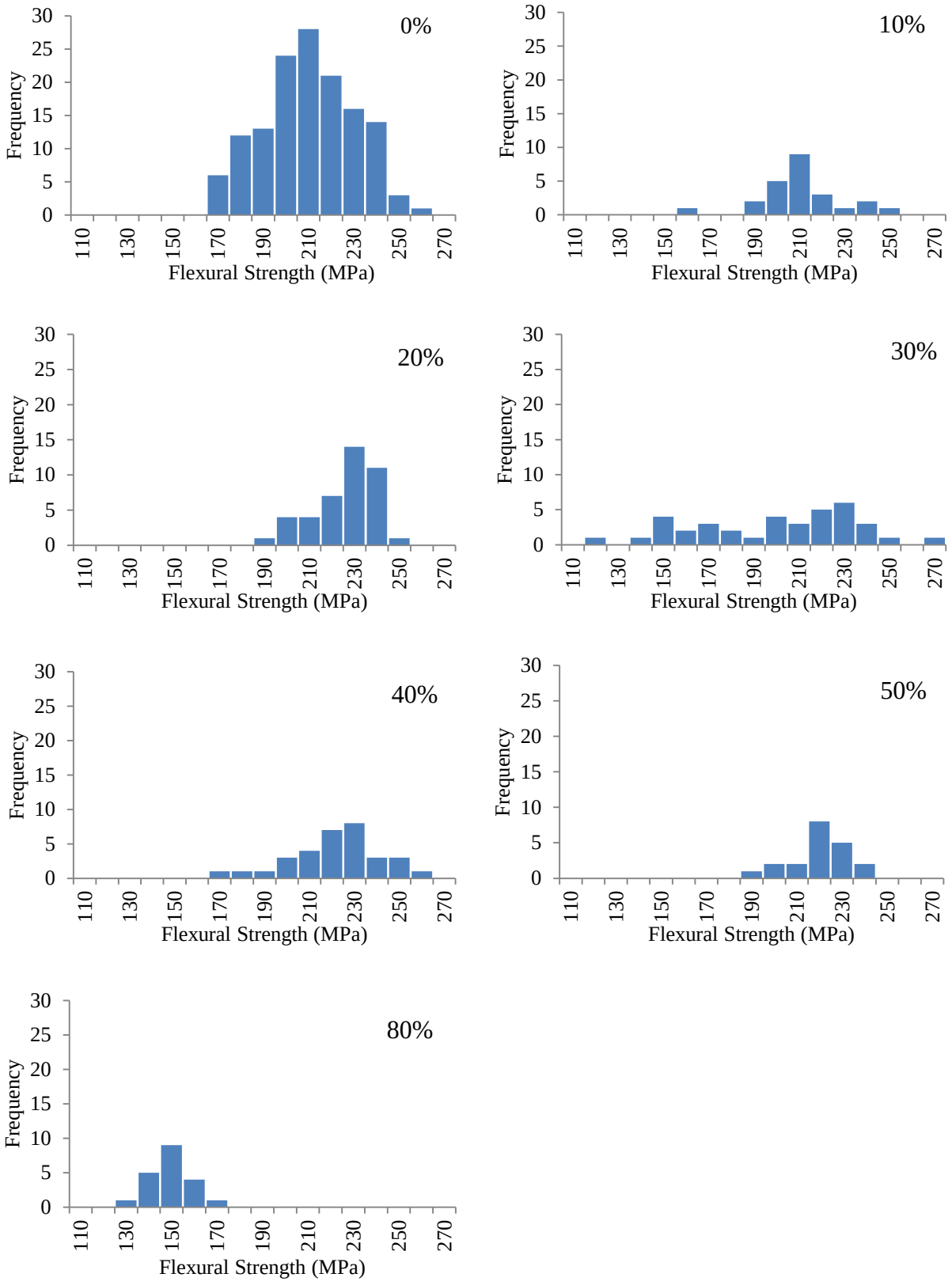

Figure 7.3. Frequency histograms comparing flexural strength values for specimens composed of Nextel 720 fibres within an alumina matrix containing 0-80% 1 micron particles.

Welch's t-test was conducted to compare mean flexural strength values obtained for composites containing 0-80% 1 micron alumina particles (Table 7.2). Flexural strength of specimens containing 80% 1 micron particles was found to be extremely statistically different from mean flexural strength of specimens containing purely submicron particles (0%) and specimens containing 50% 1 micron particles ($p<0.0001$). Mean flexural strength of specimens containing 0, 10 and 30% 1 micron particles were found to be statistically indifferent ($p>0.05$). Equally, mean flexural strength of specimens containing 20, 40 and 50% 1 micron particles were found to be statistically indifferent ($p>0.05$).

Table 7.2. Intermediate and p values obtained from Welch's t-test comparing flexural strength group values for composites containing 0-80% 1µm alumina particles.

Grp 1 (% 1µm)	Grp 2 (% 1µm)	$X_1 - X_2$	95% CI Min	95% CI Max	$\sqrt{\frac{s_1^2}{n_1}+\frac{s_2^2}{n_2}}$	t	df	p
0	10	0.77	-7.50	9.03	4.07	0.19	34	0.85
0	20	-14.75	-20.34	-9.16	2.82	5.23	95	**9.80×10^{-07}**
0	30	10.05	-2.20	22.30	6.07	1.66	42	0.11
0	40	-11.79	-19.67	-3.92	3.91	3.01	47	**0.0042**
0	50	-9.38	-16.20	-2.55	3.36	2.79	34	**0.0085**
0	80	61.24	55.67	66.82	2.78	22.09	48	**5.95×10^{-27}**
10	20	-15.52	-24.21	-6.82	4.30	3.61	39	**0.0009**
20	30	24.80	12.27	37.34	6.23	3.98	46	**0.0002**
30	40	-21.84	-35.44	-8.24	6.79	3.22	58	**0.0021**
40	50	2.42	-6.70	11.53	4.54	0.53	49	0.60
50	80	70.62	63.32	77.92	3.60	19.63	35	**1.41×10^{-20}**
10	30	9.29	-4.50	23.07	6.88	1.35	56	0.18
20	40	2.96	-5.37	11.28	4.15	0.71	54	0.48
20	50	5.37	-1.96	12.71	3.63	1.48	41	0.15

Representative stress-displacement curves for specimens including a bimodal particle distribution loaded in three-point bend are presented in Figure 7.5 to Figure 7.9. Stress-displacement curves for specimens manufactured with purely submicron alumina particles, previously termed 10wt% ACH, are shown in Figure 7.4 for reference. Typically, the stress-displacement response was linear until peak load was achieved, after which a significant decrease in load bearing capacity was evident. A small number of specimens demonstrated a region of non-linear behaviour prior to failure (Specimen 1023, Figure 7.8 and Specimen 1008, Figure 7.9).

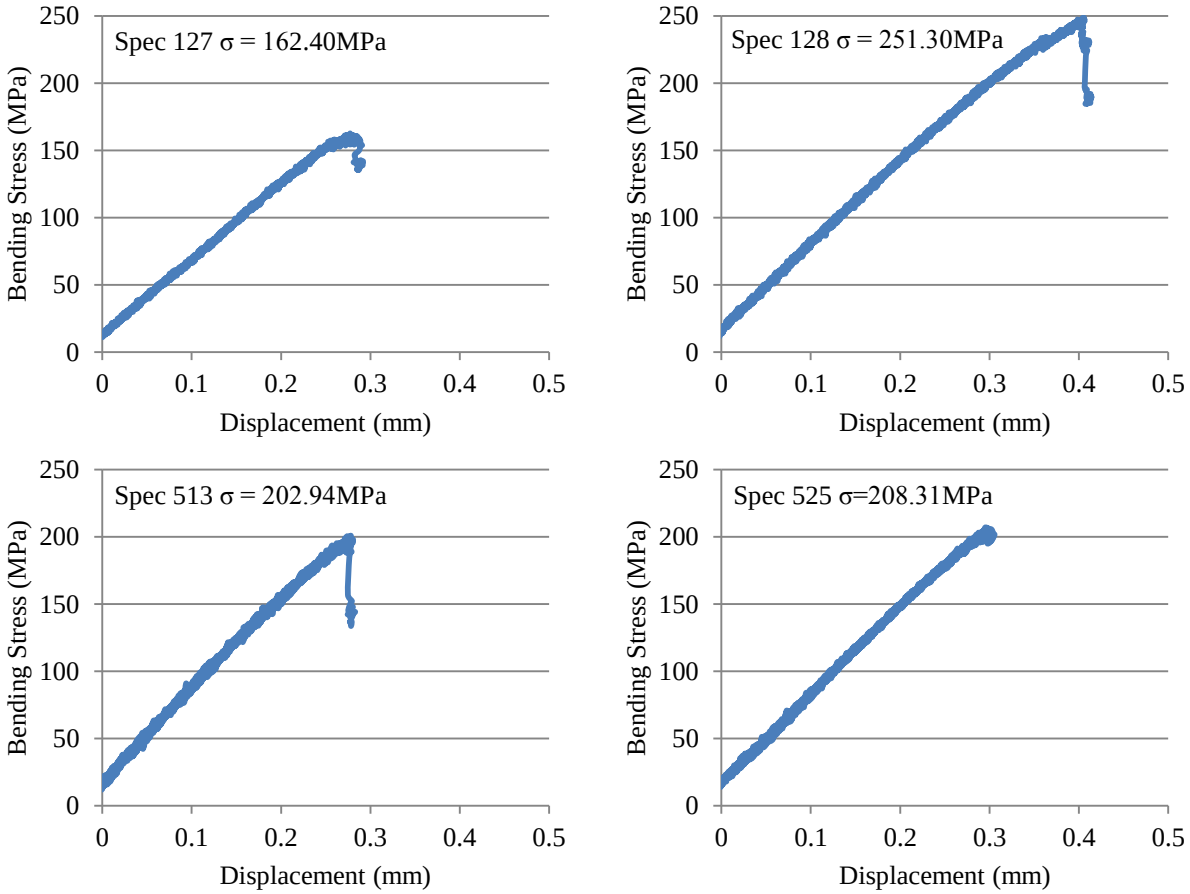

Figure 7.4. Representative stress-displacement curves for specimens composed of Nextel 720 fibres within an alumina matrix containing purely submicron particles (0% 1µm) showing minimum (Spec 127), maximum (Spec 128) and 2 average strength values (Spec 513 & Spec 525).

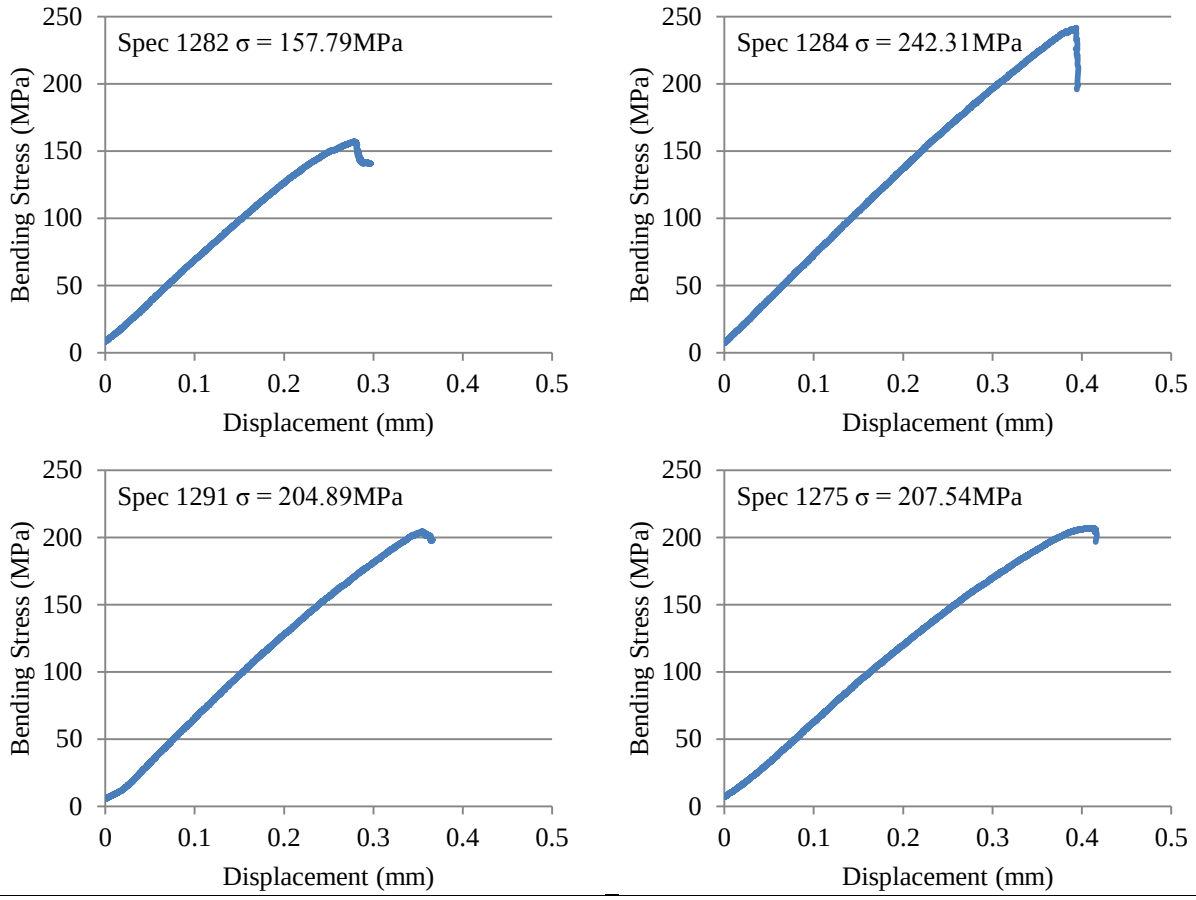

Figure 7.5. Representative stress-displacement curves for specimens composed of Nextel 720 fibres within an alumina matrix containing 10% 1µm alumina particles showing minimum (Spec 1282), maximum (Spec 1284) and 2 average strength values (Spec 1291 and Spec 1275).

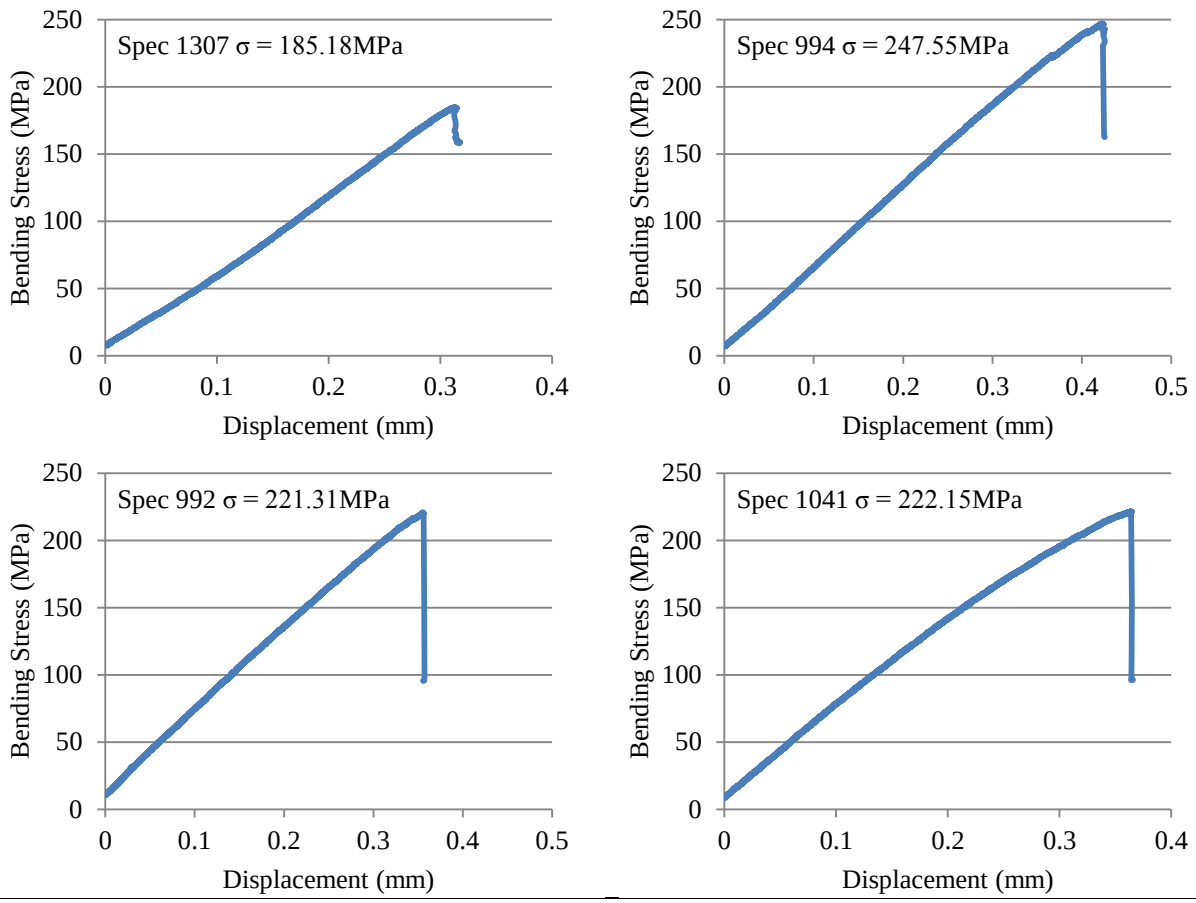

Figure 7.6. Representative stress-displacement curves for specimens composed of Nextel 720 fibres within an alumina matrix containing 20% 1µm alumina particles showing minimum (Spec 1307), maximum (Spec 994) and 2 average strength values (Spec 992, Spec 1041).

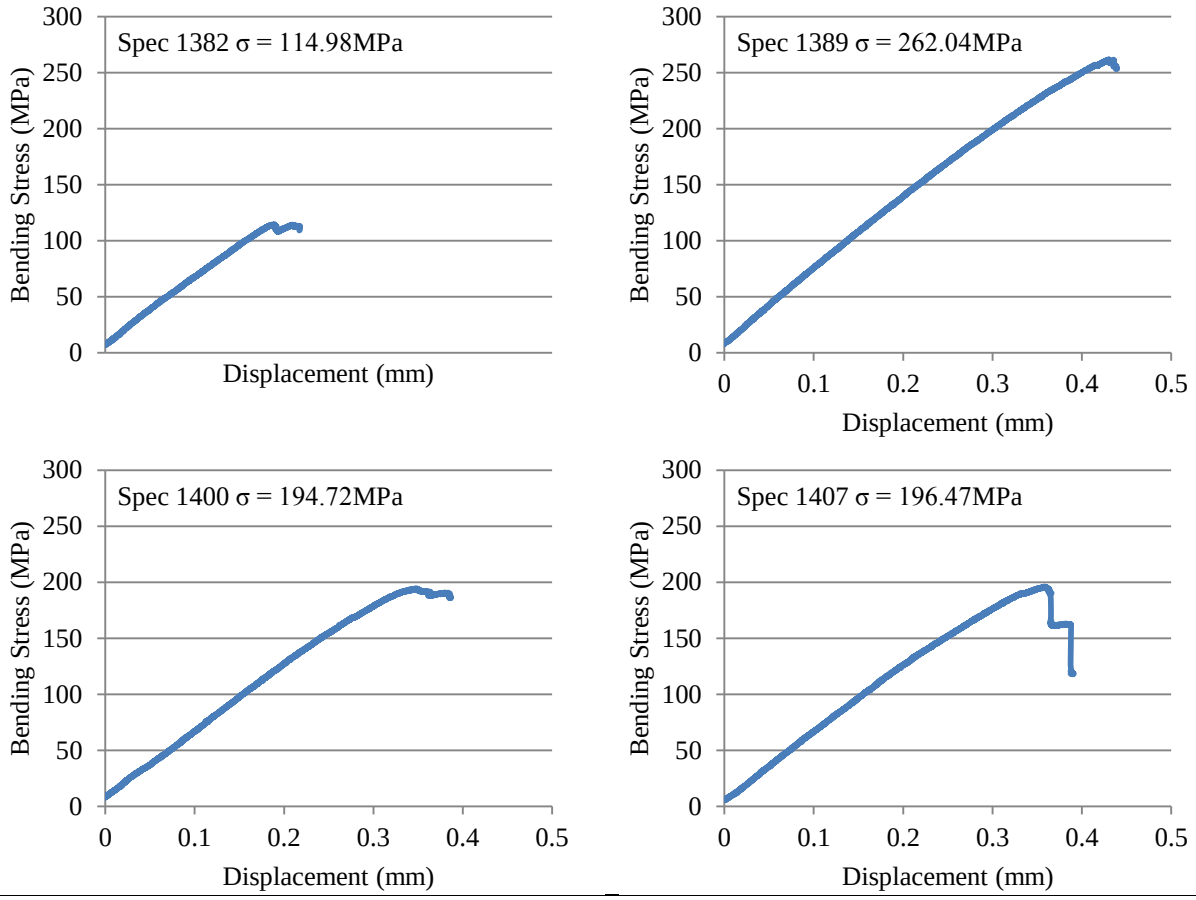

Figure 7.7. Representative stress-displacement curves for specimens composed of Nextel 720 fibres within an alumina matrix containing 30% 1µm alumina particles showing minimum (Spec 1382), maximum (Spec 1389) and 2 average strength values (Spec 1400 and Spec 1407).

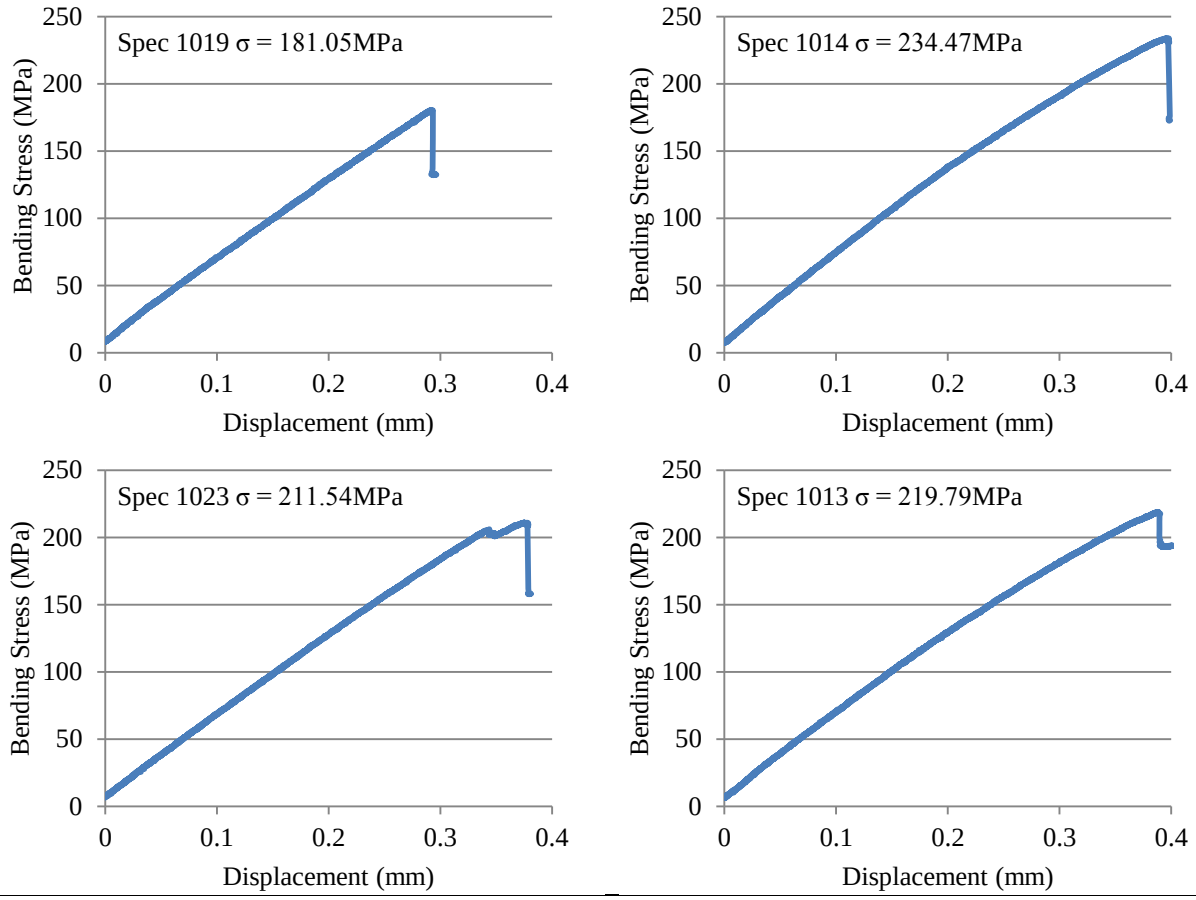

Figure 7.8. Representative stress-displacement curves for specimens composed of Nextel 720 fibres within an alumina matrix containing 50% 1µm alumina particles showing minimum (Spec 1019), maximum (Spec 1014) and 2 average strength values (Spec 1023, Spec 1013).

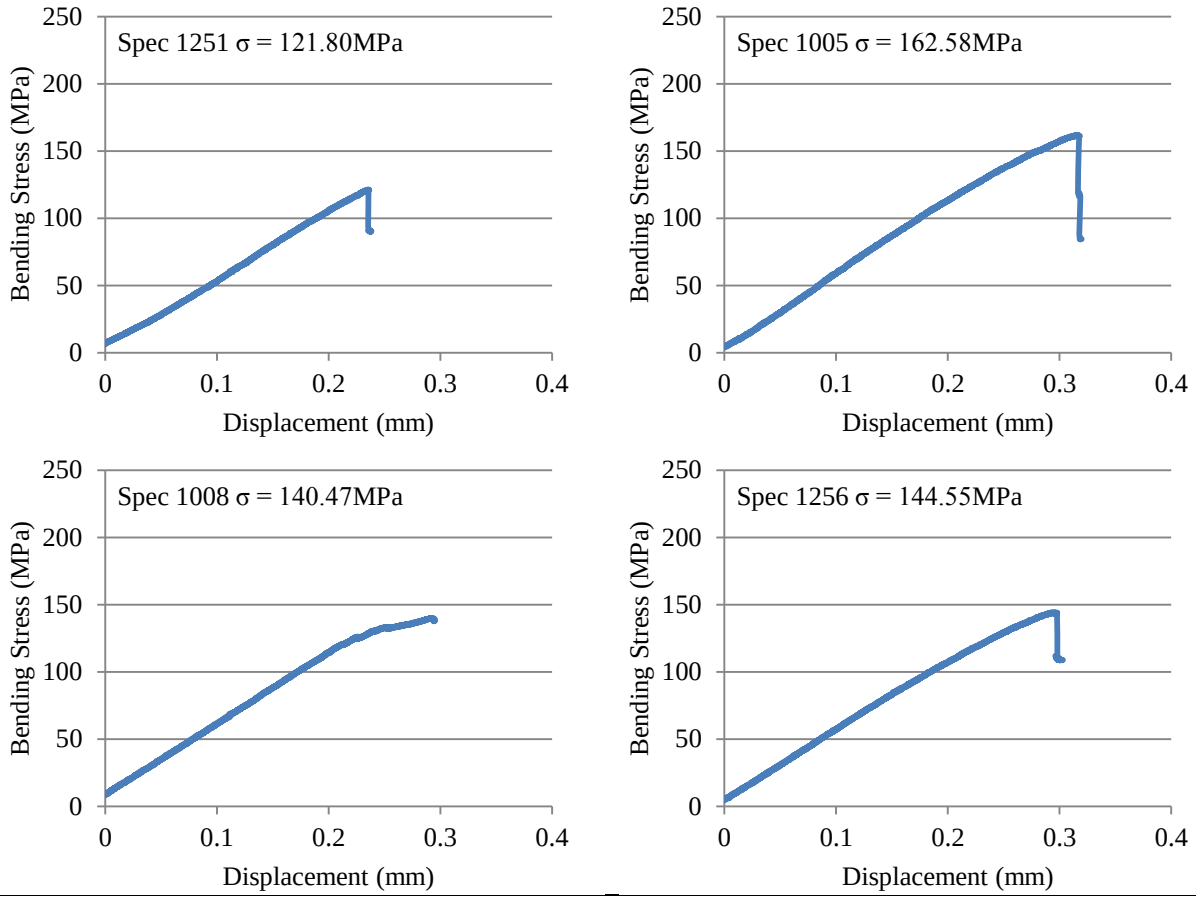

Figure 7.9. Representative stress-displacement curves for specimens composed of Nextel 720 fibres within an alumina matrix containing 80% 1μm alumina particles showing minimum (Spec 1251), maximum (Spec 1005) and 2 average strength values (Spec 1008, Spec 1256).

Low magnification SEM observations of an as-processed flexural specimen containing 20% 1 micron particles prior to testing exposed a two-dimensional fibre weave, demonstrating layers of fibre tows both parallel and perpendicular to the length of the specimen, separated by matrix-rich regions (Figure 7.10 a). Fibre tows are seemingly well infiltrated with matrix material, however large-scale pores of irregular size and distribution, and crack-like flaws perpendicular to the fibre layers in matrix-rich regions are evident. SEM observations of Specimen 999 after loading in three-point bend revealed a slight crack opening between layers after testing (Figure 7.10 b and c). It must be noted that specimens remained intact after testing, owing to termination of the test at the onset of peak load.

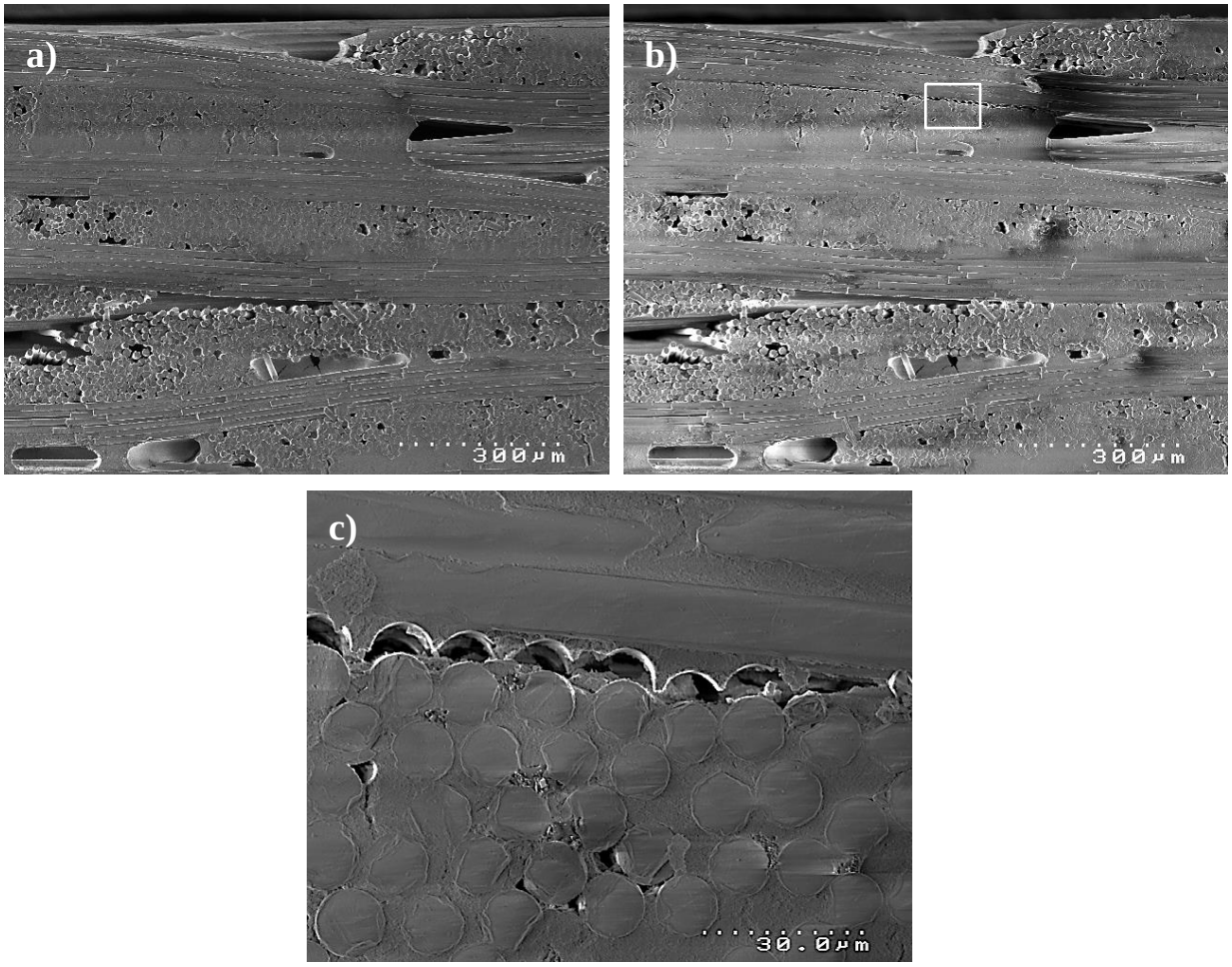

Figure 7.10. SEM micrographs of Specimen 999, manufactured with 20% 1 micron particles. a) in-plane composite structure prior to loading, b) in-plane composite structure after loading in three point bend and c) higher magnification image demonstrating debonding between layers after loading.

7.1.2. Short beam shear

Specimens containing purely submicron particles (0%) exhibited a mean short beam shear strength of 12.1MPa. Specimens manufactured with 10-50% 1 micron particles demonstrated mean shear strengths between 9.8 and 11.4MPa, whilst specimens manufactured with 80% 1 micron particles exhibited a mean shear strength of 7.2MPa (Table 7.3). Standard deviation ranged from 0.66MPa for specimens manufactured with 40% 1 micron particles to 2.89MPa for specimens manufactured with 10% 1 micron particles (Figure 7.11). Specimens manufactured with 10% 1 micron particles also exhibited the largest interquartile range (Figure 7.12). Frequency histograms presented in Figure 7.13 illustrating the distribution of data generally revealed normal distribution with the exception of 10% and 20% 1 micron particles which demonstrated random distribution.

Table 7.3. Short beam shear values for composites composed of Nextel 720 fibres within an alumina matrix containing 0-80% 1µm alumina particles.

% 1µm	Min	Q1	Median	Q3 (MPa)	Max	Mean	St. Dev	No. Tests
0	10.52	11.63	12.06	12.79	13.53	12.10	0.90	14
10	8.15	10.20	12.24	12.99	13.74	11.38	2.89	3
20	7.15	8.41	9.57	10.79	13.30	9.79	1.97	15
30	9.12	10.29	11.21	12.21	13.94	11.20	1.48	14
40	10.18	10.99	11.30	11.75	12.54	11.32	0.66	16
50	8.94	9.17	9.76	10.75	11.78	10.05	1.14	6
80	6.37	6.75	6.80	7.75	8.08	7.18	0.67	7

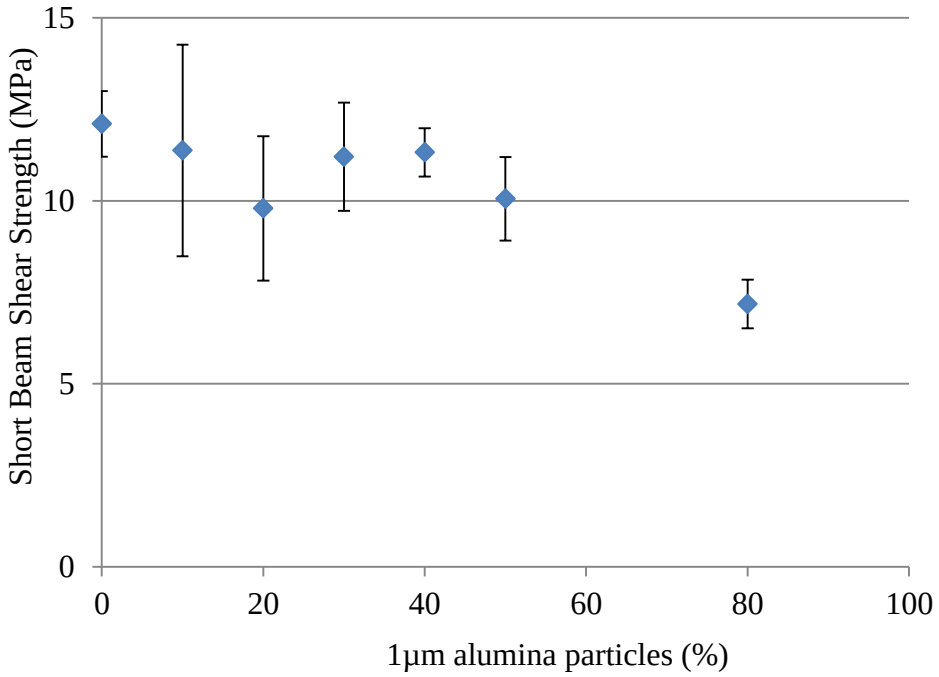

Figure 7.11. Short beam shear values illustrated by mean and standard deviation comparing composites composed of Nextel 720 fibres within an alumina matrix containing 0-80% 1 micron particles.

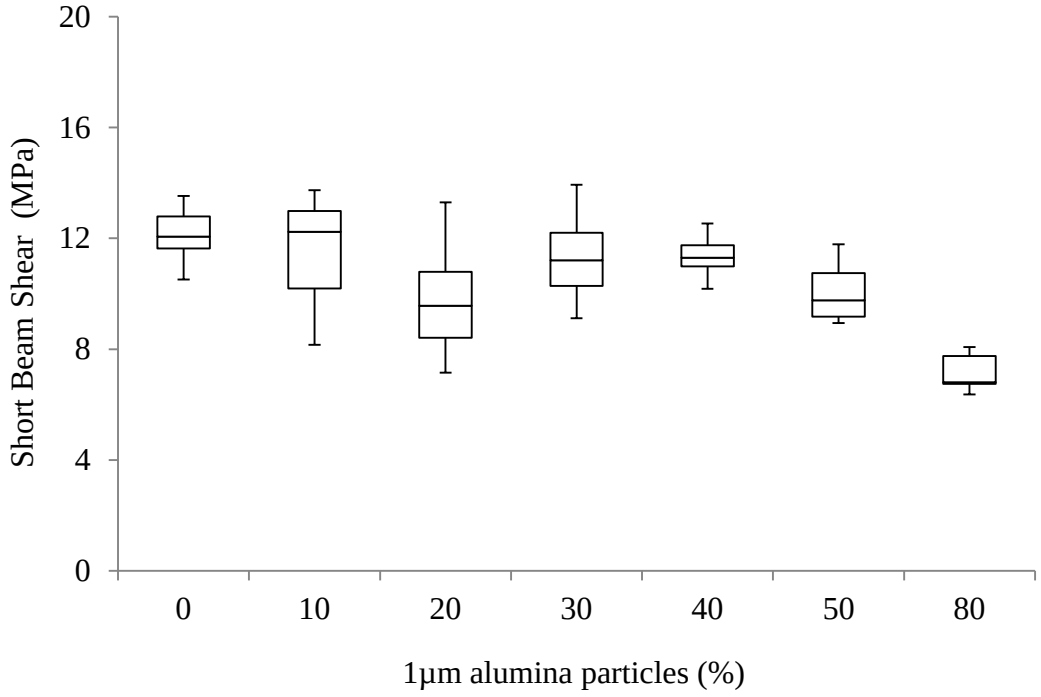

Figure 7.12. Box and whisker diagram comparing short beam shear values for composites composed of Nextel 720 fibres within an alumina matrix containing 0-80% 1 micron particles.

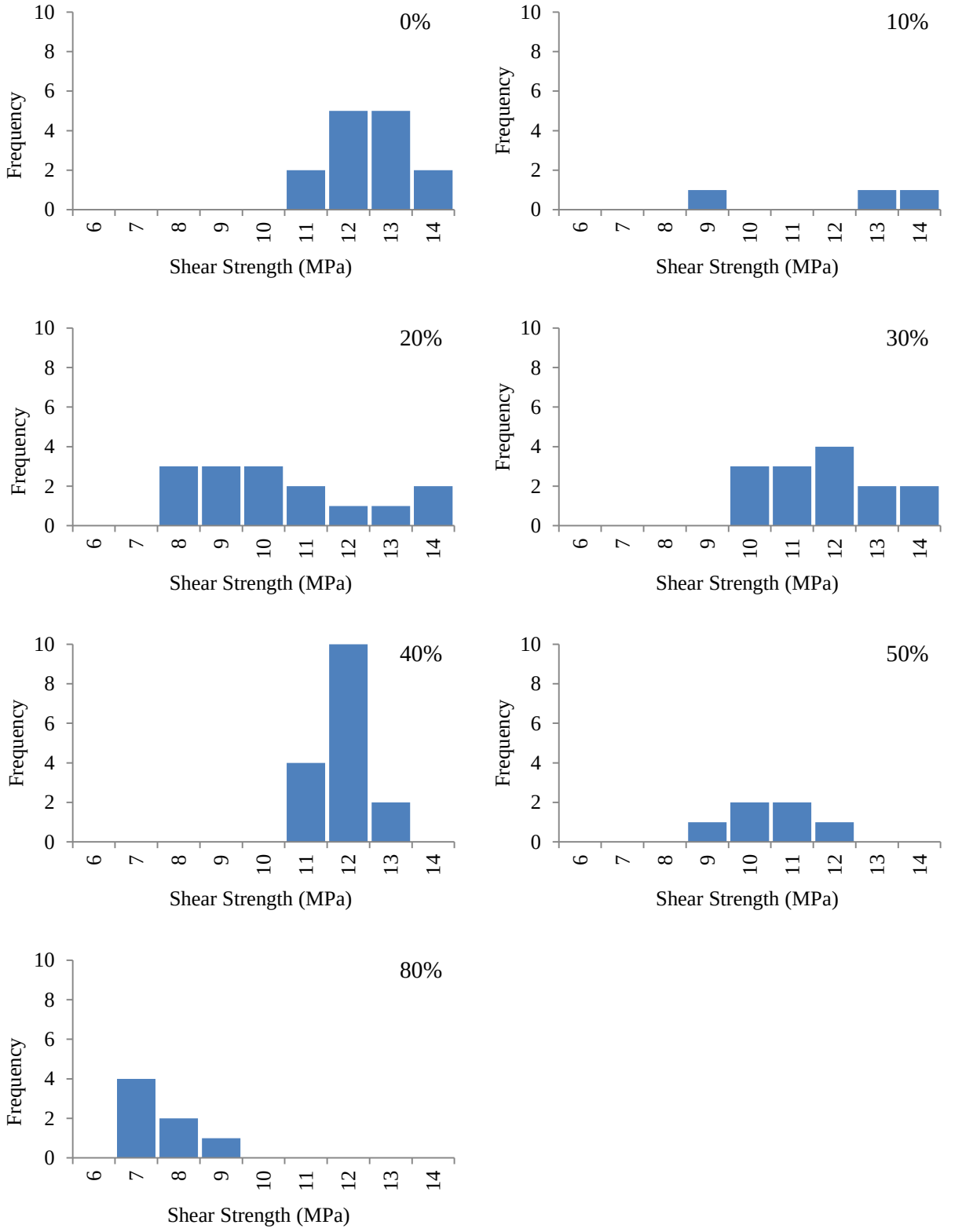

Figure 7.13. Frequency histograms comparing short beam shear values for composites composed of Nextel 720 fibres within an alumina matrix containing 0-80% 1 micron particles.

Welch's t-test was conducted to compare the mean short beam shear values for specimens containing 0-80% 1 micron alumina particles (Table 7.4). Short beam shear values for specimens containing 10% and 30% 1 micron particles were found to be statistically not different ($p<0.05$) from shear values for specimens containing only submicron particles (0%). In fact, short beam shear values for specimens containing 10% 1 micron particles were found to be statistically not different from any other group of data. Nevertheless, shear values for specimens containing 20% 1 micron particles were found to be statistically different to shear values for specimens containing 30% 1 micron particles ($p>0.05$), and 40% 1 micron particles were found to be statistically different to 50% 1 micron particles. 50% 1 micron particles were found to be extremely statistically different to 80% 1 micron particles.

Table 7.4. Intermediate and p values obtained from Welch's t-test comparing short beam shear strength values for composites containing 0-80% 1µm alumina particles.

Grp 1 (wt% ACH)	Grp 2 (wt% ACH)	$X_1 - X_2$	95% CI Min	95% CI Max	$\sqrt{\frac{s_1^2}{n_1}+\frac{s_2^2}{n_2}}$	t	df	p
0	10	0.72	-6.53	7.98	1.69	0.43	2	0.71
0	20	2.31	1.13	3.49	0.56	4.11	19	**0.00055**
0	30	0.90	-0.06	1.86	0.46	1.94	21	0.065
0	40	0.78	0.18	1.38	0.29	2.68	23	**0.014**
0	50	2.05	0.81	3.29	0.52	3.91	7	**0.0058**
0	80	4.92	4.18	5.66	0.35	14.16	15	**2.08×10^{-10}**
10	20	1.59	-5.92	9.09	1.74	0.91	2	0.46
10	30	0.17	-7.20	7.55	1.72	0.10	2	0.93
10	40	0.06	-7.16	7.27	1.68	0.03	2	0.98
10	50	1.33	-6.13	8.78	1.73	0.77	2	0.52
10	80	4.20	-3.06	11.46	1.69	2.49	2	0.13
20	30	-1.41	-2.74	-0.09	0.64	2.19	25	**0.038**
30	40	-0.12	-1.02	0.78	0.43	0.28	17	0.78
40	50	1.27	0.06	2.48	0.50	2.57	6	**0.042**
50	80	2.87	1.62	4.13	0.53	5.42	7	**0.0010**

7.1.3. Density

The density of composites containing 0 to 80% 1 micron particles was determined by mass/volume calculations. Density decreased from 2.6g/cc for pure submicron particle composite plates to 2.42g/cc for 80% 1µm composite plates (Figure 7.14). Composite flat plates manufactured with 40% 1 micron particles exhibited the smallest standard deviation, whilst those manufactured with 30% 1 micron particles exhibited the largest (Table 7.5).

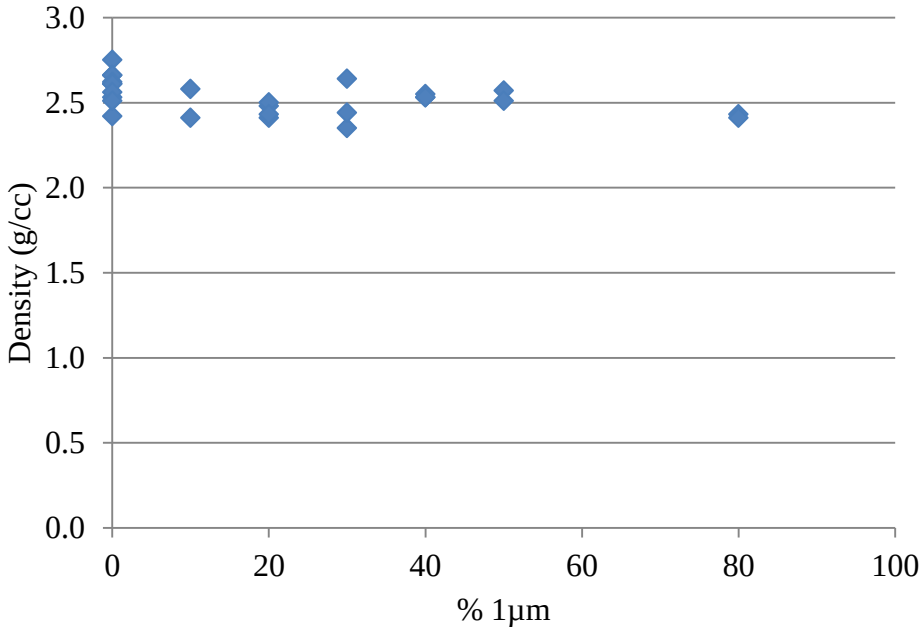

Figure 7.14. Density of composites composed of Nextel 720 fibres within an alumina matrix containing 0-80% 1 micron particles.

Table 7.5. Density values for composites composed of Nextel 720 fibres within an alumina matrix containing 0-80% 1 micron particles.

% 1µm	Density (g/cc)	St. Dev.	No. Plates
0	2.59	0.09	10
10	2.50	0.12	2
20	2.46	0.04	4
30	2.48	0.15	3
40	2.54	0.01	3
50	2.54	0.04	2
80	2.42	0.01	2

Welch's t-test was conducted to compare mean density values obtained for composites manufactured with 0-80% 1 micron particles (Table 7.6). The findings suggest that, at the 95% confidence level, mean densities of composites manufactured with 20 and 80% 1 micron particles are significantly different from the mean density of composites manufactured with a purely submicron particle distribution (0%) ($p<0.05$).

Table 7.6. Intermediate and p values obtained from Welch's t-test comparing density values for composites containing 0-80% 1 micron particles.

Grp 1 (%1 µm)	Grp 2	$X_1 - X_2$	95% CI Min	95% CI Max	$\sqrt{\frac{s_1^2}{n_1}+\frac{s_2^2}{n_2}}$	t	df	p
0	10	0.098	-1.04	1.24	0.090	1.09	1	0.4725
0	20	0.138	0.06	0.22	0.036	3.83	11	**0.0028**
0	30	0.116	-0.27	0.51	0.091	1.28	2	0.3276
0	40	0.056	-0.01	0.12	0.030	1.88	9	0.0928
0	50	0.053	-0.08	0.19	0.042	1.27	3	0.2950
0	80	0.173	0.10	0.24	0.031	5.60	9	**0.0003**

7.1.4. Linear Contraction

Linear contraction was calculated as a percentage change in plate thickness before and after sintering (Equation 7.1) for composites containing 0-40% 1 micron particles. Composite plates manufactured with purely submicron particles exhibited a mean linear contraction of 3.57% (±0.78%), whilst composites manufactured with 10-40% 1 micron particles exhibited mean linear contraction of 2.31-4.19% (Table 7.7, Figure 7.15).

$$Linear\ Contraction = 100 * \frac{Green\ thickness - Sintered\ thickness}{Green\ thickness} \quad \textbf{Equation 7.1}$$

Table 7.7. Linear contraction during sintering calculated as a percentage change in plate thickness for composites manufactured with 0-40% 1 micron particles.

% 1µm	Mean (%)	St. Dev (%)
0	3.57	0.78
10	4.19	0.51
20	3.68	1.29
30	2.31	0.52
40	2.51	0.30

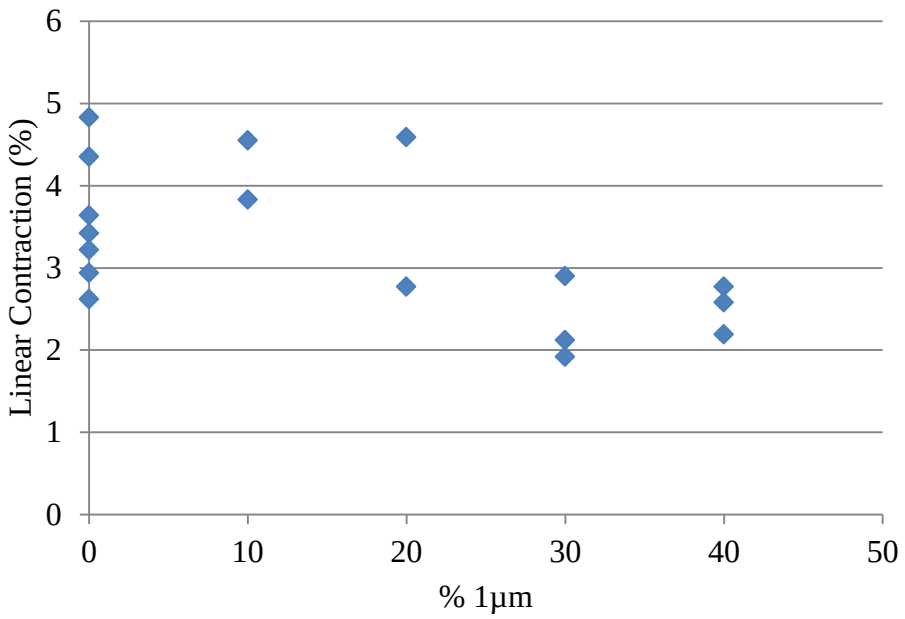

Figure 7.15. Linear contraction calculated as a percentage change in plate thickness during sintering for composites manufactured with 0-40% 1 micron particles.

Welch's t-test was conducted to compare linear contraction values obtained for composites manufactured with 0-40% 1 micron particles (**Table** 7.8). The findings suggest that, at the 95% confidence level, mean linear contraction values of composites manufactured with 10 and 20% 1 micron particles are not statistically different to composites manufactured with a purely submicron particle distribution (0%) ($p>0.05$). On the contrary, mean linear contraction of composites manufactured with 30 and 40% 1 micron particles were statistically different from the mean linear contraction of composites manufactured with a purely submicron particle distribution (0%) ($p<0.05$).

Table 7.8. Intermediate and p values obtained from Welch's t-test comparing linear contraction for composites containing 0-40% 1 micron particles.

Grp 1 (%1 µm)	Grp 2 (%1 µm)	$X_1 - X_2$	95% CI Min	95% CI Max	$\sqrt{\frac{s_1^2}{n_1} + \frac{s_2^2}{n_2}}$	t	df	p
0	10	-0.62	-2.62	1.39	0.47	1.32	2	0.317
0	20	-0.11	-12.26	12.05	0.96	0.11	1	0.930

0	30	1.26	0.18	2.34	0.42	3.00	5	**0.030**
0	40	1.06	0.26	1.87	0.34	3.12	7	**0.017**

7.1.5. Microstructural observations

Low magnification SEM micrographs of the in-plane composite structure of Specimen 1025 containing purely submicron particles revealed large matrix shrinkage cracks in matrix rich regions (Figure 7.16). SEM micrographs of Specimen 999 containing 20% 1 micron particles revealed seemingly fewer and smaller shrinkage cracks (Figure 7.17), whilst Specimen 1015 containing 50% 1 micron particles and Specimen 1010 containing 80% 1 micron particles revealed little evidence of matrix shrinkage cracking (Figure 7.18 and Figure 7.19). Fibre tows were seemingly well infiltrated with matrix material, however large-scale pores of irregular size and distribution were evident for all specimens observed.

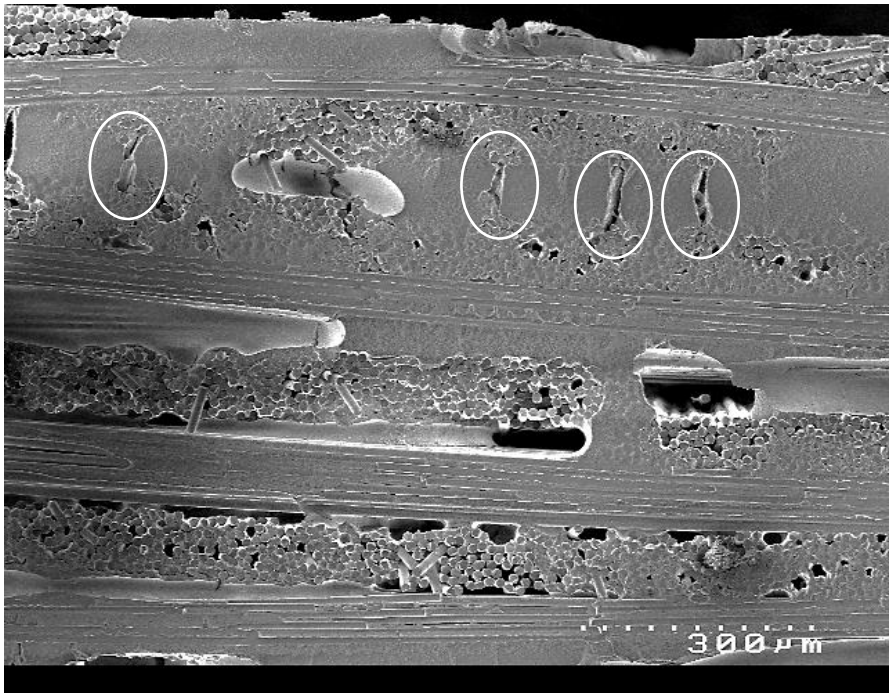

Figure 7.16. SEM micrograph of Specimen 1025 containing purely submicron alumina particles (0%) showing large shrinkage cracks in matrix rich regions.

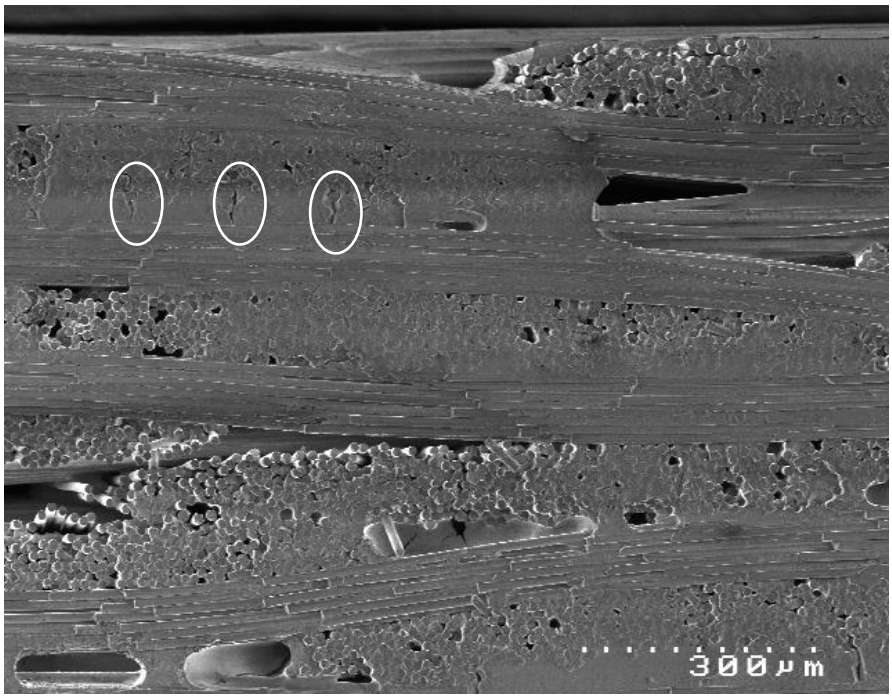

Figure 7.17. SEM micrograph of Specimen 999 containing 20% 1 micron alumina particles showing small shrinkage cracks in matrix rich regions.

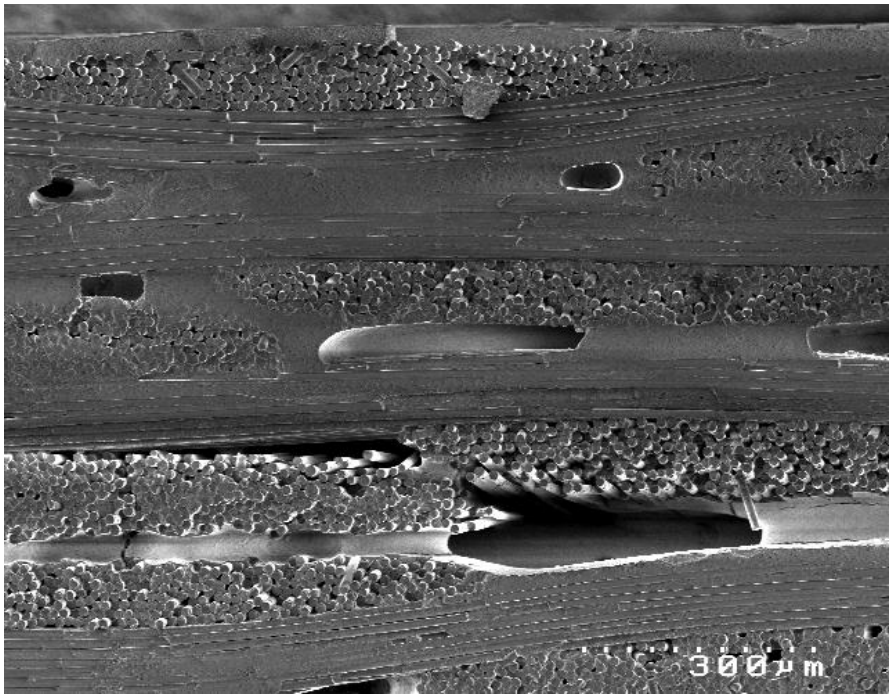

Figure 7.18. SEM micrograph of Specimen 1015 containing 50% 1 micron alumina particles showing little evidence of shrinkage cracks in matrix rich regions.

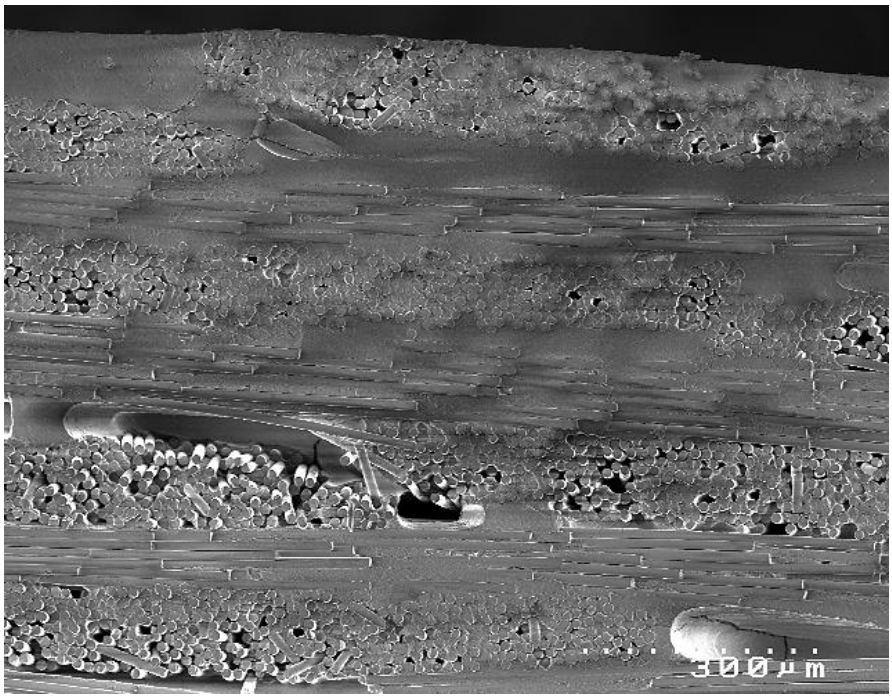

Figure 7.19. SEM micrograph of Specimen 1010 containing 80% 1 micron alumina particles showing little evidence of shrinkage cracks in matrix rich regions.

7.2. Discussion

Flexural strength values obtained for composites containing 20, 40 and 50% 1 micron particles were statistically significantly greater than composites containing purely submicron particles. Whilst values obtained for 30% 1 micron particles were not different from composites containing only submicron particles, the range of values was very large and encompassed the entire data set. It is therefore very difficult to draw any conclusions based on this data, and will be discussed in further detail below. For the purpose of discussion, composites containing 20, 40 and 50% 1 micron particles will be classified as 'moderate amounts' of 1 micron particles.

1 micron alumina particles were employed to reduce the number of shrinkage cracks and large-scale pores formed during particle densification and sintering. Hypothetically, submicron particles fill the inter-particle spaces between large particles, to achieve a high

packing density and to create a non-shrinking network (Figure 7.20). This ultimately reduces the number of shrinkage cracks and pores, subsequently improving composite performance.

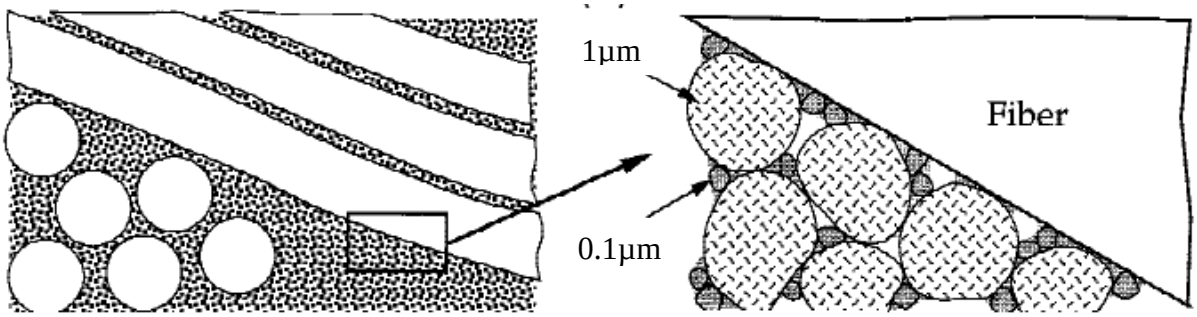

Figure 7.20. Microstructural design of an oxide-oxide CMC with a bimodal particle size distribution (After [42]**).**

The presence of a non-shrinking network was implied by calculation of linear contraction during sintering. Composites manufactured with 30 and 40% 1 micron particles revealed a significant decrease in linear contraction compared with composites containing only submicron particles. These findings suggests that moderate amounts of large particles within the matrix inhibited shrinkage during sintering, leading to less interparticle spacing and fewer shrinkage cracks, resulting in an improvement in flexural strength. Furthermore, microstructural analysis of composites containing 20% 1 micron particles revealed fewer and smaller shrinkage cracks compared with composites containing purely submicron particles, and composites containing 50% 1 micron particles revealed little evidence of shrinkage cracks. On the contrary, a significant decrease in short beam shear values obtained for composites containing 20, 40 and 50% 1 micron particles was evident. The short beam shear test is designed to induce shear stresses at the mid-plane resulting in a delamination failure, and is greatly affected by matrix strength and matrix adhesion with reinforcing fibres. As suggested previously, 1 micron particles provide a non-shrinking network that resists densification. Whilst this proved beneficial to flexural strength, incomplete densification results in both a weaker matrix and poorer fibre/matrix adhesion. Subsequently, composites

containing a moderate amount of 1 micron particles were less able to withstand shear stresses at the mid-plane, resulting in premature delamination.

Composites containing 80% 1 micron particles demonstrated significantly poorer flexural and short beam shear strength compared with composites containing 0-50% 1 micron particles. Microstructural observations revealed little evidence of shrinkage cracks in matrix rich regions, providing a more uniform structure. Nevertheless, it has already been suggested that the incorporation of less-sinterable 1 micron particles results in a less dense composite with poorer matrix strength. Calculation of composite density by mass/volume calculations revealed that composites containing 80% 1 micron particles were significantly less dense than composites containing only submicron particles. When a composite with an exceptionally weak matrix is loaded in three-point bend, it is possible that failure does not occur by tension at the top surface but by delamination at the mid-plane, resulting in premature failure. Further investigation would be required to confirm this suggestion.

Composites containing 30% 1 micron particles exhibited a large range in flexural strength data, and data was randomly distributed. Variability is an inherent characteristic of oxide composite materials and by the nature of three-point bend testing. Nevertheless, there is no reasonable explanation as to why flexural strength values obtained for composites containing 30% 1 micron particles should differ to any other data set. 37 specimens were tested in three-point bend which were diamond cut from three composite flat plates manufactured using the same processing technique. Bowles and Frimpong proposed that an increase in void content may lead to an increase in scatter [128], however it is apparent from Figure 7.21 that a large amount of variability occurred not only between plates, but also within plates, eliminating factors such as porosity, density or matrix volume fraction. Furthermore, frequency

histograms illustrating the distribution of data revealed that flexural strength values obtained for composites containing 30% 1 micron particles were randomly distributed. Conversely, flexural strength values obtained for 0, 10, 20, 40, 50 and 80% 1 micron particles demonstrated a normal distribution, whereby the mean, median and mode values are approximately equal, and the data is approximately symmetrical. Normal distribution allows a large population of data to be described completely by two parameters, mean and standard deviation.

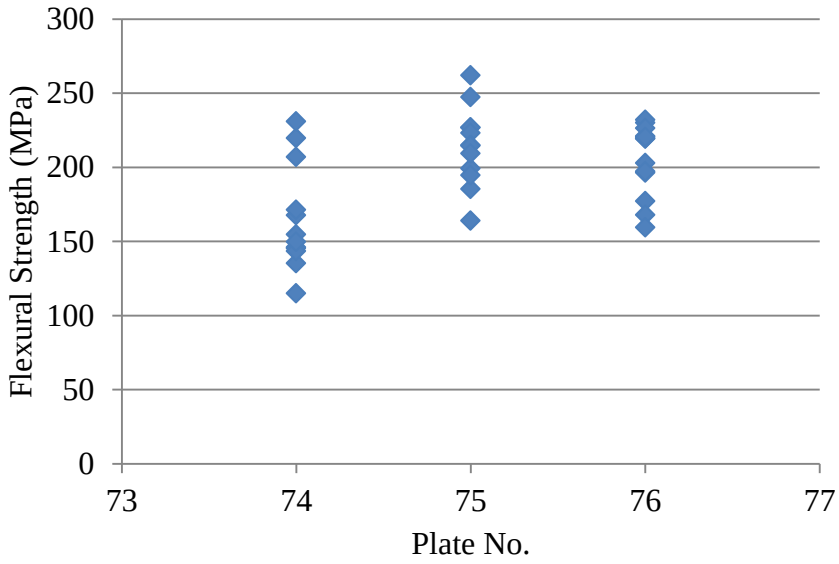

Figure 7.21. Flexural strength values for composites containing 30% 1 micron particles.

There were no observable differences in the stress-displacement response for specimens loaded in three-point bend manufactured with 30% 1 micron particles, despite a maximum strength value more than double that of minimum strength. Equally, there were no observable differences in the stress-displacement response for specimens loaded in three-point bend manufactured with 0-80% 1 micron particles. The response was typically linear elastic until peak load was achieved, after which load bearing capacity decreased significantly. A small number of specimens demonstrated a region of linear elasticity followed by non-linear

behaviour prior to failure, revealing the presence of matrix micro-cracking prior to composite failure.

7.3. Concluding remarks

Incorporating a moderate amount of 1 micron alumina particles into slurry during manufacture improved composite flexural strength, yet proved detrimental to short beam shear strength. Composites containing 10% 1 micron particles were statistically not different from composites containing purely submicron particles in both flexural and short beam shear strength. The addition of 1 micron particles did not reveal any manufacturing advantages and will therefore not be pursued throughout the remainder of the project.

Chapter 8 - The effect of sintering temperature on processing and properties of Nextel 720 fibres within an alumina matrix containing ACH

Sintering is the final phase in the production of an oxide CMC and involves burnout of polymer binders (PVA and PEG), decomposition of precursors (ACH) and densification of ceramic particles. Sintering occurs at temperatures usually between 0.5 and 0.75 of the melting temperature of the ceramic particles. Taimicron TM-DAR alumina particles have been shown to increase in density from 2.5g/cc to 4.0g/cc with an increase in temperature from 1100 to 1300°C [129]. Whilst it was recognised that Nextel 720 fibres possess a maximum temperature capability of 1200°C, the effect of sintering at temperatures between 1100 and 1300°C was investigated.

Composites flat plates of 11 ply thickness, 80x150mm, composed of Nextel 720 fibres within a submicron particle diameter alumina matrix containing 10wt% ACH were sintered at 6 temperatures between 1100°C to 1300°C (including dwell periods at 250°C, 525°C and 800°C). Composites were manufactured by both the author and Dr E.G. Butler. Twelve flexural (6 longitudinal, 6 transverse) and eight shear (4 longitudinal, 4 transverse) specimens were diamond cut from each plate flat. Specimens were tested in both three-point bend and short beam shear using the parameters outlined in sections 4.2.1. and 0. Non-coated specimens were observed using a field emission scanning electron microscope (FEG SEM) operating at 4kV acceleration voltage.

8.1. Results

8.1.1. Flexural strength

Mean flexural strength increased from 157.5MPa for specimens sintered at 1100°C, to 208.9MPa for specimens sintered at 1175°C. Specimens sintered at 1200°C, reported previously as 10wt% ACH and 0% 1 micron particles, revealed mean flexural strength of 205.3MPa. Specimens sintered at 1300°C demonstrated mean flexural strength of 99.9MPa (Table 8.1). Standard deviation ranged from 5.2MPa for specimens sintered at 1300°C, to 26.9MPa for those sintered at 1175°C (Figure 8.1). Equally, specimens sintered at 1175°C displayed the largest interquartile range, whilst those sintered at 1300°C displayed the smallest (Figure 8.2). Frequency histograms presented in Figure 8.3 illustrating the distribution of flexural strength data typically revealed a random distribution with the exception of composites sintered at 1150 and 1200°C which demonstrated normal distribution.

Table 8.1. Flexural strength data for composites composed of Nextel 720 fibres within an alumina matrix with 10wt% ACH sintered at temperatures between 1100 and 1300°C.

Temp (°C)	Min.	Q1	Median	Q3 (MPa)	Max.	Mean	St. Dev	No. Tests
1100	129.2	152.4	157.9	163.5	174.6	157.5	13.0	11
1150	178.1	195.5	206.8	215.3	253.8	205.7	15.1	52
1175	140.8	197.6	215.0	228.6	244.7	208.9	26.9	26
1200	162.4	191.6	205.8	219.8	251.3	205.3	20.4	138
1225	151.2	159.9	171.1	184.9	196.0	172.3	14.4	24
1300	91.0	95.5	101.4	104.3	106.0	99.9	5.2	12

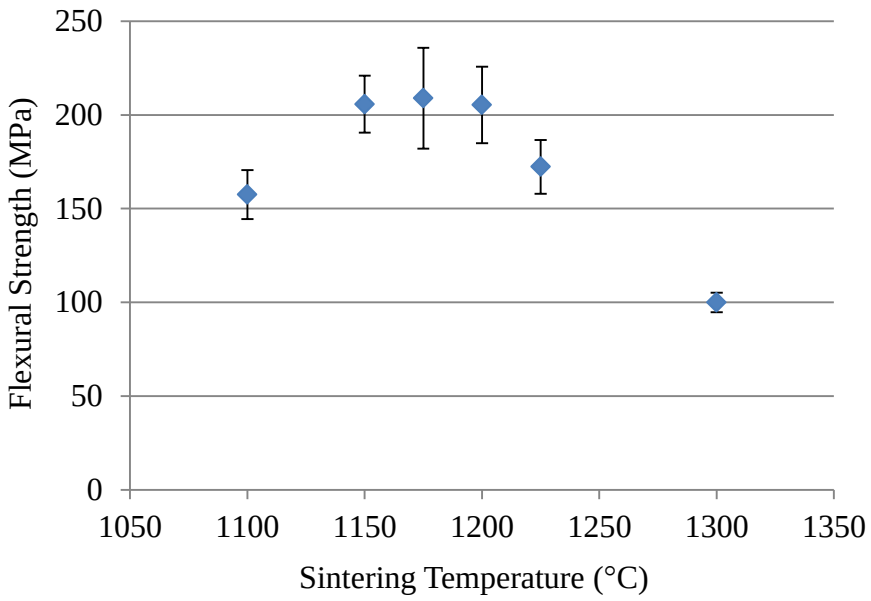

Figure 8.1. Flexural strength values illustrated by mean and standard deviation comparing composites composed of Nextel 720 fibres within an alumina matrix sintered at temperatures between 1100 and 1300°C.

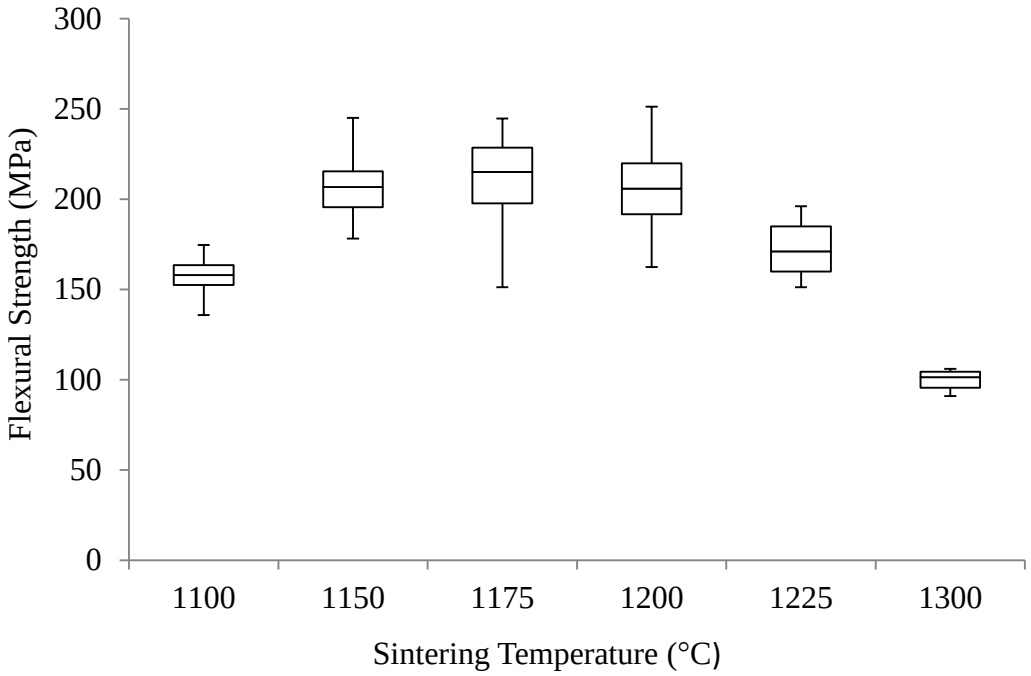

Figure 8.2. Box and whisker diagram comparing flexural strength values for composites composed of Nextel 720 fibres within an alumina matrix sintered at temperatures between 1100 and 1300°C.

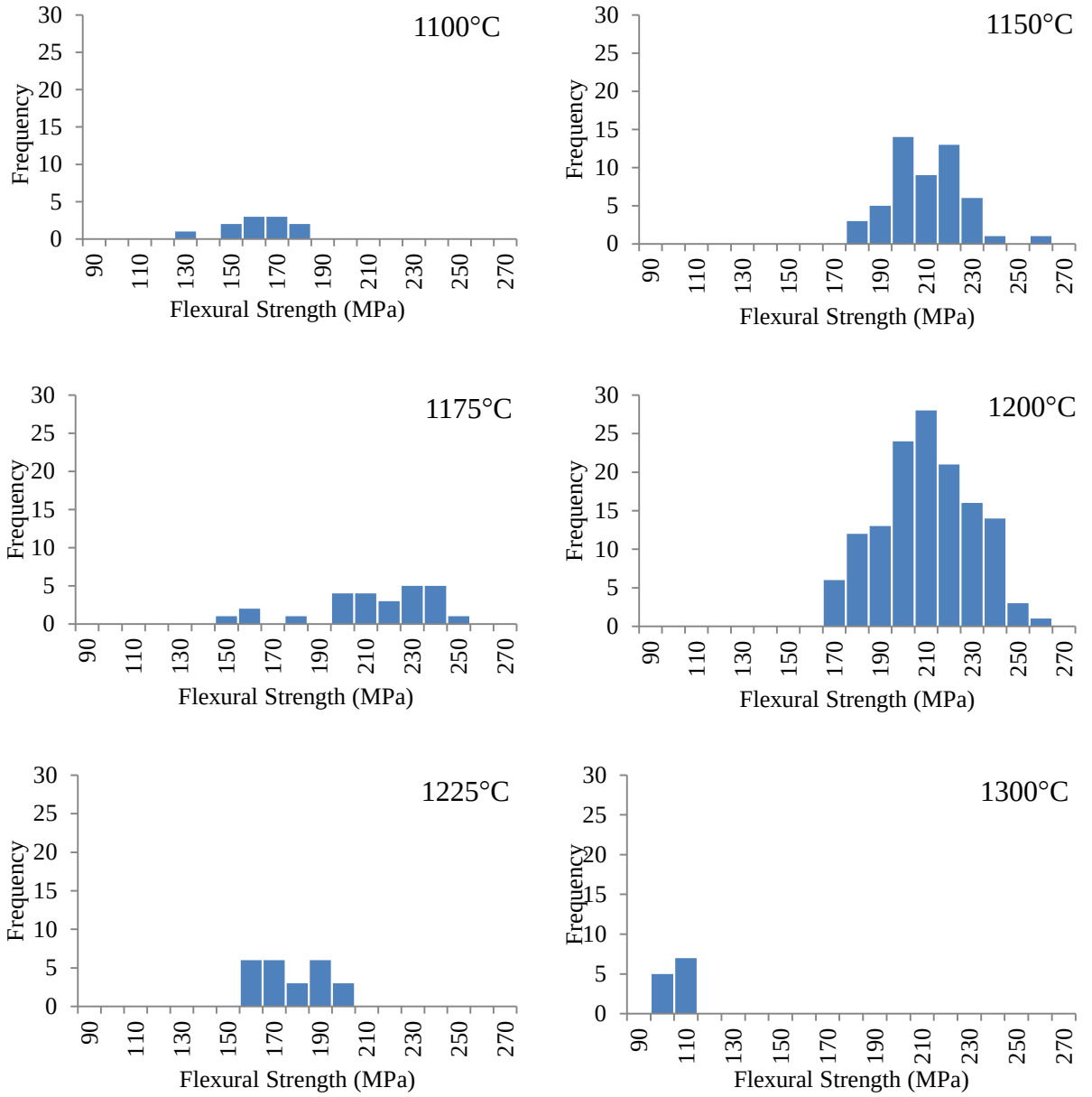

Figure 8.3. Frequency histograms comparing flexural strength values for composites composed of Nextel 720 fibres within an alumina matrix sintered at temperatures between 1100 and 1300°C.

Welch's t-test was conducted to compare mean flexural strength values obtained after sintering at 1100-1300°C with mean flexural strength after sintering at 1200°C. Flexural strength values of specimens sintered at 1100, 1225 and 1300°C were found to be extremely statistically different ($p<0.0001$) from flexural strength values of specimens sintered at 1200°C. On the contrary, flexural strength values of specimens sintered at 1150 and 1175°C

were found to be statistically not different from flexural strength of specimens sintered at 1200°C. These findings suggest that, at the 95% confidence level, flexural strength is not affected by sintering temperatures between 1150 and 1200°C.

Table 8.2. Intermediate and p values obtained from Welch's t-test comparing flexural strength values for composites sintered at temperatures between 1100 and 1300°C.

Grp 1 (°C)	Grp 2	$X_1 - X_2$	95% CI		$\sqrt{\frac{s_1^2}{n_1} + \frac{s_2^2}{n_2}}$	t	df	p
			Min	Max				
1200	1100	47.82	38.62	57.02	4.29	11.15	14	**1.99×10^{-08}**
1200	1150	-0.4219	-5.81	4.97	2.72	0.15	122	0.88
1200	1175	-3.56	-14.90	7.77	5.55	0.64	30	0.53
1200	1225	33.00	26.11	39.88	3.41	9.68	41	**3.74×10^{-12}**
1200	1300	105.39	100.77	110.01	2.30	45.82	51	**1.30×10^{-43}**

Representative stress-displacement curves for specimens sintered at temperatures between 1100 and 1300°C loaded in three-point bend are presented in Figure 8.4 to Figure 8.9. Stress-displacement curves for specimens sintered at 1200°C, manufactured with 100% submicron alumina particles containing 10wt% ACH are shown in Figure 8.7 for reference. Typically, the stress-displacement response was approximately linear until peak load was achieved, after which a significant decrease in load bearing capacity was evident. A small number of specimens demonstrated a region of non-linear behaviour prior to failure (Specimen 836, Figure 8.5 and Specimen 1198, Figure 8.6).

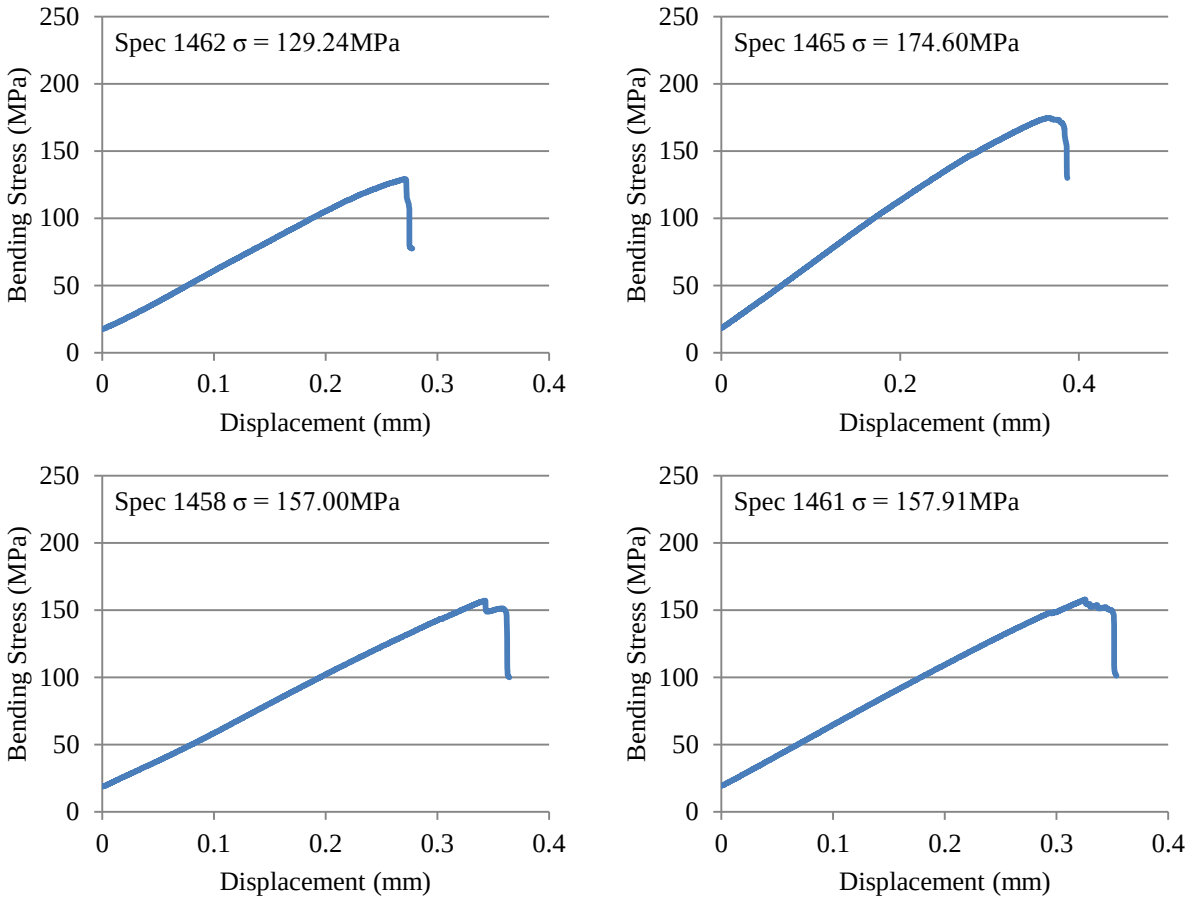

Figure 8.4. Representative stress-displacement curves for specimens composed of Nextel 720 fibres within an alumina matrix containing 10wt% ACH sintered at 1100°C showing minimum (Spec 1462), maximum (Spec 1465) and 2 average strength values (Spec 1458 & Spec 1461).

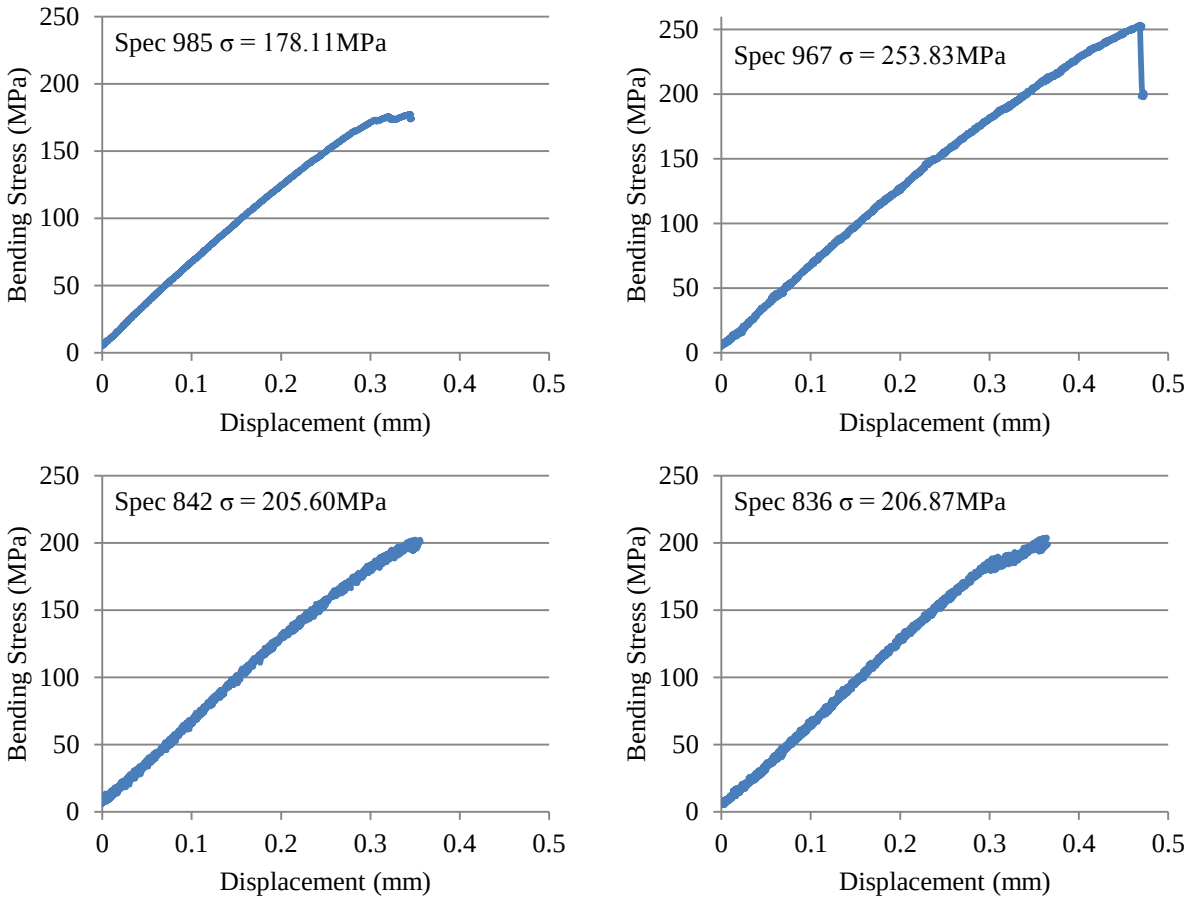

Figure 8.5. Representative stress-displacement curves for specimens composed of Nextel 720 fibres within an alumina matrix containing 10wt% ACH sintered at 1150°C showing minimum (Spec 985), maximum (Spec 967) and 2 average strength values (Spec 842 and Spec 836).

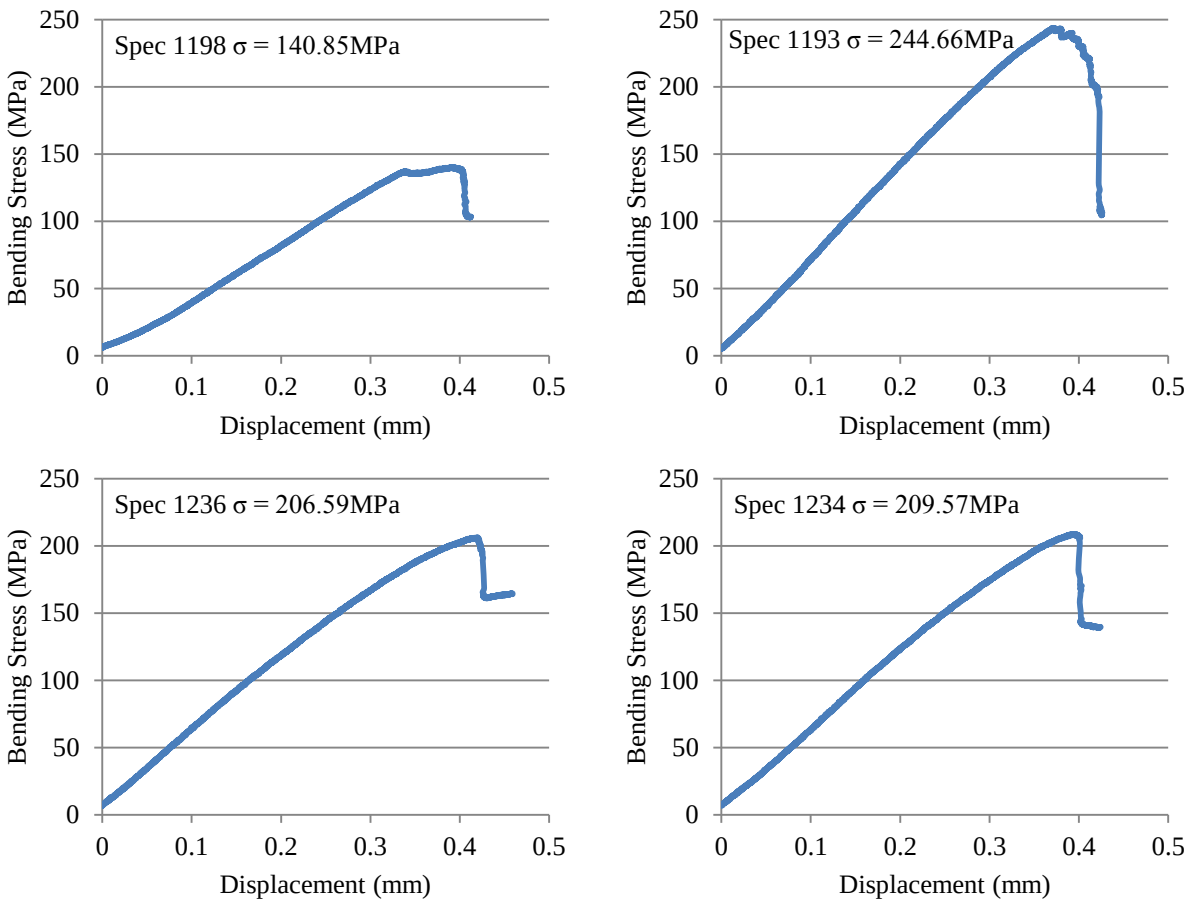

Figure 8.6. Representative stress-displacement curves for specimens composed of Nextel 720 fibres within an alumina matrix containing 10wt% ACH sintered at 1175°C showing minimum (Spec 1198), maximum (Spec 1193) and 2 average strength values (Spec 1236 & Spec 1234).

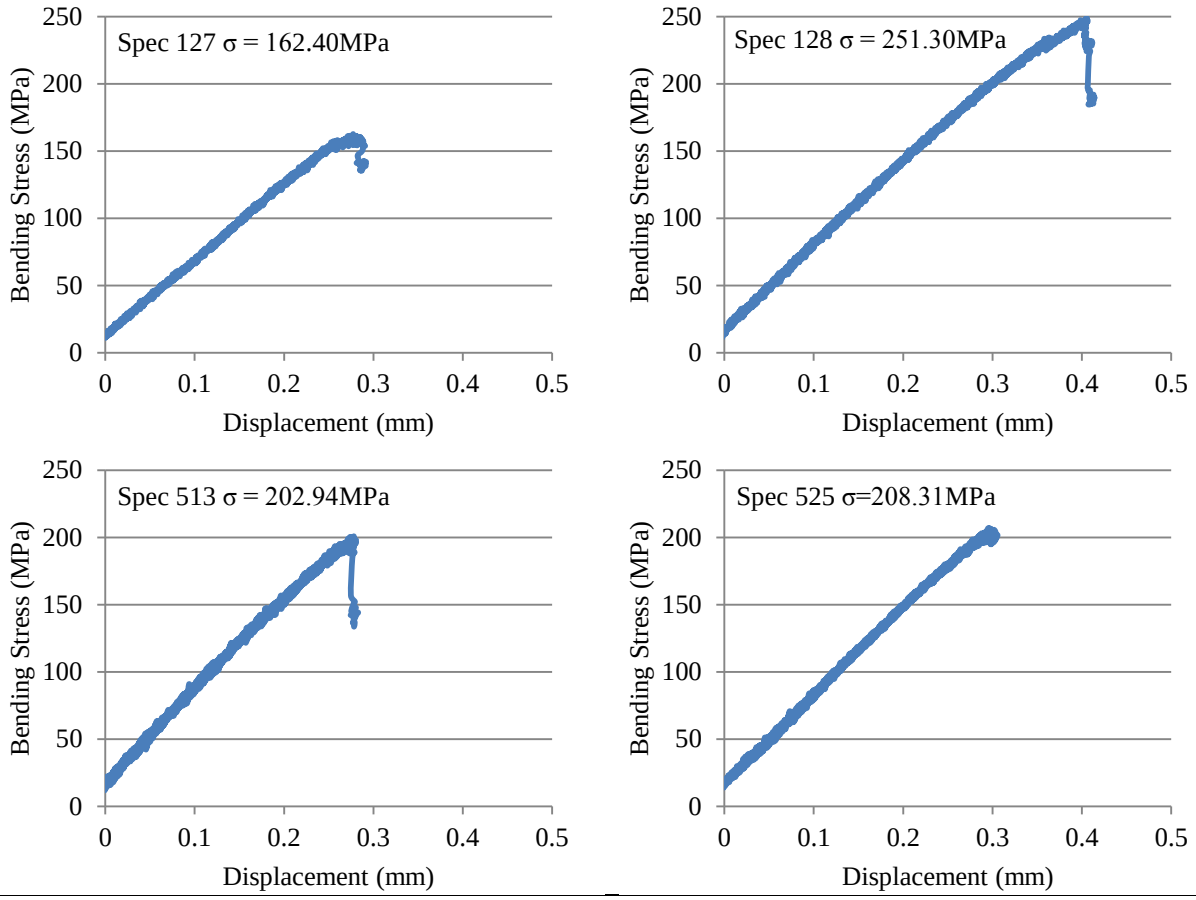

Figure 8.7. Representative stress-displacement curves for specimens composed of Nextel 720 fibres within an alumina matrix containing 10wt% ACH sintered at 1200°C showing minimum (Spec 127,), maximum (Spec 128) and 2 average strength values (Spec 513 & Spec 525).

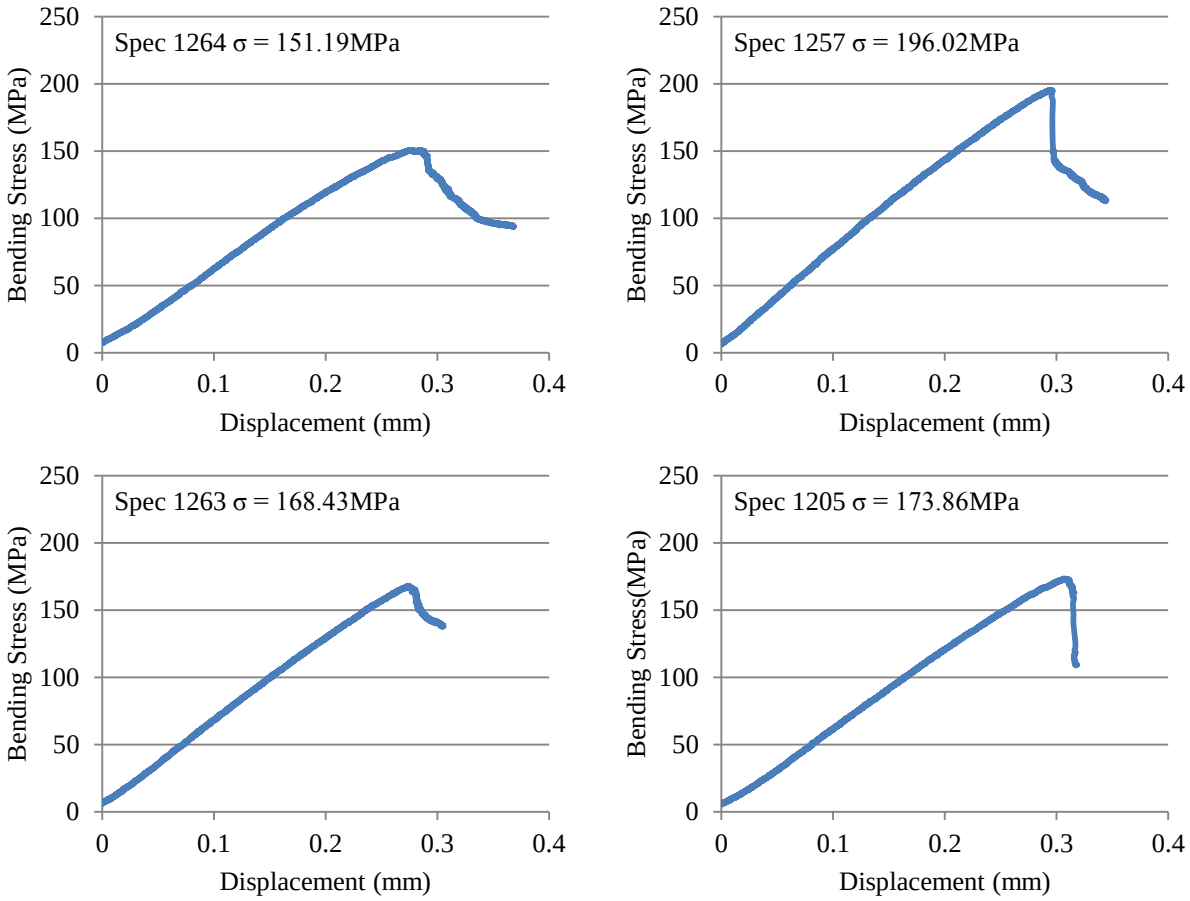

Figure 8.8. Representative stress-displacement curves for specimens composed of Nextel 720 fibres within an alumina matrix containing 10wt% ACH sintered at 1225°C showing minimum (Spec 1264), maximum (Spec 1257) and 2 average strength values (Spec 1263 & Spec 1205).

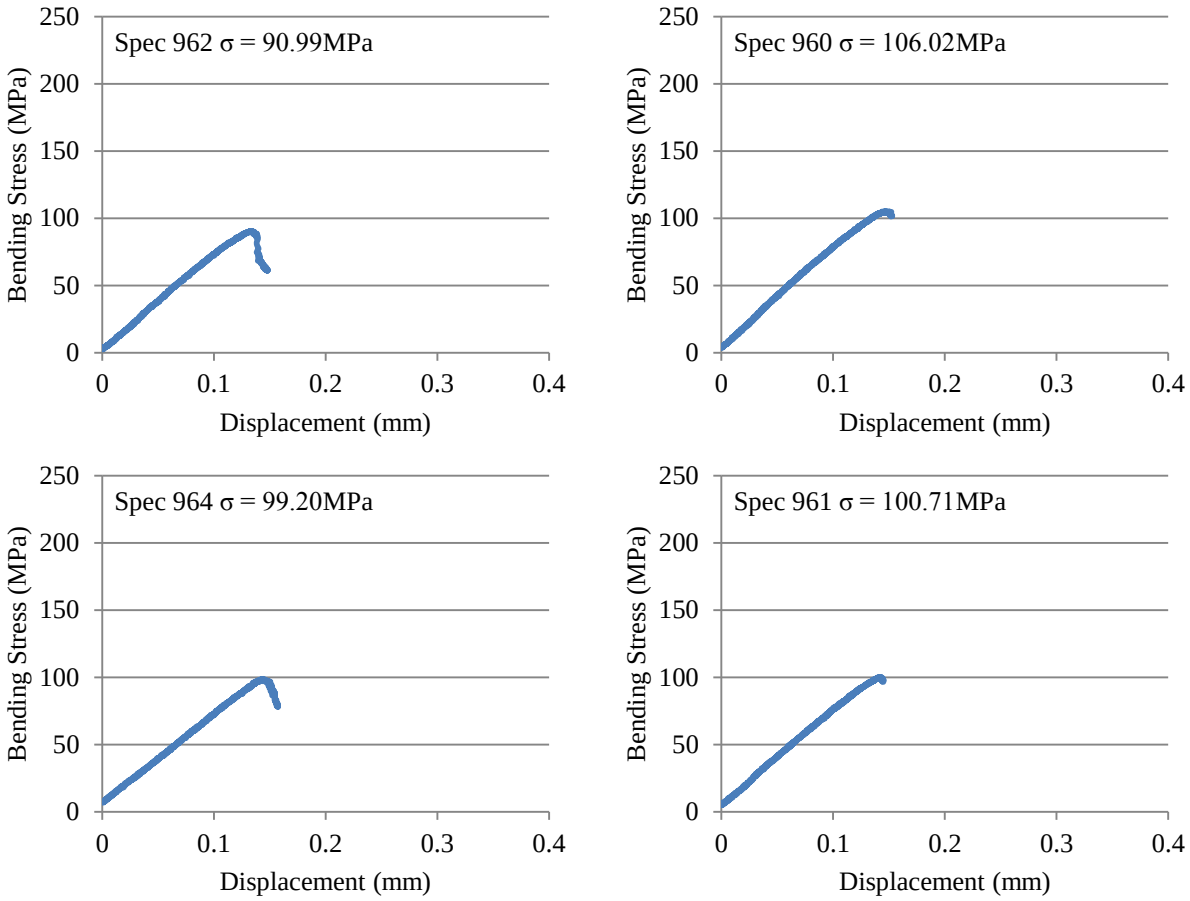

Figure 8.9. Representative stress-displacement curves for specimens composed of Nextel 720 fibres within an alumina matrix containing 10wt% ACH sintered at 1300°C showing minimum (Spec 962), maximum (Spec 960) and 2 average strength values (Spec 964 & Spec 961).

Low magnification SEM micrographs comparing the in-plane structure of specimen 845 (Figure 8.10), sintered at 1150°C, with specimen 958 (Figure 8.11), sintered at 1300°C, revealed no discernible changes with an increase in sintering temperature. Equally, low magnification micrographs of the in-plane composite structure after loading in three-point bend showed no evidence of failure in either specimen (Figure 8.10 and Figure 8.11, image a compared with b).

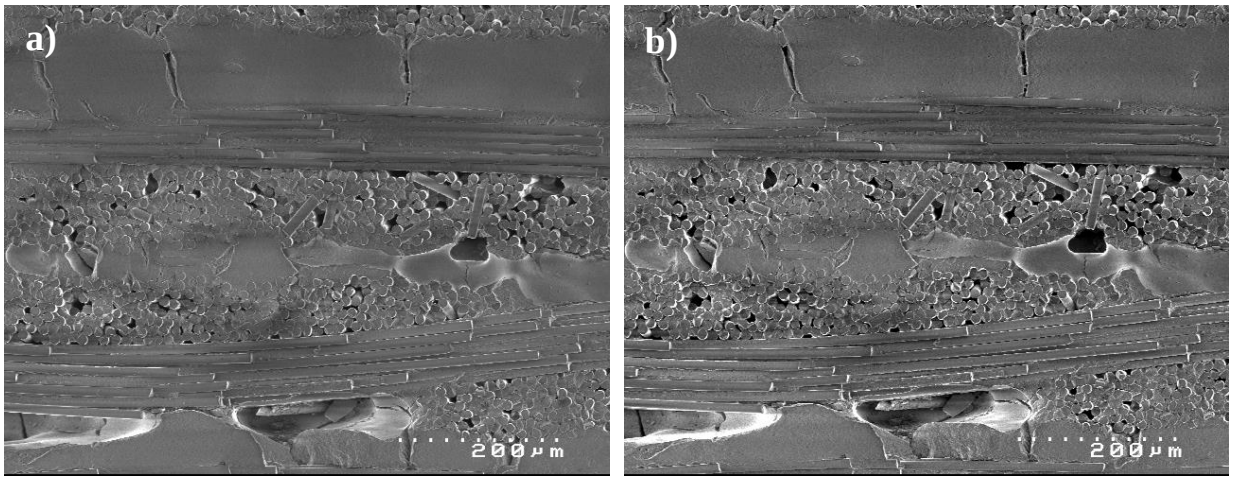

Figure 8.10. SEM micrographs of Specimen 845, sintered at 1150°C, a) in-plane composite structure prior to loading, b) in-plane composite structure after loading in three point bend.

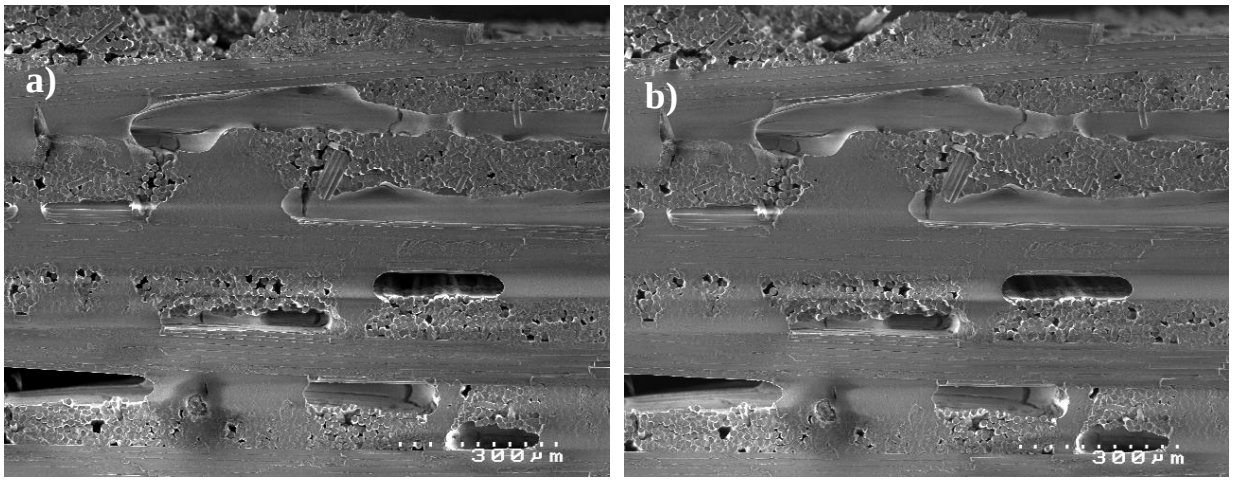

Figure 8.11. SEM micrographs of Specimen 958, sintered at 1300°C, a) in-plane composite structure prior to loading, b) in-plane composite structure after loading in three point bend.

Higher magnification SEM micrographs of the specimen top surface, directly beneath the central load roller, showed markedly different failure with an increase in sintering temperature. Specimen 921, sintered at 1200°C (Figure 8.12 a) showed evidence of fibre debonding and crack bridging whilst Specimen 958, sintered at 1300°C (Figure 8.12 b) displayed evidence of crack extension into reinforcing fibres.

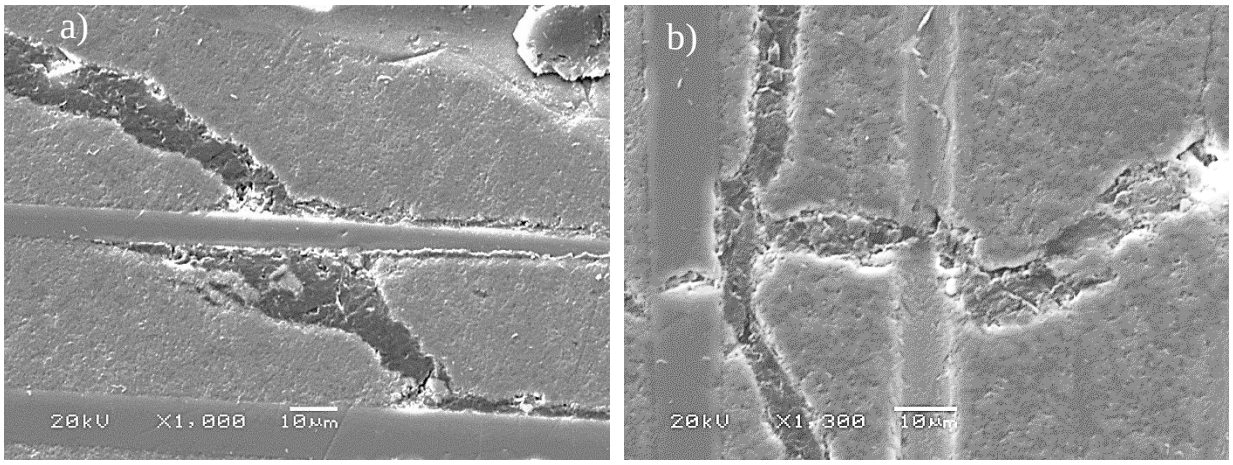

Figure 8.12. SEM micrographs of flexural test fracture surfaces showing a) fibre/matrix debonding and crack bridging (specimen 921 sintered at 1200°C) and b) damage extending directly into fibre (specimen 958 sintered at 1300°C).

8.1.2. Short beam shear

Specimens containing only submicron particles, containing 10wt% ACH sintered at 1200°C demonstrated mean short beam shear strength of 12.1MPa. Short beam shear strength increased from 8.3MPa for specimens sintered at 1100°C, to 13.9MPa for specimens sintered at 1300°C (Table 8.3). Specimens sintered at 1175°C revealed the smallest standard deviation and interquartile range, whilst those sintered at 1300°C revealed the largest (Figure 8.13 and Figure 8.14). Frequency histograms illustrating the distribution of short beam shear data for specimens sintered at 1175, 1200 and 1300°C revealed normal distribution whilst data for specimens sintered at 1100, 1150 and 1225°C demonstrated random distribution.

Table 8.3. Short beam shear values for composites composed of Nextel 720 fibres within an alumina matrix containing sintered at temperatures between 1100 and 1300°C.

Temp (°C)	Min	Q1	Median	Q3 (MPa)	Max	Mean	St. Dev	Data Points
1100	7.57	7.78	7.85	9.01	9.46	8.34	0.84	5
1150	7.09	9.58	10.52	11.19	11.94	10.25	1.41	17
1175	10.36	10.91	11.18	11.70	12.11	11.26	0.64	6
1200	10.52	11.63	12.06	12.79	13.53	12.10	0.90	14
1225	11.21	11.52	11.65	12.64	14.51	12.24	1.27	6
1300	11.89	12.81	13.53	14.94	16.16	13.87	1.53	7

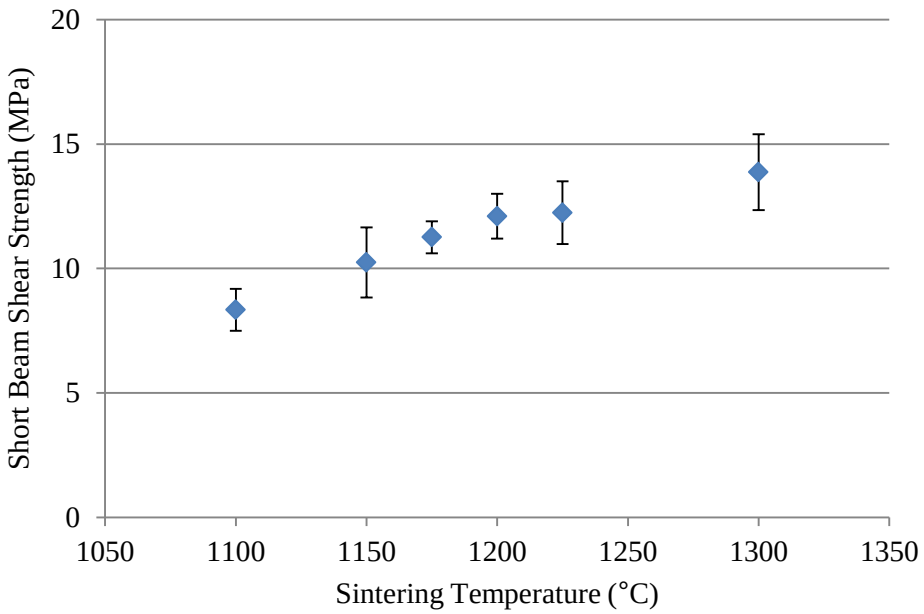

Figure 8.13. Short beam shear values illustrated by mean and standard deviation for composites composed of Nextel 720 fibres within an alumina matrix sintered at temperatures between 1100 and 1300°C.

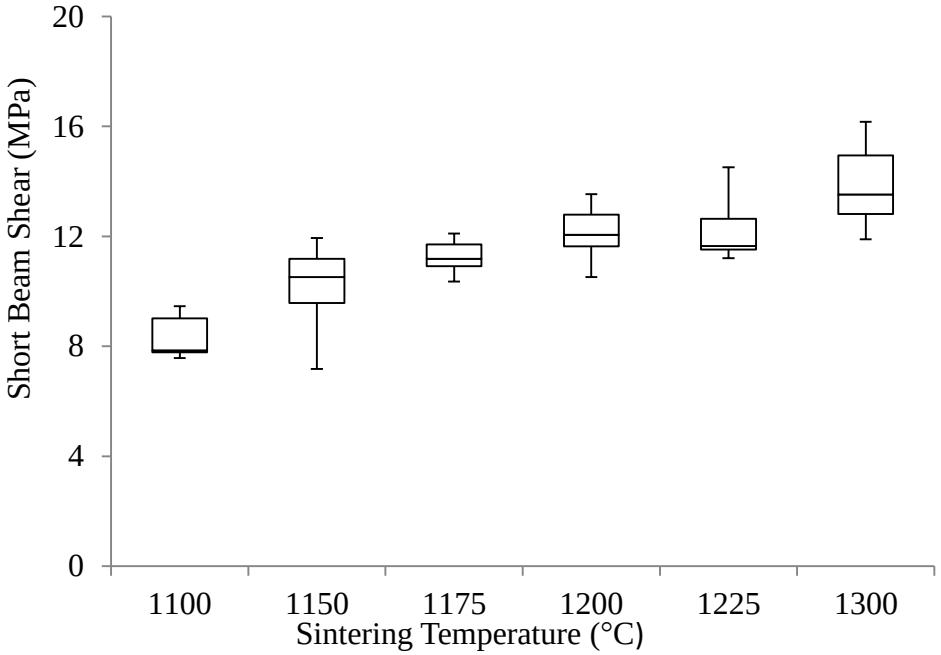

Figure 8.14. Box and whisker diagram comparing short beam shear values for composites composed of Nextel 720 fibres within an alumina matrix sintered at temperatures between 1100 and 1300°C.

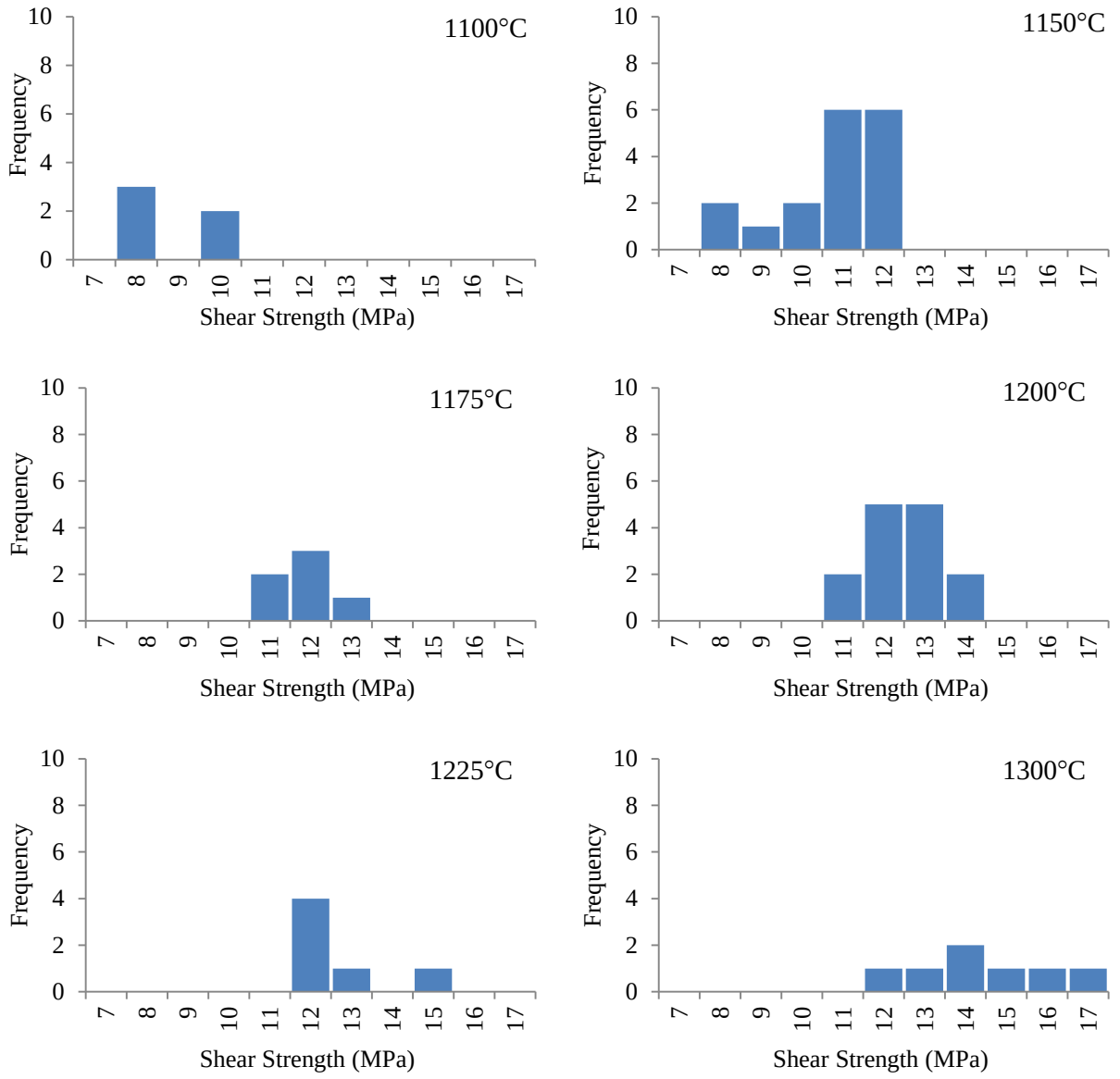

Figure 8.15. Frequency histograms comparing short beam shear values for composites composed of Nextel 720 fibres within an alumina matrix sintered at temperatures between 1100 and 1300°C.

Welch's t-test was conducted to compare mean short beam shear strength values obtained after sintering at temperatures between 1100 and 1300°C. Shear strength values of specimens sintered at 1100, 1150, 1175 and 1300°C were found to be statistically different ($p<0.05$) from shear strength values of specimens sintered at 1200°C. On the contrary, shear strength values of specimens sintered at 1225°C were found to be not statistically different from shear

strength of specimens sintered at 1200°C ($p>0.05$). These finding suggest that at the 95% confidence level, sintering at temperatures between 1200 and 1225°C does not affect short beam shear strength.

Table 8.4. Intermediate and p values obtained from Welch's t-test comparing short beam shear strength values for composites sintered at temperatures between 1100 and 1300°C.

Grp 1 (°C)	Grp 2	$X_1 - X_2$	95% CI		$\sqrt{\frac{s_1^2}{n_1} + \frac{s_2^2}{n_2}}$	t	df	p
			Min	Max				
1200	1100	3.42	2.19	4.65	0.52	6.56	7	**0.0003**
1200	1150	1.86	0.97	2.76	0.44	4.28	25	**0.0002**
1200	1175	0.85	0.08	1.61	0.36	2.38	13	**0.033**
1200	1225	-0.14	-1.49	1.20	0.57	0.25	7	0.81
1200	1300	-1.77	-3.21	-0.33	0.62	2.83	8	**0.022**

Representative stress-displacement curves for specimens sintered at 1100, 1200 and 1300°C loaded in short beam shear are presented in Figure 8.16 to Figure 8.18. For all specimens sintered at all temperatures, a nearly linear elastic response was evident during initial loading. However, markedly different behaviour was observed after maximum load was achieved. Specimens sintered at 1100°C retained their load bearing capacity once peak load had been achieved (Figure 8.16), whilst those sintered at 1200°C showed a small load drop, followed by retention of load (Figure 8.17). Specimens sintered at 1300°C showed a sharp, significant decrease in load (Figure 8.18).

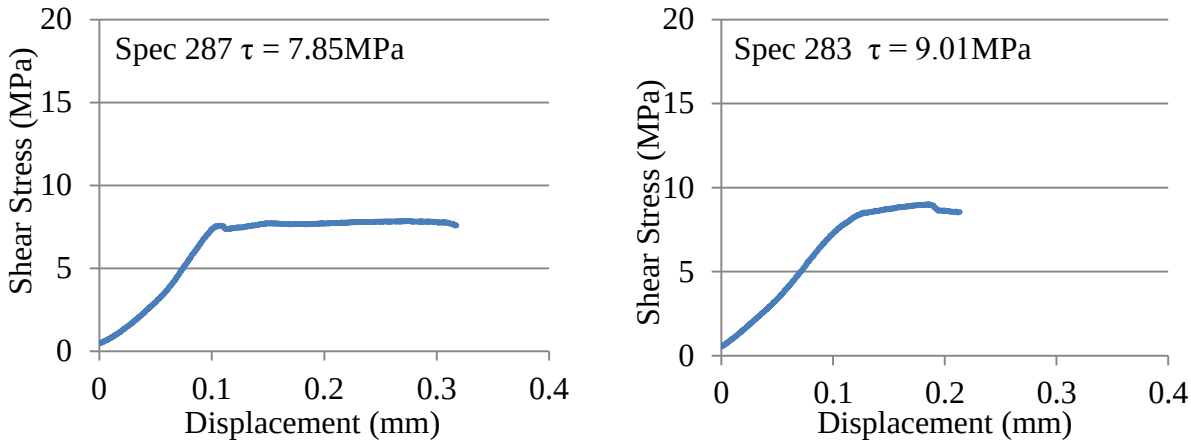

Figure 8.16. Representative stress-displacement curves for specimens composed of Nextel 720 fibres within a submicron particle alumina matrix containing 10wt% ACH sintered at 1100°C loaded in short beam shear.

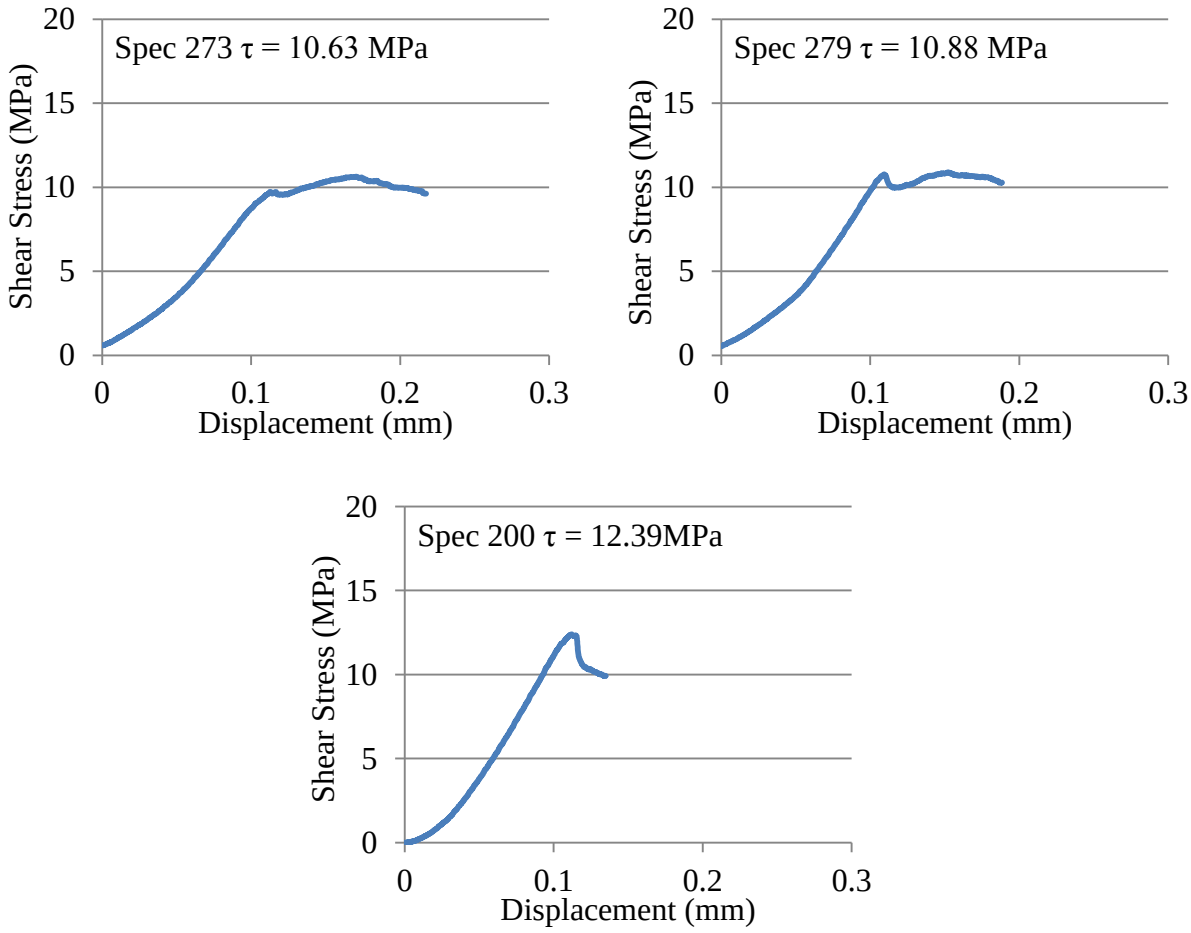

Figure 8.17. Representative stress-displacement curve for specimens composed of Nextel 720 fibres within a submicron particle alumina matrix containing 10wt% ACH sintered at 1200°C loaded in short beam shear.

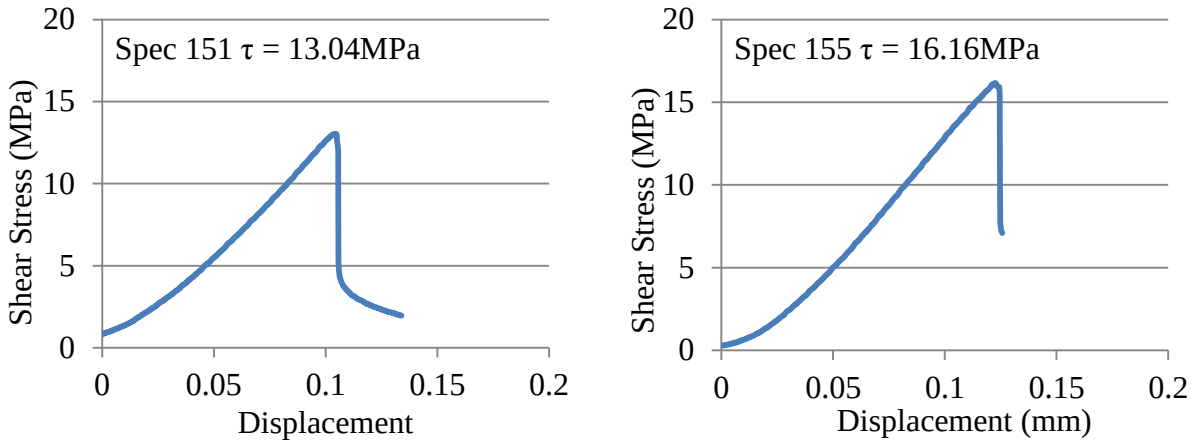

Figure 8.18. Representative stress-displacement curves for specimens composed of Nextel 720 fibres within a submicron particle alumina matrix containing 10wt% ACH sintered at 1300°C loaded in short beam shear.

Optical micrographs of specimens 286 and 287 sintered at 1100°C (Figure 8.19 a & b) reveal evidence of delamination between the outer plies, at the specimen edge. Optical micrographs of specimens 198 and 179 sintered at 1200°C (Figure 8.19 c & d) reveal evidence of delamination at the mid-plane, in the centre of the specimen. Micrographs of the in-plane structure of specimen 154, sintered at 1300°C, illustrate a combination of delamination and tensile failure (Figure 8.20 a), whilst examination of specimen 151 revealed tensile cracking on the top surface, directly beneath the central load roller (Figure 8.20 b).

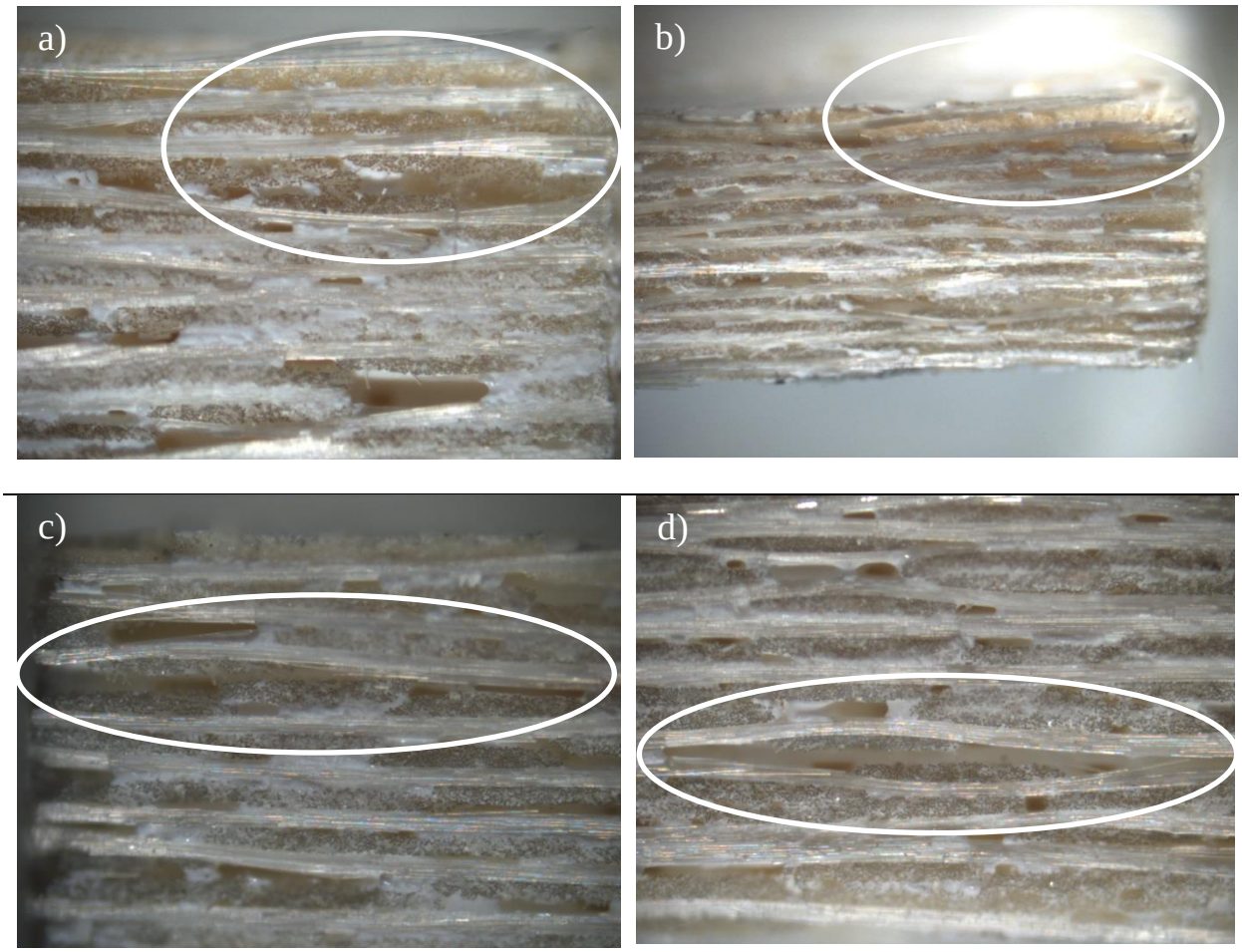

Figure 8.19. Optical micrographs of a) Specimen 286 and b) Specimen 287 sintered at 1100°C, and c) Specimen 198 and d) Specimen 179 (τ = 11.9MPa) sintered at 1200°C illustrating interlaminar shear failure.

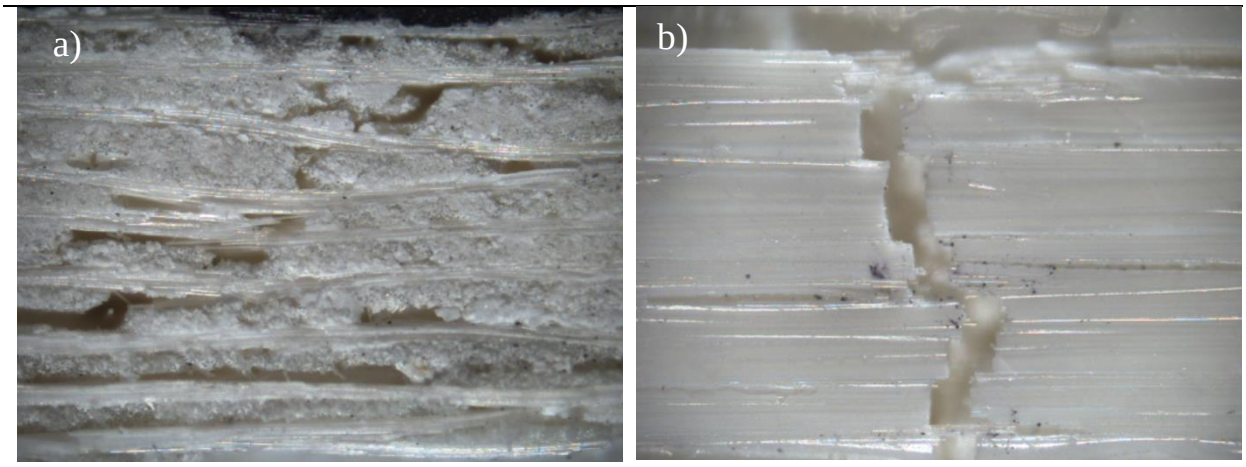

Figure 8.20. Optical micrographs of short beam shear specimens sintered at 1300°C. a) Specimen 154 front surface showing combination of interlaminar and tensile failure and b) Specimen 151 top surface showing tensile failure.

8.1.3. Density

The density of composites sintered at temperature between 1100 and 1300°C was determined by mass/volume calculations. Density increased from 2.38g/cc after sintering at 1100°C to 2.57-2.63g/cc after sintering at 1175-1300°C (Figure 8.21, Table 8.5). Welch's t-test was conducted to compare mean density values obtained for composites sintered between 1150 and 1225°C (**Table** 8.6). The findings suggest that, at the 95% confidence level, mean density of composites sintered at 1150, 1175 and 1225°C are statistically not different from composites sintered at 1200°C ($p>0.05$).

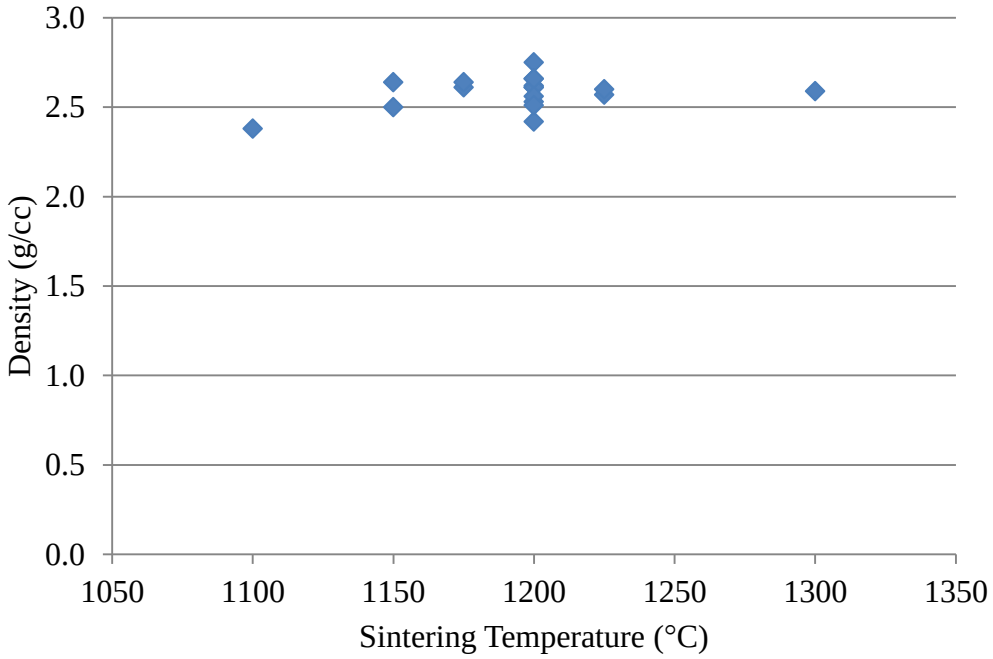

Figure 8.21. Density of composites composed of Nextel 720 fibres within a submicron particle alumina matrix containing 10wt% ACH sintered at temperatures between 1100°C and 1300°C.

Table 8.5. Density values for composites composed of Nextel 720 fibres within an alumina matrix containing 10wt% ACH sintered at temperatures between 1100°C and 1300°C.

Sintering Temp (°C)	Density (g/cc)	St. Dev	No. Plates
1100	2.38	-	1
1150	2.57	0.10	2
1175	2.63	-	2
1200	2.59	0.09	10
1225	2.59	0.02	2
1300	2.59	-	1

Table 8.6. Intermediate and p values obtained from Welch's t-test comparing density values for composites sintered at temperatures between 1150°C and 1225°C.

Grp 1 (%1 µm)	Grp 2	$X_1 - X_2$	95% CI Min	95% CI Max	$\sqrt{\frac{s_1^2}{n_1} + \frac{s_2^2}{n_2}}$	t	df	p
1200	1150	0.023	-0.94	0.99	0.076	0.30	1	0.81
1200	1175	-0.032	-0.11	0.04	0.033	0.97	8	0.36
1200	1225	0.008	-0.07	0.08	0.033	0.24	8	0.81

8.1.4. Linear contraction

Linear contraction was calculated as a percentage change in plate thickness before and after sintering for composites sintered at temperatures between 1100 and 1300°C. Linear contraction increased from 1.82% after sintering at 1100°C to 6.57% after sintering at 1300°C.

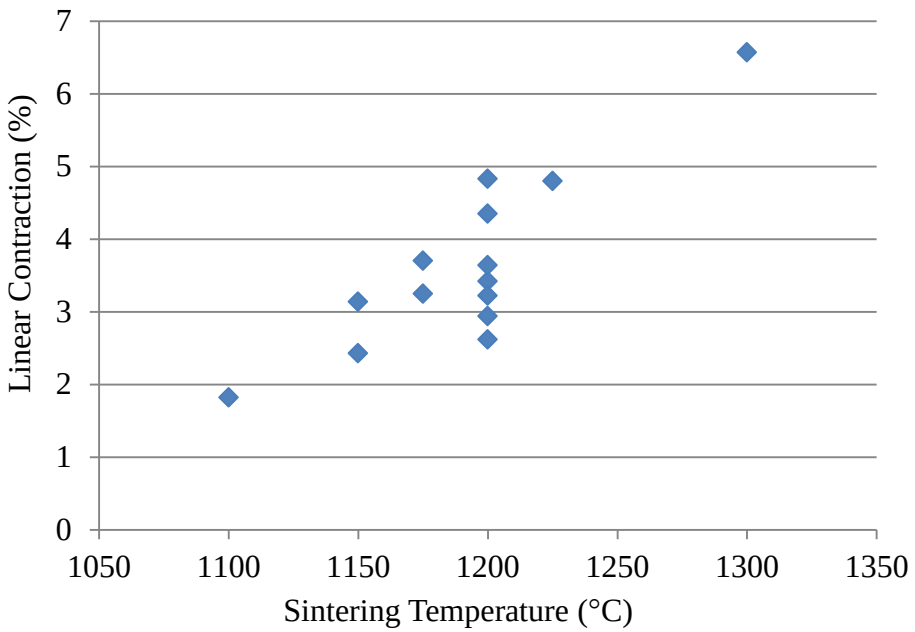

Figure 8.22. Linear contraction during sintering of composites composed of Nextel 720 fibres within a submicron particle alumina matrix containing 10wt% ACH sintered at temperatures between 1100°C and 1300°C.

Table 8.7. Linear contraction during sintering calculated as a percentage change in plate thickness for composites sintered at temperatures between 1100 and 1300°C.

Sintering Temp (°C)	Mean (%)	St. Dev (%)	No. Plates
1100	1.82	-	1
1150	2.79	0.50	2
1175	3.48	0.32	2
1200	3.57	0.78	7
1225	4.80	-	1
1300	6.57	-	1

8.2. Discussion

The effect of sintering at temperatures between 1100 and 1300°C was investigated. During the sintering process, the pores between ceramic particles close up resulting in densification of the matrix and a reduction in porosity. Taimicron TM-DAR alumina particles have been shown to increase in density from 2.5g/cc to 4.0g/cc with an increase in sintering temperature

from 1100 to 1300°C, and have been shown to be fully densified at 1300°C [119], [129]. Mass/volume calculations revealed an increase in composite density from ~2.4g/cc after sintering at 1100°C to ~2.6g/cc after sintering at 1150°C. Rather unexpectedly, no further increase in composite density was observed after sintering at temperatures above 1150°C. Shrinkage of the composite in the x-y direction was restricted by the fibre weave and therefore it is possible that density measurements did not truly reflect further densification of the matrix. Shrinkage in the z-direction, between fibre layers, was not restricted by the fibre weave and therefore linear contraction was considered an alternative method of determining particle densification during sintering. Linear contraction, calculated as a percentage change in composite thickness after sintering, increased linearly from 1.8% after sintering at 1100°C to 6.6% after sintering at 1300°C. An increase in linear contraction suggests that further densification occurred with an increase in sintering temperature.

Specimens sintered at 1100°C demonstrated significantly poorer flexural and short beam shear strength compared with specimens sintered at 1200°C. Incomplete densification of the matrix, as suggested by density and linear contraction measurements, results in a weaker matrix compared with sintering at 1200°C. Damage tolerant behaviour in oxide CMCs without a fibre coating is facilitated by a weak matrix. Nevertheless, a composite with an exceptionally weak matrix will likely fail by interlaminar shear at the mid-plane during loading in three-point bend, resulting in premature failure as shown in this study. Furthermore, incomplete densification of the matrix during sintering leads to poor fibre/matrix adhesion, which combined with an exceptionally weak matrix results in poor interlaminar properties.

Flexural strength values achieved for composites sintered at 1150 and 1175°C were statistically not different from composites sintered at 1200°C. Nevertheless, composites sintered at these temperatures were significantly poorer in short beam shear. As suggested previously, sintering at lower temperatures results in a weaker matrix and fibre/matrix adhesion. These findings suggest that a seemingly small decrease in sintering temperature of 25°C caused a significant decrease in composite interlaminar properties. In-plane properties, such as flexural strength, are fibre dominated and are therefore less sensitive to changes in the matrix compared with interlaminar properties. During loading in three-point bend, a series of cracks form in the matrix perpendicular to the load axis. Load is consequently transferred to the reinforcing fibres. Energy absorbing mechanisms such as fibre/matrix debonding and crack deflection allow the fibres to be isolated, impeding crack propagation. Fibre fracture occurs at the onset of peak load. Upon continued loading, cracks must be reinitiated in the matrix, resulting in a non-catastrophic failure.

Specimens sintered at 1300°C revealed a 50% reduction in strength compared with specimens sintered at 1150-1200°C. On the contrary, sintering at 1300°C revealed a significant improvement in short beam shear strength. Sintering at 1300°C promotes further densification of the matrix, as suggested by calculation of linear contraction, promoting better matrix strength and fibre/matrix adhesion resulting in an improvement in interlaminar properties but a reduction in damage tolerant behaviour. Furthermore, it is widely accepted that after heat treatment at 1300°C, Nextel 720 fibres retain just 70% of their room temperature strength owing to a rearrangement of the microstructure from 2:1 mullite aggregates to 3:2 facetted mullite grains [27], [130], [131]. Similar behaviour has been reported elsewhere. Holmquist and Lange observed a ~20% reduction in flexural strength after 2 hours ageing at 1300°C [90], whilst Ruggles-Wrenn et al. observed a 20-30% reduction in tensile strength after ageing

at 1330°C [95]. After ageing at temperatures above 1200°C, Simon [108] reported a gentle decrease in tensile strength whilst ILSS increased considerably. In all cases, the reported behaviour was attributed to a combination of further densification of the matrix as well as by a loss in fibre strength. Whilst the loss in strength observed in this study was far greater than reported elsewhere, it can be expected that premature failure during loading in three-point bend occurred through a combination of reduced damage tolerance and reduced fibre strength. SEM observations of the in-plane composite structure revealed little evidence of failure. Nevertheless, observations of the specimen top surface demonstrated crack propagation through Nextel 720 fibres, with no evidence of fibre/matrix debonding. These observations indicate that failure did not occur in a purely brittle manner; nevertheless, brittle tendencies were present.

There were no observable differences in the stress-displacement response for specimens loaded in three-point bend after sintering at temperatures between 1100 and 1300°C despite extremely statistically different mean flexural strength. On the contrary, representative stress-displacement curves for specimens sintered at 1100, 1200 and 1300°C loaded in short beam shear revealed markedly different behaviour after an initial linear response. Specimens sintered at 1100°C retained their load bearing capacity once peak load had been achieved. This behaviour is indicative of homogenous shear failure or permanent deformation. Specimens sintered at 1200°C showed a small load drop, followed by retention of load. This response suggests an initial interlaminar failure, followed by homogenous shear failure or permanent deformation. Specimens sintered at 1300°C showed a sharp, substantial decrease in load indicative of tensile failure [132]. Optical micrographs of specimens sintered at 1100, 1200 and 1300°C confirmed this suggestion, revealing markedly different failure mechanisms. Specimens sintered at 1100°C showed evidence of delamination between the outer plies at the

specimen edge, whilst specimens sintered at 1200°C showed evidence of delamination at the mid-plane, in the centre of the specimen. Noticeably different failure was observed for specimens sintered at 1300°C, illustrating a combination of delamination and tensile failure.

Calculating the maximum tensile stresses induced at the top surface during both in-plane flexural tests and short beam shear tests, it is apparent that the tensile stresses are essentially identical for specimens sintered at 1300°C (Figure 8.23), providing further evidence to suggest that fracture occurred by tension at the top surface during short beam shear tests. Similar behaviour was observed by Mattoni et al. [9] during investigation into the effect of matrix porosity on the mechanical performance of an all-oxide CMC manufactured by the polymer impregnation and pyrolysis method.

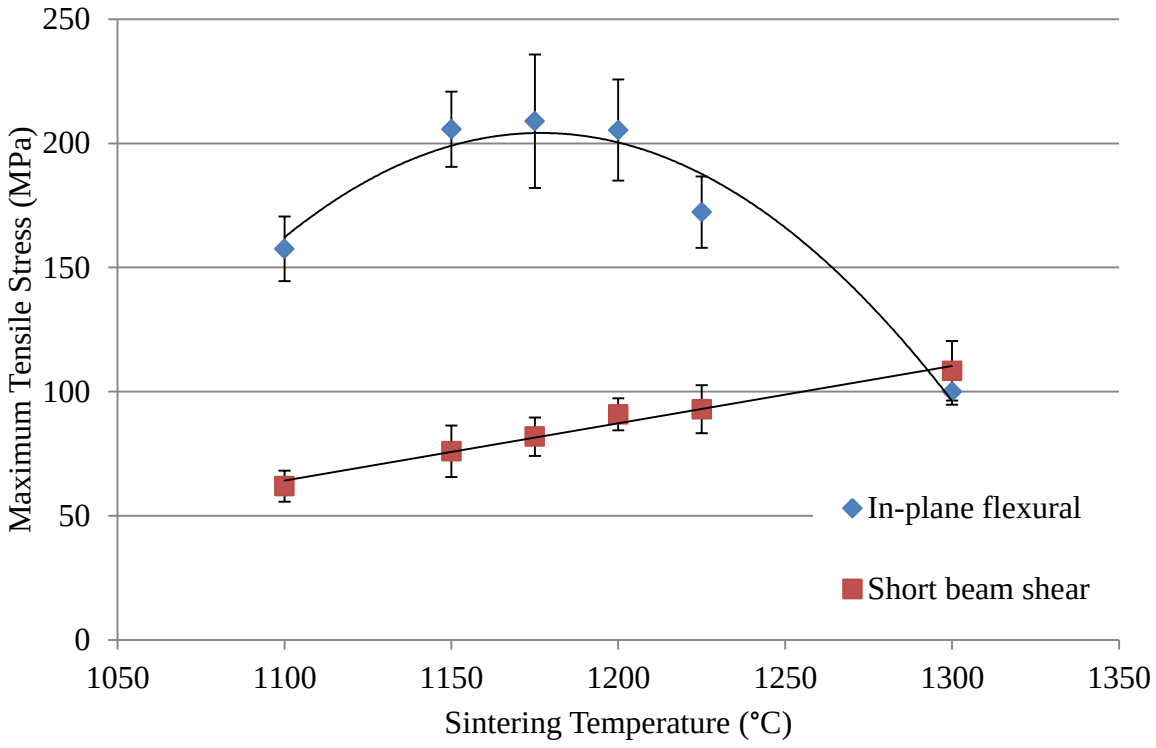

Figure 8.23. Comparison of maximum tensile stresses obtained during both in-plane flexural testing and short beam shear testing of specimens composed of Nextel 720 fibres within a submicron particle alumina matrix containing 10wt% ACH sintered between 1100°C and 1300°C (error bars: ±1 standard deviation).

Furthermore, through a comparison of the tensile stresses achieved during in-plane flexural testing and shear stresses achieved in short beam shear testing, it is evident that the condition for shear failure was not satisfied for specimens sintered at 1300°C (Equation 8.1). In the present geometry, τ/σ must be less than 0.13 to satisfy the condition for shear failure. For specimens sintered at 1300°C, $\tau/\sigma = 13.87/99.48 = 0.139$ which is above the critical value of 0.13 and therefore the condition for shear failure was not satisfied and fracture is predicted to occur in a tensile mode. In contrast, the condition for shear failure was satisfied for sintering temperatures less than 1300°C, largely due to the higher tensile stresses achieved. For example, for specimens sintered at 1200°C $\tau/\sigma = 12.1/205.3 = 0.059$ [9].

$$\frac{\tau}{\sigma} < \frac{t}{2s} \qquad \textbf{Equation 8.1}$$

Where τ is shear stress, σ is tensile stress, t is specimen thickness and s is span length.

8.3. Concluding remarks

Composites sintered between 1150 and 1200°C demonstrated mean flexural strength greater than 200MPa and were significantly equivalent. Nevertheless, short beam shear strength was significantly lower for composites sintered at 1150 and 1175°C compared with 1200°C. Composites sintered at 1300°C demonstrated superior short beam shear strength, however a ~50% reduction in flexural strength was observed. These findings indicate that a compromise on properties must be attained, for one cannot achieve both high flexural strength and high shear strength. For most structural applications, tensile or flexural strength is more desirable than interlaminar or compressive strength, and therefore composites manufactured subsequently were sintered at 1200°C.

Chapter 9 - Conclusions and further work

9.1. Conclusions

A simple, low cost processing method has been developed for the production of an oxide-oxide ceramic matrix composite composed of Nextel 720 fibres within an alumina matrix. Five processing steps were identified including 1) preparation of a polymer binder system, 2) preparation of slurry, 3) slurry impregnation to produce pre-impregnated fibres ('pre-preg'), 4) reactivation and consolidation of pre-preg plies under low temperature and load to produce a green composite and 5) pressure-less sintering to produce an environmentally stable oxide/oxide ceramic matrix composite. Preliminary research and development was carried out in light of the literature in order to produce a viable processing method. The ability to produce and store dry pre-preg in ambient conditions is a unique concept in oxide CMC manufacturing and was successfully demonstrated in this project. Further investigation into the matrix constituents and processing method was completed in order to optimise the material. This included selection of a suitable polymer binder, the effect of an alumina precursor, the influence of a bimodal particle size distribution and the effect of sintering temperature.

Polyvinyl alcohol (PVA) was identified as a suitable polymer binder. Three PVAs were investigated exploring their effect on both manufacturing and mechanical properties. Pre-preg containing PAF 2, a partially saponified liquid preparation, absorbed the least amount of water during immersion and had the quickest drying rate during reactivation. This was attributed to the presence of fewer hydroxyl groups as a result of incomplete saponification from polyvinyl acetate to polyvinyl alcohol. The saponification level and physical form of PVA had an insignificant effect on flexural strength; composites demonstrated mean flexural strengths of 154-159MPa. Nevertheless, improvements to manufacturing with use of PAF 2 were evident and therefore PAF 2 was employed throughout the remainder of the project.

The effect of an alumina precursor, Chlorohydrol 50 aluminium chlorohydrate (ACH), on manufacturing and material properties was explored. The addition of 2-15wt% ACH significantly improved composite flexural strength. Composites containing 7-15wt% ACH demonstrated flexural strength greater than 205MPa. This was attributed to an improvement in impregnation, reactivation and consolidation. Flexural strength of composites containing 20wt% ACH was statistically not different from composites manufactured without ACH. Alumina yield was shown to decrease 6% with the addition of 20wt% ACH, resulting in a significantly less dense composite. It was concluded that improvements to manufacturing were outweighed by an increase in matrix porosity. The addition of >12wt% ACH was detrimental to short beam shear strength. This was attributed an increase in matrix porosity caused by a decrease in alumina yield. Composites containing 5-10wt% ACH demonstrated short beam shear strength greater than 12MPa. Frequency histograms illustrating the distribution of shear data revealed that flexural and short beam shear values for composites containing ≤5wt% ACH demonstrated positive skew, whilst ≥12wt% demonstrated negative skew. Flexural and short beam shear values for composites containing 7-10wt% demonstrated normal distribution. Composites manufactured with 10wt% ACH revealed a mean tensile strength of 146.95MPa, however further investigation into a suitable tabbing arrangement is required to prevent slipping within the grips. The addition of 10wt% ACH was pursued throughout the remainder of the project.

The effect of combining large alumina particles with submicron alumina particles to create a bimodal particle size distribution was investigated. Composites containing a moderate amount of 1 micron particles (20-50%) demonstrated flexural strength significantly better than composites containing purely submicron particles. The addition of 1 micron particles was shown to impart a non-shrinking network, indicated by a reduction in linear contraction after

sintering with increasing large particles. Composites possessed less interparticle spacing and fewer matrix shrinkage cracks, resulting in an improvement in flexural strength. Nevertheless, incomplete densification of the matrix led to poorer matrix strength and fibre/matrix adhesion, resulting in premature delamination under shear loading. Composites containing 80% 1 micron particles demonstrated poor flexural and short beam shear strength owing to an exceptionally weak matrix. There were no evident manufacturing benefits with the addition of 1 micron particles.

The effect of sintering at temperatures between 1100 and 1300°C was investigated. Specimens sintered at 1100°C exhibited moderate flexural and poor short beam shear strength compared with those sintered at 1200°C. Incomplete densification of submicron alumina particles led to poor matrix strength and fibre/matrix adhesion, resulting in premature failure. Specimens sintered at 1300°C displayed poor flexural strength, however short beam shear strength was significantly improved. Complete densification of submicron alumina particles led to excellent matrix strength and fibre/matrix adhesion, improving the interlaminar properties of the material but decreasing damage tolerant behaviour. It was proposed that the condition for shear failure was not satisfied and subsequently tensile failure occurred during short beam shear tests, whilst failure in flexural tests was thought to occur prematurely on account of both reduced damage tolerance and fibre degradation caused by a rearrangement of the microstructure after sintering at 1300°C. Composites sintered between 1150 and 1200°C demonstrated mean flexural strength greater than 200MPa and were statistically equivalent. Nevertheless, short beam shear strength was significantly lower for composites sintered at 1150 and 1175°C compared with 1200°C. These findings indicate that a compromise on properties must be attained, for one cannot achieve both high flexural strength and high shear strength. For most structural applications, tensile or flexural strength is more desirable than

interlaminar or compressive strength, and therefore composites manufactured subsequently were sintered at 1200°C.

The properties of the optimised composite, composed of Nextel 720 fibres within a submicron alumina particle matrix with 10wt% ACH sintered at 1200°C, were compared with those reported for similar oxide CMCs highlighted in the literature. The optimised composite revealed equivalent flexural and tensile strength and superior shear strength compared with those reported previously.

9.2. Further work

The presented research work provides an understanding of the room temperature mechanical properties of composites composed of Nextel 720 fibres within an alumina matrix. It is understood from the literature that comparable oxide CMCs exhibit superior strength at elevated temperatures and therefore additional investigation is required to determine the high temperature mechanical properties of this material. It is also necessary to examine the long-term durability of the material, particularly at elevated temperatures, replicating in-service life. A solid foundation of work presented in the appendix has led to the development of a high temperature, trimodal alumina bonding material. Further development of the bonding material is required, employing a more in-depth testing programme to optimise the composition and processing of this material. It is also important to gain a more comprehensive knowledge of the properties of this bonding material, and its interaction with the CMC, at elevated temperatures.

9.3. Final remarks

The objective of this project was to develop an oxide-oxide ceramic matrix composite capable of withstanding temperatures up to and including 1200°C, with mechanical properties that meet or exceed those of commercially available oxide-oxide systems identified in the literature, manufactured by a simple, low cost processing route that offers the ability to store pre-impregnated fabric at ambient temperatures. These properties have been successfully demonstrated within this thesis, providing evidence that this material could offer potential benefits compared with conventional materials for high temperature structural applications. Furthermore, the ability to bond CMCs with a trimodal particle alumina material has been demonstrated, allowing the construction of more complex structural components.

Appendix: Preliminary development of a bonding material

Preliminary development of a bonding material was carried out to allow the construction of complex components, as well as for attaching thermal barrier coatings.

A number of requirements were identified:

1. The bond material must have a temperature capability equal to or greater than the ceramic composite.
2. The bond material must exhibit strength equal to or greater than the interlaminar strength of the ceramic composite.
3. The bond material must have a similar chemical composition to the ceramic composite in order to prevent leaching of unwanted substances into the composite.
4. The composite and bond must have a similar thermal expansion coefficient to prevent thermally induced residual stresses at the interface.
5. The bond material must not shrink during sintering. Shrinkage could cause thermally induced residual stresses at the interface.

The double notch shear strength of four bond materials was investigated. This included two commercially available high alumina refractory cements (Vitset 80 and 85, Vitcas Ltd.), and two in-house developed trimodal alumina bonds (air dried and vacuum dried). Vitset 80 and 85 are air-setting cements, offering excellent bonding properties at both ambient and operating temperatures. Additionally, Vitset cements are slightly expansile at elevated temperatures. Vitset 80 cement contains 74.0% alumina and is capable of withstanding temperatures up to 1750°C, whilst Vitset 85 cement contains 81.0% alumina and is capable of withstanding temperatures up to 1810°C [133]. A trimodal particle size alumina adhesive was developed in-house by Dr E.G. Butler, comprising 27% 0.1μm Taimicron TM-DAR alumina

powder (Taimei Chemicals Co., ltd), 16% 9µm fused alumina powder (OCON-019, Logitech UK), 50% 30µm calcined alumina powder (OCON-013, Logitech UK) and 7% Chlorohydrol 50 ACH (Summit Reheis). The ceramic powders were combined with the polymer binder system developed for CMC manufacture, containing deionised water, a partially saponified liquid preparation (Optapix PAF 2, Zschimmer & Schwarz GmbH), a low molecular weight polyethylene glycol (PEG 400, Sigma Aldrich) and 10% strength HNO_3 (see sections 3.1 and 4.1 for details). The bond slurry was ball milled for three hours to ensure an even distribution of particles within the polymer binder. Two methods of drying were investigated; air drying at room temperature and drying under vacuum at room temperature.

Two flat composite plates of ~2.6mm thickness, manufactured by Dr E.G. Butler according to the processing technique described in section 4.1, were joined using the bond materials described above, allowed to dry and sintered to 1200°C to create a rectangular plate of ~6mm thickness. The strength of the bond was determined by loading a double notched specimen in compression, adapted from ASTM C1292 [134]. Specimens were diamond cut to 25mm in length and 12mm in width, including two centrally located notches machined halfway through the thickness and spaced 6mm apart on opposing faces. Double notch shear tests were performed in position control at a constant displacement rate of 0.05mm/min (Figure A. 1.). Double notch shear strength was calculated using Equation A. 1. CMC specimens of 24 ply (approx. 6mm) thickness without a bond were tested for reference.

$$\tau = \frac{P_{max}}{d\ w} \qquad \textbf{Equation A. 1}$$

Where *Pmax* is the maximum load observed during test, *d* is distance between notches and *w* is specimen width.

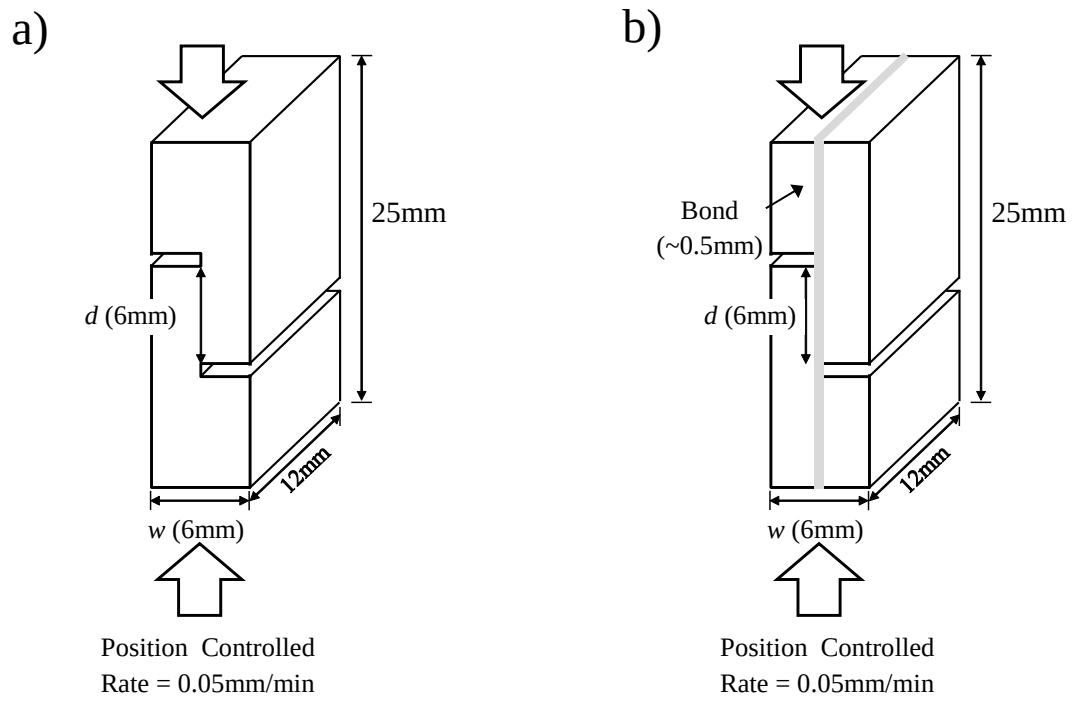

Figure A. 1. Double notch shear parameters adapted from ASTM C1292 for continuous fibre-reinforced advanced ceramics a) 24 ply CMC and b) two CMC plates joined by a ceramic bond [134]**.**

Mean interlaminar shear strength of a 24 ply composite composed of Nextel 720 fibres within a submicron alumina particle matrix containing 10wt% ACH, determined by double notch shear in compression was 8.89MPa (±0.99MPa) (Table A. 1). Specimens composed of two CMC flat plates joined by a Vitset 80 ceramic bond exhibited mean shear strength of 9.15MPa (±2.79MPa), whilst those joined by a Vitset 85 ceramic bond exhibited mean shear strength of 10.95MPa (±4.34MPa). Specimens composed of two CMC flat plates joined by a trimodal alumina bond dried in air exhibited mean shear strength of 5.62MPa (±1.45MPa), whilst those joined by a trimodal alumina bond dried under vacuum exhibited mean shear strength of 12.76MPa (±1.63MPa).

Table A. 1. Double notch shear strength data for specimens comprising two CMC flat plates joined by a ceramic bond.

	Mean (MPa)	St.Dev.	No. Tested
CMC	8.89	0.99	3
Vitset 80	9.15	2.79	4
Vitset 85	10.95	4.34	4
Trimodal alumina (air dried)	5.62	1.45	4
Trimodal alumina (vacuum dried)	12.76	1.63	6

Representative stress-displacement curves for specimens composed of Nextel 720 fibres within a submicron alumina particle matrix containing 10wt% ACH are presented in Figure A. 2. In general, the response was linear to failure. A significant decrease in load bearing capacity was observed once peak load was achieved. Macrographs of double notch shear specimens after failure illustrate delamination failure between the notches at the mid-plane (Figure A. 3).

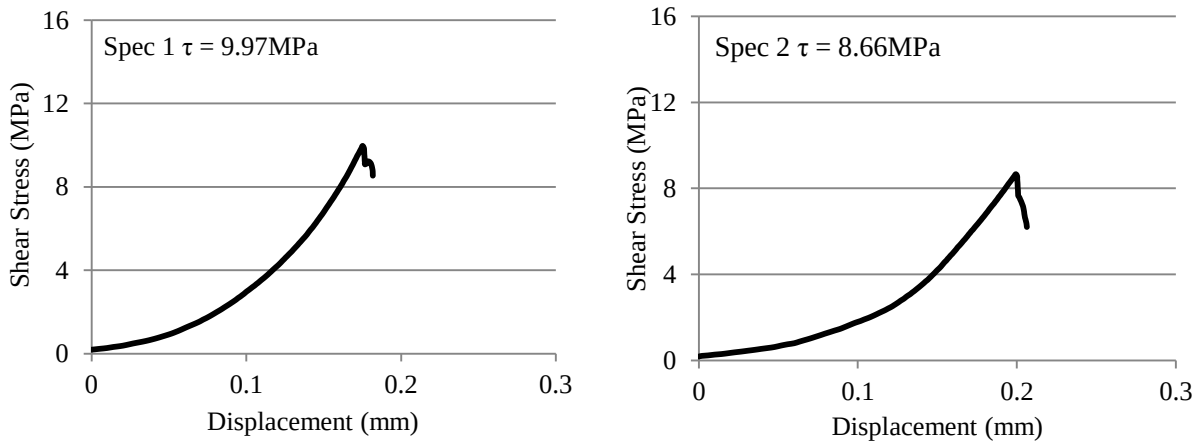

Figure A. 2. Representative stress-displacement curves for double notch shear specimens composed of Nextel 720 fibres within a submicron particle alumina matrix containing 10wt% ACH loaded in compression.

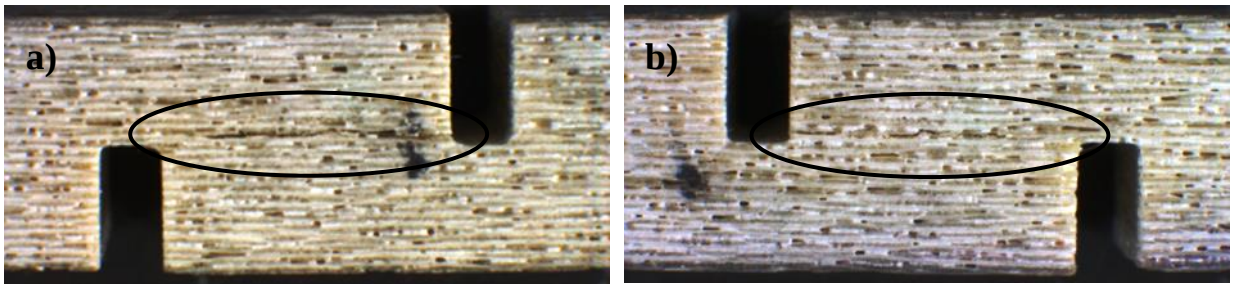

Figure A. 3. Macrographs of double notch shear specimens composed of Nextel 720 fibres within a submicron particle alumina matrix containing 10wt% ACH a) specimen 1 (τ = 9.97MPa) and b) specimen 2 (τ = 8.66MPa) showing interlaminar failure between centrally located notches at the mid-plane.

Representative stress-displacement curves for specimens composed of two CMC plates joined by Vitset 80 refractory cement are presented in Figure A. 4. In general, the response was linear to failure. Specimen 6 showed a significant decrease in load bearing capacity once peak load was achieved, whilst specimen 7 showed retention of load. Macrographs of double notch shear specimens after failure illustrate delamination failure at the CMC/bond interface (Figure A. 5).

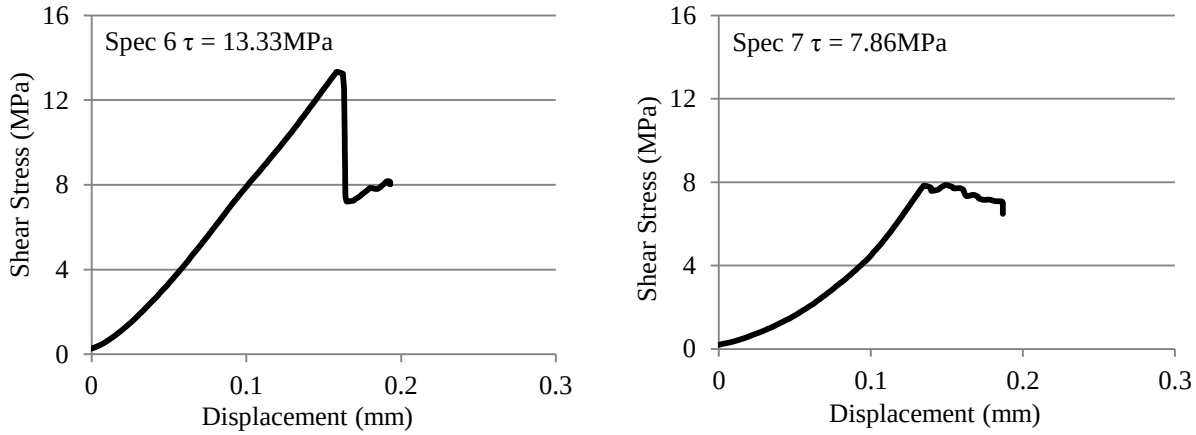

Figure A. 4. Representative stress-displacement curves for double notch shear specimens composed of two composite plates joined by Vitset 80 refractory cement loaded in compression.

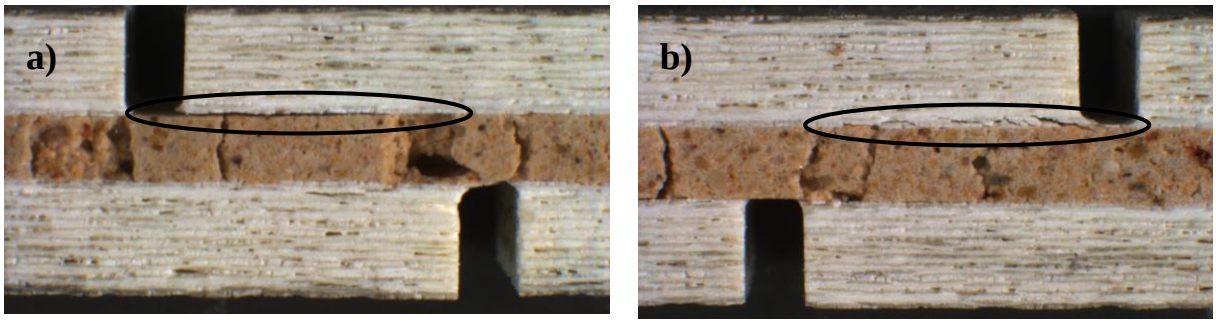

Figure A. 5. Macrographs of double notch shear specimens composed of two composite plates joined by Vitset 80 refractory cement a) specimen 6 (τ = 13.33MPa) and b) specimen 7 (τ = 7.86MPa) showing failure at the CMC/bond interface.

Representative stress-displacement curves for specimens composed of two CMC plates joined by Vitset 85 refractory cement are presented in Figure A. 6. Specimen 13 demonstrated evidence of cracking prior to peak load, followed by a gradual decrease in load. Specimen 15 displayed linear behaviour to failure, followed by a significant decrease in load. Macrographs of double notch shear specimens after failure illustrate two methods of failure. Specimen 13 illustrated delamination failure at the CMC/bond interface, whilst specimen 15 illustrated failure through the bond material adjacent to the notch (Figure A. 7).

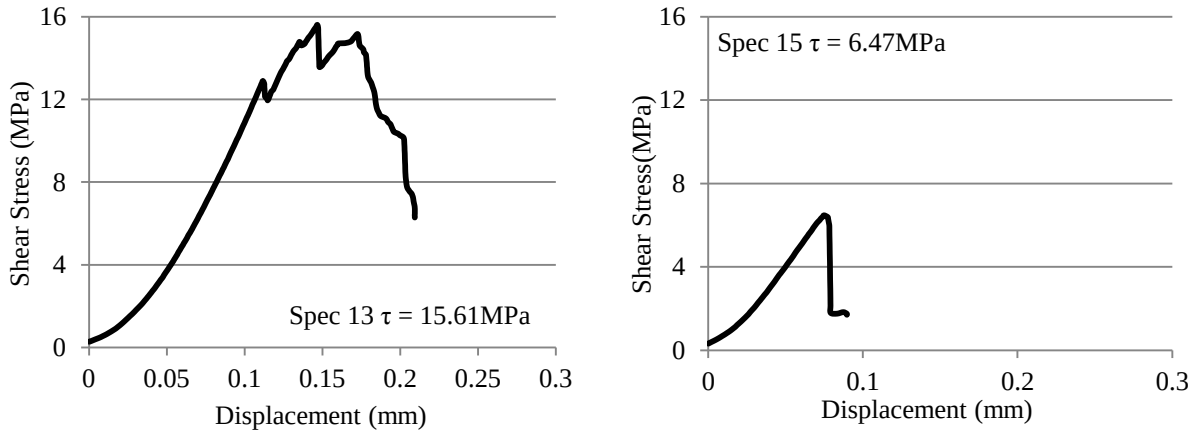

Figure A. 6. Representative stress-displacement curves for double notch shear specimens composed of two composite plates joined by Vitset 85 refractory cement loaded in compression.

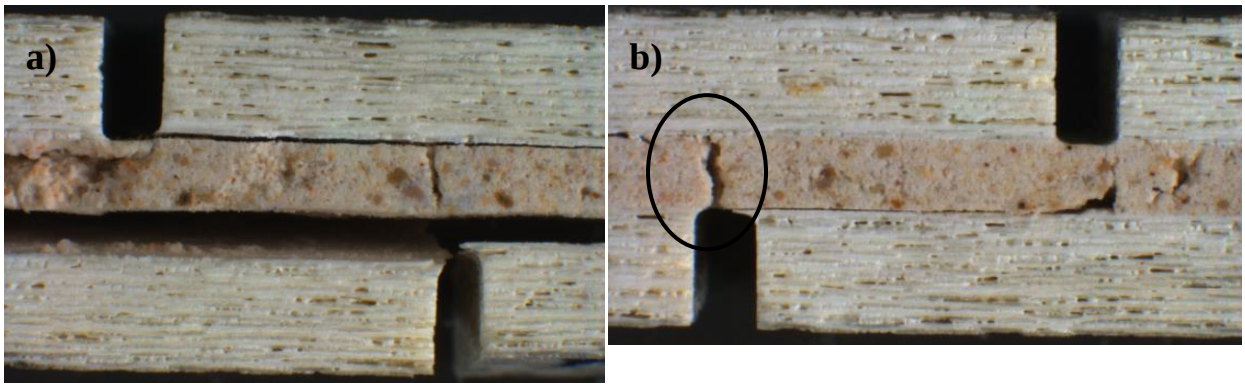

Figure A. 7. Macrographs of double notch shear specimens composed of two composite plates joined by Vitset 85 refractory cement a) specimen 13 (τ = 15.61MPa) showing interlaminar failure at the CMC/bond interface and b) specimen 15 (τ = 6.47MPa) showing failure through the bond material.

Representative stress-displacement curves for specimens composed of two CMC plates joined by an air dried trimodal alumina bond are presented in Figure A. 8. In general, the response was non-linear to failure. Macrographs of double notch shear specimens after failure illustrate delamination failure at the CMC/bond interface. Specimen 29 revealed failure across the bond layer (Figure A. 9).

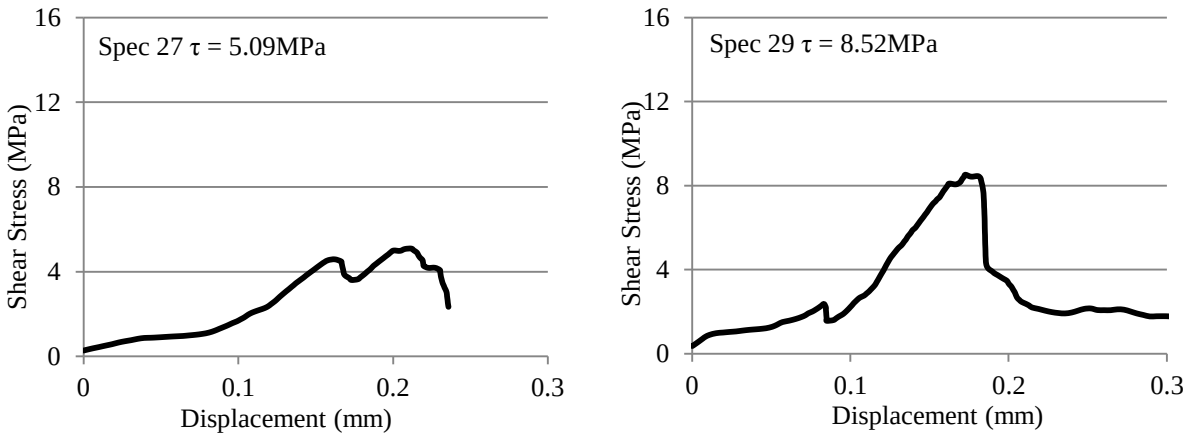

Figure A. 8. Representative stress-displacement curves for double notch shear specimens composed of two composite plates joined by an air dried trimodal alumina bond loaded in compression.

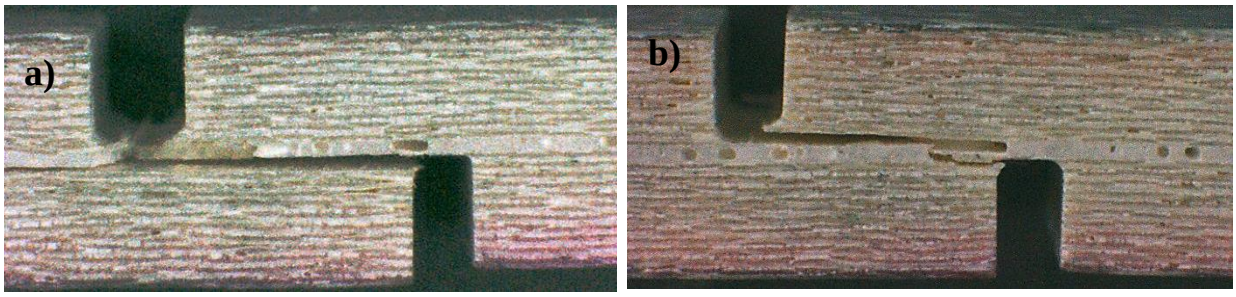

Figure A. 9. Macrographs of double notch shear specimens composed of two composite plates joined by an air dried trimodal alumina bond a) specimen 27 (τ = 5.09MPa) and b) specimen 29 (τ = 8.52MPa).

Representative stress-displacement curves for specimens composed of two CMC plates joined by a vacuum dried trimodal alumina bond are presented in Figure A. 10. In general, specimens revealed an initial drop in load, followed by a region of linearity. Non-linear behaviour was evident prior to peak load, and load decreased gradually after failure. Macrographs of double notch shear specimens after failure illustrated two methods of failure. Specimen 32 revealed delamination failure at the CMC/bond interface, whilst specimen 34 demonstrated failure across the bond layer (Figure A. 11).

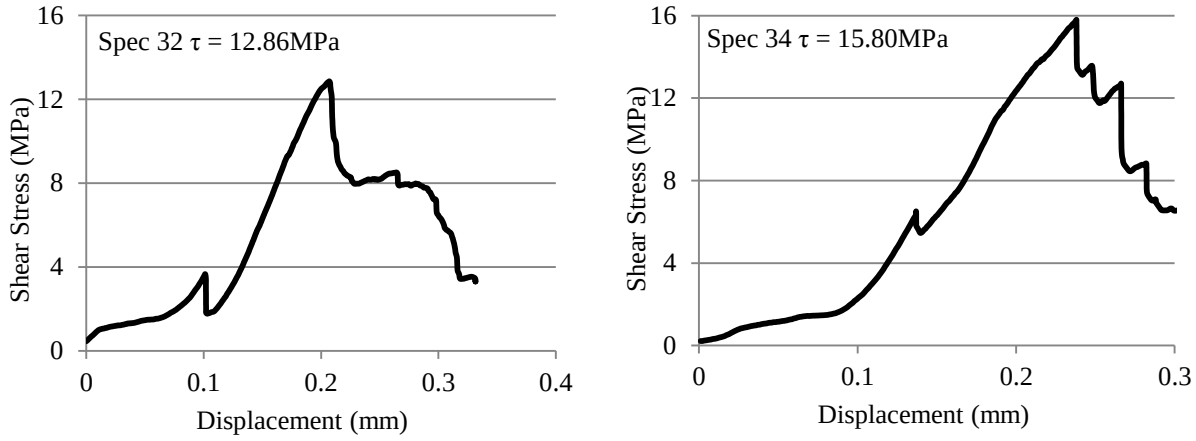

Figure A. 10. Representative stress-displacement curves for double notch shear specimens composed of two composite plates joined by a vacuum dried trimodal alumina bond loaded in compression.

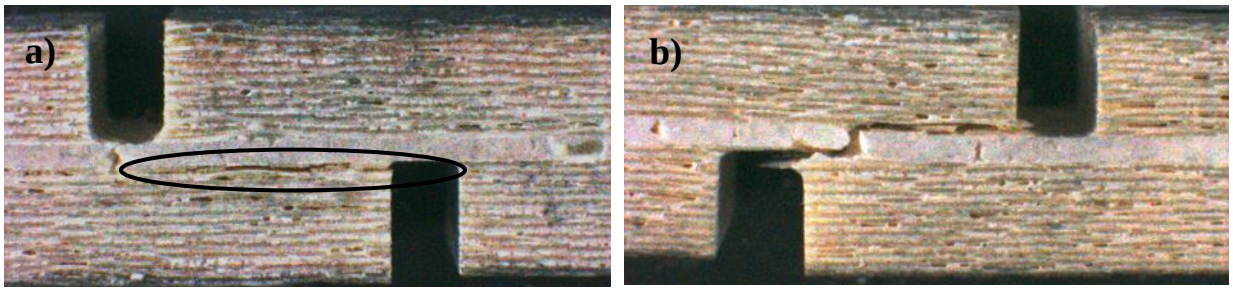

Figure A. 11. Macrographs of double notch shear specimens composed of two composite plates joined by a vacuum dried trimodal alumina bond a) specimen 32 (τ = 12.86MPa) and b) specimen 34 (τ = 15.80MPa).

Double notch shear strength of specimens composed of two CMC plates joined by Vitset 80, Vitset 85 and a vacuum dried trimodal alumina bond exceeded the shear strength of reference CMC specimens. Whilst the shear strength of the CMC determined by double notch shear was poor compared with results of short beam shear tests, double notch shear strength of the vacuum dried trimodal alumina bond exceeded that of the short beam shear strength of the CMC (τ_{SBS} =12.1MPa). SEM observations of the CMC/vacuum dried trimodal alumina bond interface showed evidence of the bond material penetrating into cracks on the CMC surface, therefore improving adhesion (Figure A. 12a). Higher magnification SEM analysis demonstrated an even distribution of large 30µm and 9µm particles within a submicron particle network (Figure A. 12b).

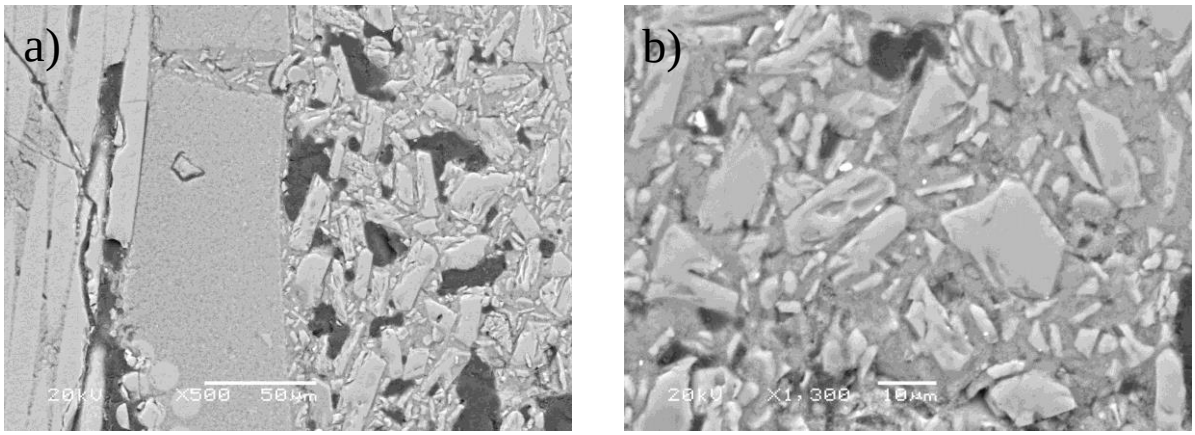

Figure A. 12. SEM observations of a) CMC/vacuum dried trimodal alumina bond interface and b) bond material at higher magnification showing trimodal distribution.

The in-house developed vacuum dried trimodal alumina bond meets many of the requirements outlined previously. It has a temperature capability that exceeds that of the CMC material and it has a similar chemical composition. Thermal expansion has not been investigated, however it would be expected that the trimodal alumina bond has a similar thermal expansion coefficient to the CMC material owing to its similar chemical composition. Shrinking during sintering is inhibited by large 30μm alumina particles, preventing thermally induced stresses at the interface. Furthermore, the strength of the bond, determined by double notch shear, exceeds that of the CMC material.

References

[1] H. Ohnabe, S. Masaki, M. Onozuka, K. Miyahara, and T. Sasa, “Potential application of ceramic matrix composites to aero-engine components,” *Compos. Part A Appl. Sci. Manuf.*, vol. 30, pp. 489–496, 1999.

[2] D. . Phillips, “Interfacial bonding and the toughness of carbon fiber reinforced glass and glass-ceramics.” pp. 1874–1854, 1974.

[3] F. W. Zok, “Developments in Oxide Fiber Composites,” *J. Am. Ceram. Soc.*, vol. 89, no. 11, pp. 3309–3324, Nov. 2006.

[4] F. F. Lange, W. C. Tu, and a. G. Evans, “Processing of damage-tolerant, oxidation-resistant ceramic matrix composites by a precursor infiltration and pyrolysis method,” *Mater. Sci. Eng. A*, vol. 195, pp. 145–150, Jun. 1995.

[5] J. J. Haslam, K. E. Berroth, and F. F. Lange, “Processing and properties of an all-oxide composite with a porous matrix,” *J. Eur. Ceram. Soc.*, vol. 20, pp. 607–618, 2000.

[6] K. A. Keller, T. Mah, T. A. Parthasarathy, and C. M. Cooke, “Fugitive Interfacial Carbon Coatings for Oxide/Oxide Composites,” *J. Am. Ceram. Soc.*, vol. 83, no. 2, pp. 329–336, 2000.

[7] “GE Aviation Moving To Apply Ceramic Matrix Composites to the Heart of Future Engines,” 2009. [Online]. Available: http://www.geaviation.com.

[8] M. Holmquist, R. Lundberg, O. Sudre, A. G. Razzell, L. Molliex, and J. Benoit, “Alumina/alumina composite with a porous zirconia interphase - Processing, properties and component testing,” *J. Eur. Ceram. Soc.*, vol. 20, pp. 599–606, 2000.

[9] M. A. Mattoni, J. Y. Yang, C. G. Levi, and F. W. Zok, “Effects of Matrix Porosity on the Mechanical Properties of a Porous-Matrix, All-Oxide Ceramic Composite,” *J. Am. Ceram. Soc.*, vol. 84, no. 11, pp. 2594–2602, 2001.

[10] K. K. Chawla, “Introduction,” in *Ceramic Matrix Composites*, 1993, pp. 1–10.

[11] K. K. Chawla, “Processing of Ceramic Matrix Composites,” in *Ceramic Matrix Composites*, 1993, pp. 126–160.

[12] K. K. Chawla, “Ceramic Reinforcements,” in *Ceramic Matrix Composites*, 1993, pp. 45–125.

[13] J. E. Sheehan, K. W. Buesking, and B. J. Sullivan, “Carbon-Carbon Composites,” *Annu. Rev. Mater. Sci.*, vol. 24, no. 1, pp. 19–44, Aug. 1994.

[14] Department of Defense Handbook, “Composite Materials Handbook Vol. 5 Ceramic Matrix Composites,” 2002.

[15] D. C. Deleeuw, J. Lipowitz, and P. . Lu, “Preparation of substantially cyrtalline silicon carbide fibres from polycarbosilane, US PAtent 5,071,600,” 1991.

[16] J. A. DiCarlo and H.-M. Yun, “Non-oxide (Silicon Carbide) Fibres,” in *Handbook of Ceramic Composites by N.P. Bansal*, 2005, pp. 33–52.

[17] R. E. Jones, D. Petrak, J. Rabe, and A. Szweda, “SYLRAMIC SiC fibers for CMC reinforcement,” *J. Nucl. Mater.*, vol. 287, pp. 556–559, 2000.

[18] COI Ceramics, “Sylramic SiC Fibre,” 2003.

[19] H. Ichikawa, “Recent advances in Nicalon ceramic fibres including Hi-Nicalon Type S,” *Ann. Chim. Sci. des Matériaux*, vol. 25, pp. 523–528, 2000.

[20] A. R. Bunsell, “Oxide Fibres,” in *Handbook of Ceramic Composites by N.P. Bansal*, 2005, pp. 3–31.

[21] A. K. Dhingra, “Alumina fibre FP,” *Philos. Trans. R. Soc. London*, vol. A294, no. 1411, pp. 411–417, 1980.

[22] A. R. Bunsell and M. Berger, “Fine diameter ceramic fibres,” *J. Eur. Ceram. Soc.*, vol. 20, pp. 2249–2260, 2000.

[23] J. C. Romine, “New High Temperature Ceramic Fiber,” *11th Annu. Conf. Compos. Adv. Ceram. Mater. Ceram. Eng. Sci. Proc.*, vol. 8, pp. 755–765, Jan. 1987.

[24] D. M. Wilson and L. R. Visser, “High performance oxide fibers for metal and ceramic composites,” *Compos. Part A Appl. Sci. Manuf.*, vol. 32, pp. 1143–1153, 2001.

[25] C. Lesniewski, C. Aubin, and A. R. Bunsell, “Property-Structure characterisation of a continuous fine alumina-silica fibre,” *Compos. Sci. Technol.*, vol. 37, no. 1–3, pp. 63–78, Jan. 1990.

[26] 3M Ceramic Textiles and Composites, “Nextel ™ Ceramic Textiles Technical Notebook,” 2004.

[27] F. Deléglise, M. H. Berger, and A. R. Bunsell, “Microstructural evolution under load and high temperature deformation mechanisms of a mullite/alumina fibre,” *J. Eur. Ceram. Soc.*, vol. 22, pp. 1501–1512, 2002.

[28] A. Poulon-Quintin, M. H. Berger, and A. R. Bunsell, “Mechanical and microstructural characterisation of Nextel 650 alumina–zirconia fibres,” *J. Eur. Ceram. Soc.*, vol. 24, no. 9, pp. 2769–2783, Aug. 2004.

[29] K. K. Chawla, H. Liu, J. Janczak-Rusch, and S. Sambasivan, “Microstructure and properties of monazite (LaPO4) coated saphikon fiber/alumina matrix composites,” *J. Eur. Ceram. Soc.*, vol. 20, pp. 551–559, 2000.

[30] R. Pedrazzani, “Sapphire Optical Fibers,” in *Speciality Optical Fibres Handbook*, 2006, pp. 651–670.

[31] R. F. Gibson, “Introduction,” in *Principles of Composite Material Mechanics*, 1994, pp. 1–33.

[32] M. M. Schwartz, “Processing of Composite Materials,” in *Composite Materials, Volume II: Processing, Fabrication and Applications*, 1996, pp. 1–276.

[33] R. L. Lehman, “Ceramic Matrix Fiber Composites,” in *Structural Ceramics*, 1989, pp. 229–291.

[34] K. K. Chawla, “Ceramic Matrix Materials,” in *Ceramic Matrix Composites*, 1993, pp. 11–44.

[35] K. K. Chawla, “Interface,” in *Ceramic Matrix Composites*, 1993, pp. 162–223.

[36] F. W. Zok and C. G. Levi, “Mechanical Properties of Porous- Matrix Ceramic Composites,” *Adv. Eng. Mater.*, vol. 3, no. 1, pp. 15–23, 2001.

[37] E. Mouchon and P. Colomban, “Oxide ceramic matrix/oxide fibre woven fabric composites exhibiting dissipative fracture behaviour,” *Composites*, vol. 26, no. 3, pp. 175–182, Mar. 1995.

[38] R. Naslain, “Design, preparation and properties of non-oxide CMCs for application in engines and nuclear reactors: an overview,” *Compos. Sci. Technol.*, vol. 64, no. 2, pp. 155–170, Feb. 2004.

[39] M. Srinivasan, “The Silicon Carbide Family of Structural Ceramics,” in *Structural Ceramics*, 1989, pp. 99–159.

[40] R. E. Tressler, “Recent developments in fibers and interphases for high temperature ceramic matrix composites,” *Compos. Part A Appl. Sci. Manuf.*, vol. 30, pp. 429–437, 1999.

[41] K. K. Chawla, C. Coffin, and Z. R. Xu, “Interface engineering in oxide fibre/oxide matrix composites,” *Int. Mater. Rev.*, vol. 45, no. 5, pp. 165–189, May 2000.

[42] C. G. Levi, J. Y. Yang, B. J. Dalgleish, F. W. Zok, and A. G. Evans, “Processing and Performance of an All-Oxide Ceramic Composite,” *J. Am. Ceram. Soc.*, vol. 86, no. 8, pp. 2077–2086, 1998.

[43] A. Licciulli, A. Chiechi, M. Fersini, K. P. Sanosh, and A. Balakrishnan, “Influence of Zirconia Interfacial Coating on Alumina Fiber-reinforced Alumina Matrix Composites,” *Int. J. Appl. Ceram. Technol.*, vol. 10, no. 2, pp. 251–256, Mar. 2013.

[44] D. B. Marshall and J. B. Davis, “Ceramics for future power generation technology : fiber reinforced oxide composites,” *Curr. Opin. Solid State Mater. Sci.*, vol. 5, pp. 283–289, 2001.

[45] P. E. D. Morgan and D. B. Marshall, “Functional interfaces for oxide/oxide composites,” *Mater. Sci. Eng. A*, vol. 162, no. 1–2, pp. 15–25, Apr. 1993.

[46] J. J. Brennan, “Interfacial studies of refractory glass-ceramic matrix/advanceed SiC fibre reinforced composites,” 1993.

[47] R. R. Naslain, “The design of the fibre-matrix interfacial zone in ceramic matrix composites,” *Compos. Part A Appl. Sci. Manuf.*, vol. 29, no. 9–10, pp. 1145–1155, Jan. 1998.

[48] P. Jackson, M. B. Ruggles-Wrenn, S. Baek, and K. Keller, “Compressive creep behavior of an oxide–oxide ceramic composite with monazite fiber coating at elevated temperatures,” *Mater. Sci. Eng. A*, vol. 454–455, pp. 590–601, Apr. 2007.

[49] J. H. Weaver, J. Yang, C. G. Levi, F. W. Zok, and J. B. Davis, “A Method for Coating Fibers in Oxide Composites,” *J. Am. Ceram. Soc.*, vol. 90, no. 4, pp. 1331–1333, Apr. 2007.

[50] R. S. Hay and E. E. Boakye, “Monazite Coatings on Fibers: I, Effect of Temperature and Alumina Doping on Coated-Fiber Tensile Strength,” *J. Am. Ceram. Soc.*, vol. 84, no. 12, pp. 2783–2792, 2001.

[51] R. S. Hay, E. Boakye, and M. D. Petry, “Effect of coating deposition temperature on monazite coated fiber,” *J. Eur. Ceram. Soc.*, vol. 20, pp. 589–597, 2000.

[52] E. E. Boakye, R. S. Hay, P. Mogilevsky, and L. M. Douglas, “Monazite Coatings on Fibers: II, Coating without Strength Degradation,” *J. Am. Ceram. Soc.*, vol. 84, no. 12, pp. 2793–2801, 2001.

[53] J. B. Davis, D. B. Marshall, and P. E. D. Morgan, “Monazite-containing oxide/oxide composites,” *J. Eur. Ceram. Soc.*, vol. 20, pp. 583–587, 2000.

[54] M. B. Ruggles-Wrenn, S. S. Musil, S. Mall, and K. A. Keller, “Creep behavior of Nextel 610/Monazite/Alumina composite at elevated temperatures,” *Compos. Sci. Technol.*, vol. 66, no. 13, pp. 2089–2099, Oct. 2006.

[55] B. Saruhan, M. Schmucker, M. Bartsch, H. Schneider, K. Nubian, and G. Wahl, “Effect of interphase characteristics on long-term durability of oxide-based fibre-reinforced composites,” *Compos. Part A Appl. Sci. Manuf.*, vol. 32, pp. 1095–1103, 2001.

[56] M. Gerendás, Y. Cadoret, C. Wilhelmi, T. Machry, R. Knoche, T. Behrendt, S. Denis, J. Göring, D. Koch, and K. Tushtev, “Improvement of oxide/oxide CMC and development of combustor and turbine components in the HiPOC program,” *Proc. ASME Turbo Expo 2011 Power Land, Sea Air*, vol. GT2011, no. 45460, pp. 1–14, 2011.

[57] K. J. Probst, T. M. Besmann, D. P. Stinton, R. A. Lowden, T. J. Anderson, and T. L. Starr, “Recent advances in forced-flow, thermal-gradient CVI for refractory composites,” *Surf. Coatings Technol.*, vol. 120–121, pp. 250–258, Nov. 1999.

[58] T. M. Besmann, B. W. Sheldon, R. A. Lowden, and D. P. Stinton, "Vapor-Phase Fabrication and Continuous -Filament Ceramic of Properties Composites," *Am. Assoc. Adv. Sci.*, vol. 253, no. 5024, pp. 1104–1109, 1991.

[59] R. Naslain, F. Langlais, and R. Fedou, "The CVI-processing of ceramic matrix composites," *J. Phys. Proc. Seventh Eur. Conf. Chem. Vap. Depos.*, vol. 50, no. C5, pp. 191–207, 1989.

[60] R. Naslain, "Chemical reactivity in the processing and the interactions with the environment of ceramic matrix composites," *Solid State Ionics*, vol. 101–103, pp. 959–973, Nov. 1997.

[61] R. R. Naslain, "Two-dimensional SiC/SiC composites processed according to the isobaric-isothermal chemical vapor infiltration gas phase route," *J. Alloys Compd.*, vol. 188, pp. 42–48, 1992.

[62] B. J. Oh, Y. J. Lee, D. J. Choi, G. W. Hong, J. Y. Park, and W. J. Kim, "Fabrication of Carbon/Silicon Carbide Composites by Isothermal Chemical Vapor Infiltration , Using the In Situ Whisker-Growing and Matrix-Filling Process," *J. Am. Ceram. Soc.*, vol. 84, no. 1, pp. 245–247, 2001.

[63] W. G. Zhang and K. J. Hüttinger, "Densification of a 2D carbon fiber preform by isothermal, isobaric CVI : Kinetics and carbon microstructure," *Carbon N. Y.*, vol. 41, pp. 2325–2337, 2003.

[64] J. Zhao, K. Li, H. Li, and C. Wang, "The influence of thermal gradient on pyrocarbon deposition in carbon/carbon composites during the CVI process," *Carbon N. Y.*, vol. 44, no. 4, pp. 786–791, Apr. 2006.

[65] I. Golecki, R. C. Morris, D. Narasimhan, and N. Clements, "Rapid densification of porous carbon-carbon composites by thermal-gradient chemical vapor infiltration," *Appl. Phys. Lett.*, vol. 66, no. 18, pp. 2334 – 2336, 1995.

[66] Y. G. Roman, M. H. J. M. De Croonb, and R. Metselaar, "Analysis of the Isothermal Forced Flow Chemical Vapour Infiltration Process. Part II : Experimental Study," *J. Eur. Ceram. Soc.*, vol. 15, pp. 887–898, 1995.

[67] J. S. Lewis, W. J. Lackey, and S. Vaidyaraman, "Model for prediction of matrix microstructure for carbon/carbon composites prepared by forced flow-thermal gradient CVI," *Carbon N. Y.*, vol. 35, no. 1, pp. 103–112, 1997.

[68] K. Sugiyama and E. Yamamoto, "Reinforcement and antioxidizing of porous carbon by pulse CVI of SiC," *J. Mater. Sci.*, vol. 24, no. 10, pp. 3756–3762, 1989.

[69] S. G. Lee, J. Fourcade, R. Latta, and a. a. Solomon, "Polymer impregnation and pyrolysis process development for improving thermal conductivity of SiCp/SiC–PIP matrix fabrication," *Fusion Eng. Des.*, vol. 83, no. 5–6, pp. 713–719, Oct. 2008.

[70] Y. Hirata, K. Hayata, T. Maeda, and M. Shibuya, "Preparation of Silicon-Titanium-Carbon-Oxygen Fabric/ Mullite Filler/Polytitanocarbosilane Laminates by Polymer

Impregnation and Pyrolysis Method," *J. Am. Ceram. Soc.*, vol. 87, no. 6, pp. 996–1001, Jun. 2004.

[71] A. Hilbig, E. Müller, R. Wenzel, G. Roewer, E. Brendler, G. Irmer, and G. Schreiber, "The microstructure of polymer-derived amorphous silicon carbide layers," *J. Eur. Ceram. Soc.*, vol. 25, pp. 151–156, Jan. 2005.

[72] M. Kotani, T. Inoue, A. Kohyama, Y. Katoh, and K. Okamura, "Effect of SiC particle dispersion on microstructure and mechanical properties of polymer-derived SiC/SiC composite," *Mater. Sci. Eng. A*, vol. 357, no. 1–2, pp. 376–385, Sep. 2003.

[73] M. Singh and D. R. Behrendt, "Reactive melt infiltration of silicon-molybdenum alloys into microporous carbon preforms," *Mater. Sci. Eng. A*, vol. 194, no. 2, pp. 193–200, May 1995.

[74] M. Singh and D. R. Behrendt, "Reactive melt infiltration of silicon-niobium alloys in microporous carbons," *J. Mater. Res.*, vol. 9, no. 7, pp. 1701–1708, 1994.

[75] Y. Xu, L. Cheng, and L. Zhang, "Carbon/silicon carbide composites prepared by chemical vapor infiltration combined with silicon melt infiltration," *Carbon N. Y.*, vol. 37, no. 8, pp. 1179–1187, Jan. 1999.

[76] E. S. Nelson and P. Colella, "Parametric study of reactive melt infiltration," in *Proceedings of the 1999 International Mechanical Engineering Congress and Exposition, Nashville, Tennessee*, 1999.

[77] J. Zhang, D. Zhu, L. Yang, and S. Li, "Wear behavior of Lanxide Al2O3/Al composite," *Wear*, vol. 215, no. 1–2, pp. 34–39, 1999.

[78] O. Salas, H. Ni, V. Jayaram, K. C. Vlach, C. G. Levi, and R. Mehrabian, "Nucleation and growth of Al2O3/metal composites by oxidation of aluminum alloys," *J. Mater. Res.*, vol. 6, no. 9, pp. 1964–1981, Jan. 1991.

[79] M. S. Newkirk, A. W. Urquhart, H. R. Zwicker, and E. Breval, "Formation of Lanxide™ ceramic composite materials," *J. Mater. Res.*, vol. 1, no. 1, pp. 81–89, 1986.

[80] A. W. Urquhart, "Novel reinforced ceramics and metals: a review of Lanxide's composite technologies," *Mater. Sci. Eng. A*, vol. 144, no. 1–2, pp. 75–82, Oct. 1991.

[81] T. Radsick, B. Saruhan, and H. Schneider, "Damage tolerant oxide/oxide fiber laminate composites," *J. Eur. Ceram. Soc.*, vol. 20, pp. 545–550, 2000.

[82] Y. Zhu, Z. Huang, S. Dong, M. Yuan, and D. Jiang, "Manufacturing 2D carbon-fiber-reinforced SiC matrix composites by slurry infiltration and PIP process," *Ceram. Int.*, vol. 34, no. 5, pp. 1201–1205, Jul. 2008.

[83] K. K. Chawla, "Ceramic Matrix Composites," in *Composite Materials: Science and Engineering*, 2012, pp. 249–292.

[84] W. I. L. Tredway, K. M. Prewo, and C. G. Pantano, “Fiber-matrix interfacial effects ni carbon-fiber reinforced glass matrix composites,” *Carbon N. Y.*, vol. 27, no. 5, pp. 717–727, 1989.

[85] C. . Brinker and G. . Scherer, *Sol-Gel Science: The Physics and Chemistry of Sol-Gel Processing*. 1990.

[86] M. K. Naskar, M. Chatterjee, a. Dey, and K. Basu, “Effects of processing parameters on the fabrication of near-net-shape fibre reinforced oxide ceramic matrix composites via sol–gel route,” *Ceram. Int.*, vol. 30, no. 2, pp. 257–265, Jan. 2004.

[87] J. A. Heathcote, X. Gong, J. Y. Yang, U. Ramamurty, and F. W. Zok, “In-Plane Mechanical Properties of an All-Oxide Ceramic Composite,” *J. Am. Ceram. Soc.*, vol. 82, no. 10, pp. 2721–2730, 1999.

[88] E. a. V. Carelli, H. Fujita, J. Y. Yang, and F. W. Zok, “Effects of Thermal Aging on the Mechanical Properties of a Porous-Matrix Ceramic Composite,” *J. Am. Ceram. Soc.*, vol. 85, no. 3, pp. 595–602, Dec. 2004.

[89] M. a. Mattoni and F. W. Zok, “Strength and Notch Sensitivity of Porous-Matrix Oxide Composites,” *J. Am. Ceram. Soc.*, vol. 88, no. 6, pp. 1504–1513, Jun. 2005.

[90] M. G. Holmquist and F. F. Lange, “Processing and Properties of a Porous Oxide Matrix Composite Reinforced with Continuous Oxide Fibers,” *J. Am. Ceram. Soc.*, vol. 86, no. 10, pp. 1733–1740, 2003.

[91] M. G. Holmquist, T. C. Radsick, O. H. Sudre, and F. F. Lange, “Fabrication and testing of all-oxide CFCC tubes,” *Compos. Part A Appl. Sci. Manuf.*, vol. 34, pp. 163–170, 2003.

[92] R. A. Jurf and S. C. Butner, “Advances in Oxide-Oxide CMC,” vol. 122, no. April, pp. 202–205, 2000.

[93] COI Ceramics, “Oxide CMC Fabrication Process,” *www.coiceramics.com*.

[94] S. G. Steel, L. P. Zawada, and S. Mall, “Fatigue Behavior of a Nextel 720\Alumina (N720\A) Composite at Room and Elevated Temperature,” in *25th Annual Conference on Composites, Advanced Ceramics, Materials, and Structures: A: Ceramic Engineering and Science Proceedings, Volume 22, Issue 3*, 2001, vol. 22, pp. 695–702.

[95] M. B. Ruggles-Wrenn, S. Mall, C. A. Eber, and L. B. Harlan, “Effects of steam environment on high-temperature mechanical behavior of Nextel720^{TM}/alumina (N720/A) continuous fiber ceramic composite,” *Compos. Part A Appl. Sci. Manuf.*, vol. 37, no. 11, pp. 2029–2040, Nov. 2006.

[96] S. Mall and J.-M. Ahn, “Frequency effects on fatigue behavior of Nextel720^{TM}/alumina at room temperature,” *J. Eur. Ceram. Soc.*, vol. 28, no. 14, pp. 2783–2789, Oct. 2008.

[97] M. B. Ruggles-Wrenn and J. Braun, “Effects of steam environment on creep behavior of Nextel™720/alumina ceramic composite at elevated temperature,” *Mater. Sci. Eng. A*, vol. 497, no. 1–2, pp. 101–110, Dec. 2008.

[98] J. Mehrman, M. B. Ruggles-Wrenn, and S. Baek, “Influence of hold times on the elevated-temperature fatigue behavior of an oxide–oxide ceramic composite in air and in steam environment,” *Compos. Sci. Technol.*, vol. 67, no. 7–8, pp. 1425–1438, Jun. 2007.

[99] M. B. Ruggles-Wrenn, G. T. Siegert, and S. S. Baek, “Creep behavior of Nextel™720/alumina ceramic composite with ±45° fiber orientation at 1200°C,” *Compos. Sci. Technol.*, vol. 68, no. 6, pp. 1588–1595, May 2008.

[100] M. B. Ruggles-Wrenn and B. A. Whiting, “Cyclic creep and recovery behavior of Nextel™720/alumina ceramic composite at 1200°C,” *Mater. Sci. Eng. A*, vol. 528, no. 3, pp. 1848–1856, Jan. 2011.

[101] M. B. Ruggles-Wrenn, A. Radzicki, S. Baek, and K. Keller, “Effect of loading rate on the monotonic tensile behavior and tensile strength of an oxide–oxide ceramic composite at 1200°C,” *Mater. Sci. Eng. A*, vol. 492, no. 1–2, pp. 88–94, Sep. 2008.

[102] M. B. Ruggles-Wrenn and N. R. Szymczak, “Effects of steam environment on compressive creep behavior of Nextel™720/Alumina ceramic composite at 1200°C,” *Compos. Part A Appl. Sci. Manuf.*, vol. 39, no. 12, pp. 1829–1837, Dec. 2008.

[103] M. B. Ruggles-Wrenn, G. Hetrick, and S. S. Baek, “Effects of frequency and environment on fatigue behavior of an oxide–oxide ceramic composite at 1200°C,” *Int. J. Fatigue*, vol. 30, no. 3, pp. 502–516, Mar. 2008.

[104] S. Wannaparhun and S. Seal, “Combined Spectroscopic and Thermodynamic Investigation of Nextel-720 Fiber/Alumina Ceramic-Matrix Composite in Air and Water Vapor at 1100°C,” *Engineering*, vol. 30, no. 187408, pp. 1628–1630, 2003.

[105] M. B. Ruggles-Wrenn and P. Laffey, “Creep behavior in interlaminar shear of Nextel™720/alumina ceramic composite at elevated temperature in air and in steam☆,” *Compos. Sci. Technol.*, vol. 68, no. 10–11, pp. 2260–2266, Aug. 2008.

[106] S. Mall and M. A. Sullivan, “Creep Rupture and Fatigue Behavior of a Notched Oxide/Oxide Ceramic Matrix Composite at an Elevated Temperature,” *Int. J. Appl. Ceram. Technol.*, vol. 8, no. 2, pp. 251–260, Mar. 2011.

[107] S. Mall and B. H. Boyer, “Cyclic and sustained loading behaviors of oxide/oxide Nextel™720/alumina composite with double edge sharp notch,” *Compos. Part A Appl. Sci. Manuf.*, vol. 43, no. 7, pp. 1153–1159, Jul. 2012.

[108] R. A. Simon, “Progress in Processing and Performance of Porous-Matrix Oxide/Oxide Composites,” *Int. J. Appl. Ceram. Technol.*, vol. 2, no. 2, pp. 141–149, Mar. 2005.

[109] R. a. Simon and R. Danzer, “Oxide Fiber Composites with Promising Properties for High-Temperature Structural Applications,” *Adv. Eng. Mater.*, vol. 8, no. 11, pp. 1129–1134, Nov. 2006.

[110] P. S. Thomas, J. Guerbois, G. F. Russell, and B. J. Briscoe, “FTIR STUDY OF THE THERMAL DEGRADATION OF POLY (VINYL ALCOHOL),” vol. 64, no. 2001, pp. 501–508, 2007.

[111] K. J. Moeggenborg and P. E. Reed, “United States Patent 5 487 855,” 1996.

[112] T. Chartier, D. Merle, and J. L. Besson, “Laminar Ceramic Composites,” *J. Eur. Ceram. Soc.*, vol. 15, pp. 101–107, 1995.

[113] D. Hotza and P. Greil, “Review : aqueous tape casting of ceramic powders,” *Mater. Sci. Eng. A*, vol. 202, pp. 206–217, 1995.

[114] S. Somiya, *Handbook of Advanced Ceramics: Materials, Applications, Processing and Properties*. 2013.

[115] F. F. Lange, “Powder Processing Science and Technology for Increased Reliability,” *J. Am. Ceram. Soc.*, vol. 72, no. 1, pp. 3–15, 1989.

[116] M. Szafran and G. Rokicki, “New Polymeric Binders in Ceramic Processing,” *Adv. Sci. Technol.*, vol. 45, pp. 453–461, 2006.

[117] Zschimmer & Schwarz GmbH & Co KG - Chemische Fabriken, “Product information on polyvinyl alcohol preparations.”

[118] “http://www.taimei-chem.co.jp/product/english/01.html. Accessed 15/03/2012.” .

[119] J. Echeberria, J. Tarazona, J. . He, T. Butler, and F. Castro, “Sinter-HIP of alpha-alumina powders with sub-micron grain sizes,” *J. Eur. Ceram. Soc.*, vol. 22, no. 11, pp. 1801–1809, Oct. 2002.

[120] J.-J. Luo and I. M. Daniel, “Sublaminate-based lamination theory and symmetry properties of textile composite laminates,” *Compos. Part B Eng.*, vol. 35, no. 6–8, pp. 483–496, Sep. 2004.

[121] J. W. Gilman, D. L. VanderHart, and T. Kashiwagi, “Thermal Decomposition Chemistry of Poly (vinyl alcohol),” *Fire Polym. II Mater. Test Hazard Prev. Am. Chem. Soc.*, vol. ACS Sympos, 1995.

[122] “Standard Test Method for Flexural Properties of Continuous Fiber-Reinforced,” *Annu. B. ASTM Stand.*, vol. C1341, no. 06.

[123] “Standard Test Method for Short-Beam Strength of Polymer Matrix Composite Materials,” *Annu. B. ASTM Stand.*, vol. D2344, no. 00 (Reapproved 2006).

[124] “Standard Test Method for Monotonic Tensile Behavior of Continuous Fiber-Reinforced Advanced Ceramics with Solid Rectangular Cross-Section Test Specimens

at Ambient Temperature," *Annu. B. ASTM Stand.*, vol. C1275, no. 00 (Reapproved 2005).

[125] J. A. Rodríguez-González and F. Avilés, "A modified short beam shear specimen for characterization of interfacial strength in nanocomposites," *Polym. Test.*, vol. 31, no. 6, pp. 792–799, 2012.

[126] T. R. Walter, G. Subhash, B. V. Sankar, and C. F. Yen, "Monotonic and cyclic short beam shear response of 3D woven composites," *Compos. Sci. Technol.*, vol. 70, no. 15, pp. 2190–2197, 2010.

[127] V. C. S. Chandrasekaran, S. G. Advani, and M. H. Santare, "Role of processing on interlaminar shear strength enhancement of epoxy/glass fiber/multi-walled carbon nanotube hybrid composites," *Carbon N. Y.*, vol. 48, no. 13, pp. 3692–3699, 2010.

[128] K. J. Bowles and S. Frimpong, "Void Effects on the Interlaminar Shear Strength of Unidirectional Graphite-Fiber-Reinforced Composites," *J. Compos. Mater.*, vol. 26, no. 10, pp. 1487–1509, Jan. 1992.

[129] Taimei Chemicals Co. Ltd, "Taimicron High Purity Alumina," 2011.

[130] D. M. Wilson, "New High Temperature Oxide Fibers."

[131] F. Deléglise, M. H. Berger, D. Jeulin, and A. R. Bunsell, "Microstructural stability and room temperature mechanical properties of the Nextel 720 Fibre," *J. Eur. Ceram. Soc.*, vol. 21, pp. 569–580, 2001.

[132] B. K. Daniels, N. K. Harakas, and R. C. Jackson, "Short beam shear tests of graphite fiber composites," *Fibre Sci. Technol.*, vol. 3, no. 3, pp. 187–208, 1971.

[133] Vitcas, "High Refractory Alumina Mortars." [Online]. Available: http://www.vitcas.com/high-alumina-refractory-mortars. [Accessed: 22-Feb-2015].

[134] "Standard Test Method for Shear Strength of Continuous Fiber-Reinforced Advanced Ceramics at Ambient Temperatures," *Annu. B. ASTM Stand.*, vol. C1292, no. 00 (Reapproved 2005).